FORMABILITY OF HIGH STRENGTH

ALUMINIUM SHEET

ANGUS GORDON RICHARD McCLELLAND

A thesis submitted in supplication for the

degree of Doctor of Philosophy

Department of Metallurgy and Materials Engineering

University of Aston in Birmingham

September 1982

Summary

The University of Aston in Birmingham

Title: Formability of High Strength Aluminium Sheet
Author: Angus Gordon Richard McClelland
Degree: PhD, 1982

An initial review of the subject emphasises the need for
improved fuel efficiency in vehicles and the possible
role of aluminium in reducing weight. The problems of
formability generally in manufacture and of aluminium in
particular are discussed in the light of published data.
A range of thirteen commercially available sheet aluminium
alloys have been compared with respect to mechanical
properties as these affect forming processes and behaviour
in service.

Four alloys were selected for detailed comparison. The
formability and strength of these were investigated in
terms of underlying mechanisms of deformation as well as
the microstructural characteristics of the alloys
including texture, particle dispersion, grain size and
composition.

In overall terms, good combinations of strength and
ductility are achievable with alloys of the 2xxx and
6xxx series. Some specific alloys are notably better
than others. The strength of formed components is affected
by paint baking in the final stages of manufacture.
Generally, alloys of the 6xxx family are strengthened
while 2xxx and 5xxx become weaker. Some anomalous
behaviour exists, however.

Work hardening of these alloys appears to show rather
abrupt decreases over certain strain ranges which is
probably responsible for the relatively low strains at
which both diffuse and local necking occur. Using data
obtained from extended range tensile tests, the strain
distribution in more complex shapes can be successfully
modelled using finite element methods.

Sheet failure during forming occurs by abrupt shear
fracture in many instances. This condition is favoured
by states of biaxial tension, surface defects in the form
of fine scratches and certain types of crystallographic
texture. The measured limit strains of the materials can
be understood on the basis of attainment of a critical
shear stress for fracture.

Key words: Aluminium; Formability; Limit Strain;
              Shear Fracture.

CONTENTS

LIST OF TABLES

LIST OF FIGURES

2.   INTRODUCTION

At the end of 1975 there were 17 884 000 licensed vehicles in the
United Kingdom. Of these
14 061 000 were private cars and vans
   114 000 public transport vehicles
 1 813 000 commercial vehicles
 1 173 000 motorcycles, mopeds and scooters
the remainder being agricultural tractors, civil engineering machinery
and military vehicles.

The overall automotive fuel requirement for 1974-75 was:
Petrol   15.87 x 10^6 tons
Derv   5.33 x 10^6 tons
which represents 24.6% of the total oil consumption in the U.K. for
that year.

There has been a continuous increase in the past in the number of
licensed vehicles and this trend is likely to carry on well into the
future. It is apparent therefore that any improvement in vehicle
fuel efficiency will lead to appreciable savings in total fuel
consumption. The popular demand for larger, more powerful vehicles
was conditioned by the relative cheapness of motor fuel. However,
the fourfold increase in crude oil price by O.P.E.C. in 1973 and its
subsequent impact with value added tax (V.A.T.) on petrol prices
served to highlight the need for fuel economy. From 1973 onwards
fuel prices increased at a relatively stable rate until the later

half of 1978 and 1979 when petrol prices rose by up to 50%.

The rise in price coupled with a further increase in the rate of V.A.T. increased pressure on automobile manufacturers to produce vehicles with higher fuel efficiencies and subsequently there is now increasing demand for smaller and more economical models.

There are several ways in which increased fuel efficiency could be achieved:

.   To consider improvements in design to internal combustion engines and transmissions leading to reduced fuel consumption.

.   To consider improvements in vehicle design leading to reduced fuel consumption.

The latter method may be further divided:

.   Improved design to reduce drag and frictional losses - the current average drag coefficient for British cars is 0.45. Changes in design have produced drag coefficients as low as 0.23 which it is estimated would give a 20% reduction in fuel consumption.

.   Improved utilisation of materials to reduce vehicle weight.

Reduction of vehicle weight through the use of lighter materials includes:

.   A primary saving resulting from the direct substitution of a lighter for a heavier material in a component.

.   A secondary weight saving resulting from the lighter structural loads to be carried by the chassis, suspension system, etc.

Research carried out in the United States indicates that 36 kg of aluminium can replace approximately 90 kg of heavier material in production and prototype vehicles. This gives a direct weight saving of 54 kg or a primary weight saving of 1.5 kg for each kilogram of aluminium used. Estimated secondary weight savings average 50% of the primary resulting in a total saving of around 2.25 kg for each kilogram of aluminium used.

This research is based on the investigation of suitable aluminium alloys for automotive applications with a view that a reduction in vehicle body weight of upto 30% may be achieved producing a subsequent increase in fuel efficiency.

3.   LITERATURE REVIEW

3.1.   THE CASE FOR ALUMINIUM

If we are to tackle seriously the problem which is now becoming evident it would appear that we must make more efficient use of fuel used in automobiles.

Evaluating the energy saving potential of a material depends on three basic factors:

. Weight differences between alternative materials
. Relationship between fuel economy and weight
. Energy content of both materials and fuel

Aluminium requires large amounts of energy to produce. 14 - 16 KWh/Kg (1) is required in the electrolytic reduction process. The cost of recycling aluminium scrap is, however, low. Calculations of the return in terms of energy saved over a ten year life, on the investment of energy in producing aluminium for motor cars show a ratio of 9:1 as the result of direct substitution. For a complete re-design taking full advantage of aluminium the savings on energy investment could be in the ratio 22:1.

There is a direct correlation between vehicle weight and petrol mileage (2). E.P.A. figures show an average of 10.06 Km/1 for a 907 Kg car versus 4.61 Km/1 for a 1814 Kg car.

The relationship between fuel economy and the weight of an automobile can be calculated from empirical formulae derived by interpolating published data covering both urban and open highway driving. For urban driving an average fuel consumption/weight coefficient of 1.15×10^{-4} 1/Kg Km was calculated from fuel economy figures (2). The corresponding coefficient developed for open highway driving was 2.71×10^{-5} 1/Kg Km (3).

Fuel savings from vehicle weight reduction are roughly four times greater for urban than for open highway driving. This fact arises from the inherently greater amount of fuel consumed in stop/go urban driving and the effect of aerodynamic drag which reduces the relative advantage of weight savings in open highway driving.

Accurate evaluations of weight reduction through substitution of lighter for heavier materials are difficult because of the number of performance requirements ie. strength, stiffness, heat conductivity, mass, resistance to corrosion, appearance, etc. They can best be determined from experience gained from production and prototype vehicles.

Alternative Materials

High strength steels have been proposed, in recent years, as relatively cheap, high strength to weight ratio metals which could be substituted in place of low carbon steel for vehicle body manufacture in preference to aluminium. High strength low

alloy (H.S.L.A.), high strength cold rolled (H.S.C.R.) and Micro-duplex steels provide a viable substitute for mild steels and possess improved fatigue and impact resistance, adequate corrosion and welding characteristics but have reduced formability.

H.S.L.A. steels rely on the addition of small percentages of carbide and nitride forming elements, which produce particles within the metal during hot rolling, for their strength. Niobium, titanium and vanadium or combinations of these elements are used. The carbides restrict recrystallization and grain growth of the hot-worked austenite, which upon transformation gives a fine ferrite grain size and thus a high strength material. A precipitation hardening effect can also be obtained depending on whether the particles form during the following process or are precipitated subsequently as a fine dispersion in the ferrite.

The use of H.S.L.A. steel is limited in the automobile industry due to the relatively thick minimum gauges that are currently available. H.S.C.R. steels were introduced to overcome this difficulty. Just as with H.S.L.A. steels, solid solution hardening, precipitation hardening and grain refinement are used to produce a product with the required hot band yield strength. The material then undergoes cold reduction to produce a range of as-rolled yield strengths. A recovery anneal or full anneal can be used to produce metal with yield strengths of 0.8 - 0.9 or 0.3 - 0.45 of the as-rolled yield strength respectively. Finally, a temper-rolling pass can be used to produce the required thickness control, surface finish and suppression of discontinuous yielding.

High strength microduplex steels have recently been developed
and consist of a duplex microstructure of ferrite and martensite.
It is produced by heating a vanadium containing steel of the H.S.L.A.
type for a short time at a temperature in the intercritical two-phase
austenite-ferrite region. On cooling, a duplex microstructure is
produced consisting of a ferrite matrix with a less deformable
second phase of martensite and a fine distribution of vanadium
carbide precipitates. More recent developments allow the dual phase
structure to also be achieved without the addition of alloying
elements.

3.2 STRUCTURAL CONSIDERATIONS

In general, vehicle design criteria can be grouped into three
categories:
.   Static load design criteria
.   Dynamic load design criteria
.   Crashworthiness load design criteria

The first two design criteria arise from functional and service
requirements and the third from imposed safety standards. From
a structural view point, the objectives of these criteria can be
related to four types of structural requirements:
.   Stiffness
.   Strength
.   Vibration
.   Crash

The stiffness design requirement can be defined as the maximum allowable deflection of a structure under a specific load. Similarly, the strength design requirement is defined as the maximum allowable stress under a specific loading and the vibration design requirement, as the desired frequency and mode of response. The crash design requirements are related to energy absorption and management. Unlike the requirements for stiffness, strength and vibration, which are also often considered in conventional structural designs, the crash characteristic is a very special requirement in automobile structures and only a small quantity of literature and design guidelines are available in this area because the relationship between various deformation modes and occupant protection is only partially understood.

Local Stiffness

Most outer panels have areas not supported by inner panels. Loads applied to the outer panel in these areas will cause the panel to deflect; the amount of deflection is dependent on load, thickness, geometry and material. The deflection of essentially flat panels is sometimes referred to as oil-canning. Under identical loading the deflection of an aluminium panel is greater than that of a steel panel having the same size and thickness because of the difference in the modulus of elasticity. In Fig. 1. (4), for a given load, the measured deflection of the aluminium panel is not three times that of the steel panel as might be expected from the relative values of modulus of elasticity but is less than twice the deflection of the steel panel.
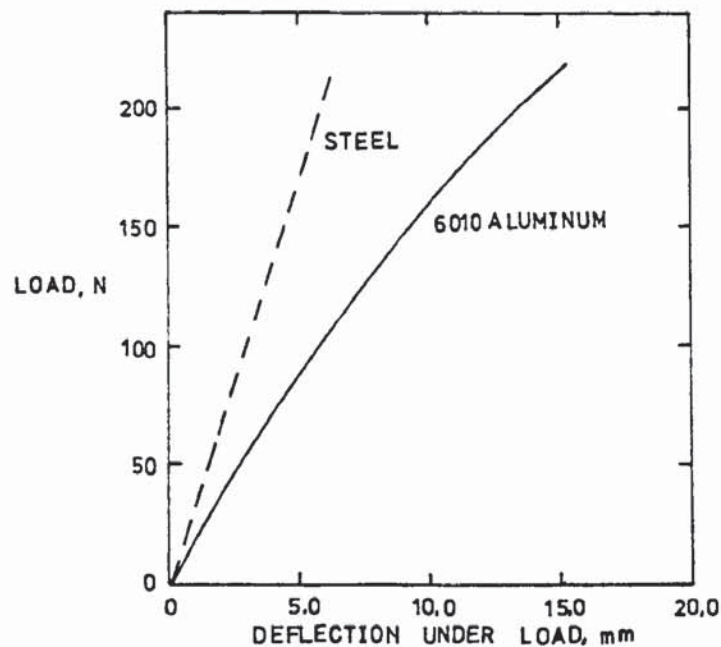
FIG.1. Load-deflection tests of production hoods . (4).

Finite element analyses and load deflection tests have been
conducted to determine the significant perameters that influence
local deflection of outer panels. The equation for calculating the
local deflection of nearly flat outer panels was determined to be: (4)

$$\Delta = \frac{KL}{t \sqrt{E}} \qquad (1)$$

where

Δ = Deflection for a given load.

K = Coefficient that varies primarily with load on the
    outer panel.

L = Length of shortest side of unsupported area (function
    of rib spacing).

t = Thickness of outer panel.

E = Modulus of elasticity of material of the outer panel.

Good agreement was found between calculated and measured deflections
in steel and aluminium panels.

Two changes can be made to an aluminium assembly to minimize outer panel deflection:

. The inner rib spacing can be decreased.

. The outer panel thickness can be increased.

Reducing the inner rib spacing greatly reduces weight but retains performance equivalent to an assembly in which the thickness of the outer panel is increased to obtain the desired local stiffness. Local stiffness can be improved, if clearance requirements do not allow a full depth inner panel rib to be employed, by not cutting out a strip of inner panel. Increasing the depth of the strip by down flanging the edges is also beneficial.

For bending stiffness to be the same in the new material, the new thickness can be found by: (5)

$$\frac{t_2}{t_1} = (\frac{E_1}{E_2})^{\frac{1}{3}} \qquad (2)$$

Hence, for any assemblies, which carry bending loads, the thickness has to be increased.

The thickness of an outer panel in aluminium compared to the thickness of a steel outer panel for equivalent local stiffness is: (4)

$$\frac{t_1}{t_2} = \frac{L_1}{L_2} \cdot \sqrt{\frac{E_2}{E_1}} \qquad (3)$$

where

L_1, L_2 = Length of the shortest unsupported area of aluminium and steel respectively.

E_1, E_2 = Modulus of aluminium and steel respectively.

Strength

An assembly needs to have resistance to yielding or failure under
loads causing bending of inner panel ribs (bending or torsion of
the assembly). Yielding and crippling are considered. Thickness
requirements to prevent crippling and yielding of assemblies can
decrease with an increase in yield strength as shown in Fig. 2. (4).
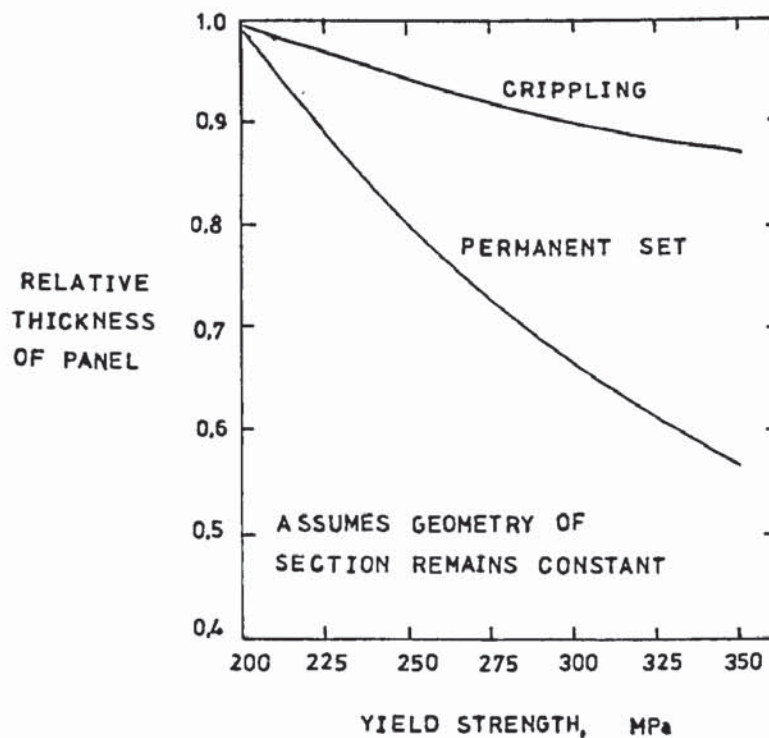
FIG.2. Thickness and yield strength variations for beam
        crippling and permanent set. (4)

Thickness has been normalized to a value of 1.0 for an aluminium
yield strength of 200 MPa. Thus from the standpoint of yielding
(resistance to permanent set), and crippling, minimum weight designs
would result from the use of high strength aluminium alloys.

The thickness of aluminium compared to steel for equivalent resistance
to permanent set for the same geometry is inversely proportional to
yield strength. Younger (6) has shown that theoretically the new

-11-

gauges for a different material in a bending mode can be determined from:

$$\frac{t_1}{t_2} = \frac{(\sigma y_2)^{\frac{1}{2}}}{\sigma y_1^2} \qquad (4)$$

As stated previously, for tensile and compressive loads, thickness is inversely proportional to yield strength. Therefore, to have equal strength in the tensile mode:

$$t_1 = t_2 \cdot \frac{\sigma y_2}{\sigma y_1} \qquad (5)$$

Crippling is a phenomenon that can occur in thin walled shapes subjected to bending. It is a type of instability of the section in which failure occurs at stresses less than the yield strength of the material. Crippling strength depends on the width-to-thickness ratio of the elements of the part, the yield strength of the material and the modulus of elasticity. For a given bending moment and shape of section, the thickness required is roughly proportional to: (7)

$$\sqrt{\sigma y \cdot E} \qquad (6)$$

For equivalent crippling strengths of aluminium and steel, the width-to-thickness ratio of aluminium $(b/t)_1$ compared to steel $(b/t)_2$ is (4)

$$\frac{(b/t)_1}{(b/t)_2} = \frac{t_1}{t_2} \cdot \frac{y_1}{y_2} \cdot \frac{E_1}{E_2} \qquad (7)$$

Dent Resistance

Dent resistance can be described in many ways and numerous types of tests have been employed to define it. Speed of loading, shape of part, stiffness of part and mass of the impacting object are a few

of the many variables that can be considered. In spite of the large
number of variables and the differences in test procedures and
analyses employed by investigators, published studies (8-14)
show that dent resistance increases with yield strength and thickness.
The depth of dent as determined from a simple drop weight test
(230g steel ball dropped 3m) decreases as the product of yield
strength and thickness increases, see Fig. 3 (4). The curve in
Fig. 4 (4) demonstrates the reduction in thickness that can be
achieved with increasing yield strength for aluminium outer panels
having dent resistance equivalent to panels of 200 or 350 MPa yield
strength steels.
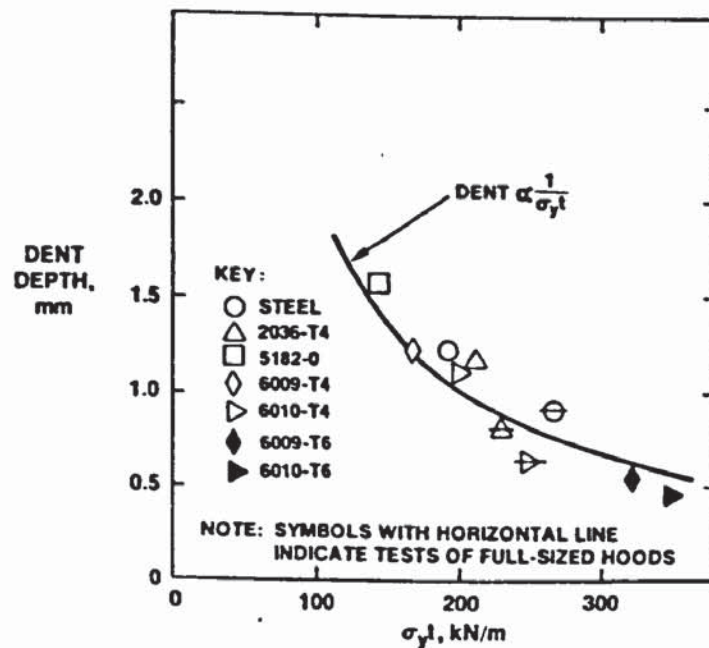
FIG.3.   Dent resistance of minihoods and fullsized hoods. (4)
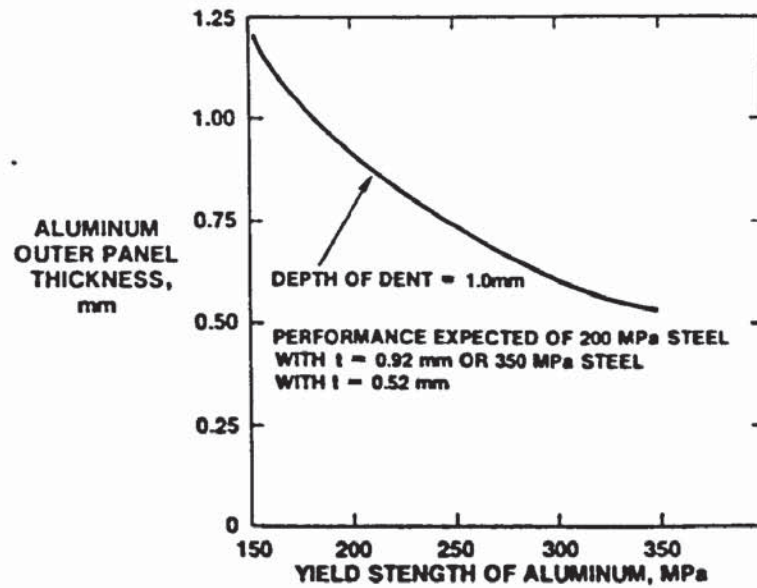
FIG.4.   Dent resistance as a function of yield strength and
         thickness. (5)

It was found (4) that aluminium alloys 2036-T4, 6009-T6 and

6010-T6 provide the same or better dent resistance as 200 MPa steel

for the same gauge.   A high strength aluminium alloy such as 6010-T6

must be used to have equal performance on a gauge-for-gauge basis

with a 250 MPa steel.   Based on equivalent dent resistance the

thickness of aluminium compared to steel for an outer panel is as

follows: (8)

$$\frac{t_1}{t_2} = \frac{\sigma y_2}{\sigma y_1} \qquad (8)$$

As per Dicello and George (10), when a weight reduction is made by

changing the material, the dent resistance of new material can be

found by:

$$\frac{(\sigma y)_1^2}{S_1} \cdot t_1^4 = \frac{(\sigma y)_2^2}{S_2} \cdot t_2^4 \qquad (9)$$

-14-

where

S$_1$, S$_2$ represent panel stiffness, we get:

$$\frac{(t_1)^4}{(t_2)^4} = \frac{(\sigma y_2)^2}{(\sigma y_1)^2}$$

3.3   PROBLEMS ENCOUNTERED IN MATERIALS SUBSTITUTION

The substitution of aluminium in place of low carbon steel gives rise to many problems in manufacturing not least of which is the reduced formability of aluminium alloys when compared with conventional sheet steels. Fig. 5 compares the formability of a typical aluminium alloy BA2117 (CP) with low carbon 1010 steel and microduplex Hi-Form 8od.
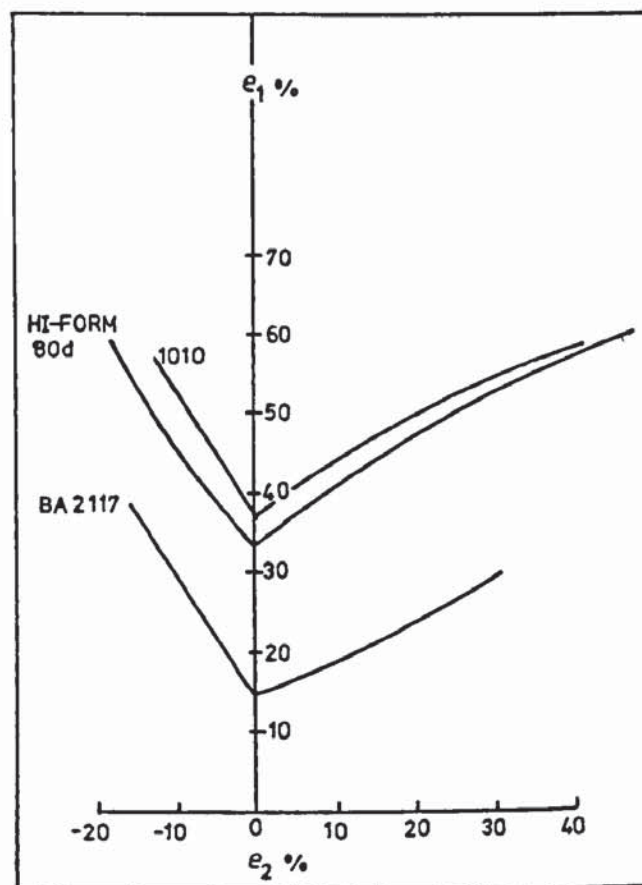
FIG.5.   A comparison of limit strains for an aluminium alloy (BA2117CP), low carbon steel (1010) and Microduplex steel (Hi-Form 8od).

Limit strains in the case of 1010 steel are only marginally superior to Hi-Form 8od. Aluminium, however, shows a reduction of ~20% in limit strains in the region o$\leqslant e_2$. This difference slowly but steadily decreases when e_2 becomes increasingly negative.

Material strength plays an important role in sheet metal pressing operations. If the yield strength is too high or the material too hard damage to the dies may occur over a period of several pressings. Fig. 6 shows stress-strain curves for BA2117 (CP) and three types of sheet steel. It is evident that the strength levels of BA2117 (CP) and 1010 steel are very similar although ductility differs. Microduplex and H.S.L.A. steels are much stronger and so afford the opportunity to reduce sheet thickness saving weight.
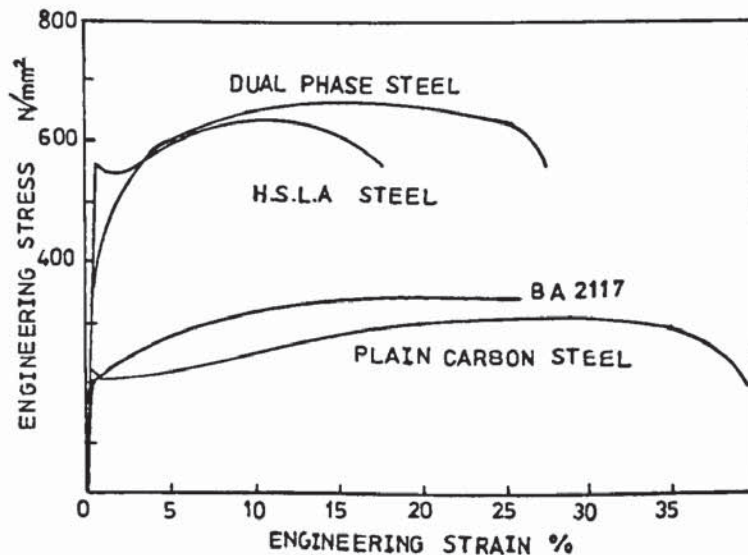
FIG.6. Comparison of stress-strain data for an aluminium alloy, low carbon steel, HSLA steel and Microduplex steel.

When aluminium is formed under press conditions similar to those used for steel, problems of material pick-up on die surfaces are often encountered. This pick-up gives rise to surface damage of the sheet and imparts an unacceptable finish to the pressing. Frequent cleaning of the die surfaces is therefore necessary which is both time consuming and expensive.

The joining characteristics of aluminium present problems not normally encountered with steel. Because the specific heat of aluminium is twice that of steel and aluminium conducts heat four times faster, welding plant must provide an intense localised source of heat. The oxide film is chemically stable and reforms rapidly in air, therefore the process must be able to remove or break up the oxide film and prevent its reformation. In the manufacture of automobiles spot welding is probably the most widely used joining process. Because of its afore-mentioned characteristics, aluminium requires higher spot welding currents and electrodes require dressing more frequently. This can increase process costs dramatically.

3.4 ASSESSMENT OF FUNDAMENTAL MATERIAL PROPERTIES

3.4.1 Work Hardening Behaviour

The descriptions of the process of strain hardening at modest plastic strains are capable of quantification in terms of both the detailed structural descriptions of dislocation accumalation and the rates and geometry of dislocation motion. A number of reviews (15, 16)

have been produced which discuss the details of the hardening process. However, at large plastic strains the description of the plastic flow of both single crystals and polycrystals is much more empirical in form. Lücke and Mecking (17) have pointed out that one of the essential features of a description of large strain deformation is the occurence of dynamic recovery which leads to a gradual decrease in work hardening rate because the hardening processes which are dominant at low strains are supplemented by softening processes. In cold forming strain hardening is the dominant source of necking resistance and because the flow strength increases and the rate of strain hardening decreases quite rapidly with increasing strain, room temperature stretching limits are severely restricted.

Strain Hardening Index

The n value is defined as the slope of the log true stress (log σ) - log true strain (log ϵ) curve. Conventionally the n value is measured in the tensile test between the limits of yield and maximum load, ie. before the onset of diffuse necking.

$$d(\log \sigma)/d(\log \epsilon) = n \qquad (10)$$

Provided the power law (18)

$$\sigma = K \epsilon^n \qquad (11)$$

is a good approximation to the true stress-strain curve then n will be independent of strain. Theoretically, for an isotropic metal in uniaxial tension, the onset of diffuse necking will occur at a strain numerically equal to n (19,20),

$$\text{viz. } n = \epsilon_u \qquad\qquad (12)$$

or in terms of engineering strain

$$n = \ln (1 + (\epsilon_o)_u)$$

whilst failure, localised necking, does not begin until the strain $\epsilon = 2n$. Deformation behaviour during diffuse necking was studied by Ghosh (21) who recognised that hardening (or softening) behaviour during necking was controlled by stress state, strain hardening and strain-rate hardening. Arbel (22) obtained, by experiment, a general relationship between the L.D.R. attained in formal deep drawing with a flat headed punch and n. However, Swift (23) found no correlation to exist between $(\epsilon_o)_u$ and L.D.R.

Approximate Equations for Stress-Strain Curves

Various attempts have been made to write empirical equations that would fit experimentally observed stress-strain curves. Within the elastic range of most metals the relationship between stress and strain is described by the equation

$$\overline{\sigma} = E \, \overline{\epsilon} \qquad\qquad (13)$$

For situations where the metal may be deformed into the plastic range it is desirable to have the stress-strain curve for the material described by some mathematical equation. The four which are most commonly used are:

-19-

$$\sigma = A + B\varepsilon^n \qquad (14) \quad \text{Ludwik} \quad (24)$$

$$\sigma = K_1\varepsilon^n \qquad (15) \quad \text{Hollomon} \quad (18)$$

$$\sigma = A(B + \varepsilon)^C \qquad (16) \quad \text{Swift} \quad (25)$$

$$\sigma = A - (A - B)\exp(-\varepsilon/c) \qquad (17) \quad \text{Voce} \quad (26)$$

where σ and ε are the true stress and true plastic strain respectively and the other perameters are constants. Some equations describe the deformation behaviour of a specific material better than others. For instance, the curves of annealed and deformed copper are best fitted by the Voce equation (27).

Plastic Instability

In 1885 Considere (28) first formulated a criterion for the instability strain in tension. At high rates of strain Zener and Hollomon (29) observed a shear plastic instability which they attributed to thermal softening and called adiabatic shear. Backofen (30) considered strain rate and adiabatic heating to arrive at the instability strain for the specific case of parabolic uniaxial tensile deformation. Hillier (31) developed criteria for instability in plane strain biaxial loading. The Considere theory of the tensile test was extended to include strain rate sensitivity and several definitions of instability by Hart (32). Argon (33) extended Hart's theory to include the effect of pressure and adiabatic heating. Anisotropy effects were added by Duncombe (34,35). Others (21, 36, 37) have also published related work.

In recent years many authors have investigated a class of instabilities which can be defined as phenomena related to the growth of a locally thinned region or neck, in a material containing defects, upon the application of a stress. Four criteria have been proposed in terms of different choices of variable for describing the onset of instability. Hart (32) proposed that the behaviour of a cross-sectional inhomogeneity σ_A be monitored whereas several other authors (34, 35, 38) chose to consider the behaviour of a relative cross-sectional inhomogeneity σ_ϵ. Local length (39) and dislocation density (40) were also proposed as plastic instability criteria.

Recently questions have been raised about prior treatments in particular Hart's (32) treatment, by Jonas et al (41) and others (42). Jonas et al (41) distinguished two types of defect on a tensile specimen. They called them mechanical defects and geometric defects. As noted by Kocks (42), these defects have usually been considered separately, the deformation defect being treated by some investigators (32 - 35) and the geometric defect by others (38, 43).

Different criteria for the onset of plastic instability have been given for the two types of defects by Jonas et al (44). The viewpoint that these two types of defect should be distinguished where the onset of plastic instability is considered phenominologically was questioned (45) and it was subsequently suggested that Hart's (32) criterion applies for both deformation and geometric defects.

In recent work, Ghosh (46) considered the influence of strain rate on plastic instability and presented a convincing argument that

increasing the strain rate would decrease the strain at maximum load, and at localised necking prior to fracture. These arguments are confirmed, at least for low strain rate loads, by the experiments of Sagat and Taplin (47) and the theories of Hutchinson and Neale (48). In the high strain rate loading condition the results appear to be quite different and considerable evidence exists that an increase in strain rate can result in an increase in the ductility of most metals (49). If strain rate sensitivity is decreased by increased prestraining Fyfe and Rajendran (49) found their results confirmed the theoretical development of Hutchinson and Neale (48) namely, the onset of plastic instability occurs at lower strains for a reduction in strain rate sensitivity.

For most practical purposes, the strain at which the load reaches a maximum deformation also corresponds to the formation of a diffuse neck. For plane stress situations with $\alpha = \sigma_2/\sigma_1$ where σ_1 and σ_2 represent the maximum and intermediate principal stresses respectively, a diffuse neck forms when

$$\frac{d\bar{\sigma}}{d\bar{\epsilon}} = \frac{\bar{\sigma}}{Zi} \qquad (18)$$

where $\bar{\sigma}$ is the effective stress, $\bar{\epsilon}$ is the effective strain and Zi is the critical subtangent. The effective stress (strain) is that function of the stress (strain) components which is representative of or equivalent to the stress (strain) under uniaxial tension. For an isotropic material obeying the Von Mises yield criterion these may be expressed as:

$$\bar{\sigma} = \frac{1}{\sqrt{2}} \left[(\sigma_1 - \sigma_2)^2 + (\sigma_2 - \sigma_3)^2 + (\sigma_3 - \sigma_1)^2 \right]^{\frac{1}{2}} \tag{19}$$

$$d\bar{\epsilon} = \frac{\sqrt{2}}{3} \left[(d\epsilon_1 - d\epsilon_2)^2 + (d\epsilon_2 - d\epsilon_3)^2 + (d\epsilon_3 - d\epsilon_1)^2 \right]^{\frac{1}{2}} \tag{20}$$

Z_i is a function of stress ratio. A graphical representation (known as Considere's construction) is shown in Fig. 7 for different values of Z_i. Two modes of unstable flow are indicated.
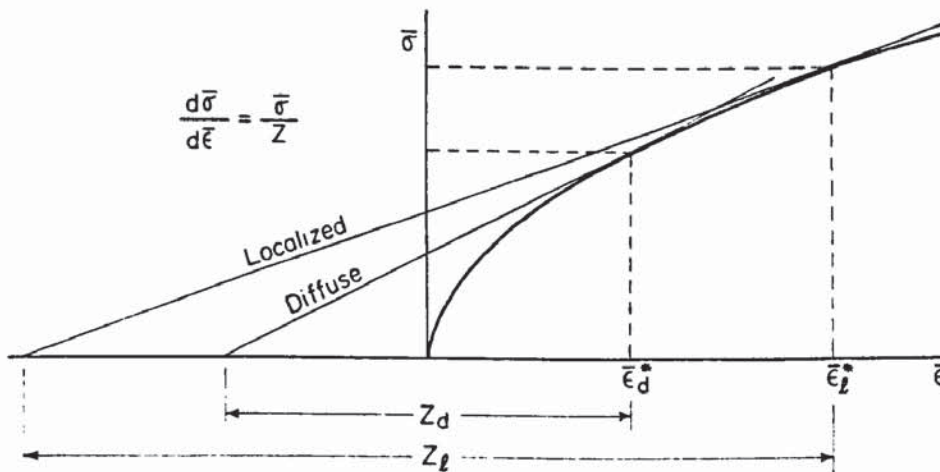
FIG. 7. Graphical determination of instability strain in a sheet uniformly loaded in its plane. Z is a function of the principal stress ratio σ_2/σ_1 ($\sigma_3 = 0$); Z_d relates to the beginning of diffuse and Z_L to the beginning of localised necking. For uniaxial tension, $\bar{\sigma} = \sigma$, $\bar{\epsilon} = \epsilon_1$, $Z_d = 1$ and $Z_L = 2$. (50).

-23-

For a particular stress system Zi can be found in terms of the stress ratio α and n the strain hardening exponent can be found experimentally. For an isotropic material in uniaxial tension $Z_{diffuse} = 1$ and $Z_{local} = 2$. Hill (51) also analysed this problem with particular reference to local instability. However, instability does not necessarily require the occurrence of localised necking, for when there is no line of zero extension in the plane of the sheet, a local neck is not possible. Keeler and Backofen (50) have shown that diffuse necking occurs when

$$Z_D = 4(1 - \alpha + \alpha^2)^{3/2} / [(1 - \alpha)(4 - 7\alpha + 4\alpha^2)] \qquad (21)$$

and localised necking when

$$Z_L = 2(1 - \alpha + \alpha^2)^{\frac{1}{2}} / (1 - \alpha) \qquad (22)$$

Equations 21 and 22 assume particular loading conditions. When $\alpha = \frac{1}{2}$, $Z_D = Z_L$ and the two modes of instability become equivalent. When $\alpha > \frac{1}{2}$ there is no direction of zero extension and so local necking is not possible. However, local necks have been seen to develop during biaxial stretch forming operations (52).

If the stress-strain curve can be represented by the power law

$$\bar{\sigma} = K\bar{\epsilon}^n$$

then
$$\frac{d\bar{\sigma}}{d\bar{\epsilon}} = n K\bar{\epsilon}^{(n-1)} = \frac{n\bar{\sigma}}{\bar{\epsilon}} \qquad (23)$$

From equations 39 and 42

$$\bar{\epsilon} = nZ \qquad\qquad (24)$$

Changes in both stress state and strain rate are associated with
diffuse necking, which might modify the apparent strain hardening
behaviour and result in a change in ϵ_1 for local necking. The
effects of a change in stress state in the neck have been considered
by several investigators (53, 54). It has also been pointed out
that the stress state may have an effect on the effective hardening
behaviour (55, 56).

3.4.2 Plastic Anisotropy

The phenomenon of anisotropy ie. "Mechanical directionality" and
"Crystallographic directionality" (or preferred orientation), is
known to play a significant role in sheet metal behaviour in the
plastic range. Certain anisotropic metals which possess higher
strength in the thickness direction than in the plane of the sheet
have been found to exhibit better drawing qualities than isotropic
metals. This phenomena has been studied by several investigators,
eg. (57-60).

Normal Anisotropy

The normal plastic anisotropy of a sheet metal is generally expressed
in terms of the r_θ coefficient defined as the ratio of the width-to
thickness strains in the uniaxial tensile test specimen orientated

at $\theta°$ to the sheet rolling direction. The idea of measuring anisotropy
in this way and the procedure of the test itself were proposed almost
simultaneously in 1949 by Krupkowski and Kawinski (59) and in 1950
by Lankford et al (57). In the first method the plastic strain
ratio was expressed in terms of conventional elongations in the width
and thickness directions and in the second method as the ratio of
partial true strains. Both authors proposed the measurement of the
value of this coefficient at the deformation corresponding to the
limit of uniform elongation.

However, the value of strain ratio calculated in this way is not a
counterpart of anisotropy of the tested metal, its value being changed
in the test itself by the formation of fibre texture. In order to
obtain the value of strain ratio fully characterising the anisotropy
of the metal under test, Truszkowski (61) proposed the determination
of r_0 coefficient by measuring the strain ratio values at different
degrees of straining, and extrapolating the function $r = f(\varepsilon)$ back
to the initial state.

The course of the $r = f(\varepsilon)$ relationship may be explained by the
influence of fibre texture which forms during the tension test on
the initial deformation or recrystallisation texture. The lack of
a well defined preferred orientation in the initial state results
in a continuous change in the r value with strain. In completely
texture free metal it might be expected to obtain a constant r value
equal to unity over the range of uniform elongation. In the case
of a well defined preferred orientation, however, the fibre texture
appearing during the tension test influences the texture of the

initial state and as a result two different zones on the $r = f(\epsilon)$ relationship arise (61).

Several authors (62) have studied the effects of various factors such as specimen size, strain measurement location, number of specimens tested, etc. on the value of r obtained. Some of their results clearly indicate a strain dependence of the r value. Work done by Hu (63) has demonstrated that changes in the r value of sheet specimens during uniform elongation in tension depend on the r value of the sheet. For specimens having r = 1.00 (random textured sheet) the r value is independent of strain; for those having r < 1.00 (poor drawability sheet - strong (100) textured specimens) the r value increases with strain; and for those having r > 1.00 (deep drawing sheet - strong (111) texture) the r value decreases with increasing strain. However, Arthey and Hutchinson (64) have subsequently demonstrated that the apparent variation of r-value with strain in fact originates from two separate but discrete values which pertain to firstly inhomogeneous yielding and then to later homogeneous flow.

The strain ratio r is defined as the ratio of the natural strains in the width and thickness directions for a specimen extended in tension and is a function of the particular crystallographic anisotropy of the sheet (65).

$$r = \frac{\ln \dfrac{W_0}{W_f}}{\dfrac{t_0}{t_f}} \qquad (25)$$

where

W_0 = initial width

t_0 = initial thickness

Wf = final width

tf = final thickness

Early investigators measured width and thickness strains directly. To avoid the direct measurement of thickness strains, Burns (66) assumed that the volume of gauge length remained constant and used a modified parameter.

$$r = \frac{\ln \dfrac{W_0}{Wf}}{\ln \dfrac{\dfrac{Wf}{Lf}}{\dfrac{Wo}{Lo}}} \qquad (26)$$

Much has been written on the measurement of normal anisotropy (67-69) and its variation with strain (70).

It is generally agreed that the strain ratio value obtained is hypersensitive to errors in measurement. Atkinson and Maclean (67) pointed out that when equation 26 is used to calculate r, propogation of measurement errors produces an increasing uncertainty in r as the magnitude of r increases.

Atkinson (62) showed that even with very careful specimen preparation, inhomogeneities exist in plastic flow which can cause significant variability in r. For this reason two to three specimens for each test direction in the sheet are invariably required for reliable results.

Because of crystallographic texture the magnitude of r_θ will vary with θ. For this reason an average strain ratio r is determined conventionally and is defined by

$$\bar{r} = \frac{r_0 + 2r_{45} + r_{90}}{4} \qquad (27)$$

Stickles and Mould (71) working with low carbon steels showed that a statistical correlation can be made between angular variation and Youngs Modulus in the plane of textured sheet metals and the angular variation of the plastic strain ratio. They also showed that the angular variation of the elastic modulus could be used to characterise empirically the formability of a sheet with respect to both deep drawability and earing behaviour. Liu and Alders (72-75) have used measurements of the anisotropy of Youngs Modulus to study deformation textures in f.c.c. metals but this approach is not applicable to aluminium which is elastically isotropic.

Specific linear correlations between r value and L.D.R. have been established (67, 76, 77). The limited published data for aluminium indicate a rather tenuous connection between the two criteria (78,79). A number of investigators have demonstrated a direct relationship between r and deformation behaviour (79-81).

Lankford et al (57) found that the product $\bar{r} \times \bar{n}$ produced a favourable correlation with the drawability of steel sheet. Rennhack (82) found orientations of maximum and minimum r demonstrated little or no relation to the directionality in n. Solution treatment and natural ageing tended to accentuate planar anisotropy, increase $\bar{r}$ and decrease $\bar{n}$.

Planar Anisotropy

Planar anisotropy occurs where the properties in the plane of the sheet vary with respect to the rolling direction. Whilst normal anisotropy can improve drawability, planar anisotropy is in most cases undesirable (83). A well recognised manifestation of planar anisotropy is the earing effect encountered during deep drawing (57, 84, 85). Planar anisotropy has normally been measured by the change in "r" value with orientation, that is,

$$\Delta r = \frac{r_0 - 2r_{45} + r_{90}}{2} \tag{28}$$

3.4.3 Yield Criteria

The yield criterion defines the condition under which a material subjected to a stress system yields. Criteria which express a similar relationship after plastic strain has occured are known as flow criteria.

Criteria for Isotropic Metals

If a material is isotropic the yield condition must depend on the magnitude of the applied stresses and not upon their orientation.

Tresca (86) carried out tests on the extrusion of metals through various shaped dies and observed that the maximum shear stress τ_{MAX} reached a definite value when plastic flow started. Assuming the convention $\sigma_1 \geq \sigma_2 \geq \sigma_3$ then

$$\tau_{MAX} = \frac{\sigma_1 - \sigma_3}{2} = \text{constant} \qquad (29)$$

where $\sigma_1, \sigma_2, \sigma_3$ = principal stresses

A second criterion for isotropic metals is that of Von Mises (87). This was suggested earlier by Huber (88) but, being published in Polish, went unnoticed. The theory was introduced by Von Mises on Mathematical grounds and defines a yield surface in stress state with reference to the three mutually perpendicular principal stresses (no shear components) which must be reached by the imposed stress loading path before yielding begins (89).

$$(\sigma_1 - \sigma_2)^2 + (\sigma_2 - \sigma_3)^2 + (\sigma_3 - \sigma_1)^2 = 2Y^2 = 6K^2 \qquad (30)$$

Where   Y = Yield stress in simple uniaxial tension

              K = Yield shear stress for a state of pure shear

Hencky (90) later suggested that yield occurs when the elastic energy of distortion reaches a critical value. Thus a hydrostatic

pressure does not cause yielding in an isotropic material since it produces only elastic energy of dilation. The theory is independent of the sign of the stress since the terms are all squared and the convention that $\sigma_1 \geqslant \sigma_2 \geqslant \sigma_3$ is not required.

Criteria for Anisotropic Metals

In 1948, Hill (91) proposed a yield criterion based on Von Mises initial criterion, containing six parameters which specified the state of anisotropy. Hill argued that since the Von Mises criterion described fairly accurately the yielding of isotropic materials, then the simplest criterion for a material which was anisotropic was one which reduced to that of Von Mises when the anisotropy was vanishingly small. The mathematical form of Hills criterion is (92)

$$2f(\sigma ij) \equiv F(\sigma_y - \sigma_z)^2 + G(\sigma_z - \sigma_x)^2 + H(\sigma_x - \sigma_y)^2$$
$$+ 2L^2_{yz} + 2M^2_{zx} + 2N^2_{xy} = 1$$

Where F, G, H, L, M, N are parameters characteristic of the current state of anisotropy. This criterion when applied to metals with only normal anisotropy becomes (93)

$$\sigma_1^2 + \sigma_2^2 - (\frac{2r}{1 + r})\sigma_1\sigma_2 = Y^2$$

The stress required to deform a sheet under balanced biaxial loading, σb, is often compared with that attained under uniaxial load, σu, which in turn is directly related to the transverse plastic strain ratio r. Hill's theory predicts increasing stress ratio $\sigma b/\sigma u$ with increasing r; when r <1 theory predicts $\sigma b/\sigma u < 1$ and with r = 1, $\sigma b/\sigma u = 1$,

with $\sigma b/\sigma u > 1$ then $r > 1$ (94). Recent experimental work on steel
and aluminium has suggested that these conditions are not always
fullfilled (55, 95) which is inconsistent with Hill's plasticity
theory. The discrepancy between theory and experiment has been
attributed to deficiencies in the continuum approach, where the
crystallographic aspects of deformation are not considered. In
order to overcome this discrepancy, Hill's theory has been modified
by several investigators (96).

3.4.4 Strain Rate Sensitivity

Strain hardening and strain rate hardening have often been expressed
by the power law relationship,

$$\sigma = K\epsilon^n \dot{\epsilon}^m \tag{33}$$

where σ = flow strength

k = contant

ϵ = strain

$\dot{\epsilon}$ = strain rate

n = strain hardening index

m = strain rate hardening index

The effect of strain rate and temperature on the mechanical behaviour
of aluminium and its alloys has been reported by several investigators
(97-101). Although there is agreement that the flow stress of
aluminium is strain rate sensitive, the exact nature of this relation-
ship is not clear. Dynamic ageing due to interaction between
dislocations and diffusing solute atoms complicates the strain rate

sensitivity of many alloys. The strength of this source of
resistance to dislocation motion is sensitive to temperature, which
influences the rate of solute diffusion, and strain/strain rate which
influence dislocation velocities (102).

Negative strain rate sensitivity, as observed in the aluminium
alloy used in experiments by Ghosh and Hecker (103), is developed
under conditions of straining in which an increase in strain rate
leads to a reduction in the strength of the dynamic ageing reaction
which is sufficient to cause a reduction in flow strength.
Negative strain rate sensitivity therefore tends to promote strain
localisation and it leads to the shear type fractures frequently
associated with solution treated aluminium alloys deformed at room
temperature. It also gives rise to jerky flow phenomena which are
commonly observed in tensile tests.

Recently there have been some useful theoretical studies of the
combined influences of strain rate sensitivity of the flow stress
and the strain rate sensitivity of strain hardening on the development
of tensile instability (42, 104). Ghosh and Ayres (36) showed that a
good correlation between terminal m value before fracture and ductility
was feasable whereas correlation between initial m value and ductility
was not. It is therefore m value near fracture and not m value at
initial yield that would be expected to control elongation at fracture.

3.4.5 Ductile Fracture

The phenomenon of ductile fracture is widely observed among metallic materials. Several reviews have been made amongst which are those by Orowan (105, 106), Cottrell (107), Backofen (30) and Meakin and Petch (108).

Experimental results show that the mechanism of ductile fracture in materials consists basically of three stages. In the first stage internal microscopic cavities (microvoids) are nucleated at the site of inclusions and second phase particles; as the matrix undergoes bulk plastic deformation (109, 110) the number of micro-voids tending to increase with increased plastic straining. The second stage consists of the continuous volumetric growth and shape change of the voids, under the applied stress and strain fields, with the volume fraction of microvoids remaining sufficiently small for the overall macroscopic deformation of the matrix to approximate to that of an incompressible plastic solid. The third stage consists of a localised internal necking of the intervoid matrix, over a single sheet of microvoids, to produce a ductile fracture surface (107, 111) a process known as void coalescence.

An important feature of the process of void coalescence is the abrupt intervention of a ductile fracture surface in a hitherto continuous process of plastic flow, as demonstrated by results (112, 113) showing the microvoids, in regions immediately adjacent to ductile fracture surfaces, to be relatively small and widely

spaced. Such results suggest (114) that the onset of ductile
fracture by void coalescence is due primarily to a loss of
stability by the intervention of a highly localised mode of unstable
plastic flow in the intervoid matrix with adjacent regions of the
matrix remaining virtually rigid after the onset of void coalescence.

Modes of Fracture

Ductile fracture of commercial metals and alloys can occur by two
basic modes, the fibrous mode and the shear mode. Fibrous fracture
is characterised by the formation and growth of voids from non-
metallic inclusions or second phases leading to a fracture surface
covered with equiaxed dimples. The mechanism of this mode of
fracture is fairly well understood (115, 116).

The shear mode of ductile fracture gives rise to fracture surfaces
covered with strongly oriented parabolic dimples. This mode of ductile
fracture occurs in a number of different situations including the
outer portion of cup and cone fractures, the tensile fracture of sheet
materials and the fracture of some materials under hydrostatic
pressure (117). A general model for shear fracture has been proposed
(116) which involves the development of zones of heavy shear deformation
within which sheets of voids form, followed by fracture due to axial
tensile stress. Additional features of this type of fracture are
that where there is a strong inclusion - matrix interface such as in
aluminium alloys, voids develop only just prior to fracture and void
coalescence occurs rapidly and only close to the fracture path.

Cavity formation at Inclusions

Optical and electron metallography (111, 115, 116) and fractography
(109) have shown that the voids responsible for fracture are
frequently associated with second phase particles. Although it has
generally been recognised that some plastic strain is necessary to
form holes at inclusions most quantitative developments have compared
experimentally computed strains for hole growth and coalescence
(118, 119). There are many observations which show that large plastic
strains are often required to tear inclusions free or produce internal
fracture in them (110, 120, 121). It has been generally observed
(115, 122) that while inclusions with large aspect ratios may undergo
multiple internal fracturing, equiaxed inclusions almost always
nucleate holes by interfacial separation.

Considerations of inclusion separation can be grouped into three
categories, energy criteria, local stress criteria, and local strain
criteria. Gurland and Plateau (123) proposed that cracks at interfaces
could form when the locally concentrated elastic strain energy which
could be released on decohesion becomes comparable to the energy
of the surfaces to be generated. The effect of the relative surface
energies is to influence the mode of void formation by either interface
failure or by particle failure. The two possibilities are governed
by the expressions:

$$\gamma = \gamma m + \gamma p - \gamma mp \qquad (34)$$

for fracture of the interface, and

$$\gamma \simeq 2\gamma p \qquad\qquad (35)$$

for fracture of the particle

where γm = surface energy of the matrix

γp = surface energy of the particle

γmp = surface energy of the particle-matrix interface

Variations in the value of σ along the surface of an individual particle, presumably by some form of contamination, have been shown to inhibit void formation locally (124).

Gurland and Plateau (123) have attributed cavity formation to impingement of dislocation pile-ups at inclusions in the manner proposed by Zener (125). Ashby (126) has discussed an alternative in which primary deformation incompatabilities do not produce cavities directly, but initiate highly organised secondary slip by punching out dislocation loops form the matrix/inclusion inter-face to reduce the local shear stresses. These loops then form reverse pile-ups and can build up increasing interfacial tensile stresses until they reach the interfacial tensile strength when a cavity if formed.

It has been shown (127) that interfacial stress will increase with strain hardening and triaxiality. Both of these effects reduce ductility. Both theoretical (119) and experimental (128) results suggest that a state of triaxial tension promotes microvoid coal-essence. Such a stress state is obtained in a necked uniaxial tensile specimen, or in thick sheet, below the root of a notch

in bending or tension.

Models of Ductile Fracture

Over a number of years many models have been proposed to explain
some of the experimental observations in ductile fracture.

In the models of Gurland and Plateau (123) and of McClintock (129)
a continuum mechanics approach was used. Cavities were assumed
to be present in the unworked material or to form at inclusions
at the onset of plastic deformation. The Gurland and Plateau
model shows that the strain at fracture is a function of the volume
fraction of particles or inclusions present, which is in agreement
with the experimental observations of Edelson and Baldwin (130), and
the mean free path between particles.

The models of Ansell and Lenel (131), Ashby (126) and McLean (132)
use dislocation mechanisms to calculate the onset of yield, void
formation and growth. The model of Ansell and Lenel (131) was
proposed to explain the effects of a dispersion of second phase
particles on the yield strength of metals. The yield stress was
shown to be proportional to the reciprocal square root of the inter-
particle spacing in agreement with the experimental work of Roberts
et al (133) and Lenel et al (134). In the Ashby (126) model the
back stress, exerted by dislocation loops formed around particles
during plastic flow, is relieved by a process of secondary slip.
The details of the calculation show that the stress increases linearly
with strain and with particle diameter. Hence, large particles
will form interfacial voids before small ones, a fact observed

experimentally (123, 124). The model proposed by McLean (132) is based upon the formation and subsequent growth of a vacancy loop at the particle matrix interface. Growth of the loop into a crack is considered to occur by coalescence with other loops or by absorption of edge dislocations.

More recently models have been proposed by Melander (135, 136) and Needleman and Rice (137). These can be divided into two types. In one category of models (135, 136) a detailed study is made of the influence of the initial void distribution on the fracture strain. The flow properties of the matrix material are, however, described in a crude way and the arrangement of voids is only two dimensional. The other category (137) studies macroscopic shear instabilities caused by void growth. The void distribution in these models is usually assumed to be in a regular three-dimensional network. The work hardening properties of the matrix material are taken into consideration.

In most commercial materials voids are created at second phase particles. In several of the above mentioned models the voids are assumed to grow as if the particles were not present. In a recent study (138) it has been shown, however, that the void volume and shape are significantly influenced by the particles.

3.5   FORMABILITY

3.5.1   Assessment of Formability

Traditional evaluations of formability are based on both fundamental
and simulative tests. Within the first category are direct measure-
ments of mechanical properties derived from a standard tensile test,
such as yield stress, tensile strength, total elongation and
measurements of hardness (139-142). Property levels required for
successful stampings are determined either from an accumulation of
many past trial and error attempts on similar stampings, or from
long statistical correlations with press performance data.

The relationship between test results and press performance data is
often unclear. Specifications so established are only partially
valuable for selected stampings. Work by members of the International
Deep Drawing Research Group (I.D.D.R.G.) (143-147) has contributed
to a better understanding of this problem.

3.5.1.1. Simulative Tests

Swift (148-151) carried out a basic scientific study of the stresses
and strains induced in a sheet during the drawing operation, press
load requirements and limitations of the drawing process. Particular
attention was given to the Wedge-drawing test (152) and he subsequently
proposed a deep drawing test (153, 154) known after his name.

The problem of assessing the deep drawing qualities of sheet metal
has been the subject of extensive investigations and is frequently
referred to in literature on sheet metal working (155-159).

-41-

Stretch Forming Tests

In these tests the material is mainly subjected to a system of balanced biaxial tension, stretch forming being effected by means of a solid punch or through fluid pressure. Methods include the Erichsen Test (160-162), hydrostatic bulge test (163), K.W.I. expanding test (164, 165) and Güths stretch test (166, 167). The Erichsen test has recently been modified (168, 169) to improve its reliability and assessed for reproducibility between different laboratories (170).

Wedge-Drawing Tests

These tests consist of drawing a wedge-shaped specimen through a similar shaped die in a tensile testing machine. Test results are evaluated in terms of the maximum drawable width or length of wedge. Sachs test (171) is an example of this method of test procedure.

Deep Drawing Tests

Here, specimen blanks undergo a true deep-drawing operation in a press, the basis of measurement and comparison being the maximum diameter of blank that can be drawn with a punch of specified size and geometry. This test gives rise to the value known as the limiting drawing ration (L.D.R.)

$$L.D.R. = \frac{(Do)\ Max}{do} \qquad (36)$$

where

Do = blank diameter

do = punch diameter

Examples of these tests include Blume's draw value (172), the A.E.G. test (173-174), Schmidts method (175), Swift's cup drawing test (147, 153, 154), Beisswangers cup redrawing test (176) and the conical cup test (177, 178).

3.5.1.2 Combined Simulative Tests

Due to a lack of real success using the previous test methods, attempts to assess deep drawability were made by means of various combinations of simulative test. In all of these tests the material undergoes an initial forming operation which simulates, either partly or fully the deep-drawing operation. This is followed by stretch forming (179, 180) expanding or tearing off tests (181-187) performed for the exhaustion and consequent evaluation of the residual capacity for deformation of the sheet material tested.

3.5.1.3 Forming Limit Diagrams

In 1946 Gensemer (188) demonstrated that deformation at the point of fracture varied with the ratio of principal strains. Thus by measuring the principal surface strains, e_1 and e_2, the formability of sheet metals might be assessed. The experimental measurement of these strains, carried out by Keeler (189) and Goodwin (190) formed the basis of the forming limit diagram (F.L.D.). A technique developed by Nakazima (191) appears to be the most practical for the investigation of limit strains as it utilizes equipment already present in most metallurgical test laboratories without the need

for excessive specimen preparation.

Other investigators have used different techniques to vary major (e_1) and minor (e_2) strains at failure. These include punches of various shape (50) and lubrication, elliptical shaped blanks with variable hold down (192, 193), tensile specimens of differing configurations (194, 195), hydraulic bulges of various geometries (193, 196) and the stretching of variable eccentricity, reduced thickness patches in the plane of the sheet (37).

Explanations have been put forward for the existence of forming limit curves, based on either ductile fracture (50), diffuse instability (197), localised strain concentration or a combination of these theories (198-200).

Measurement of the F.L.C.

The first attempt to develop a technique which could assess the strain distribution in a material was the one inch square test (201, 202). For many automotive stampings, however, a grid spacing of one inch is too large to measure strain distributions and peak strains accurately (189, 190, 203), since the critical strain may exceed over as little as 0.2 square inches (189). Furthermore, the squares are seldom oriented to indicate directly the principal or maximum strain. The scribe mark can also introduce stress concentrations as evidenced by breakage along scribed lines. It was quickly realised that the use of a grid

composed of circles had major advantages over squares.

Early attempts at creating a rapid grid marking system involved the use of a rubber stamp and marking ink (204). Resolution, accuracy, and the adhesion of the grids were limited. Photographic methods (204, 205) produced the first accurate and highly detailed grids. The system currently in common use for producing small diameter circular grids, or any other desired pattern, is electrochemical marking (206-209). The circle grid method and its applications have been reported by several authors (210-212). Several grid methods have been developed (213-215) which enable a step wise analysis of the deformation and hence the analysis of strain path.

There is much controversy about the limit strains which define the F.L.C. Up to the present time there is no clear understanding as to which distorted circles must be measured. Woodthorpe and Pearce (193) and Veerman (217) proposed graphical and interpolative methods. In the absence of strain gradients, both methods are equivalent to that of Keeler (50). A more stringent laboratory definition, such as the onset of diffuse necking (218) or a strain gradient (37) does not take full advantage of the material's ability to deform. Any definition more lenient, such as fracture (194, 219), permits the existence of local necks which are unacceptable structural and appearance defects.

A change in surface roughness has been used as a criterion for the forming limit (220, 221).

Factors Influencing the F.L.D.

Parameters such as sample orientation, cleanness of the metal, sheet thickness, strain path, strain gradient, strain rate, temperature and test procedure have all been reported to influence the level of the F.L.C. (221-224).

The avoidance of forming problems by use of a thicker sheet is a widely used practice. Kleemola and Kumpulainen (225) found that sheet thickness does not influence the limit strains if a "correct" experimental procedure and limit strain definition is used. They suggest the improvement in formability with sheet thickness is due to an increased necking zone and not to a thickness dependence of the limit strains.

Ayres and Wenner (226) investigated the effects of temperature and strain rate on F.L.D.'s. They found for aluminium that at 130°C a modest increase in limit strains results only at the slowest punch rates. At 200°C the F.L.D. becomes a much stronger function of punch rate. For both 130°C and 200°C they found a tendency for the biaxial portion of the F.L.D. to extend to larger values of e_2 for slow punch rates. Strain rate hardening was found to more than offset any decrease in strain hardening due to elevated temperature. Even at constant punch rate, the strain rate varies in the deformed sheet because of strain gradients which develop as punch height increases. The strain rate gradient alters the local values of n and m to effect the strain distribution. It is known (227) that

-46-

aluminium alloys behave differently under biaxial tension than under uniaxial tension and also that the rate of hardening may decrease markedly at strains larger than those found in the tensile test (228).

Recent work on sheet metal formability has shown that the position of the F.L.D. depends not only on the material properties but also on certain geometrical factors related to the method of determination. It has been shown that the limit strains increase with increasing punch curvature (1/R), at constant material thickness (222). Strain gradients alone, under essentially plane stress conditions, have been shown to cause an increase in limit strain (229, 230).

According to Ghosh and Hecker (229) the presence of strain gradients modifies the instability condition which applies for in-plane stretching and retards the formation of a local neck. This would suggest that for a given material the particular F.L.C. corresponding to the proper material thickness and radius of curvature should be used in actual strain analysis problems.

Analysis of F.L.D.'s obtained using two different strain measurement techniques showed that limit strains obtained from photoelastic coating measurements were invariably greater than those obtained from circle grid measurements (231). It was found that the largest difference between the two curves occured when a fracture criteria was used for F.L.D. determination, reaching as much as 12% in plane strain. This difference decreased when F.L.D.'s were determined

using a loss of stability criterion.

Workers (232) have found that the deviation of forming limits is much greater than could be accounted for by an analysis of the experimental technique. This suggests that the failure process in sheet may be a probabilistic phenomenon.

Theoretical Estimate of the F.L.D.

Theoretical examination of the F.L.D. has been based on plastic instability conditions. Following Hill, Keeler and Backofen (50) derived local and diffuse instability conditions for various states.

For the purpose of analysis the F.L.D. can be divided into two parts, one region where $e_2 < 0$ and one where $e_2 > 0$. In practice, most failure sites in pressed sheets occur in the biaxial stretching range and in the vicinity of plane strain. On the left hand side the F.L.C. can usually be represented by a straight line between the points of simple tension, $\alpha = 0$ $\beta = -0.5$ (where α = the stress ratio σ_2/σ_1, and β = the strain ratio ϵ_2/ϵ_1,) and plane strain, $\alpha = 0.5$ $\beta = 0$. The region $e_2 > 0$ is representative of stretch forming operations upto biaxial tension, $\alpha = 1$ $\beta = 1$.

According to Hill (51) when $\alpha > \frac{1}{2}$ there can be no line of zero extension in the plane of the sheet and so local necking should not be possible. However, local necks are observed during biaxial stretch forming operations (52).

Marciniak et al (198) have shown that the phenomenon can be explained
if it is assumed the material contains an initial inhomogeneity.
The Marciniak and Kuczynski (M-K) theory describes failure in a
sheet which is deforming in a proportional biaxial straining process.

An inhomogeneity in the form of a shallow groove is assumed to
exist within the sheet. The thickness of the sheet is t_A and the
residual thickness at the groove is t_B so that the non-uniformity
is defined by an initial thickness factor fo.

$$fo = \frac{t_B}{t_A} \qquad \text{where} \quad fo < 1 \qquad\qquad (37)$$
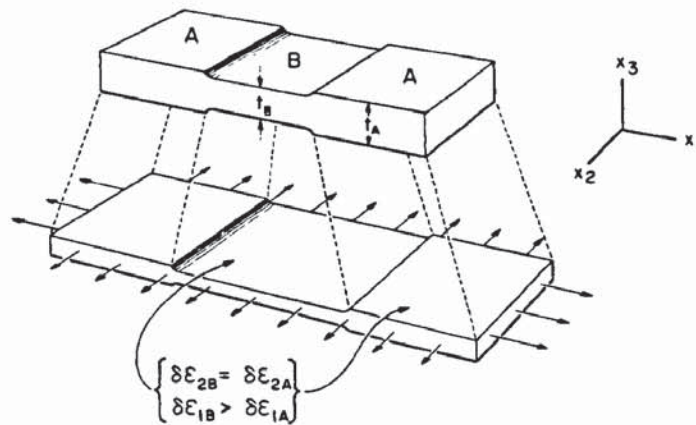
FIG 8. A schematic view of how the strain state in an incipient
        trough (B region) can approach plane strain while propor-
        tional straining is maintained outside (A region). (37).

Uniform proportional straining takes place in regions of the sheet
remote from the inhomogeneity, while within the groove region the
strain levels are increased and the strain state changes progres-
sively. Failure occurs when the strain rate in the groove reaches
some critical value or when a state of plane strain $(d \epsilon_2)_B = 0$
is reached. Non-uniformities could arise from many different sources
such as voids, inclusions, geometric factors and surface defects.

Azrin and Backofen (37) showed experimentally that artificial
troughs have to be much deeper than those predicted by the M-K theory.
Marciniak et al (43) extended their theory by taking into account
the strain rate sensitivity and the possibility of fracture before
plane strain is reached in the trough. Yamamoto (233) demonstrated
that ductility in plane strain and axisymmetric tension predicted
on the basis of a model of void growth was unrealistically high unless
an initial imperfection consisting of a perturbation in void content
was assumed.

Kaftanoglu (234, 235) has developed a strain propagation theory
which can predict the onset of fracture in hydraulic bulging
and stretch forming. The theory is difficult to apply because of
the large computer programme and extensive numerical analysis
required. Ghosh and Hecker (103) have predicted a criteria for punch
stretching based on the maximum punch load and experimental measure-
ment of strains during incremental straining. They found no need
for the assumption of initial troughs to explain local necking as
has been stated by Marciniak and Kuczynski (198). Experimental

evidence does not support the 'M-K' theory conclusively (37, 232) and it is now widely believed that the important inhomogeneities may not exist in the original sheet but instead are created during straining as a result of the discrete nature of the plastic deformation process (236).

3.5.1.4   Fracture Maps

In addition to the F.L.C. there is also a second envelope which can be drawn in principal strain space, and this is shown schematically by the broken line in Fig 9.
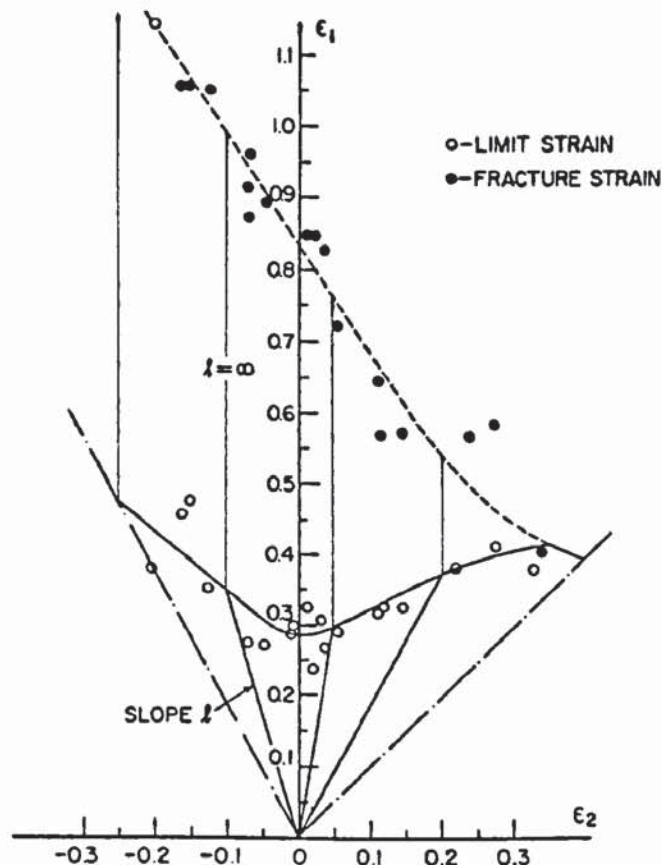
FIG 9. Limit strain curve and fracture strain curve in the case of an Al-Mg alloy, 5154, tested at room temperature in the annealed condition. ϵ_1 and ϵ_2 are the major and minor strains in the plane of the sheet respectively (237).

This indicates the strain in the material when fracture occurs and lies at major strains greater than the F.L.C., due to the additional non-uniform plastic strain associated with the strain concentration or localised necking process (237, 238). The straining process between the limit strain and fracture tends towards plane strain (239), so that the strain path is curved. The work of Glover et al (238) demonstrated that in sheet metal processes, formability is not only determined from the strain path and F.L.C., but there is also a competition between necking and fracture which can control formability in some cases, Fig. 10.
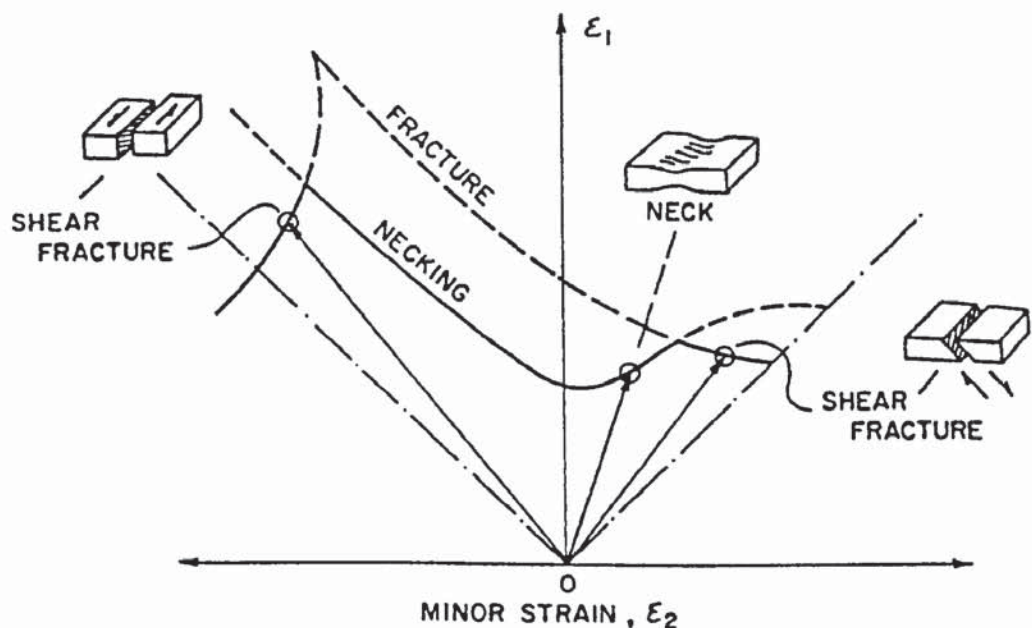
FIG.10. Forming limit curve showing a maximum shear stress fracture curve superimposed on a forming limit curve (238).

There are a variety of possible failure criteria that may be applied to sheet materials, although each criterion will be relevant only to a limited number of materials, metallurgical conditions, forming

operations, or loading paths. One of the reasons for using these mapping techniques, is to provide a basis for comparison of failure mechanisms occuring under different loading paths, when failure criteria can be expressed in terms of the microstructural variables of the material.
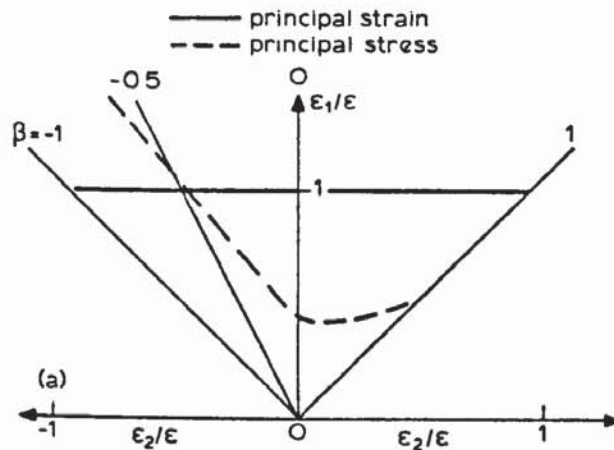
(a)
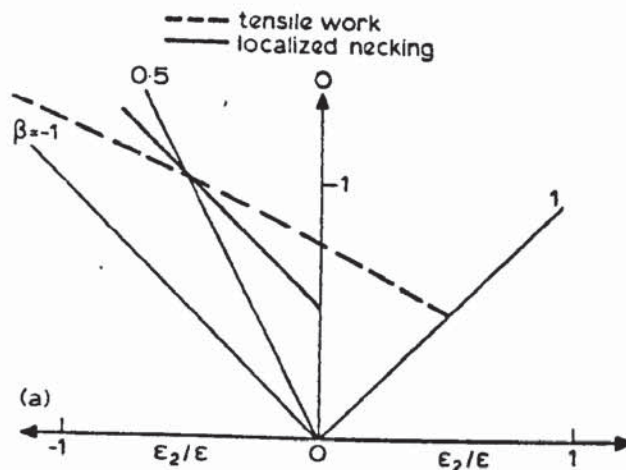
(b)

FIG.11. Schematic diagrams showing (a) the failure curves for the criterion that the maximum principal strain at failure ε_1, has a constant value (full line) and that the maximum principal stress at failure has a constant value (dashed line) (b) failure curves based on theory of localised necking (full line) and of constant value of tensile work done at failure (dashed line).

The usefulness of these diagrams can be demonstrated by superimposing the maps for these criteria to see how the governing criterion may depend on stress or strain path.

3.5.2   Effect of Load Path on Formability

The effect of stress state on the flow stress can be estimated using Hills model of anisotropy (92). Experimental work shows that Hills model cannot be used in describing the biaxial flow behaviour of many sheet materials (240-242). Recently Hill (243) proposed a new yield function to account for these anomalies. However, several investigations (56, 244) indicate that in addition to the amount of prior plastic deformation, the strain history influences the flow stress. This can be explained by the finding that the texture and microstructure developing during deformation depend on the stress state (245, 246). The influence of loading path on instability has been investigated experimentally (247-248).

3.5.3   Effect of Strain Path Changes on Formability

There is evidence that changes in the mode of deformation can alter the formability of sheet steel (56, 249). Biaxial prestraining has been found to reduce the uniaxial ductility of low carbon steel when compared with its ductility in continuous uniaxial tensile deformation (56). It was shown that such effects might arise from increased hardening under biaxial tension, resulting in a premature loss of stability when the deformation mode is changed from biaxial to uniaxial tension. Experimental work (249) shows that prior

straining along a uniaxial tensile path enhances subsequent biaxial ductility. Because of a failure to identify the useful formability parameters Laukonis and Ghosh (250) carried out a study to investigate possible differences in behaviour between material belonging to different crystallographic classes. They concluded that, for the metals investigated, the residual formability was reduced in proportion to the magnitude of balanced biaxial prestrain; for 2036-T4 aluminium the plane strain level of the FLD remained unchanged whereas for A-K steel it decreased. Biaxial n for steel was found to be greater than uniaxial n and vice-versa for aluminium. The magnitude of r dropped with prestrain for A-K steel, for aluminium no measureable change in r was detected.

3.6   CHARACTERISTICS OF ALUMINIUM ALLOYS

Alloying aluminium with other metals increases the strength and hardness but this generally involves some sacrifice to ductility and the modification of other characteristics. The principal alloying elements are copper, magnesium, silicon, manganese and zinc which, either singly or in combination, are added to produce the properties required. A description of alloy characteristics will be limited to the three groups utilized in the research programme, namely 2xxx, 5xxx and 6xxx series alloys.

3.6.1   The Al-Cu and Al-Cu-Mg System

Copper is one of the most important alloying elements added to aluminium. It is mainly added to increase the strength, at low temperature by heat treatment, at high temperature through the formation of compounds with aluminium, iron, manganese, etc. (251).

The addition of magnesium to Al-Cu alloys accelerates and substantially increases the room temperature or natural ageing responses of these alloys. A small addition of manganese also improves the strength without affecting ductility.

Ageing Responses of Al-Cu Alloys

In the age hardening of Al-Cu alloys, five structures can be recognised. Age hardening at room temperature is due to the formation of Guinier-Preston (G.P.) zones from a supersaturated solid solution (S.S.S.S.) as follows:-

$$S.S.S.S. \rightarrow G.P.(1) \rightarrow G.P.(2) \rightarrow \theta' \rightarrow \theta \ (CuAl_2)$$

G.P.1 zones consist of plate-like clusters of copper atoms segregated onto the (100) planes of the aluminium matrix (252). Natural ageing of these alloys, irrespective of copper content, produces zones which are only a few atoms thick and reach a maximum diameter of approximately 50 Å. The formation and growth of G.P.1 zones is accompanied by hardening and decreased ductility which has been attributed to distortion of the lattice (253) and pinning of

dislocations (254).

G.P.1 zones are eventually replaced by G.P.2 zones. This replacement
occurs during the time that the hardness remains constant (255).
The G.P.2 zones, often designated θ", are larger than G.P.1 zones
and their number correspondingly smaller (256) since the amount of
copper in the zones does not change radically. There is some dis-
agreement as to whether the G.P.2 zones form separately or from the
G.P.1 zones (251) or by independent nucleation and growth within the
G.P.1 zones (258).

Some authors (259) maintain that the θ' phase forms by independent
nucleation whereas others (260) report that θ' phase forms from the
G.P.2 zones. It is generally accepted that θ' is a definite phase,
separate from the matrix (261) so that no coherency strains exist, but
with each particle surrounded by a ring of dislocations (262).

Eventually the θ' phase is replaced by θ $(CuAl_2)$ which has the same
structure and composition as the θ phase formed by solidification (263).
θ can form from θ' or directly from the matrix. When it forms from
θ', direct formation by rearrangement of the atoms has been suggested
(264), but most investigators accept independent nucleation and
growth in or near the θ' phase (265).

Ageing Response of Al-Cu-Mg Alloys

The Al-Cu-Mg alloys also harden at room temperature by the formation
of G.P. zones. These zones consist of groups of Cu and Mg atoms

which cluster on the (210) planes of the aluminium matrix (266). The exact shape of these zones is not clear although it has been suggested that they are rod shaped (266). Stacking faults are a preferred site for precipitation.

The next stage in the ageing sequence is the rearrangement of dis-ordered zones to form ordered zones designated S". These zones are still coherent with the matrix as they grow.

Further rearrangement within the S" zones results in the formation of the transition phase S' ($CuMgAl_2$) which is semi-coherent with the matrix. Eventually the S' phase grows until the particles are no longer coherent with the matrix and the equilibrium S phase ($CuMgAl_2$) is formed.

The ageing sequence for Al-Cu-Mg alloys is therefore
$$S.S.S.S. \rightarrow G.P. \text{ zones} \rightarrow S" \quad S' \rightarrow S \ (CuMgAl_2)$$

3.6.2. The Al-Mg System

Magnesium, when alloyed with aluminium, provides significant strengthening and a high rate of work hardening. Because Mg has a large solubility in aluminium, precipitation does not normally occur. Thus the Al-Mg (5xxx) series alloys are non-heat-treatable. A small amount of manganese may be added to increase effectively the tensile strength. The main effect of Mg is to increase the work-hardening capacity of aluminium, possible through an effect on stacking fault

energy, which gives greatly improved stretchability in sheet alloys.

3.6.3 The Al-Mg-Si System

These 6xxx series alloys are precipitation hardenable. Levels of Mg, Si and Cu are controlled to provide required yield strengths and, in addition, optimum response to artificial ageing. Levels of Mn, Fe and Ti are controlled to optimize fabricability and to promote a structure conducive to good formability.

Ageing Response of Al-Mg-Si

Precipitation hardening in Al-Mg-Si alloys commences with the formation of small Mg and Si rich spherically shaped, G.P. zones (267). At a very early stage in the ageing sequence these zones elongate in the (100) matrix direction to form coherent, needle shaped, precipitate particles designated as β'' (268).

On further ageing these needles transform by three dimensional growth to produce the semi-coherent, rod shaped β' (Mg_2Si) particles. The final stage of transformation in the ageing sequence is the nucleation of the equilibrium (Mg_2Si) phase at the β' matrix interface which grows at the expense of the β' phase to form plate-like particles.

The ageing sequence is therefore

$$S.S.S.S. \rightarrow G.P. \text{ zones} \rightarrow \beta'' \rightarrow \beta' \ (Mg_2Si) \rightarrow \beta \ (Mg_2Si)$$
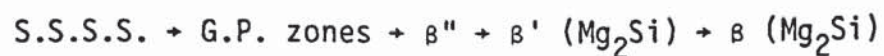
3.6.4. <u>Aluminium Alloys: A Comparison</u>

Aluminium alloys generally available for use in the automotive pressing industry are shown in table 1 together with Mechanical property levels claimed by the manufacturers.

Alloy	0.2% Proof Stress (N/mm^2)	U.T.S. (N/mm^2)	%El on 50 mm	VHN	n	r	IE
2117 CP-TB	184	329	25	81	.241	.79	9.0
2117 A-TB	180	330	24				
2002	185	335	24				
2036-TB	190	330	24		.244		
BB2	60	160-200	18	48			
BB3	85	215-275	14	59			
5182-0	148	285	20		.334		8.4
6009	128	230	24		.230	.70	
6010	180	294	23		.220	.70	

Table 1. Mechanical properties of some commercially available aluminium alloys - manufacturers specifications.

2xxx and 6xxx series alloys are normally supplied in the T.B.-temper, as defined in BS1470, while 5xxx alloys are usually O-temper. Both 2xxx and 6xxx alloys possess mechanical properties and other physical characteristics approximating to mild steel pressings which it is intended to replace in vehicle cabs and automobiles.

The 5xxx alloys are primarily intended for use on low strength panel sections where higher formability is required as is 6009.

Ageing characteristics for the heat treatable alloys are generally quoted as being between 4-7 days at room temperature. Some of these heat treatable alloys may benefit from longer ageing times eg. BA 2117 because of the subsequent suppression of Luders bands.

Corrosion resistance of all alloys is said to be better than that of steel. However, some sources have reported several of the 2xxx alloys suffer from inferior resistance to corrosive environments when compared with 5xxx or 6xxx alloys.

Spot weldability of these alloys has been widely investigated and figures between 200-2000 have been claimed for the number of spot weld operations performed before re-dressing of the electrode tips is required. These figures aer usually claimed for laboratory trials but have not been substantiated by press shop data.

Alloy availability is in most cases limited so that adequate supplies would not be forthcoming should a motor vehicle manufacturer decide to utilise aluminium in the components on his production line.

Because of the lack of reliable or consistent data on alloy properties published by bodies involved in the production and supply of aluminium it was decided that the initial phase of this research should be to establish true alloy characteristics. By doing this a valid comparison of alloy performance could be made and the most promising alloys selected for further detailed investigation.

4.   EXPERIMENTAL PROCEDURE

4.1   Materials

The alloys investigated during the course of this research programme
were supplied by Leyland Cars Ltd., and British Aluminium Co Ltd.,
and were manufactured according to the specification of the Aluminium
Federation. Alloys are referred to by the designations laid down in
AFNOR Norm A02-104. All alloys had chemical compositions within the
limits specified by AFNOR A 50-451. Identity, condition and composition
of each alloy are shown in table 2.

4.2   Heat Treatment

Standard tensile specimens 165.1 mm (6½ inches) were machined from the
as received sheets in five directions. Small samples were cut along
with the tensile specimens for subsequent metallographic work or
alternatively a small piece was eventually cut from the tensile grip
end of the samples after they had been heat treated. These were then
used for optical metallography and the determination of hardness values.

The main part of the materials were divided into two groups for heat
treatment as follows.

Group 1

This group consisted of tensile samples cut at 90°, 45° and 0° to
the sheet rolling direction. It was comprised of two further subgroups

-64-

both solution treated prior to further processing.

Group 1A

Tensile samples in this group were solution treated at 504 $\pm$ 2°C for
4 hours in an air circulating furnace. Furnace temperature was
constantly monitored using a chromel-alumel thermocouple positioned in
the close vicinity of the samples. After removal from the furnace the
samples were hot water quenched and refrigerated in a chest freezer at
-15 to -18°C. Samples were subsequently allowed to age naturally,
for periods ranging from 1-32 days, at room temperature.

Group 1B

These tensile samples were solution treated in the same way as group 1A.
They were then heat treated for 15 minutes at 150, 170, 190 and 210 $\pm$
2°C in an air circulating furnace to simulate possible paint stoving
cycles. Furnace temperature was stabalized before insertion of the
samples. Temperature was constantly monitored using a chromel-alumel
thermocouple positioned in the close vicinity of the samples. After
removal from the furnace the samples were hot water quenched and
refrigerated in a chest freezer at -15 to -18°C to await mechanical
testing.

Group 2

As for group 1 this group consisted of tensile samples cut at 90°,
45° and 0° to the sheet rolling direction. It was comprised of two

further subgroups which were processed from the as received condition.

Group 2A

Samples were heat treated as before in an air circulating furnace for 15 minutes at 150, 170, 190 and 210^{+}_{-} 2°C. Temperature was monitored as for groups 1A and B. After removal from the furnace the samples were hot water quenched and refrigerated in a chest freezer at -15 to -18°C.

Group 2B

Samples in this group were marked with a 50mm gauge length in the centre section of the specimen. These specimens were then prestrained 15% on a 50mm gauge length using an Inston 5 tonne tensile testing machine model TT-CM with a preset crosshead speed of 2mm/min. The specimens were then heat treated and stored as for group 2A.

4.3   Mechanical Testing

4.3.1   Uniaxial Tensile Testing

Tensile tests were carried out on an Instron 5T tensile testing machine model TT-CM using a crosshead speed of 2mm/minute. Specimens were marked with 30mm and 50mm gauge lengths. Specimen width was measured, at three positions along the gauge, accurate to $\pm$ 0.005mm using a micrometer and averaged. The specimens were subsequently pulled to

failure.

From the load extension curve obtained values of 0.2% offset yield stress, tensile strength and total elongation were obtained and conversions to true stress and strain were made using the relations

$$\sigma_t = \frac{P}{A} \ (1 + e) \tag{38}$$

$$\varepsilon = \ln (1 + e) \tag{39}$$

where σ_t = True stress

ε = True strain

P = Load

e = Engineering Strain

A = Original cross-sectional area

The uniform elongation was taken to be the elongation at maximum load. This was derived using the relations

$$Lf = Lo \ (1 + u) + N \tag{40}$$

$$Lf30 = 30 \ (1 + u) + N$$

$$Lf50 = 50 \ (1 + u) + N$$

$$(Lf50 - Lf30) = 20 \ (1 + u)$$

where Lf(i) = Final value of initial gauge length i

u = Uniform elongation

N = Elongation due to necking

Elongation values obtained from gauge length measurements were validated by strain gauge data.

-67-

An Instron 50mm strain gauge with 50% extension capability was used in conjunction with an X - Y graph plotter.

The range of straining during the tensile test was extended to values approaching twice the norm by the following method. Tensile specimens were strained to approximately 90% of their uniform elongation value. These specimens (two for each alloy investigated at 0°, 45° and 90° to the sheet rolling direction) were then attached to a carrier strip, in the form of a tensile specimen of the same material cut at the same angle to the sheet rolling direction, using 'superglue'. This was found to produce a good bond providing the specimen surfaces had been adequately degreased and cleaned prior to gluing.

The composite specimen was strained until failure approached. Specimens were separated using a sharp knife and a new composite produced using the original tensile specimen and a new carrier strip. The new composite specimen was then pulled to failure.

Elongation values measured during extended tensile straining were recorded by the use of an infra red non-contacting extensometer, 1000mm extension, model TTOX 100 built by J.J. Instruments Ltd. Small stick on markers with high infra-red radiation reflection were used to mark a 50mm gauge length. The conventional method of using lightly scribed lines was also employed as a cross-check facility. Output was to a calibrated X - Y graph plotter.
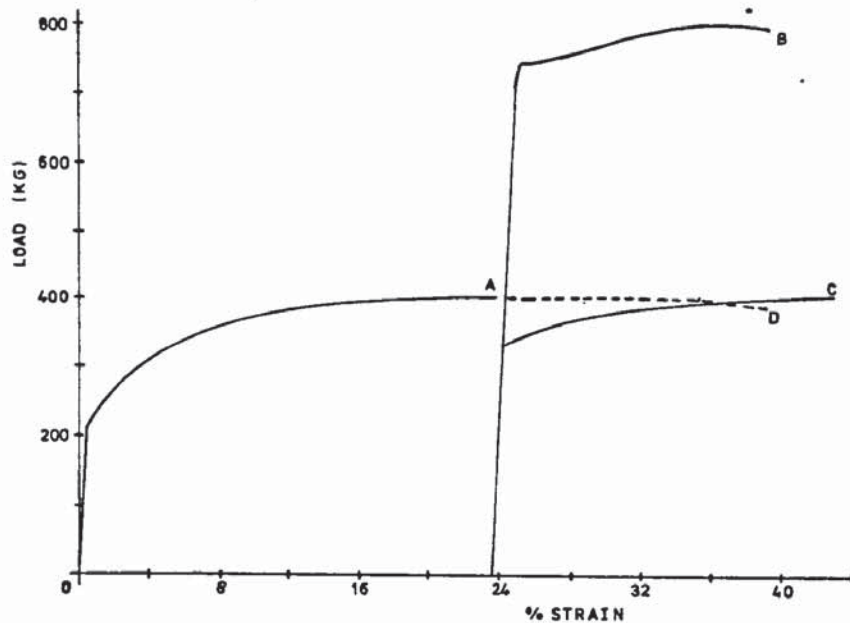
FIG.13.   Load-strain curve showing analysis of alloy behaviour
           in the extended strain range.

Fig 13 shows typical load/strain curves produced. Curve A
represents material behaviour for a single tensile specimen strained
to 24%. Uniform elongation would be approximately 25-26%. The
specimen, when glued to a prestrained (5%) backing strip, would,
if pulled to failure, produce a curve of type B. Curve C
represents the behaviour of a single test specimen after 5% prestrain.
If curve C is subtracted from B we arrive at curve D which is
representative of the behaviour of the specimen undergoing extended
straining.

4.3.2 r Value Measurement

The strain ratios were determined as

$$r = \frac{\varepsilon_W}{\varepsilon_t} = \frac{-\varepsilon_W}{\varepsilon_W + \varepsilon_l} = \frac{\ln(wo/wi)}{\ln \frac{(LoWi)}{(LoWo)}}$$

Where ε_W = True strain in the width direction

ε_t = True strain in the thickness direction

ε_l = True strain in the length direction

Wo = Original Width

Lo = Original length

Wi = Width at strain increment i

Li = Length at strain increment i

Tensile specimens were machined such that the measured portion of the gauge length was parallel to better than 0.01mm total deviation within 20mm either side of the centre line. The specimen was marked out as shown in Fig 14.
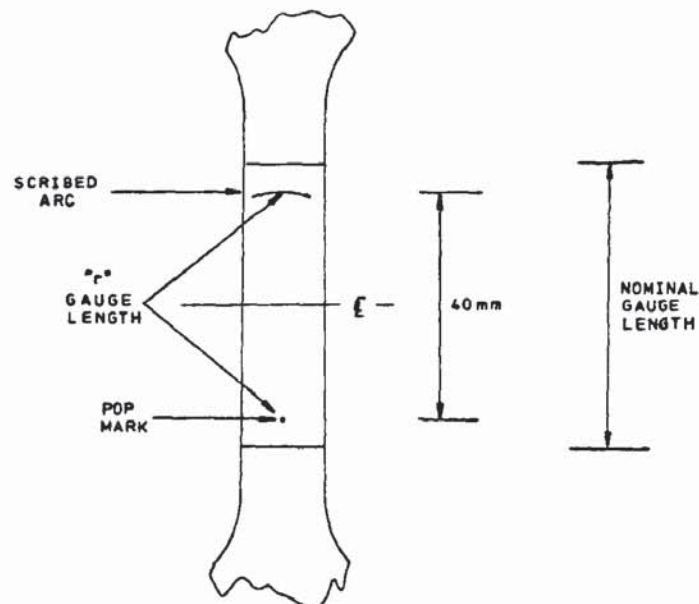

FIG.14   Dimensions and marking of r - value specimens.

The arc was scribed using a pair of dividers and the pop mark
was as light as possible.

The width of the specimen was measured in three places along the
40mm scribed gauge length, accurate to $\pm$ 0.005mm, using a micrometer
and averaged. A pair of callipers were set to a fixed strain
increment (1mm) and the specimen strained at a crosshead speed of
2mm/min until the calliper leg coincided with the scribed arc, the
other leg sitting in the pop mark. Using callipers the gauge length
could be measured accurately to $\pm$ 0.02mm.

When the strain increment was reached straining stopped and width
measurements were taken to the best 0.005mm at three places and
averaged. Width measurements were discarded if they were not
similar to within 0.01mm. At the end of the test necking was found
to cause the width measurements to fall outside the allowed band.
Measurements then ceased and the specimen was strained to failure.
Using a graph of width strain against length strain, the r-value
is readily calculated from the slope and any variation of r-value
with strain level is apparent as non-linearity.

4.3.3 Strain Hardening Coefficient (n)

The n value was determined by plotting a log true stress versus
log true strain curve to produce a line of slope n. This measurement
assumes that the material obeys the equation

$$\sigma = K\epsilon^n$$

n values were determined for aluminium alloys in the as received condition at 0°, 22½°, 45°, 67½° and 90° to the sheet rolling direction.

4.3.4 Punch Test

The alloys under investigation were subjected to the Erichsen test as stipulated in B.S. 3855, 1965. The equipment used was an Erichsen sheet metal testing machine model 131 incorporating an indentor, die and blankholder conforming to the above British Standard. All tests were carried out at room temperature. The circular material blanks and indentor were degreased and a solid film lubricant (polythene, 0.08mm thick) used. Blankholder load was set at 1000Kgf and ram speed at 10mm/minute. The end point was teken to be the point at which a crack accured through the full thickness of the test piece sufficient to allow light through part of its length. Depth of indentation was measured to the nearest 0.1mm.
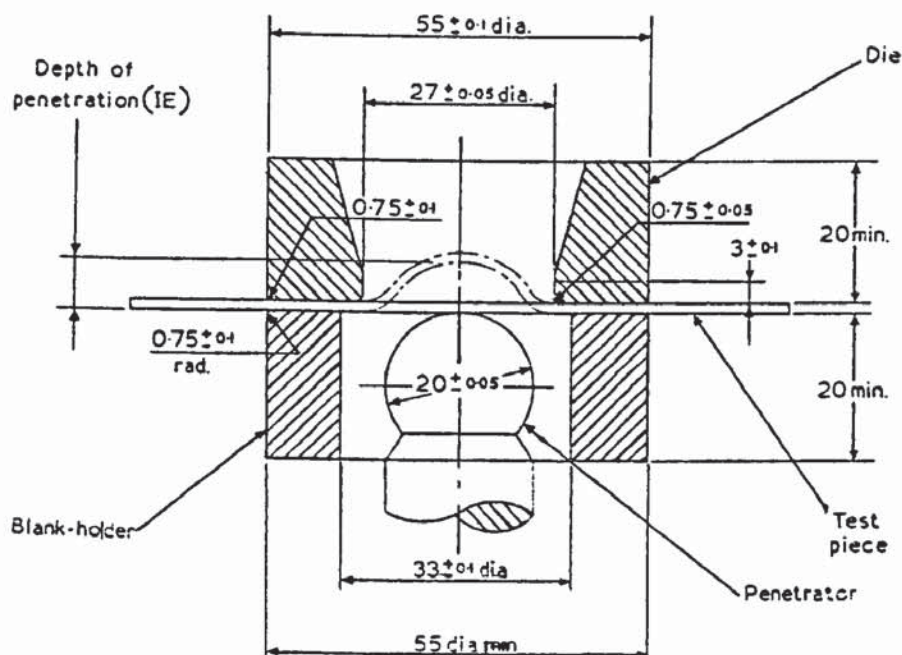
FIG.15. Dimensions (in millimeters) of punch test penetrator, die and blankholder.

-72-

4.3.5 Bulge Testing

Hydraulic bulge tests were carried out on a machine produced by Mand Precision Engineering Co. Ltd and shown in Fig. 16.
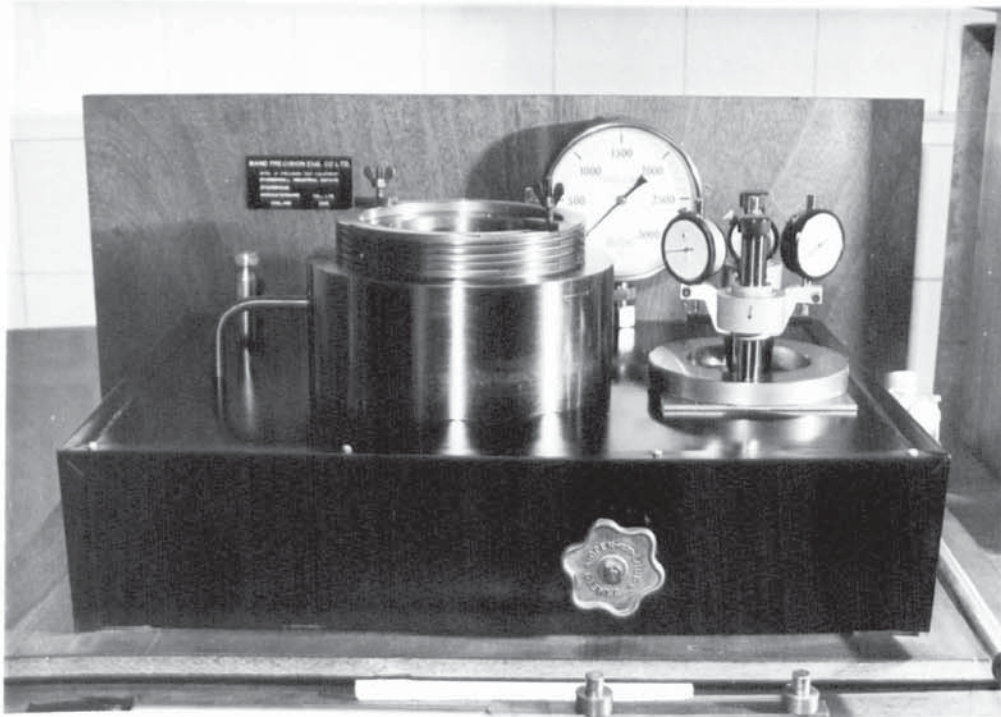
FIG.16   Hydraulic bulge test machine and extensometer.

The extensometer unit was essentially an instrument for measuring both the curvature, and the extension of the central region of the specimen as it deformed under hydraulic pressure through a circular die. The unit rested on the surface of the deforming sample and rose with it during testing. Movements of the two devices within the extensometer were registered using dial gauges. The

hydraulic pressure being applied to the specimen was measured via a pressure gauge. Effective stress and strain in the deforming sheet were then calculated. The strain in the polar region could be calculated by considering the increase in the diameter of a circle at the pole (initial diameter Do on the undeformed sample) as measured by the extensometer shown in Fig 17(a).
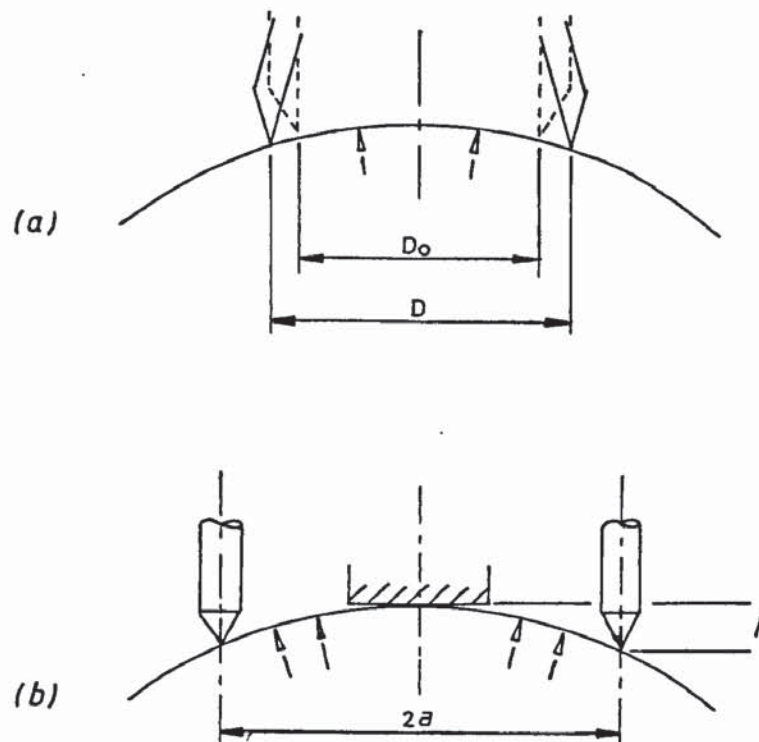
FIG.17   Schematic diagram of (a) the extensometer unit (b) the spherometer unit used in the hydraulic bulge test.

If the strains in the pole region are assumed to be uniform, then the membrane strain in all directions at the pole is given by

$$\epsilon = \ln \frac{D}{D_o} \qquad (41)$$

where D = diameter of circle D_o at any given degree of deformation

Now assuming that the specimen in the pole region is part of a spherical shell, the membrane stress is given by

$$\sigma = \frac{PR}{2t} \qquad (42)$$

where   P = Hydrostatic Pressure

      R = The current radius of curvature as measured by the spherometer. Fig 17 (b)

      t = Current thickness

The current radius of curvature can be calculated from

$$R = \frac{a^2 + h^2}{2h} \qquad (43)$$

where a and h represent the quantities shown in Fig 17(b).

The current thickness t is geven by the relation

$$t = t_o \exp(-2\epsilon) \qquad (44)$$

where t_0 = Initial specimen thickness

Using the well known equations of effective stress ($\bar{\sigma}$) and effective strain ($\bar{\epsilon}$)

$$\bar{\sigma} = \sqrt{\{[(\sigma_1 - \sigma_2)^2 + (\sigma_2 - \sigma_3)^2 + (\sigma_3 - \sigma_1)^2]/2\}}$$
$$\bar{\epsilon} = \sqrt{\{2[(\epsilon_1 - \epsilon_2)^2 + (\epsilon_2 - \epsilon_3)^2 + (\epsilon_3 - \epsilon_1)^2]\}/3}$$

it can be shown that

$$\bar{\sigma} = \sigma \qquad (45)$$
and $$\bar{\epsilon} = 2\epsilon \qquad (46)$$

The above analysis however is based on the assumption that the sheet is isotropic, and that measurements taken in the X and Y directions would be identical. The interpretation for anisotropic sheet can therefore be more difficult as reviewed by Duncan et al (269). They have suggested however that the effective stress and effective strains for materials with planar isotropy, such as aluminium, can be calculated as above and that these are equal to the through thickness stresses and strains.

4.3.6 Forming Limit Diagrams

The procedure used for determining F.L.D.'s for the various alloys was similar to that described by Hecker (270). Samples were first gridded with 1.93mm diameter overlapping circles, as described in

section 4.3.7, so that the limit strains could be measured. F.L.D.'s were determined using friction and nonfriction conditions.

Forming limits determined under friction free conditions were produced by using a combination of eliptical dies during hydraulic bulge testing and shaped tensile specimens. For strains in the region $\varepsilon_1 > \varepsilon_2 > 0$ specimens were bulged through a circular die 118mm in diameter and three eliptical dies with critical aspect ratios of 0.68, 0.55 and 0.44. Plane strain and tension conditions were obtained using tensile test pieces of varying gauge length: width ratio. Due to the size and shape of these tensile specimens it was necessary to pull them to failure using a 50T Denison Compression machine model T42 B4.

The second method used to produce F.L.D.'s under frictional conditions was that due to Nakazima (185). The sheet metal specimens were blanked to a diameter of 115mm using an Erichsen sheet metal testing machine model 123, clamped at the periphery and stretched over a 50mm diameter hemispherical steel punch using an Erichsen sheet metal testing machine model 131. The die faces were grooved and sufficient clamping pressure was applied to prevent any draw-in.

Several specimen widths and two types of lubrication were used to determine the F.L.D.'s over the required range of strain ratios. Specimens ranging from 115mm - 5mm in width were stretched over the punch with either no lubrication, Solid film lubricant (polythene 0.08mm thick), or molybdenum disulphide grease.

As well as tests carried out on defect free sheet specimen inhomogeneities were introduced into some of the test specimens in the form of grooves with known geometry and depth. These were cut into the material using a Vickers microhardness testing machine incorporating a diamond tip normally used for applying surface grid lines. Loads varying from 50gr to 300gr were applied to produce shallow V-notch scratches with an included angle of 120°.

Forming limit curves were then constructed from strain measurements of the gridded pattern. Only ellipses next to but not intersected by fracture or localized necking were chosen. This produced a conservative estimate of the F.L.C. Ellipses close to the region of fracture initiation were measured as fractures can propogate into low strain regions due to stress concentration effects.

4.3.7 Gridding of Specimens

Gridding of the specimens was preceeded by thorough degreasing and scouring of the samples using a stiff nylon pad and Teepol. The method of electrochemically etching a grid pattern onto the sheet metal surface was originally used. The apparatus consisted of a power supply manufactured by Electromark G.B.Ltd., model T25, an electrolyte and a marking stencil with 2.5mm diameter circles. The electrolyte was made up of 40gr. KCL, 45gr. NaCl, 50ml. HNO_3 and 50ml. HCl dissolved in 2.25 litres of water. A felt pad approximately 2mm thick was thoroughly dampened with electrolyte and placed ontop of the stencil which had previously been positioned on the specimen.

The specimen was made the cathode and a steel roller the anode. The power source was set to the required voltage and the roller pushed across the felt pad, with a firm smooth action, several times. The effect was to produce an etched pattern of circles as shown in Fig. 18 (a).

These grids were found to be of unacceptable quality for accurate strain measurement and so a photoresist technique was subsequently adopted which was developed and tested by the author during a period of approximately two months. This consisted of a modified process for producing printed circuit boards. The specimens were degreased as described previously. They were then sprayed with a mixture of 60pts Fotolac (available from Millwards Ltd., Birmingham) and 40pts engineers blue using an air brush to apply a thin even film over the specimen surface. When dry (~2-3 minutes) the specimens were placed in a vacuum frame which when evacuated pulled a negative of the grid pattern into very close contact with the metal surface. This was necessary to ensure clear, sharp reproduction of the grid pattern.

The specimen was then exposed for a period of 90-120 seconds to a strong ultraviolet source supplied by a Philips E/99/2 U.V. bulb in a suitably constructed protective housing. The specimen and negative were then removed from the vacuum frame and the specimen immersed in a solution of NaOH (200gr/litre) to develop the grid. This method was found to be very successful although care had to be exercised during the developing procedure as the grid could easily be removed by excessive aggitation or rubbing. The specimens were then thoroughly

(a)

(b)
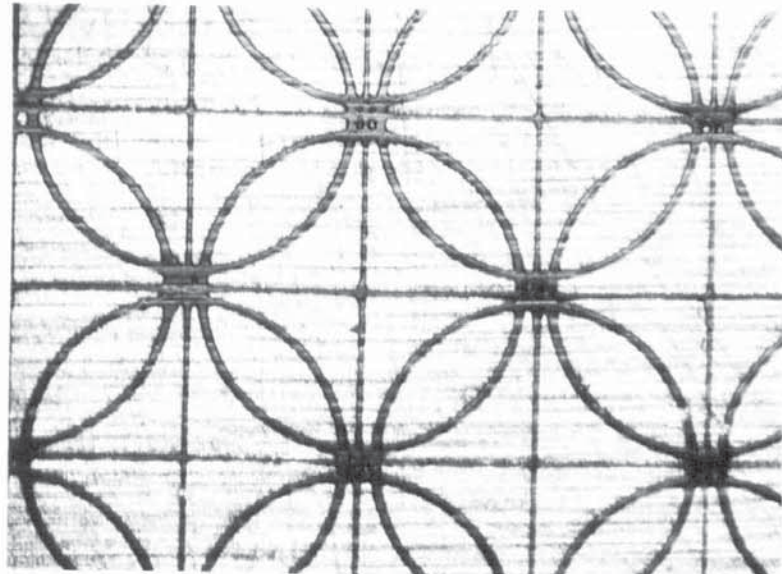
FIG.18   Photomacrographs of (a) electroetched grid pattern with
         a line thickness of 0.2-0.3 mm and (b) photoresist grid
         pattern having a line thickness of 0.05-0.075 mm.

rinsed in clean water and carefully dried in air. To fix the grid and produce a surface resistant to scuffing a thin film of Kodak Linagraph Laquer was applied and found to be highly successful. This method was greatly superior to the electro etch technique and can be seen in Fig. 18 (b).

4.4   Metallography

4.4.1 Optical Microscopy

Small samples of each alloy were taken and cold mounted in an epoxy resin mounting medium. They were mechanically polished on silicon carbide papers down to 1200 grit, then polished using 6µm and 1µm diamond paste.

Some difficulty was encountered when trying to etch the specimens by conventional means. The method eventually employed involved anodising and polarized light microscopy. The specimens were anodised in either a solution of

    70 pts   Orthophosphoric acid

    2.5pts Distilled water

    26.5pts Ethylene glycol

    1pt   Hydrofluoric acid

.

or Barkers reagent, a solution of

    4-5ml   Hydrofluoroboric acid (48%)

    200ml   Distilled water

The latter solution produced the more consistent results. The cathode was stainless steel and the anode the specimen. The specimen was treated for 40-80 seconds at 20V dc (about $0.2A/cm^2$) at room temperature.

Specimens were examined under a Vickers desk microscope utilizing crossed polariser/analyser plates and a quartz ¼ wave tint plate, or a Vickers projection microscope set in the polarizing mode. Photomicrographs were taken where necessary to show typical microstructures.

4.4.2 Electron Microscopy
Size Distribution of Second Phase Particles

Specimens to be prepared for second phase particle analysis were cold mounted in an epoxy resin mounting medium and mechanically polished on silicon carbide papers down to 1200 grit. They were then transferred to a Nashton Metallurgical vibratory polisher, type M14, for further polishing down to 1µm. Specimens were then examined using a cambridge scanning electron microscope 2A modified to incorporate a back scattered electron detector. Photomicrographs were taken at X1270 using the back scattered electron detector mode to produce sharp second phase particle images. The photomicrographs were enlarged during printing to produce a final magnification of X 2540.

Four fields were chosen at random for each alloy under examination. The size distribution of the second phase particles were determined from the prints using a Zeiss TGZ3 manually operated particle size counter. The counter was set in the "E" and "Lin" mode to produce a linear distribution analysis.

4.4.3   Fractography

Samples for fracture analysis were cut from the alloy test specimens after failure using a Bueler diamond saw. These specimens were then ultrasonically cleaned in ethyl alcohol and mounted on electron microscope stubs, electrical conductivity between specimen and stub being completed by using Aquadag, a solution of colloidal graphite in water. The fracture surfaces were investigated with a Cambridge 150 scanning electron microscope at varying magnifications. Fractographs were taken to show typical surface features of the alloys.

4.5   Texture Determination

The textures of all alloys under investigation were determined using the x-ray diffractometer method as required by A.S.T.M. Standard E81-63 (1974).

A specimen of each alloy approximately 20mm square was mechanically thinned to nearly half thickness using 320 grit silicon carbide paper. Final thinning was carried out by painting the unground side of the specimen with laquer followed by immersion in hydrofluoric acid. This removed any evidence of mechanical working of the alloy which may have been introduced by the grinding procedure. The specimens were then lightly bent and straightened to eliminate extinction effects which may give variable intensities.

Pole figures were determined by a counter technique with a Siemens power supply and texture goniometer, scintillation counter and conventional counting equipment. (200),(111) and (220) pole figures were determined using the Schulz reflection method (271) with Cu Kα radiation at 30KV and 20 mA and a nickel filter.

5. EXPERIMENTAL RESULTS AND OBSERVATIONS

5.1 Comparison of Commercially Available Sheet Aluminium Alloys

5.1.1 Tensile Test Properties

Table 3. shows the mechanical properties of all alloys investigated in the "as received" condition averaged over five directions in the sheet. As can be seen the ratio of proof stress: U.T.S. is indicative of the material temper and ductility. Ultimate tensile strength for the alloys ranges between 214-331 N/mm^2, proof stress values between 119-266 N/mm^2.

Alloy HS30/3 has the highest proof stress value probably due to mechanical working of the sheet prior to delivery. This is evidenced by the low associated value of elongation. HS30/3 also has the lowest n value in the group so that a non-uniform strain distribution might be expected to develop at an early stage leading to the low elongation value observed. In the 6xxx series of alloys levels of Mg, Si and Cu are controlled to give high yield strengths in the T.B. temper. Table 2. shows alloy HS30/3 to have the highest combined Mg and Si content of the four 6xxx series alloys present. Alloy 6010 has strengths in the same range as HS30/3 but a much higher capacity for plastic deformation. Levels of Cu in the two alloys differ significantly. HS30/3 has very little Cu whereas 6010 has a content of 0.33. Small amounts of Cu are added to Mg_2Si alloys to improve strength without substantial loss of corrosion resistance. Alloys 6009 and 609 are similar to each other in

all respects. Proof stress is slightly lower for alloy 609 and the elongation, correspondingly slightly higher. This may be a consequence of material processing and/or may be due to the fact that alloy 609 has lower Mg, Mn and Cu contents with almost twice the quantity of Si. All the 6xxx series alloys have a moderate amount of Fe present. Mn is sometimes added to these alloys as an Fe corrector which could partly explain the comparatively high amounts of Mn in HS30/3 although alloy 609 has very little Mn present and an Fe content higher than 6009 or 6010.

Looking at the 5xxx series alloys Sidal and BB2 were supplied in a cold worked condition evident from their low elongation and high proof stress values. A more realistic indication of 5xxx series alloy properties is given by BB3 and 5182 both supplied in the O-temper. Alloy BB3 has an n value of 0.33 which is slightly greater than that for 5182, a lower proof stress and lower U.T.S yet 5182 has a significantly higher elongation. From table 2.it can be seen that 5182 and BB3 have similar levels of Si, Fe, Cu and Mn. However, 5182 has a much higher Mg and Ti content. The solid solution and grain refining effects of these elements would be expected to produce higher hardness, increased strength and lower ductility. Because it is normal practice to produce 5xxx series alloys from the higher purity grades of aluminium (99.7% or better) Fe and Si contents are usually lower than in other aluminium alloys. Table 2.shows all 5xxx series alloys investigated to have relatively high Fe and Si contents which is unusual although Fe is sometimes added to increase the recryst- allisation temperature and Si to improve fluidity.

Of the 2xxx series, alloy 2002 combines the highest proof stress, U.T.S. and elongation of the group of five. The good ductility is borne out by its high IE (Erichsen) value. This alloy is apparently from a high purity base material as is alloy 2117 HP. Fe and Mn contents for these alloys are very low when compared to the rest of the group. The Si and Mg content of 2002 is relatively high. Mg is added to accelerate and increase age hardening at room temperature following solution heat treatment and quenching. Cu is the main alloying element of the 2xxx series and is added mainly to increase the strength at low temperature by heat treatment.

Fig 19 (a) - (m) shows the directionality of tensile properties for alloys in the "as received" condition. In general all alloys show little systematic variation of proof stress and U.T.S. It can be seen, however, that total and uniform elongation values do not strictly follow strength properties. Figs 19 (a) and (b) would tend to suggest that elongations are influenced quite strongly by r value but this is not borne out by the rest of the group. The r value shows large fluctuations according to test direction which highlights the texture related dependency of sheet properties. Where fluctuations occur it is generally observed that high r values exist at 90° to the sheet rolling direction. These values may be as much as twice the value at 0° to the sheet rolling direction as seen in Figs 19 (e) and (f). The observed n values, although differing between alloy types, are relatively insensitive to the direction of testing.

5.1.2   Ageing Characteristics

Natural Ageing Response

Figs 20 (a) - (m) show the tensile properties of alloys after natural
ageing, at room temperature, for periods upto 32 days.

The 6xxx series alloys show a marked drop in strength and rather similar
properties after solution heat treatment. HS30/3 has the highest proof
stress in the solution heat treated condition followed closely by
6010. Alloys 609 and 6009 have similar but lower proof stress values
consistent with tensile properties in the "as received" condition.
The ageing response of HS30/3 is clearly faster than the other alloys,
reaching peak strength between 24 and 48 hours after solution heat
treatment. After this period properties appear stable upto 32 days.
Alloy 609 takes somewhat longer to reach optimum strength, a period
between 4-8 days after which further ageing has relatively little
effect. 6010 and 6009 gain approximately 85-90% peak strength after
2-4 days ageing. This process is continued, however, upto 32 days so
that the natural ageing response for these alloys is in excess of 1
month.

The 5xxx series alloys are generally considered to be non-heat-
treatable. A large drop in strength is observed for Sidal and BB2
after solution heat treatment confirming that these alloys were
cold worked prior to delivery. Alloys BB3 and 5182 show almost no
change in properties. When comparing tensile properties of these alloys

in a similar temper it is clear that 5182 has the highest strength although the elongation values are very similar. BB3 appears to show a slight increase in strength continuously over a period upto 32 days.

The 2xxx series alloys gain their strengthening effect from both solid solution and precipitation hardening due to Cu content. As can be seen from Figs 20 (b), (i), (1), (j) and (k) alloys 2002, 2117A, 2036, 2117HP and 2117CP decrease in strength considerably when solution heat treated. All alloys revert to proof stress values between 60-90 N/mm^2, except 2036 which retains a high proof stress (155 N/mm^2) and correspondingly high U.T.S. Elongation values generally tend to decrease as ageing progresses and strength properties rise. 2117A demonstrates rather poor elongation while that of 2002 is better than average. All five alloys have an optimum ageing response of 2-4 days with peak strengths being reached and stabalised after approximately 16 days for 2002 and 32 days for 2036, 2117A, 2117HP and 2117CP. Initial ageing response of 2117HP, 2117CP and 2002 is much faster than that of 2117A and 2036.

Artificial Ageing Response

Figs 21 (a) - (m) show the tensile properties of alloys during artificial ageing, from the solution heat treated condition, for 15 minutes at temperatures between 150-210°C.

The 6xxx series alloys shown in Figs 21 (b), (c), (d) and (m) all show an increase in strength when aged at 150°C. The U.T.S. value of alloy 6009 is very nearly equal to the original value prior to solution heat treatment. This is not true of the proof stress, however, which remains somewhat lower. Alloys 6010 and 609 show a moderate recovery of properties. HS30/3 gives only a small response to heat treatment which does not improve as the temperature is increased. The results suggest that for 6xxx alloys there is a plateau between 150-190°C where temperature variation produces little further increase in strength. Between 190-210°C there is a change in the ageing process which in 6009 and 609 produces tensile strength superior to the pre-solution heat treated values. In 6010 tensile strength is approximately equal to the original "as received" value. The increase in strength of 6009, 609 and 6010 is accompanied by a large reduction in elongation. HS30/3 does not show a comparable effect.

The 5xxx series alloys in Figs 21 (e), (f), (g) and (.l) show practically no change in properties when aged between 150-210°C except for a slight increase in U.T.S. in alloys BB2 and Sidal.

Figs 21 (a), (h), (i), (j) and (k) show the artificial ageing responses of the 2xxx alloys. 2117A shows a negligable increase in strength with ageing upto 210°C. Alloys 2117HP and 2117CP in contrast, show a marked increase in strength when aged at 150°C but a steady decrease thereafter. Elongation values remain constant. 2002 exhibits the best response to artificial ageing and displays a plateau, similar to the 6xxx alloys, between 150-190°C. Above 190°C

-90-

there is an increase in strength superior to the original "as received" values but at the expense of elongation. Optimum ageing from the solution heat treated condition appears to be between 150-170°C. This gives rise to near original strength coupled with superior elongation.

5.1.3   Effect of Prestrain on Post Heat Treatment Tensile Properties

Figs 22 (a) - (m) show the ageing response of alloys in the "as received" condition and after 15% prestrain. These alloys were aged at 150-210°C for 15 minutes. The value of 15% prestrain was selected as an arbitrary average strain induced in motor vehicle body panels during sheet metal pressing operations.

Alloys HS30/3, Sidal and BB2 were not subjected to the prestrain as their initial ductility was less than 15%. In general all alloys showed a difference of approximately 10% in elongation values between "as received" and prestrained specimens after ageing.

The 6xxx alloys show an initial loss of strength when aged between 150-170°C. This was probably due to a stress relieving effect. After ageing at higher temperatures, between 190-210°C, it can be seen that 609, 6009 and 6010 show a distinct increase in strength and loss of ductility whereas HS30/3 remains stable. Prestrain has the effect of moving the strength curves up and the elongation curves down. The difference between "as received" and prestrained properties remains consistent upto about 180°C, above which strength and

elongation differences begin to decrease.

The only 5xxx alloys capable of 15% prestrain were BB3 and 5182 both in the O-temper condition. Figs 22 (h) and (m) show that after prestrain alloy strengths are increased considerably and elongations reduced. Ageing at 150°C appears to have little effect in restoring ductility but at higher temperatures we can see that elongation values begin to increase and strength to decrease.

The 2xxx series alloys show differing reactions to ageing from the "as received" condition. Alloys 2036, 2117A, 2117HP and 2117CP all show a loss in properties when aged. Initially at temperatures around 150-170°C this loss may be explained by the stress relieving effect apparent for some of the 6xxx alloys. At higher temperatures, however, it would seem that this stress relieving effect is replaced by reversion of the alloys and so the properties continue to fall. Elongation is not affected as much as strength. Only 2117A shows a marked increase in elongation. Alloy 2002 appears to react to ageing in a similar manner to 6xxx alloys. Initially 2002 suffers a loss in strength but at temperatures above 170°C strength begins to increase and above 190°C may be superior to the "as received" values. Only at ageing temperatures in the region of 190-210°C do the differences in "as received" and prestrained properties begin to decrease.

ALLOY	TEMPER	Si	Fe	Cu	Mn	Mg	Cr	Zn	Ti	V
2002	TB	0.40	0.08	1.8	0.02	0.52	0.07	0.02	0.03	0.01
6009	TB	0.79	0.25	0.31	0.26	0.51	-	0.03	0.04	0.01
6010	TB	0.94	0.19	0.33	0.26	0.87	-	0.03	0.03	0.01
HS30/3	TB	0.94	0.37	0.04	0.51	0.92	0.02	0.03	0.01	0.01
SIDAL	M	0.17	0.27	0.007	0.23	1.95	-	0.02	0.009	0.01
B164-BB2	M	0.10	0.27	0.002	0.21	2.0	-	0.01	0.01	0.01
B164-BB3	O	0.18	0.40	0.03	0.38	3.6	0.05	0.02	0.03	-
2117HP	TB	0.12	0.06	2.0	0.03	0.38	0.01	0.02	0.03	-
2117CP	TB	0.24	0.42	2.2	0.07	0.38	0.02	0.03	0.03	-
2117A	TB	0.12	0.28	1.88	0.16	0.18	0.01	0.02	0.01	-
2036	TB	0.30	0.29	2.10	0.28	0.32	0.02	0.06	0.03	-
5182	O	0.20	0.33	0.02	0.35	4.78	0.01	0.02	0.35	-
609	TB	1.17	0.28	0.07	0.08	0.49	<0.005	0.02	0.02	-

Table 2.   Identity, condition and composition of aluminium alloys under investigation.

ALLOY	SHEET THICKNESS (mm)	0.2% PROOF STRESS (N/mm^2)	U.T.S. (N/mm^2)	PROOF STRESS U.T.S.	TOTAL % ELONGATION	$\bar{r}$	Δr	ERICHSEN HEIGHT (mm)		$\bar{n}$
								DRY	LUBRICATED	
2002	1.49	191	331	0.577	26.1	0.75	+0.09	9.4	9.8	0.25
6009	1.65	147	244	0.602	23.1	0.61	-0.03	9.8	10.1	0.25
6010	1.61	202	315	0.641	23.4	0.58	+0.06	9.3	9.3	0.21
HS30/3	1.51	266	284	0.937	9.1	0.68	-0.11	8.8	9.4	0.07
SIDAL	1.59	183	214	0.855	8.4	0.68	+0.19	8.9	9.5	0.12
B164-BB2	1.58	175	212	0.825	7.8	0.79	+0.15	8.8	9.4	0.14
B164-BB3	0.92	119	235	0.506	20.6	0.61	+0.00	10	10.2	0.33
2117HP	0.99	157	291	0.539	26.6	0.88	+0.06	9.2	9.5	0.27
2117CP	0.99	157	311	0.505	25.9	0.71	+0.02	9.2	9.7	0.31
2117A	0.97	168	241	0.697	14.6	0.64	+0.05	9.4	9.9	0.16
2036	0.87	181	304	0.595	20.9	0.54	-0.02	8.8	9.3	0.22
5182	0.93	141	284	0.496	23.6	0.62	-0.01	9.8	10.5	0.29
609	0.96	137	241	0.568	24.7	0.62	+0.12	9.6	9.8	0.24

$$\bar{X} = \frac{(X_0 + 2X_{45} + X_{90})}{4}$$

$$\Delta X = \frac{(X_0 + 2X_{45} + X_{90})}{2}$$

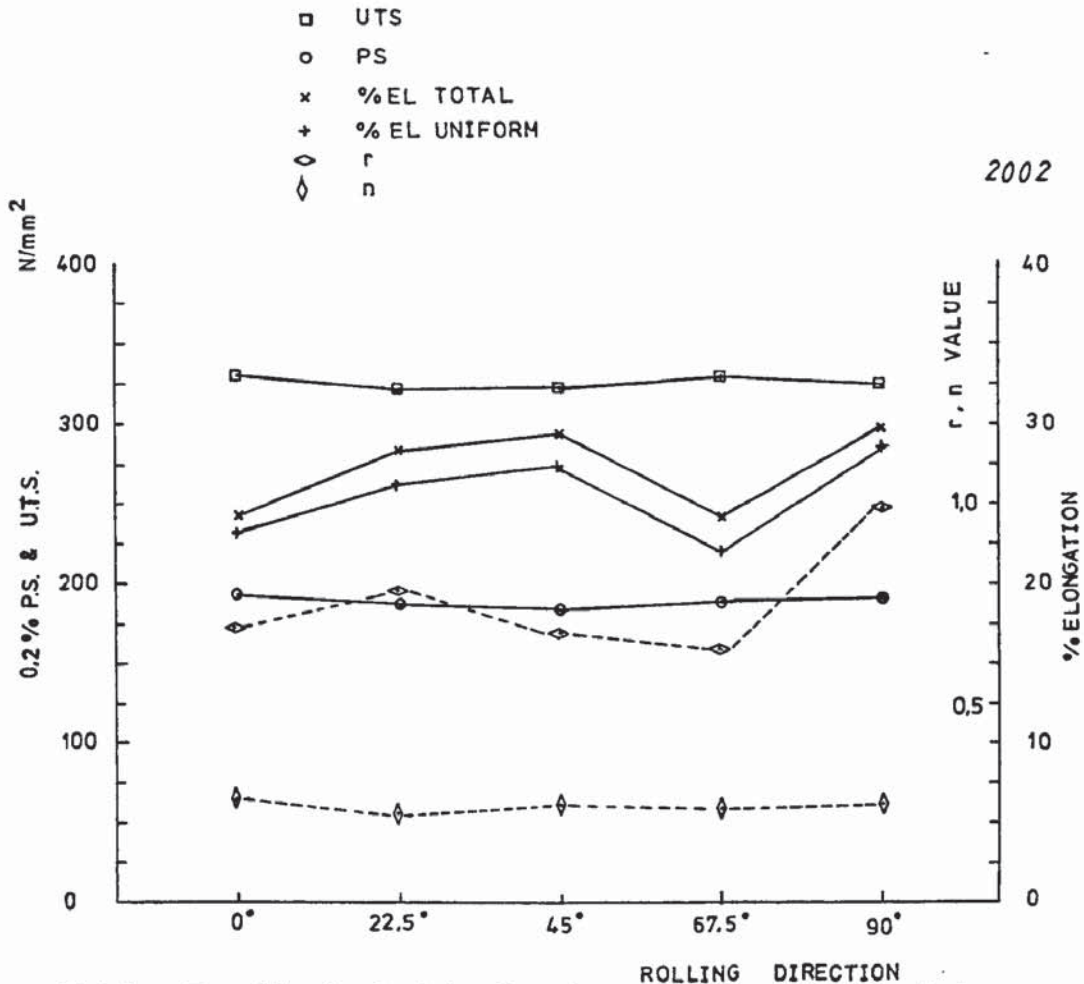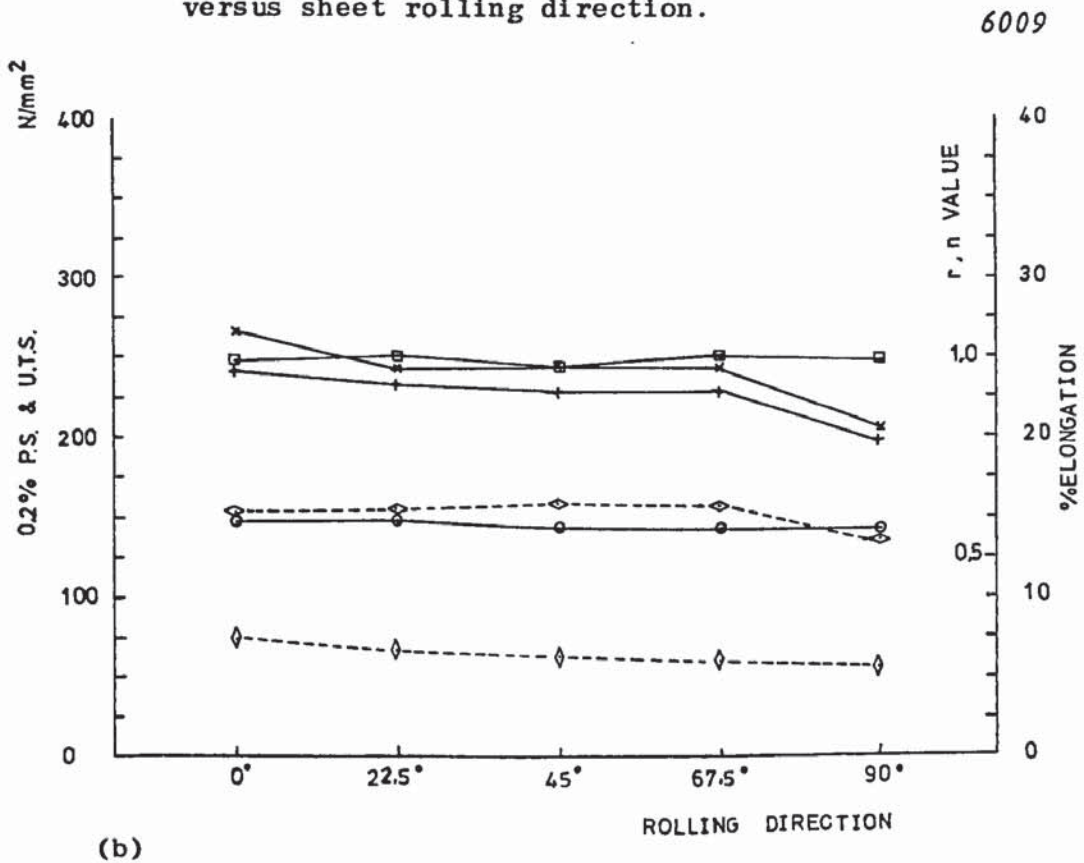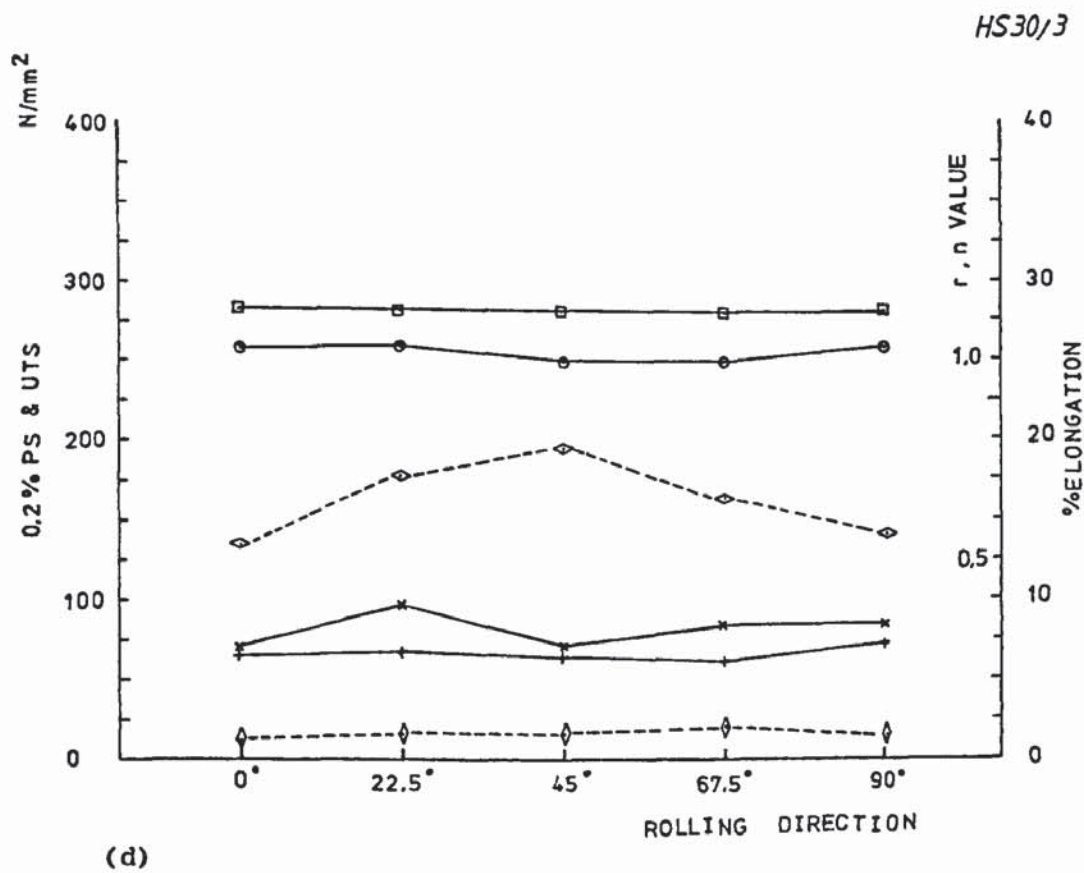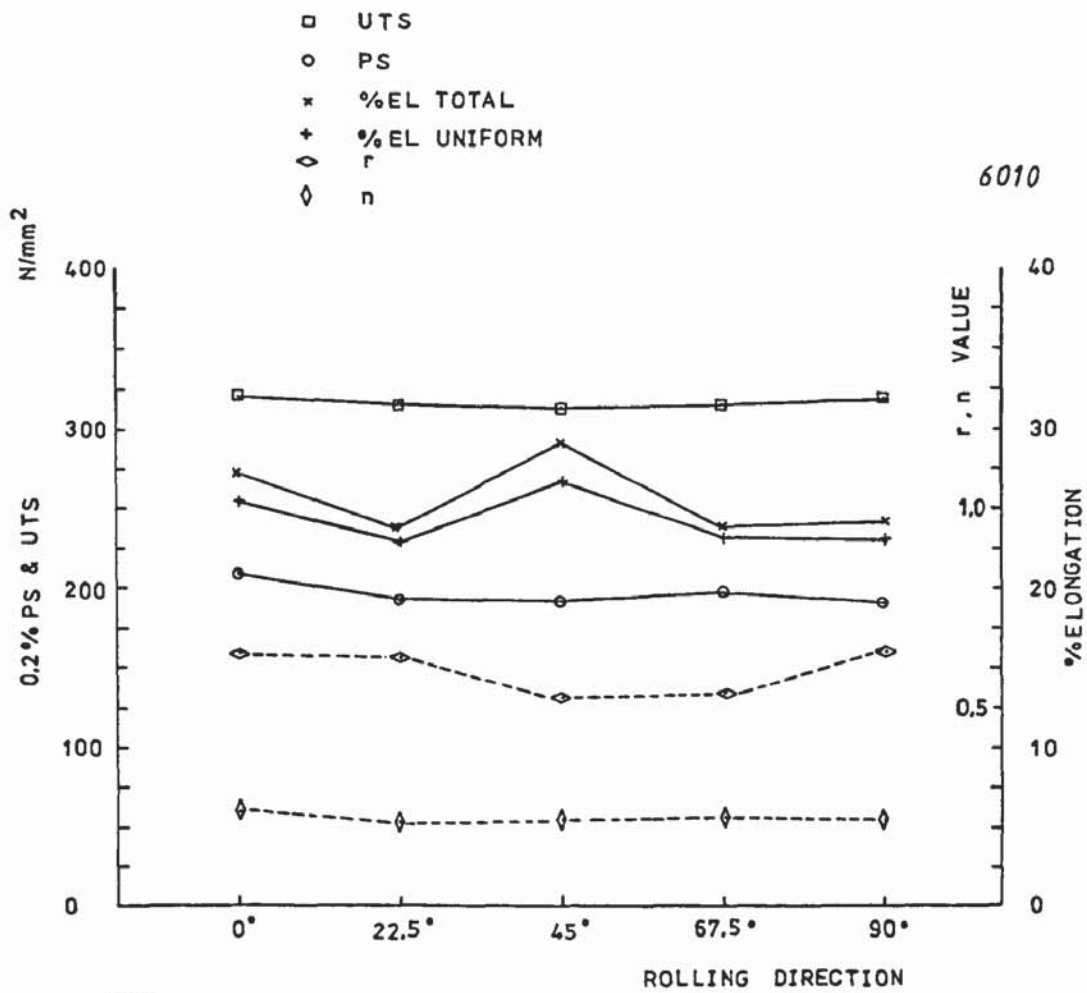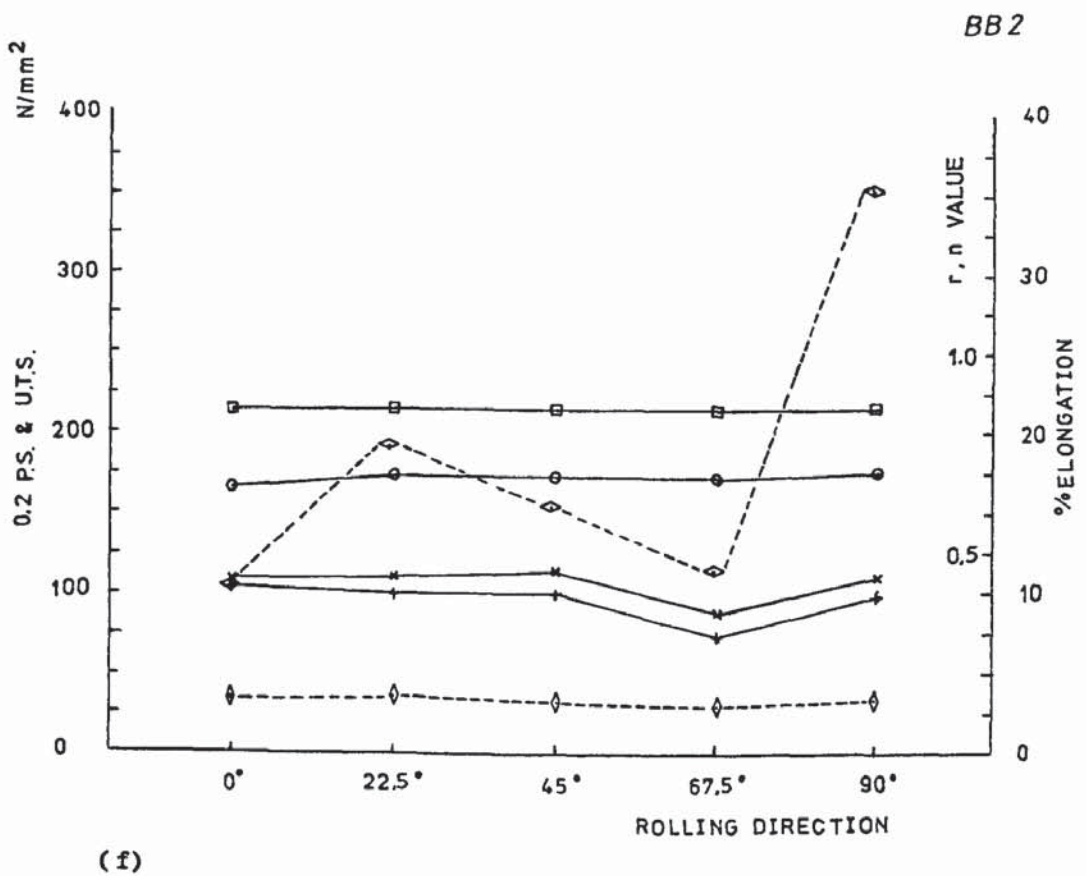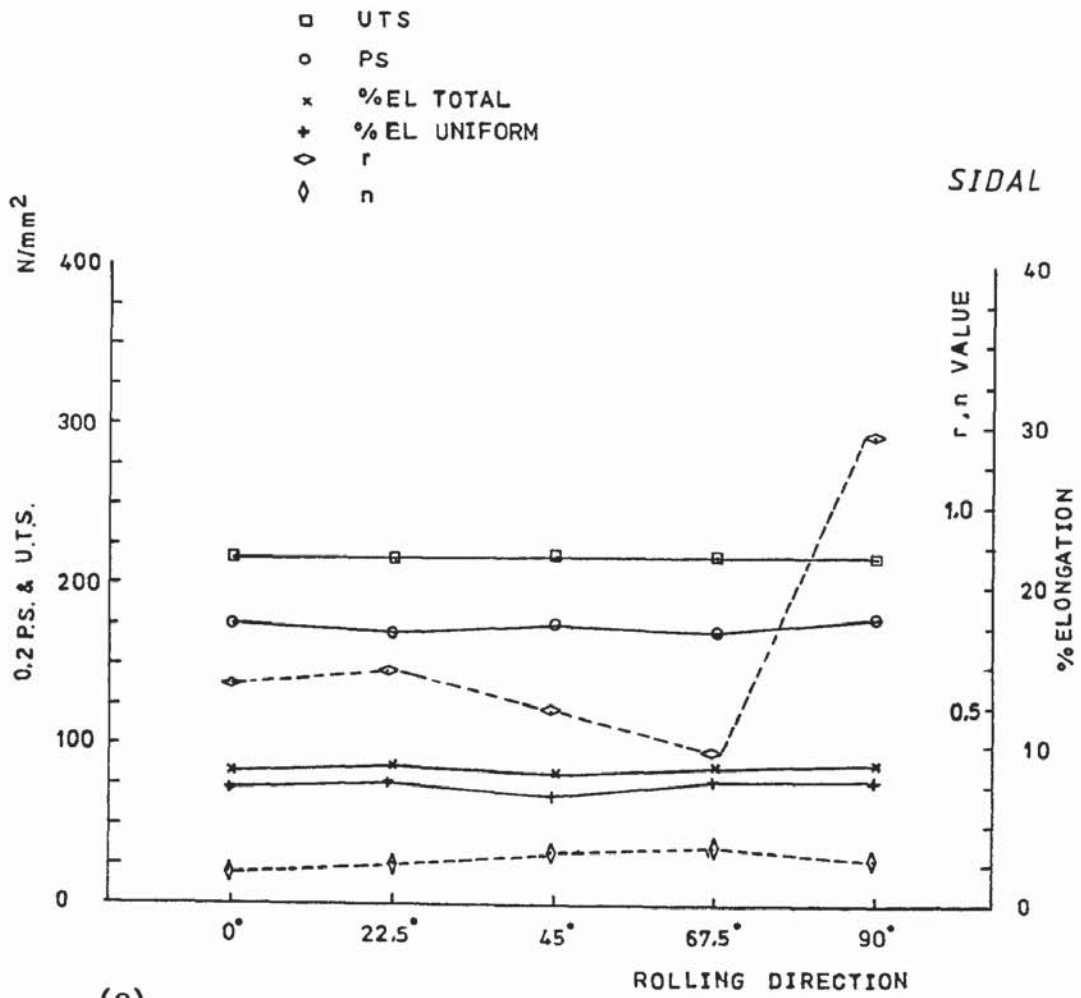Table 3.   Average tensile properties of alloys in the ' as received ' condition.

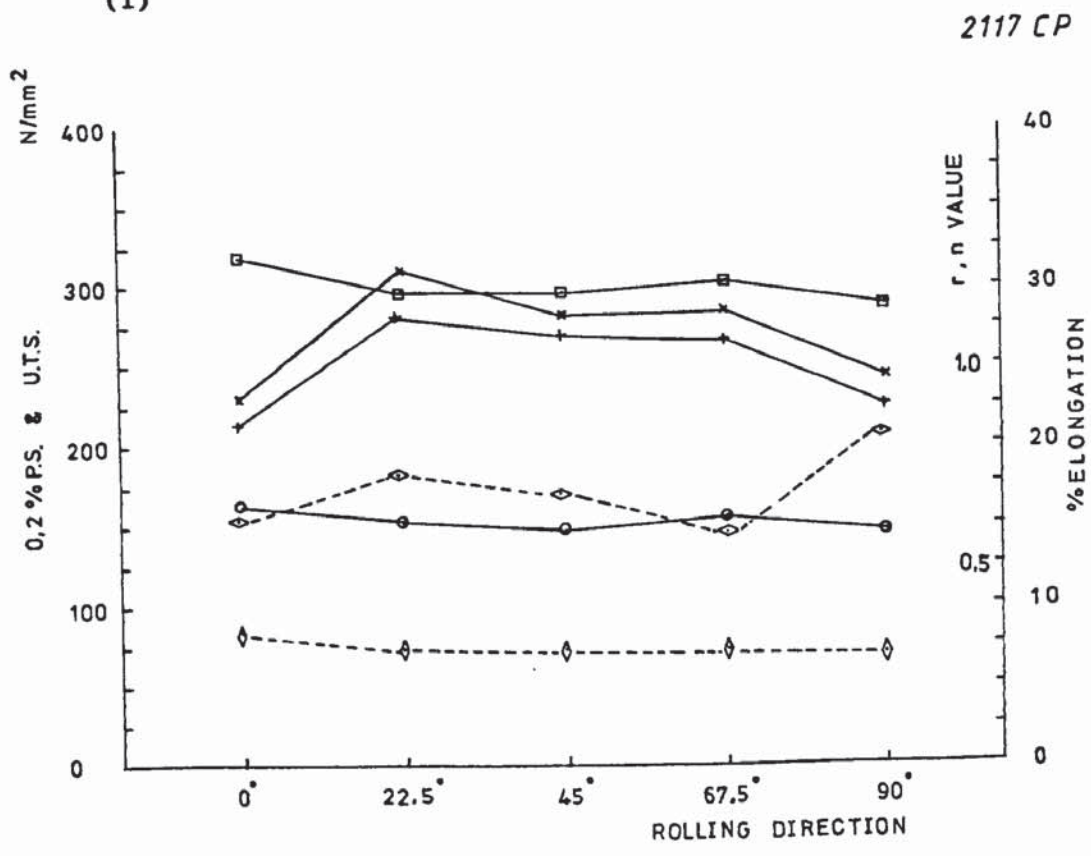Fig. 19(a)   Tensile test data for ' as received ' materials versus sheet rolling direction.

(b)

(c)

(d)

(e) SIDAL

(f) BB 2

Legend:
□ UTS
○ PS
× %EL TOTAL
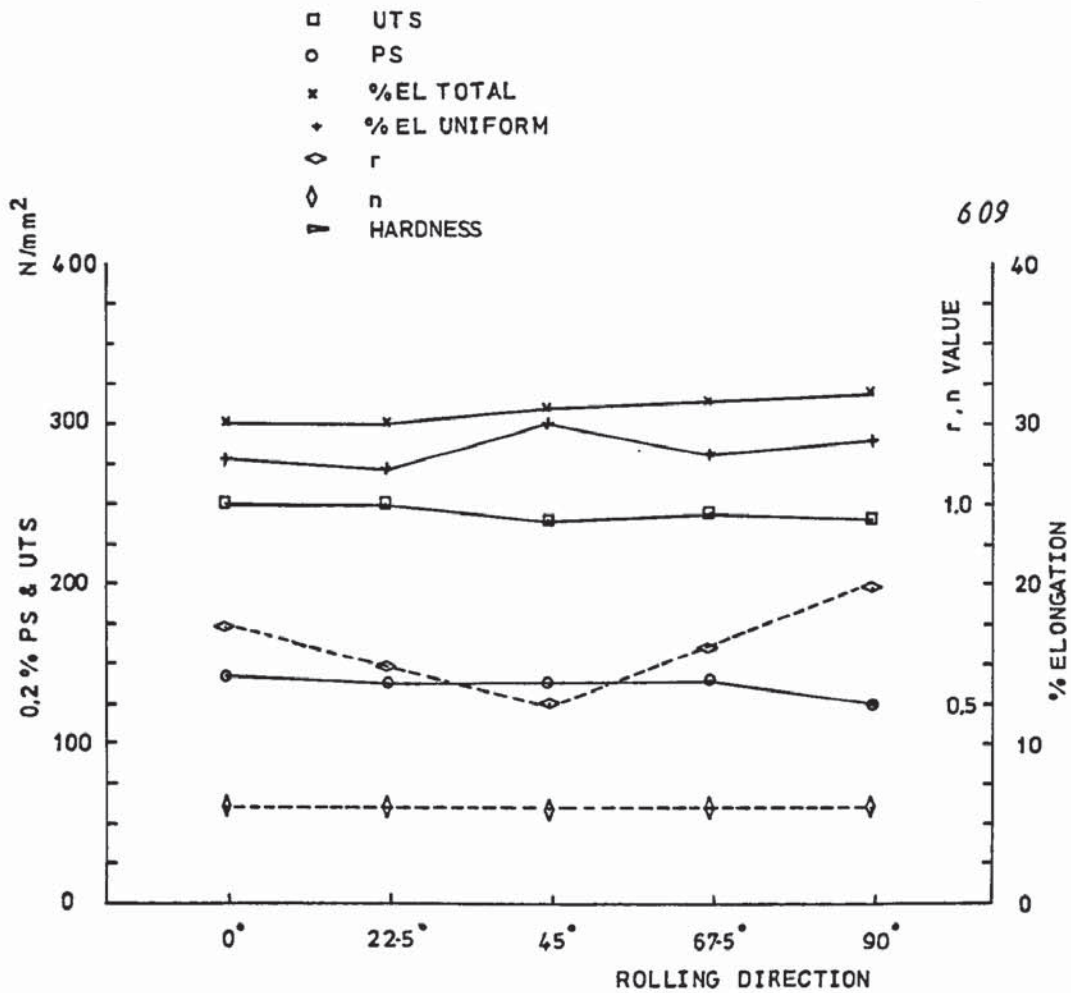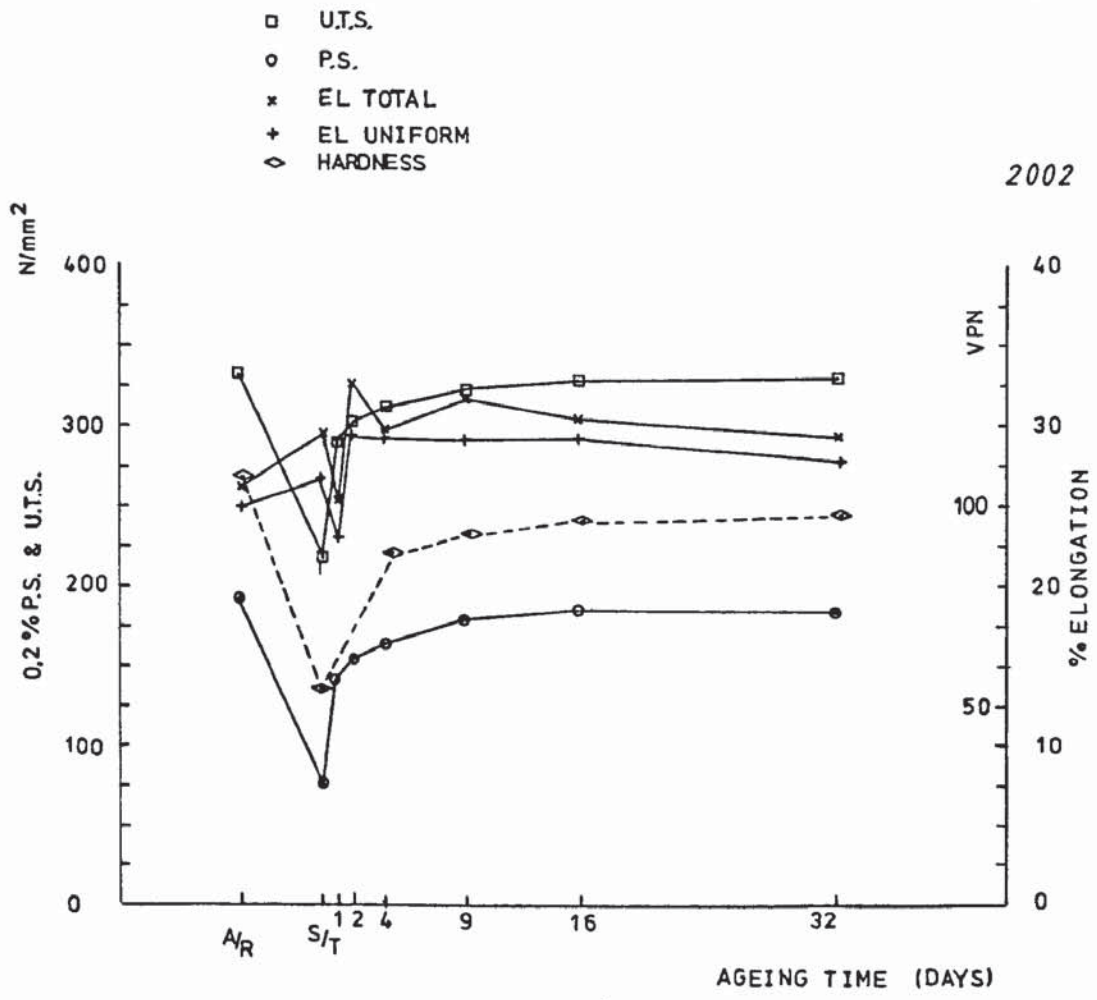+ %EL UNIFORM
◇ r
◊ n
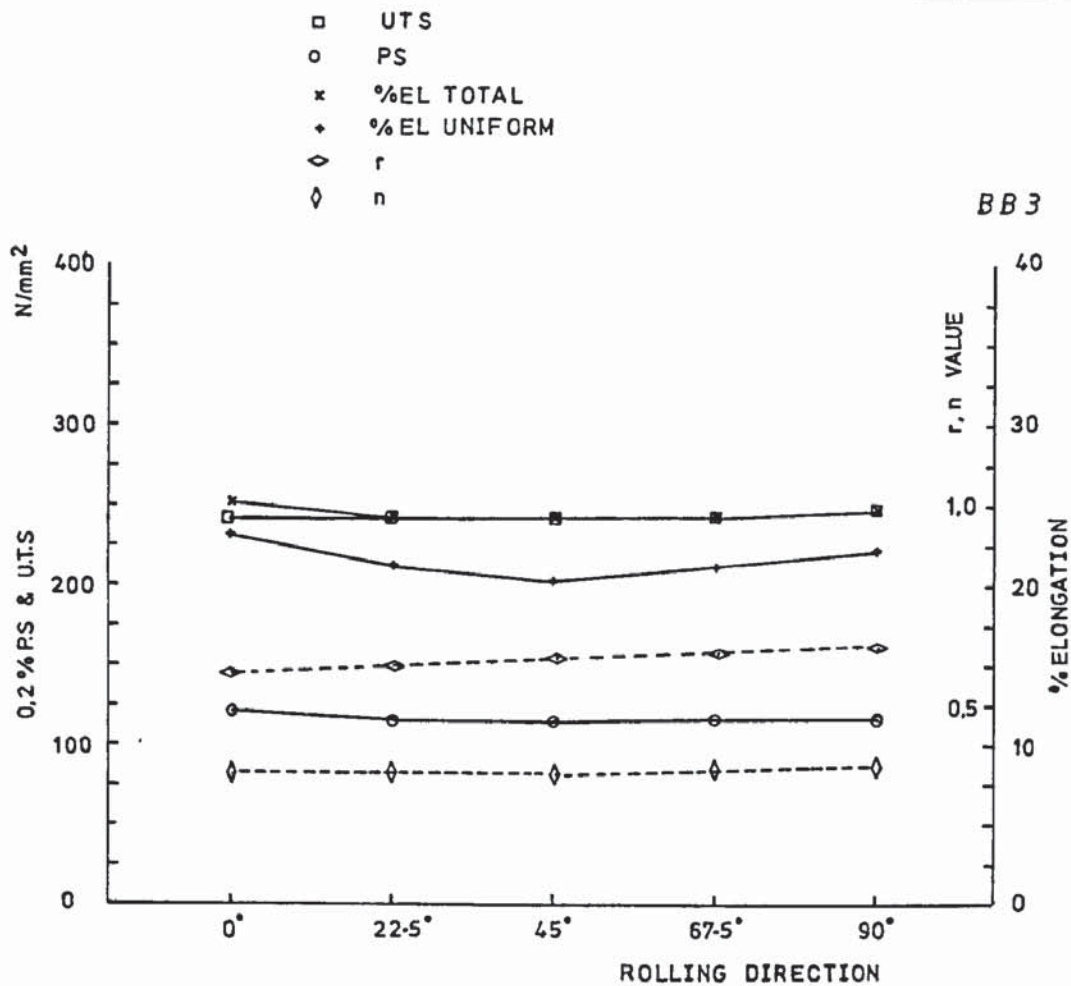
(g)
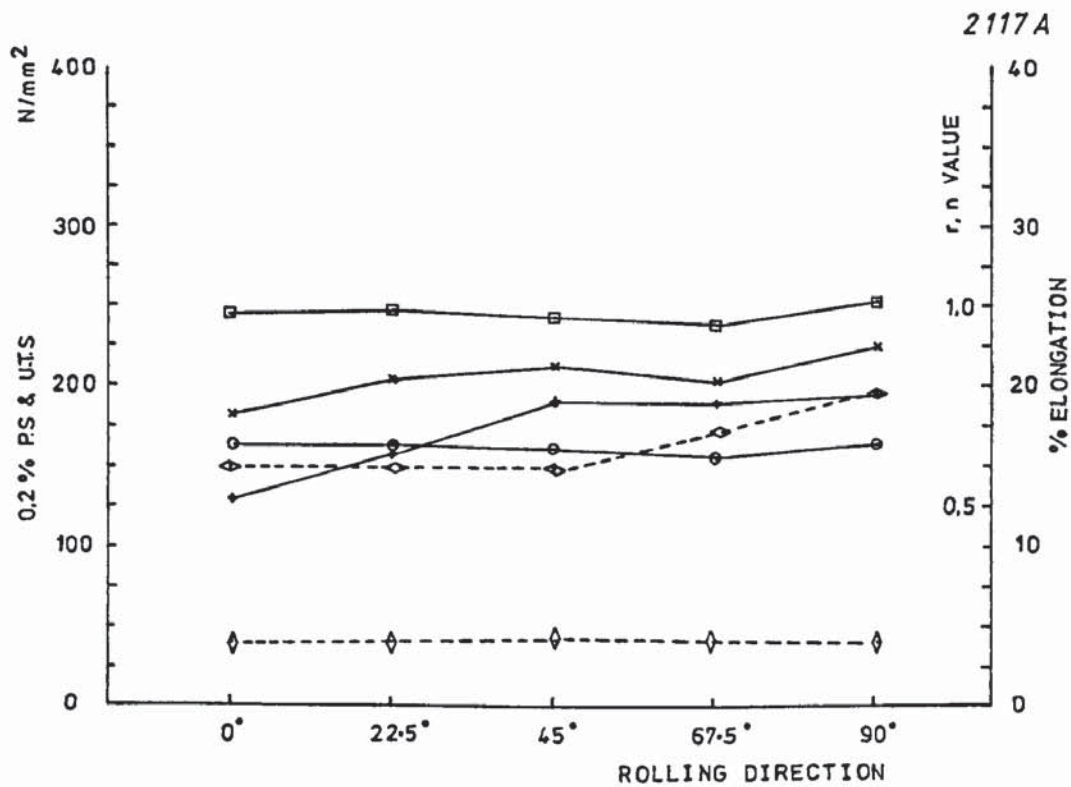
(h)
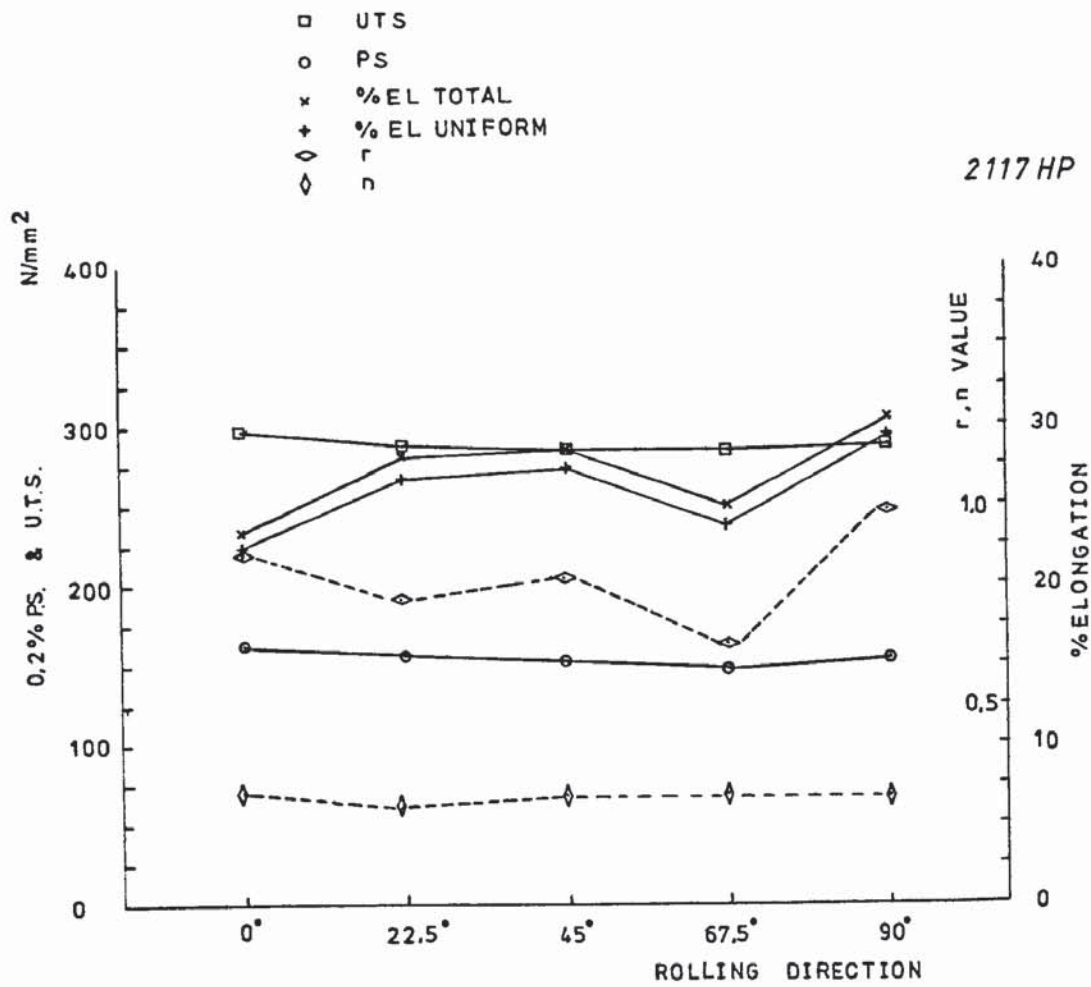
(i)

(j)
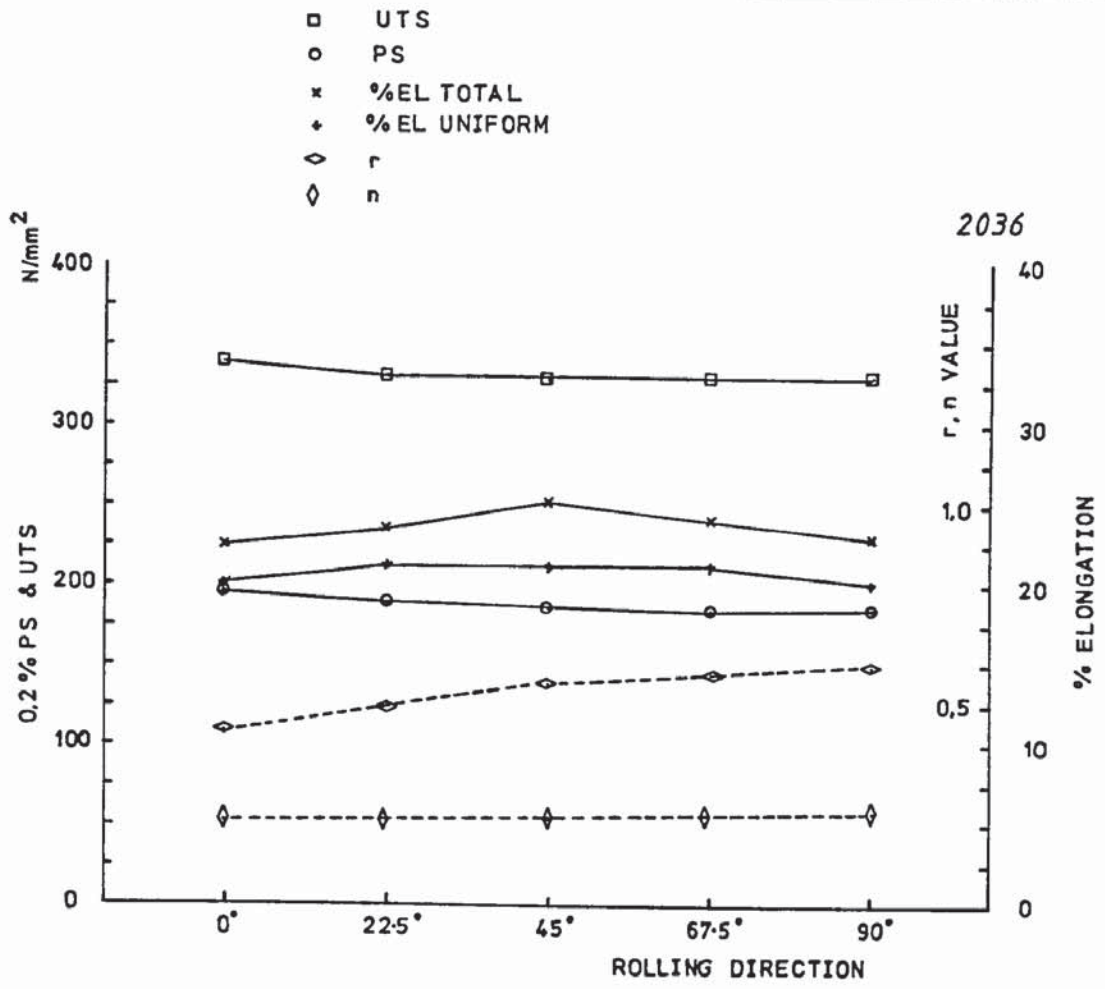
(k)
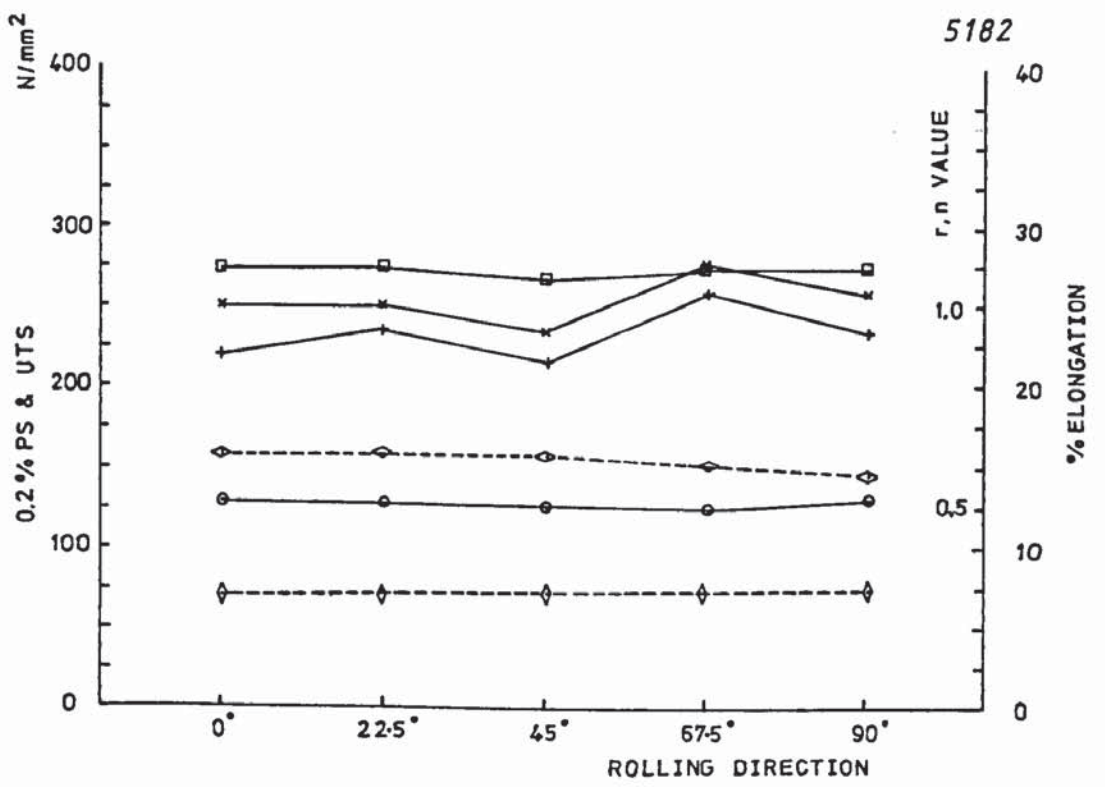
(l)
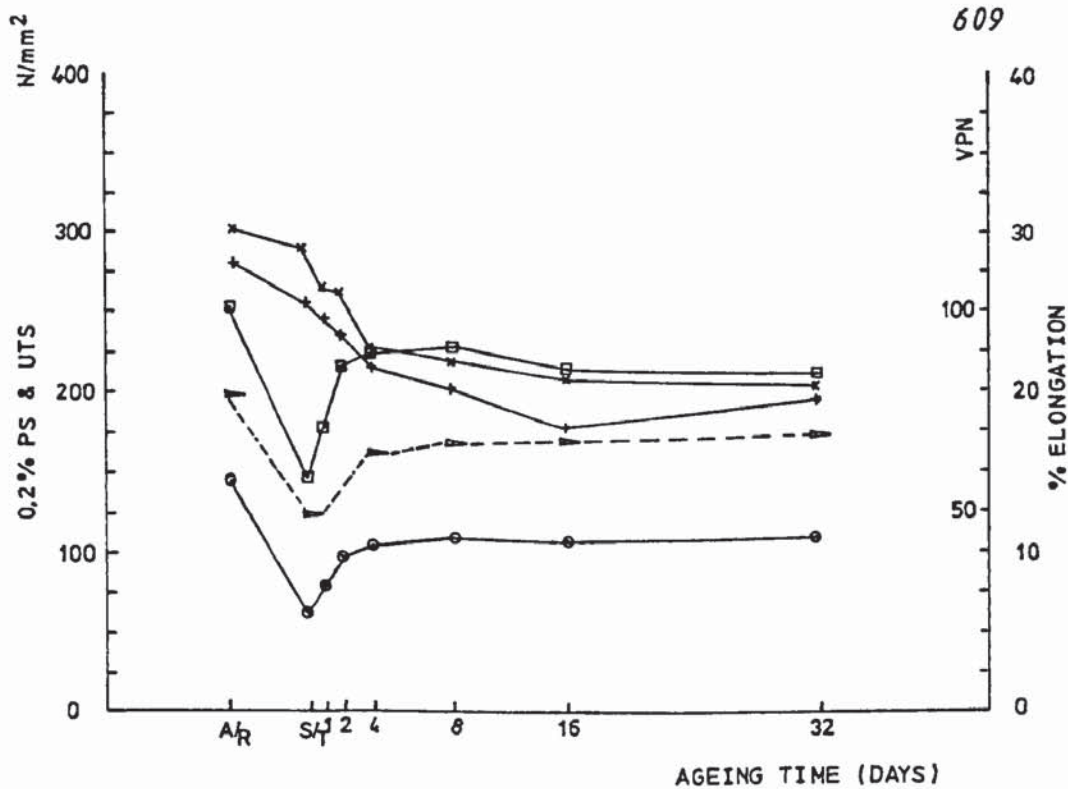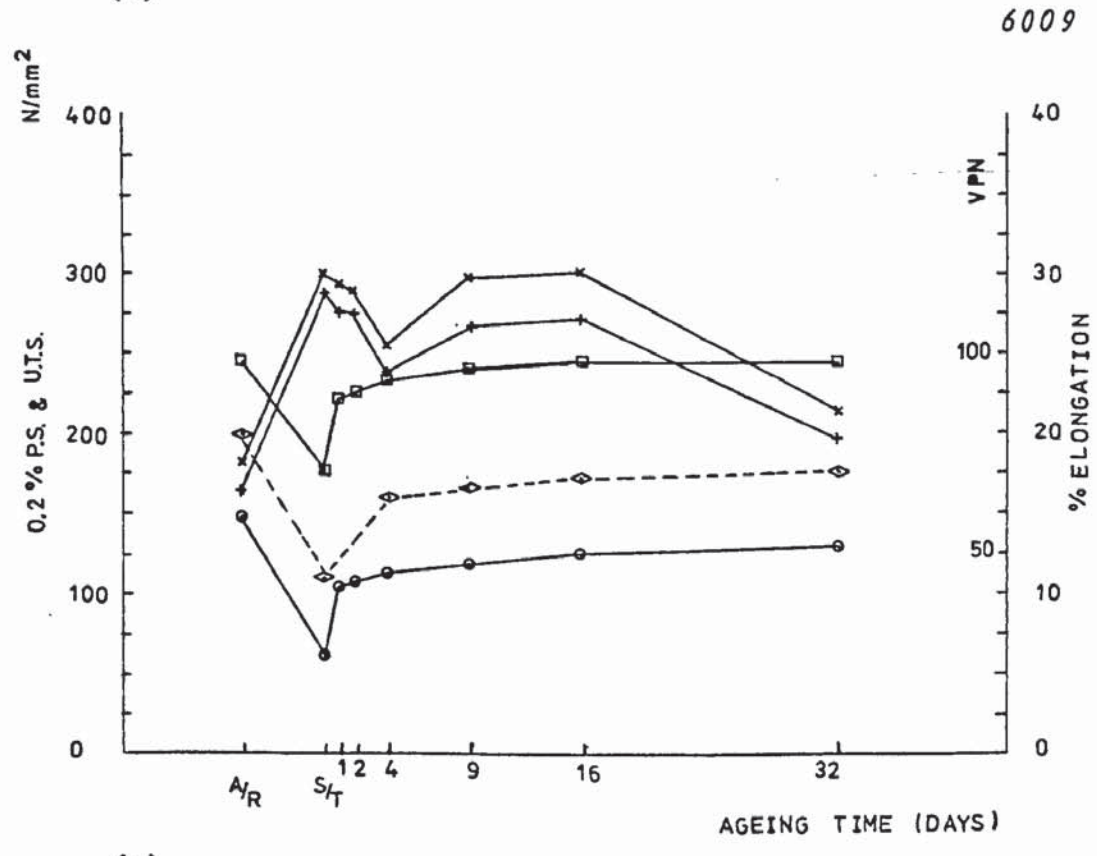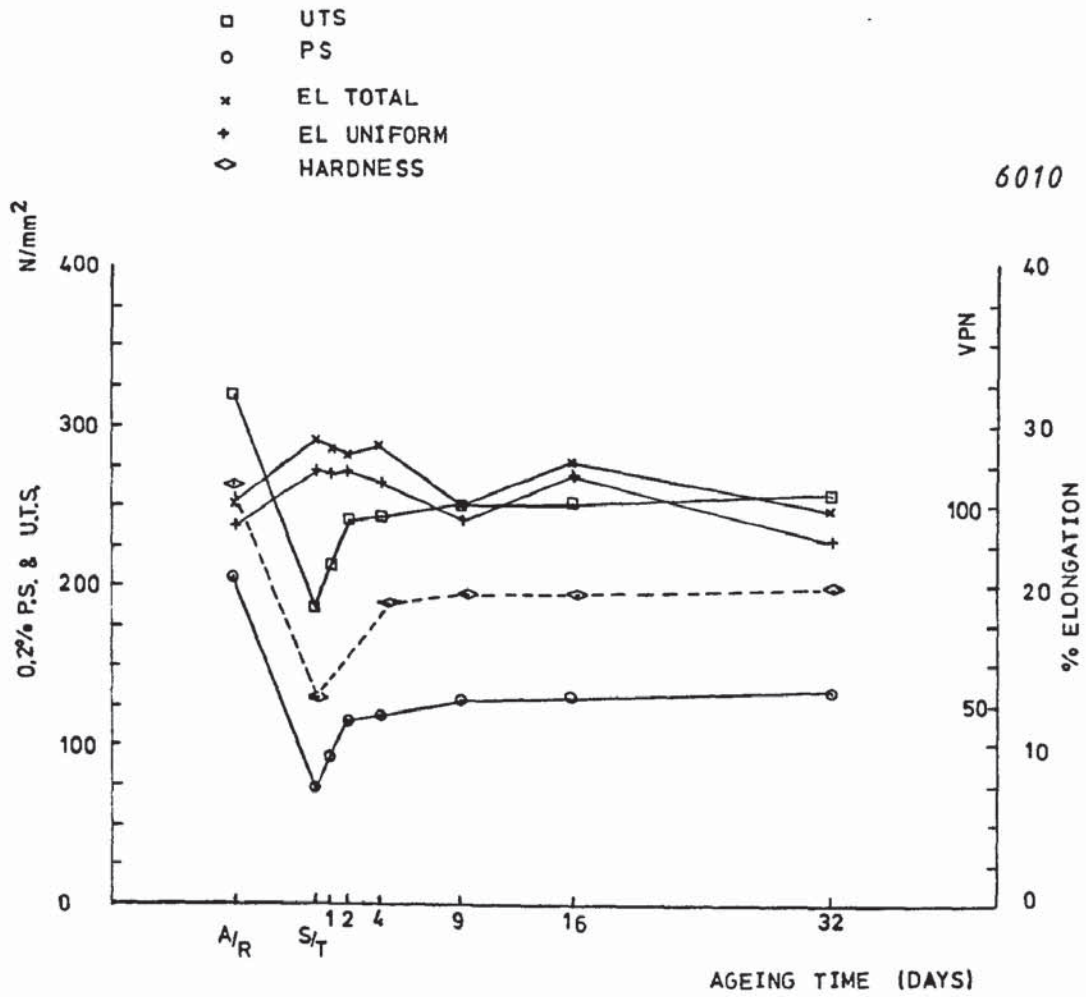
Fig. 20(a)   Average tensile properties of alloys during natural ageing at room temperature for periods between 0 - 32 days.

Legend:
□ U.T.S.
○ P.S.
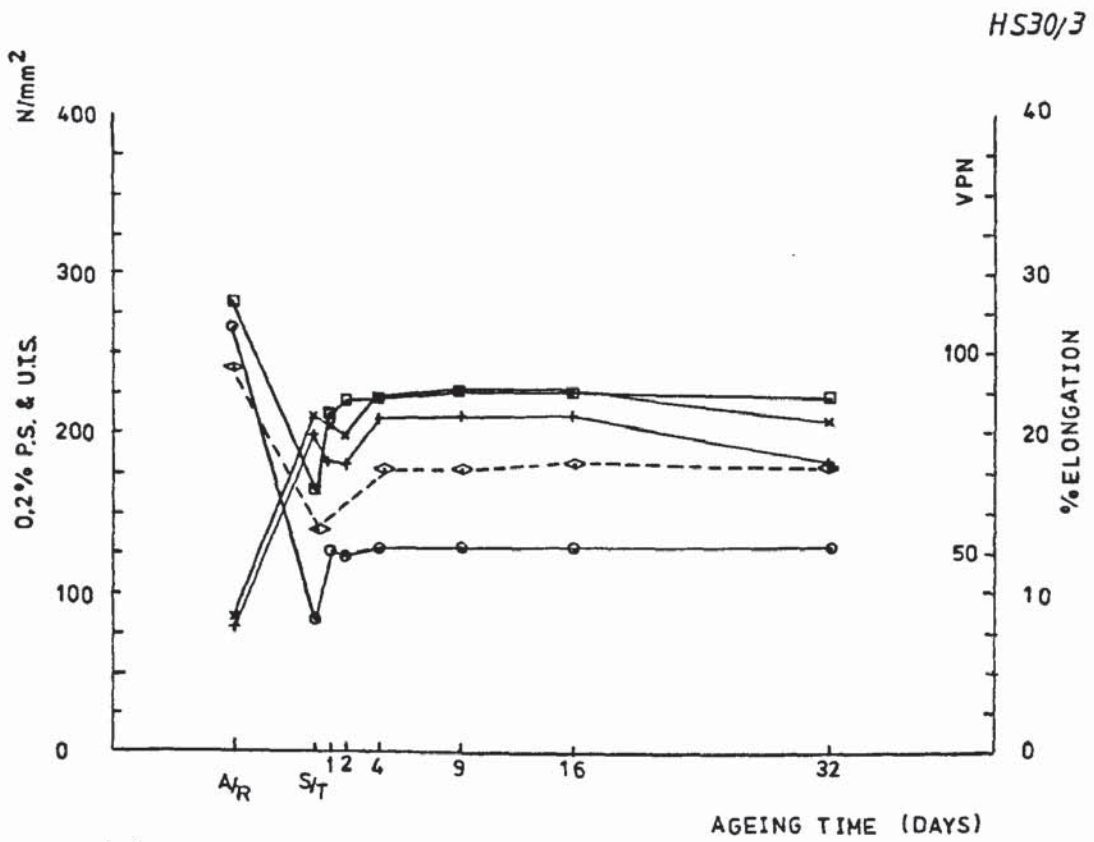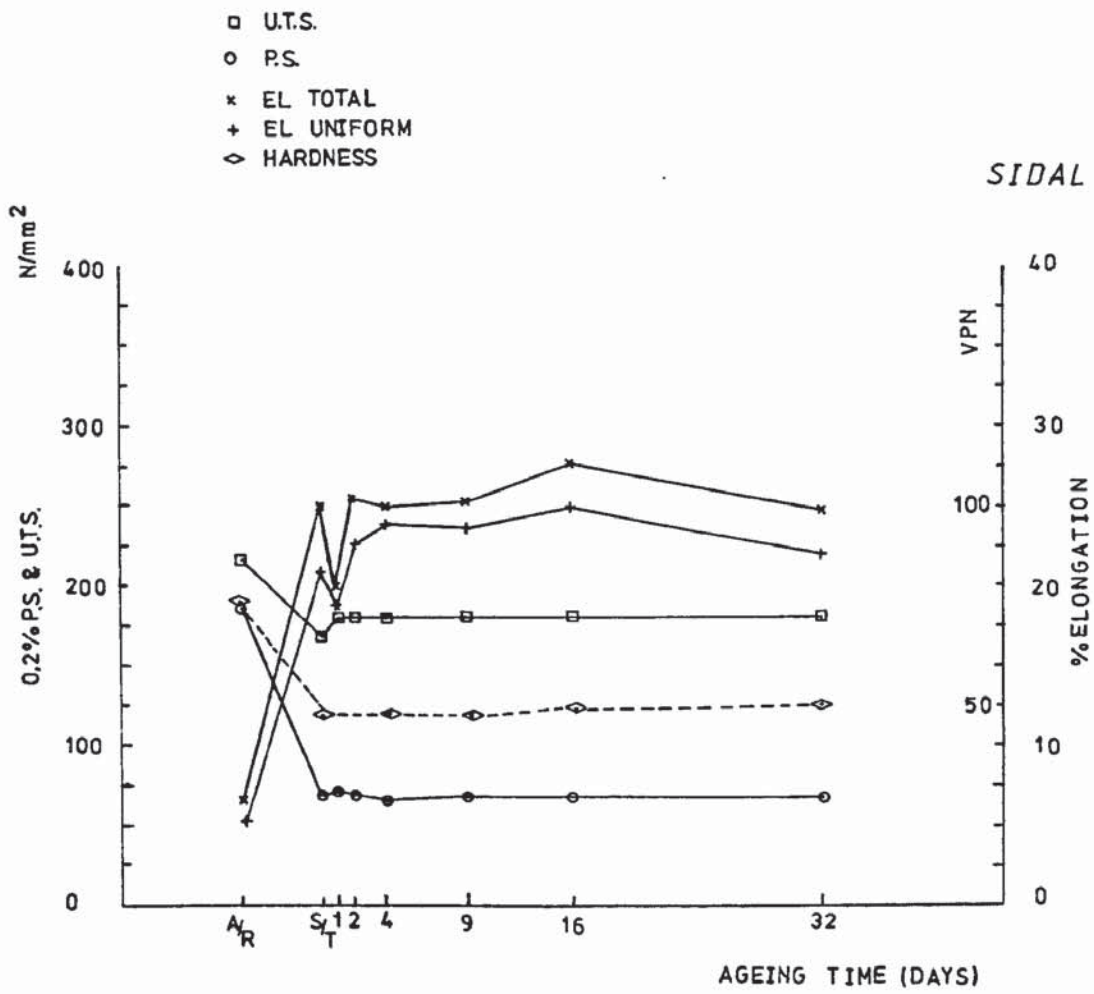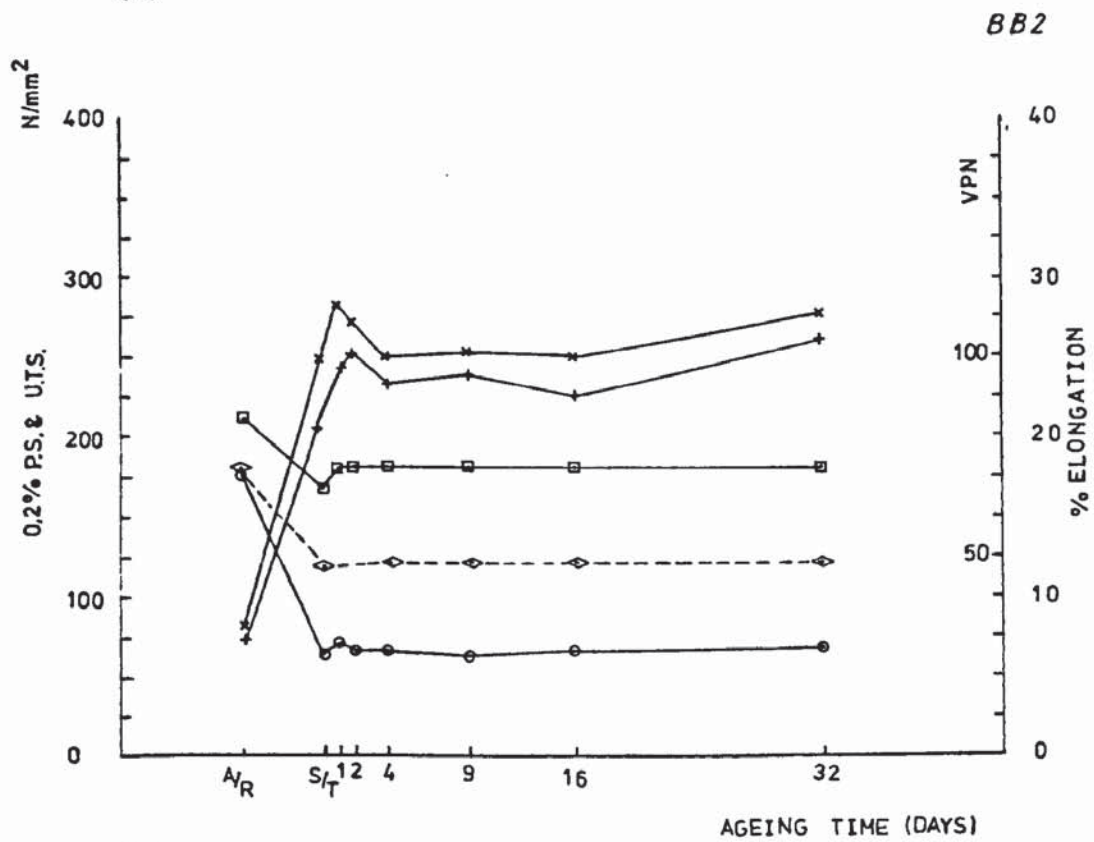× EL TOTAL
+ EL UNIFORM
◇ HARDNESS

(b) 2002

(c) 6009

(d)

(c)

SIDAL

(f)

BB2

(g)

UTS
PS
%EL TOTAL
%EL UNIFORM
HARDNESS

BB3

(h)

2117A

(i)

(j)

(k)

UTS □

PS ○

%EL TOTAL ✕

%EL UNIFORM +

HARDNESS ◇

2036

N/mm²

400

300

200

100

0

VPN

40

30

20

10

0

0.2% PS & UTS

% ELONGATION

A/R S/T 1 2 4   8   16   32

AGEING TIME (DAYS)

(1)

5182

N/mm²

400

300

200

100

0

VPN

40

30

20

10

0

0.2% PS & UTS

% ELONGATION

A/R S/T 1 2 4   8   16   32

AGEING TIME (DAYS)
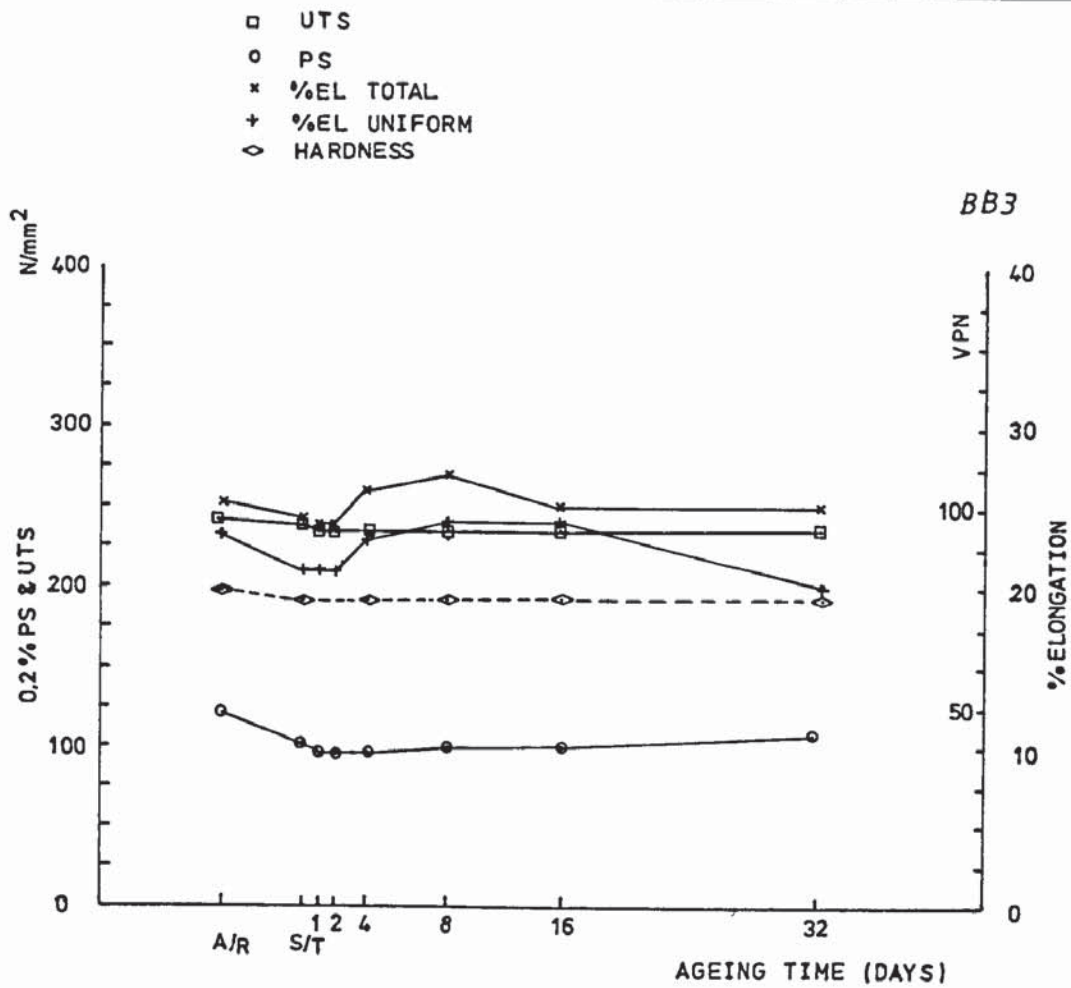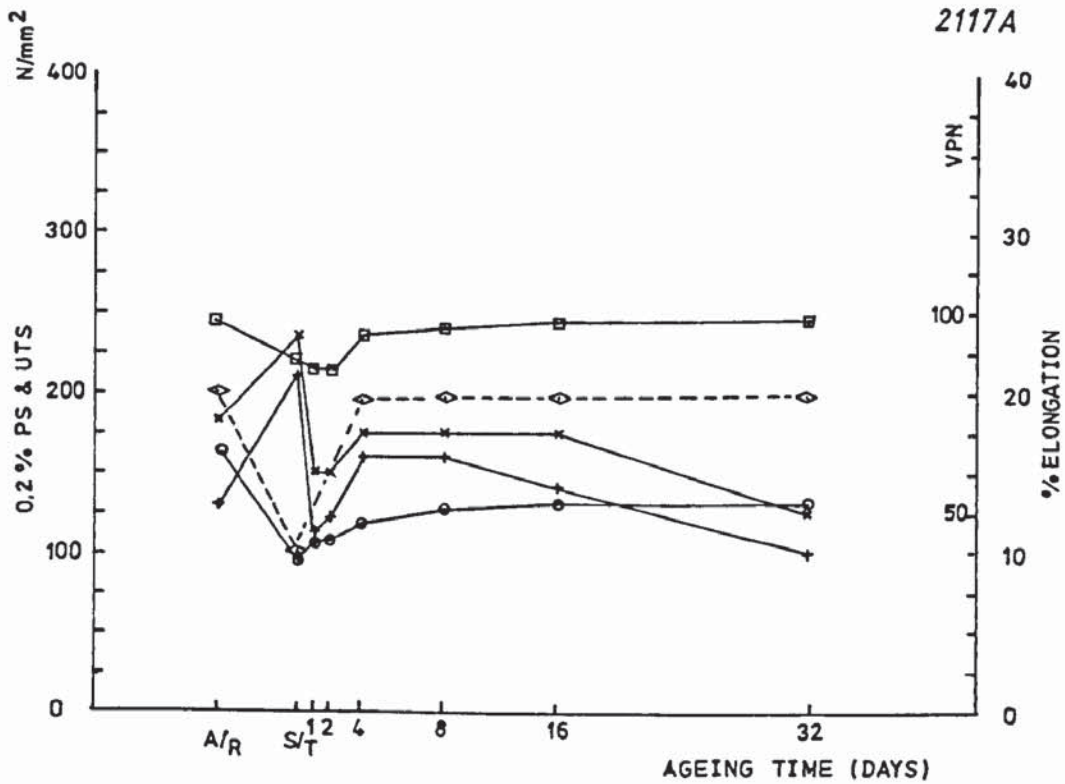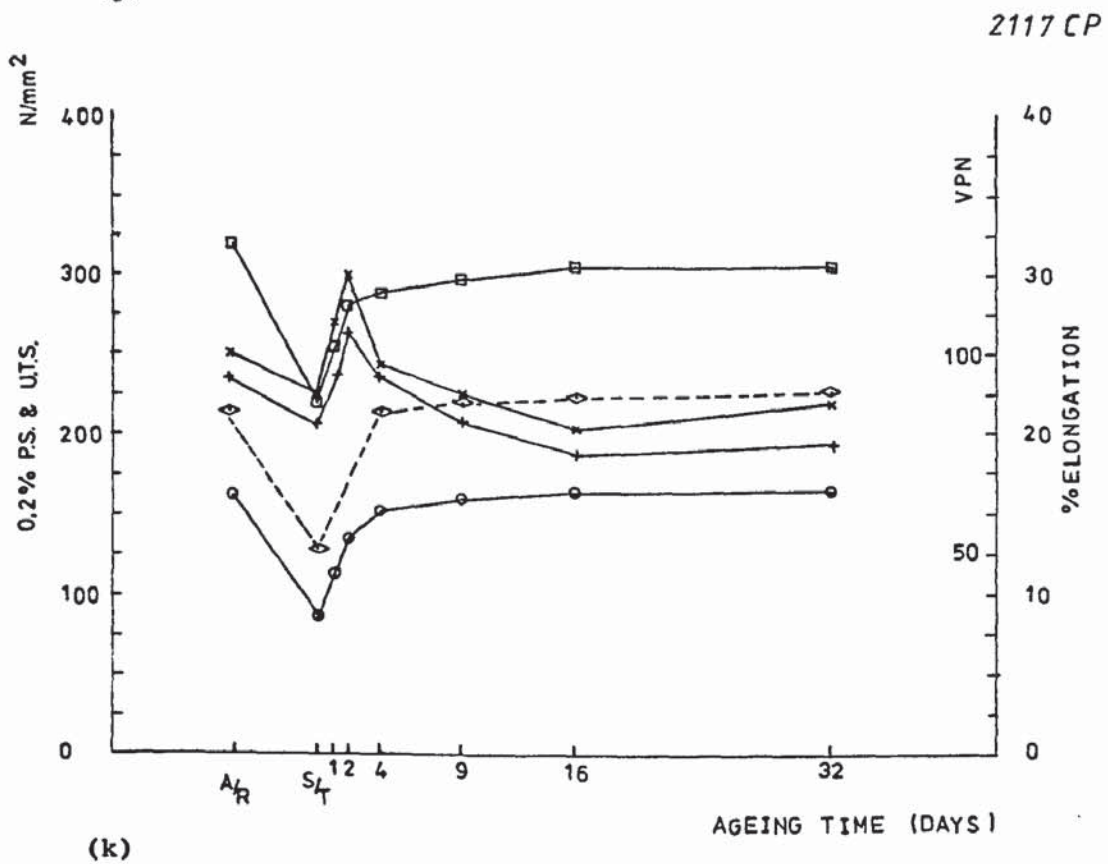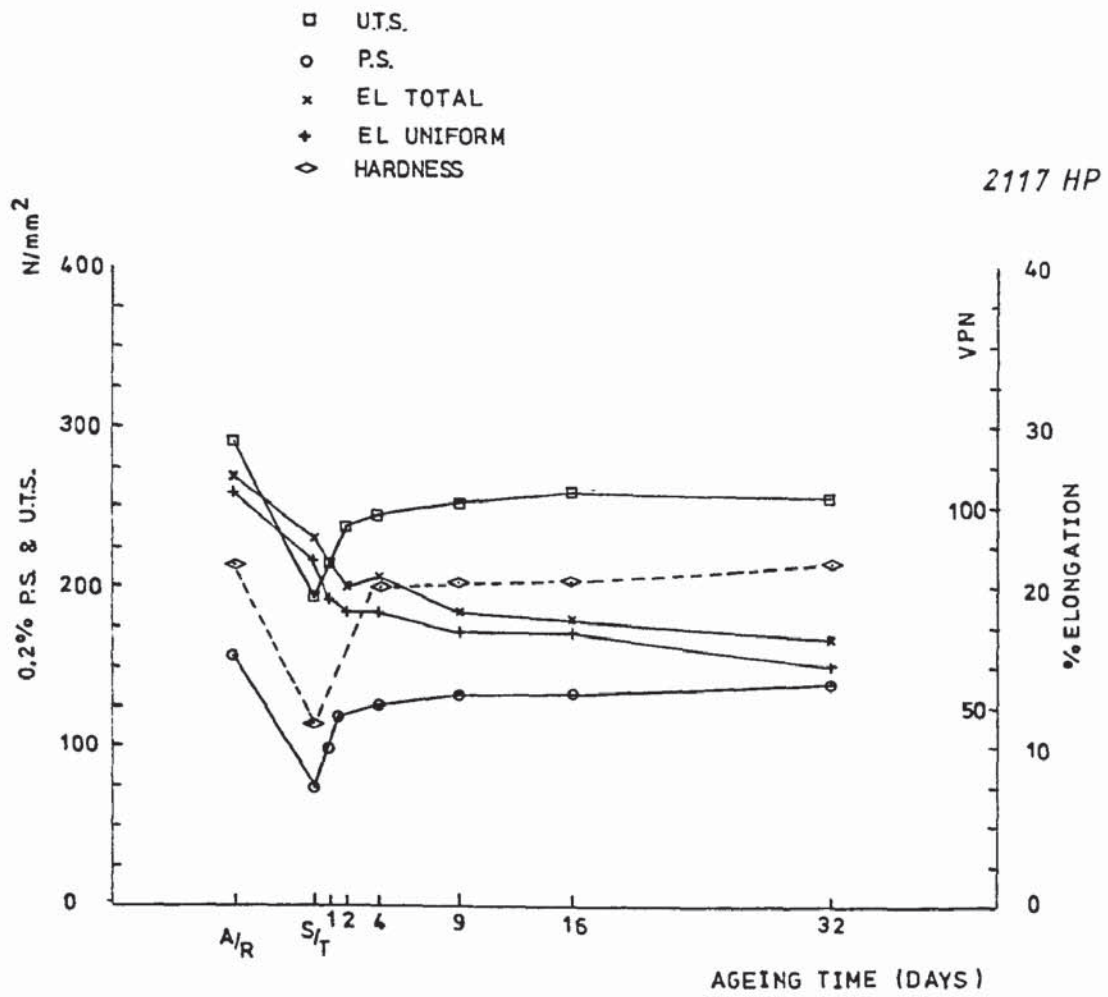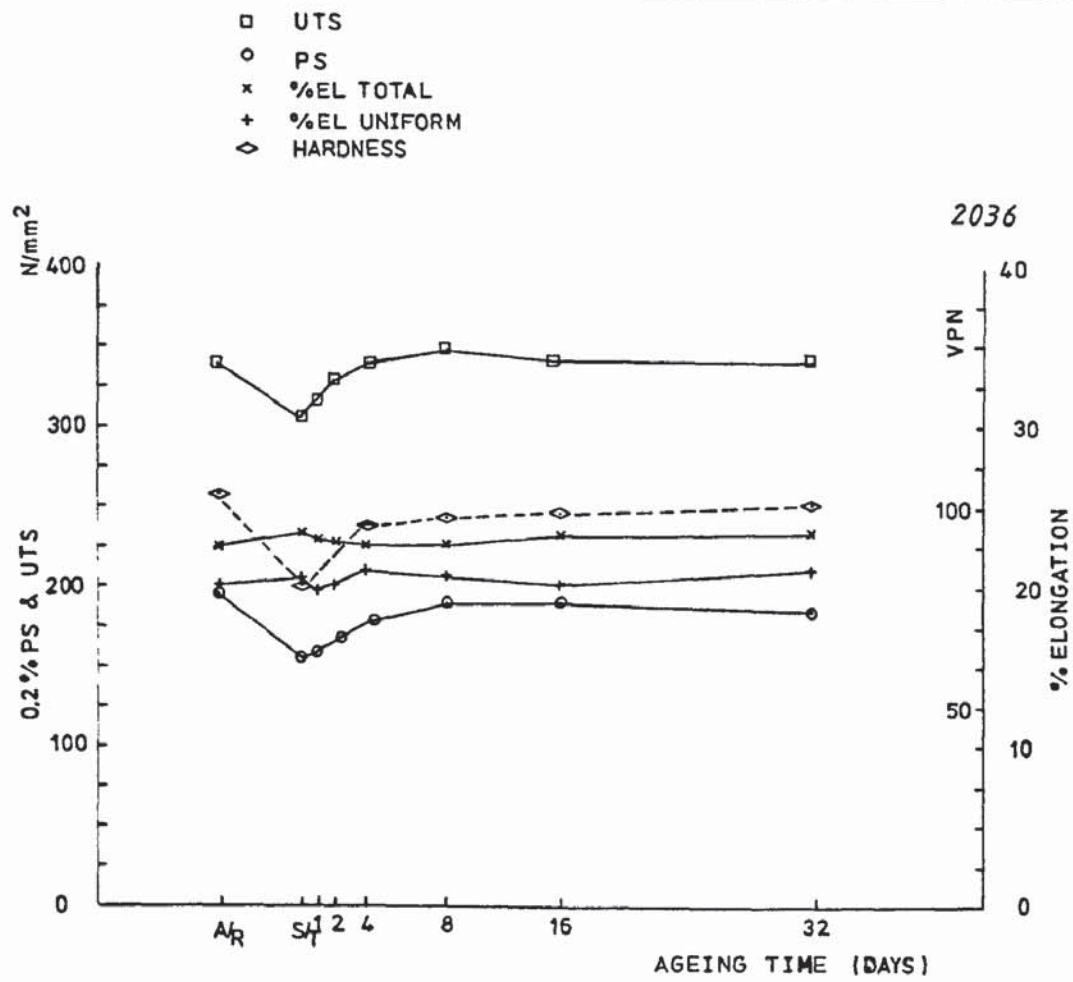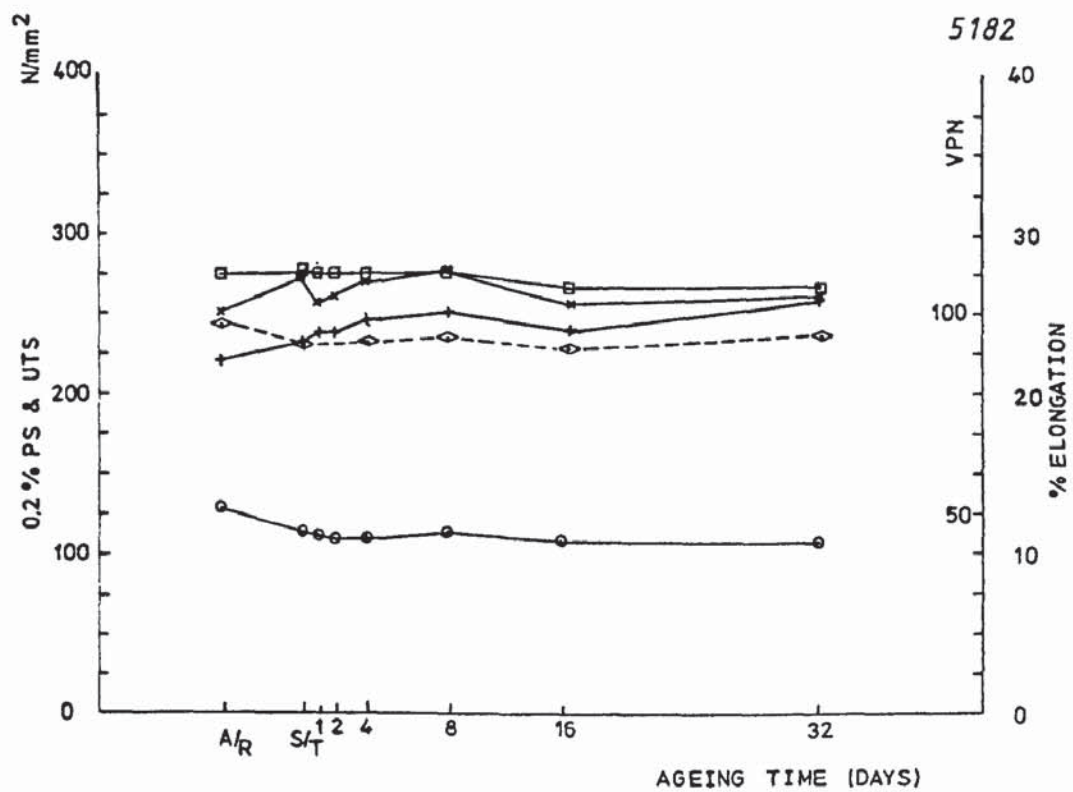
(m)
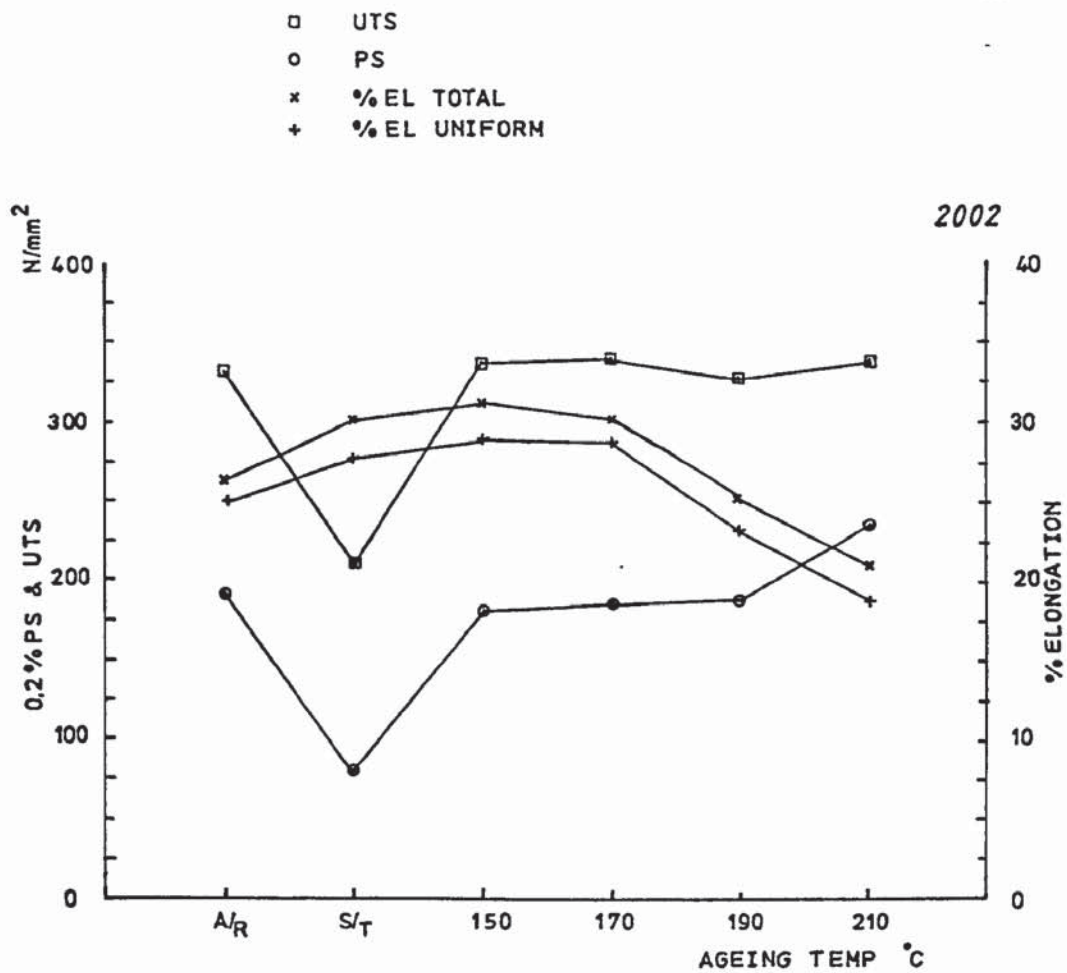
Fig. 21(a) Average tensile properties of alloys artificially
aged, from the solution heat treated condition, for
15 minutes at temperatures between 150 - 210 C

(b)

(c)

(d)

(e)

(f)

(g)

(h)

Legend:
- □ UTS
- ○ PS
- × % EL TOTAL
- + % EL UNIFORM

(i) 2117 HP

(j) 2117 CP

Legend:
- □ UTS
- ○ PS
- × % EL TOTAL
- + % EL UNIFORM

(k) 2036

(l) 5182
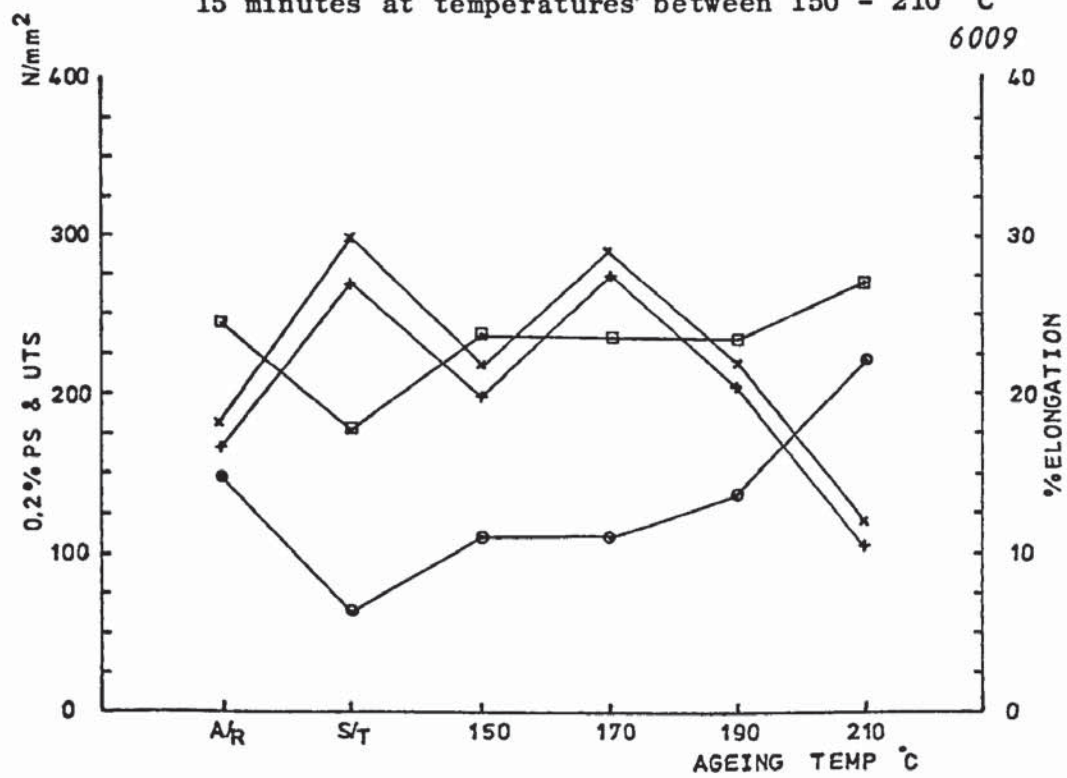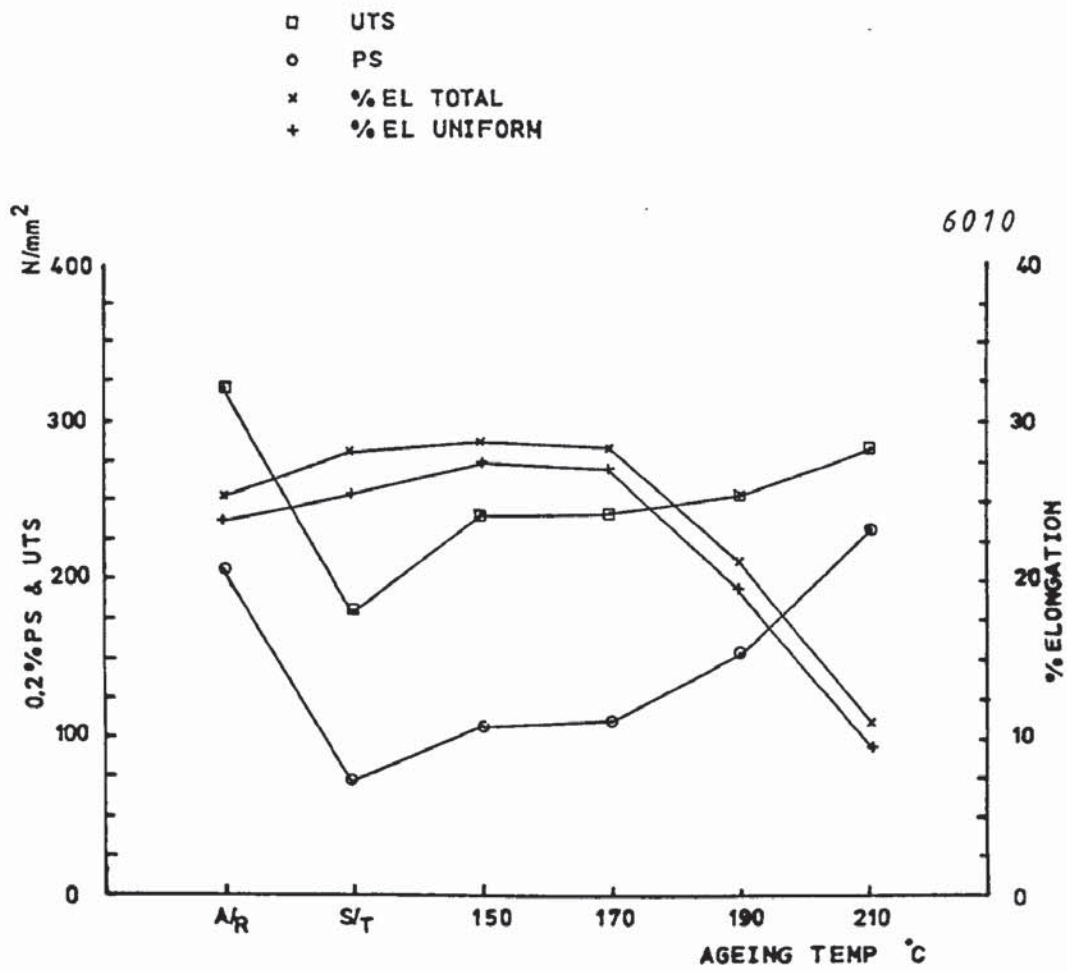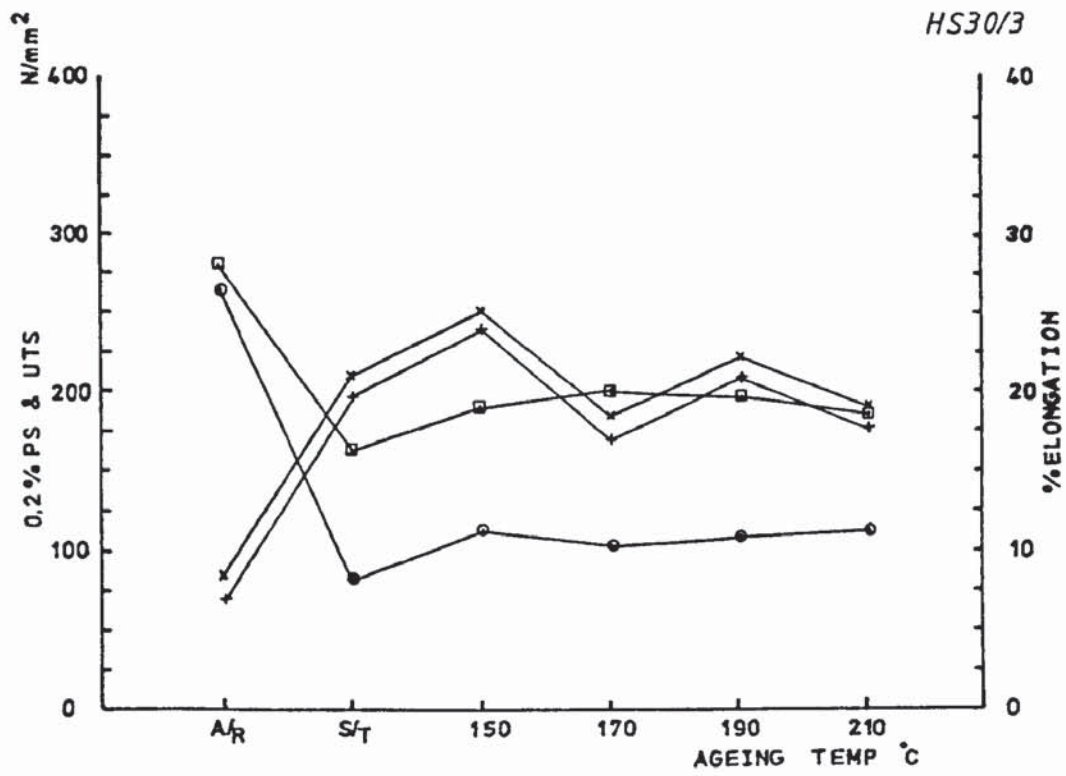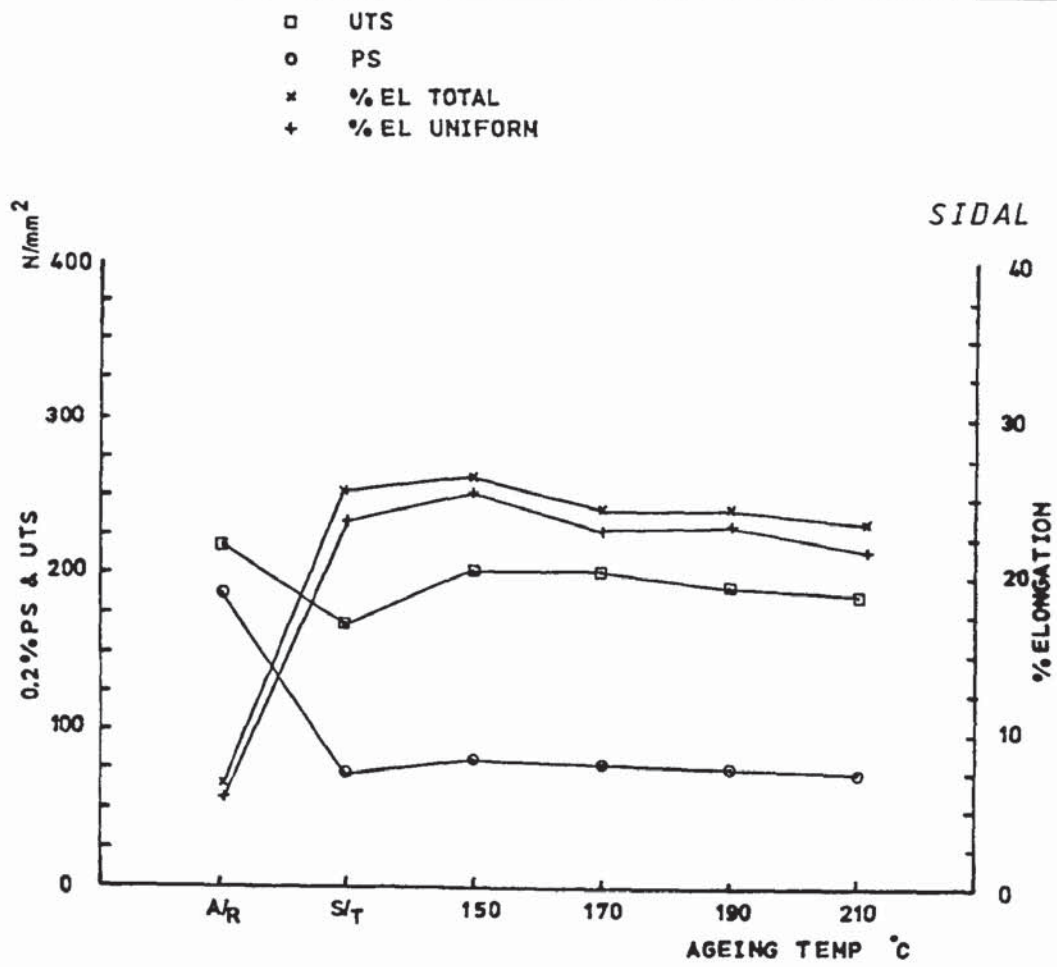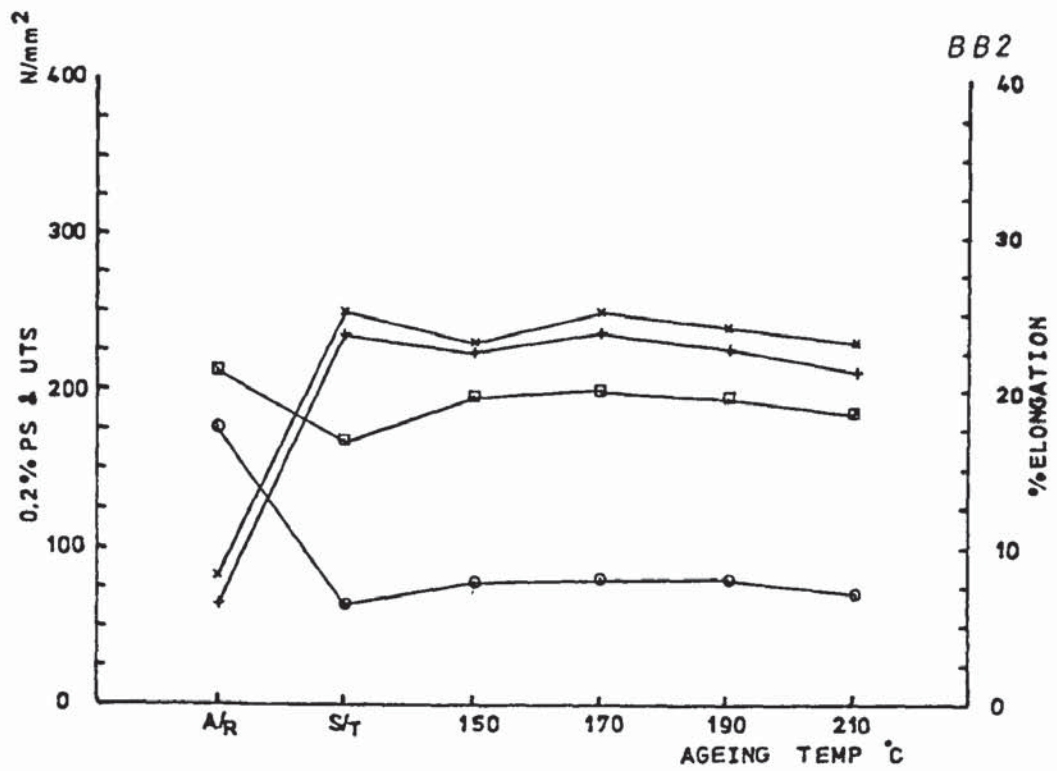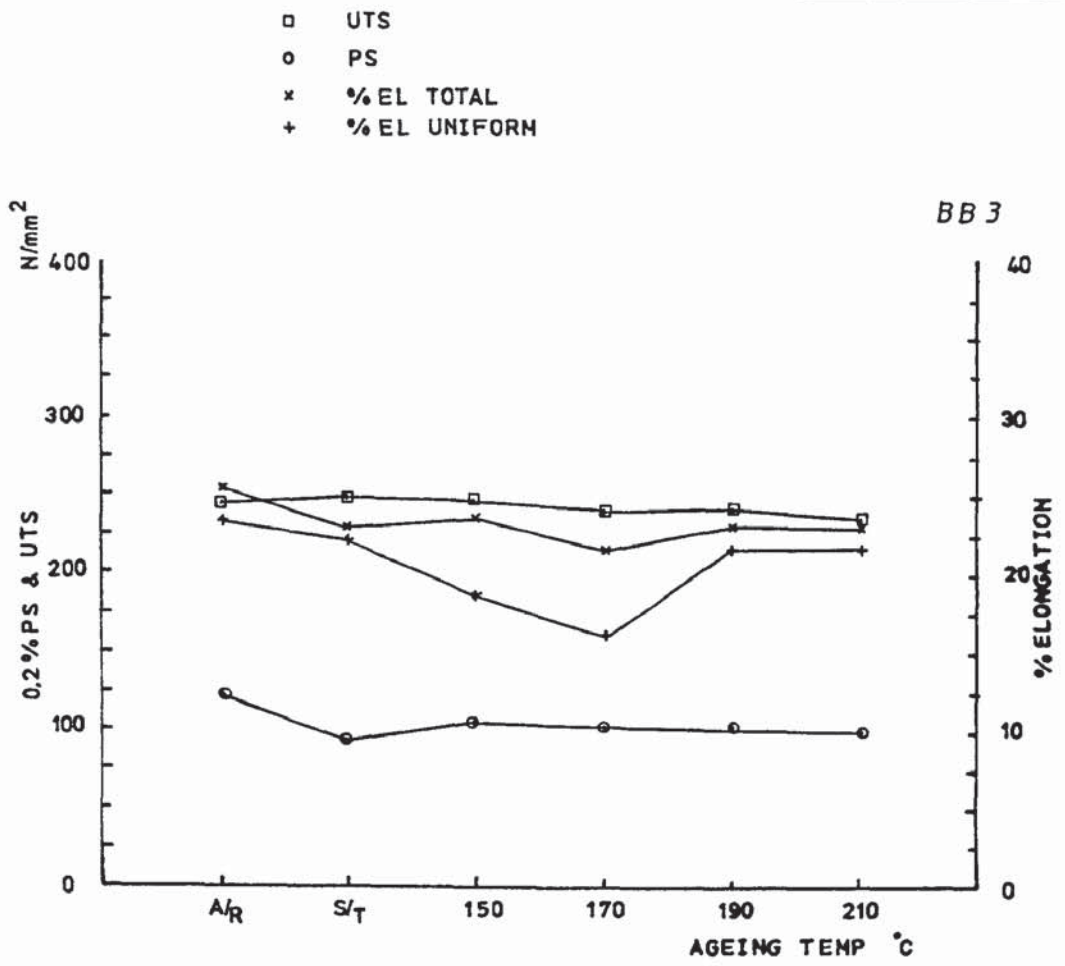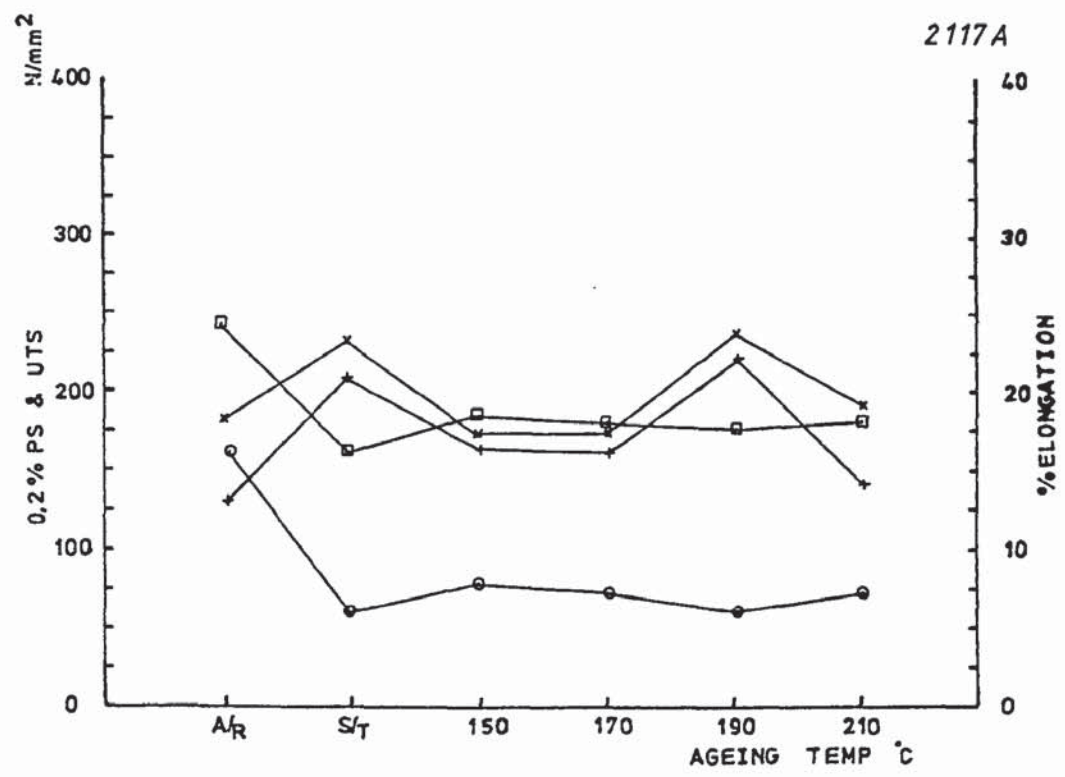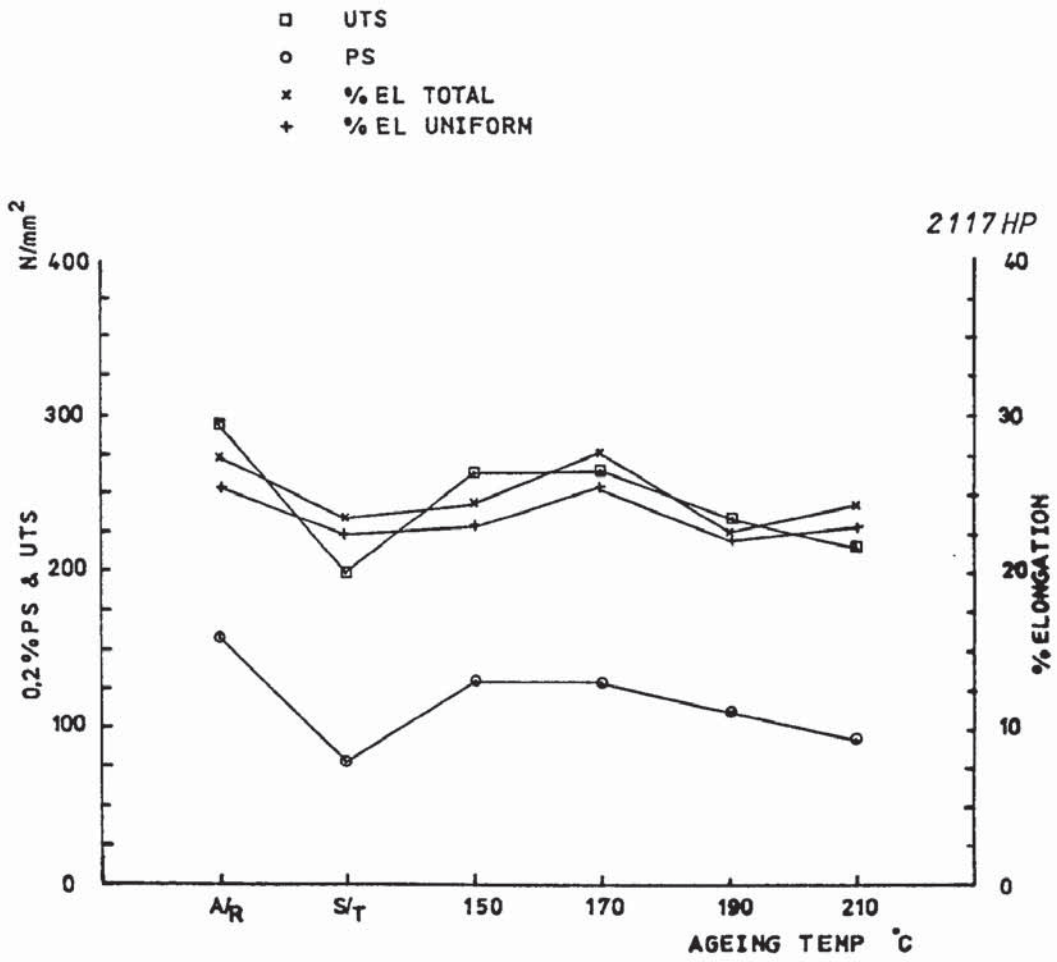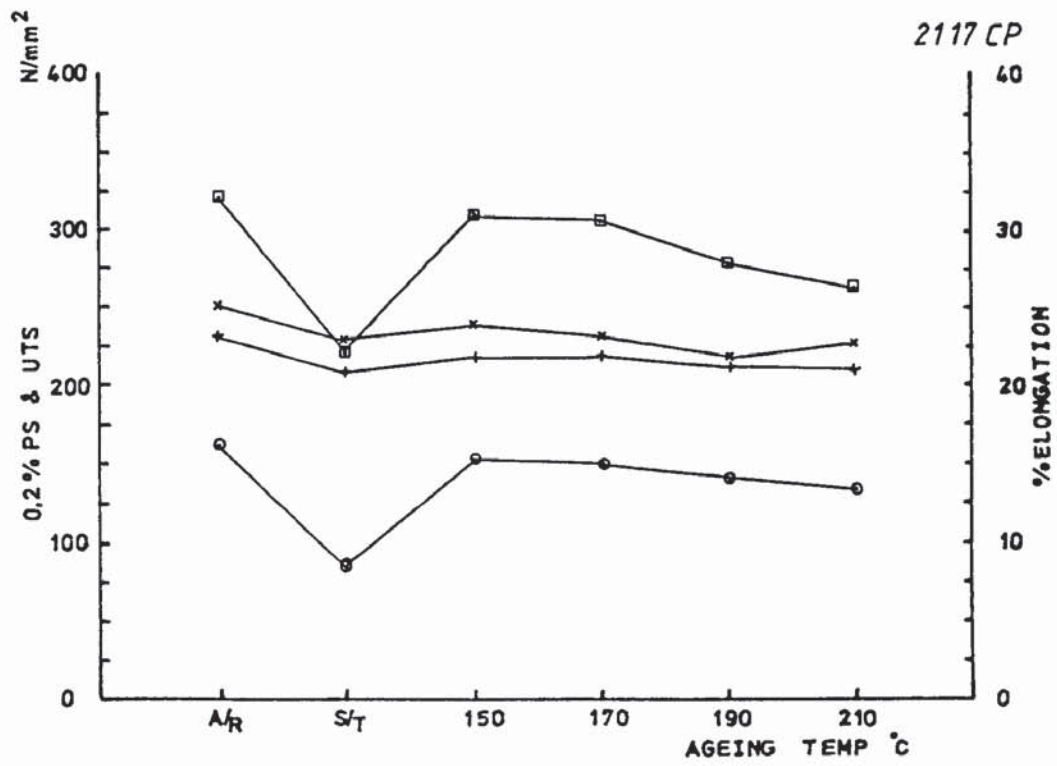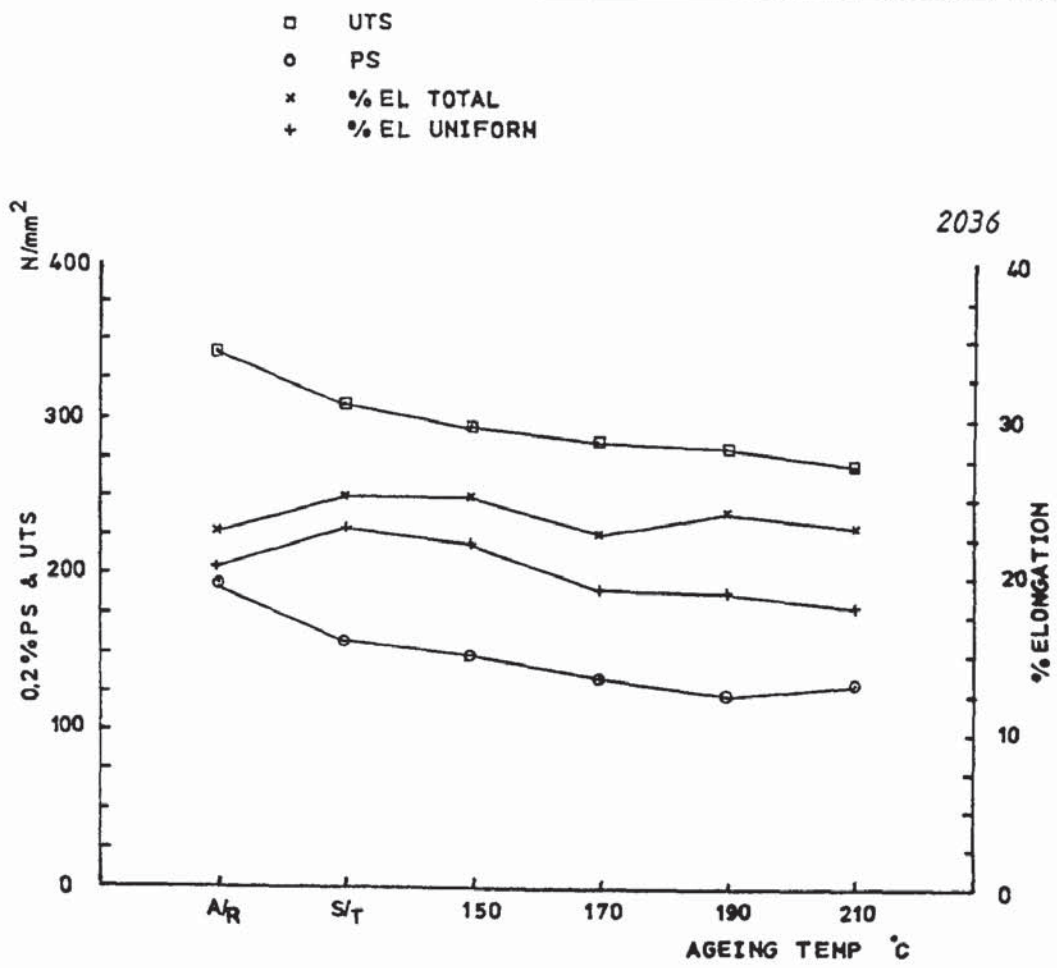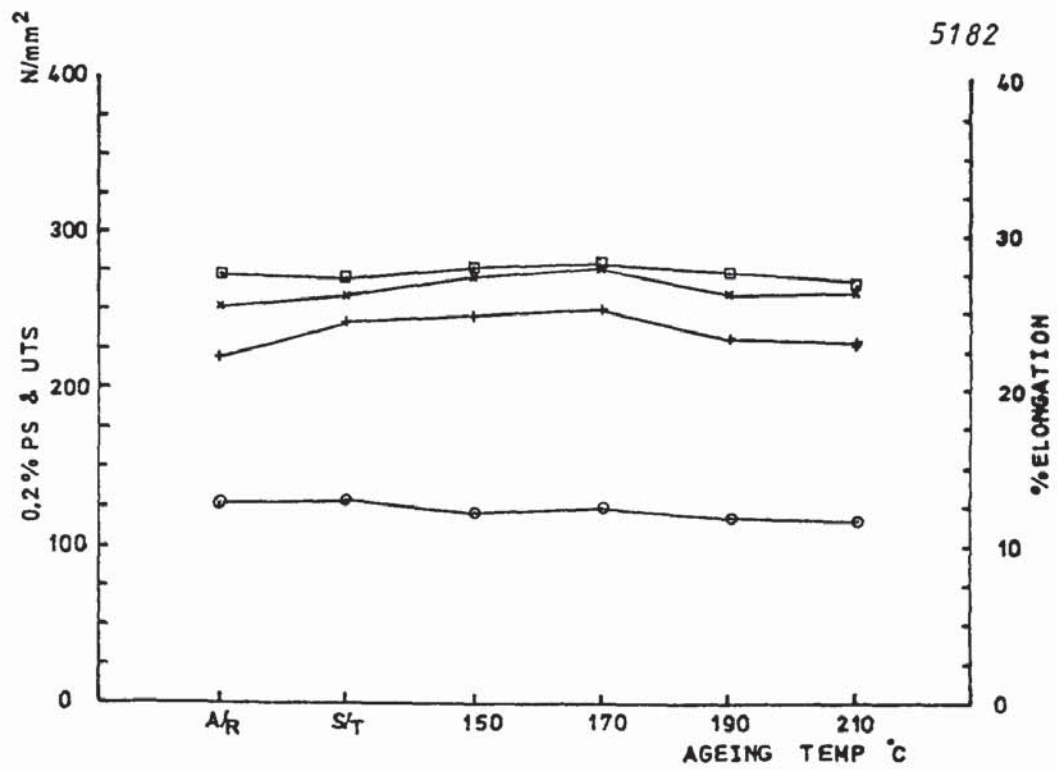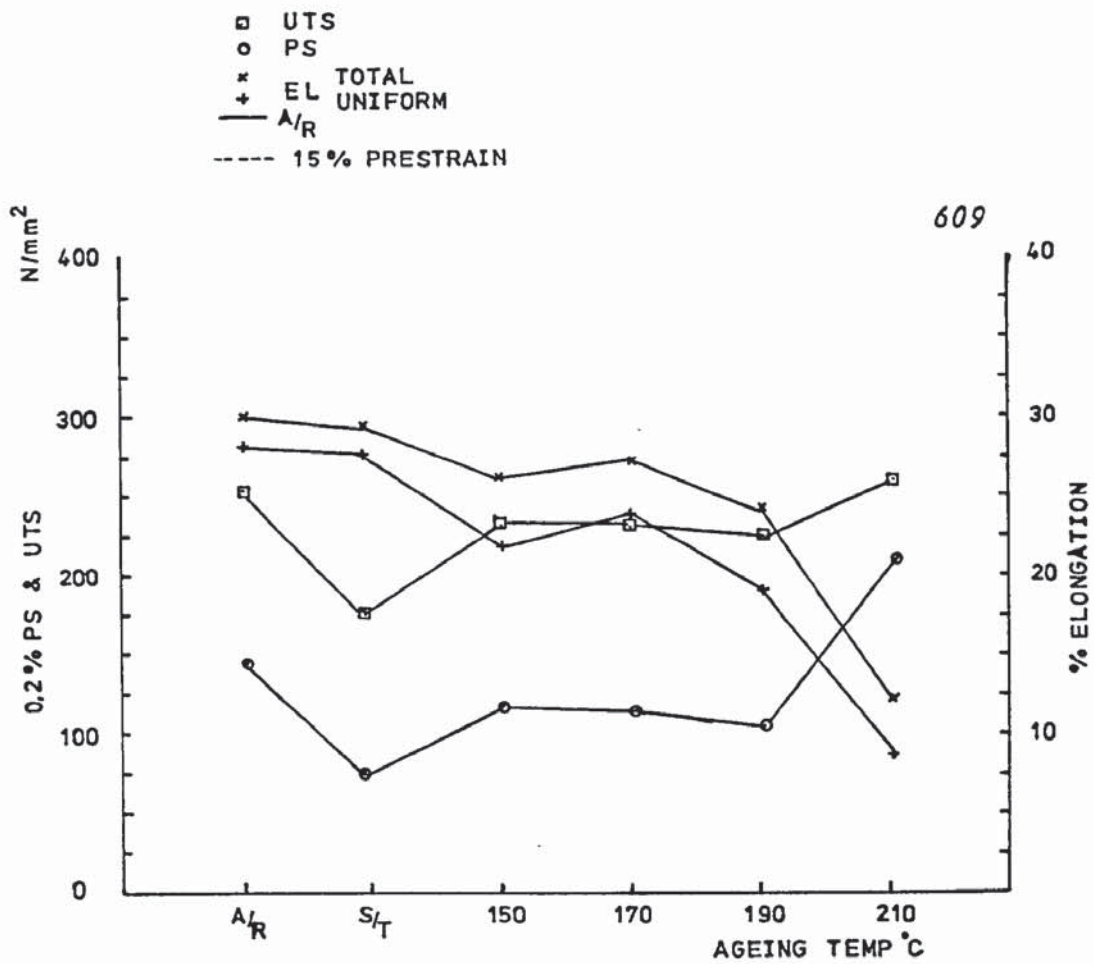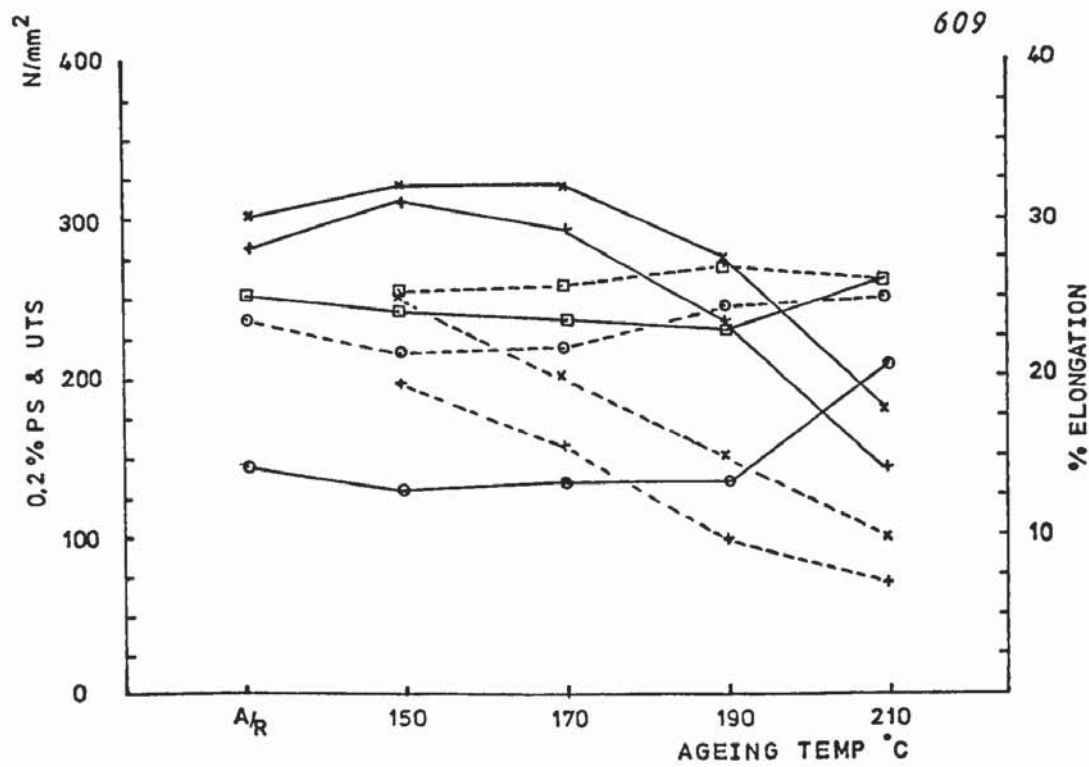
Fig. 22(a)   Average tensile properties of alloys artificially
              aged from the ' as received ' condition for 15 minutes,
              before and after 15% prestrain, at 150 - 210   C

(b)

(c)

(d)

(e)

(f)

(g)

UTS □
PS ○
EL × TOTAL
+ UNIFORM
A/R ———
15% PRESTRAIN -------

BB3

N/mm²

0.2 % PS & UTS

% ELONGATION

A/R   150   170   190   210

AGEING TEMP °C

(h)

2117A

N/mm²

0.2 % PS & UTS

% ELONGATION

A/R   150   170   190   210

AGEING TEMP °C

(i)

(j) 2117 HP

(k) 2117 CP

Legend:
- □ U.T.S.
- ○ P.S.
- × EL TOTAL
- + UNIFORM
- —— A/R
- ----- 15% PRESTRAIN
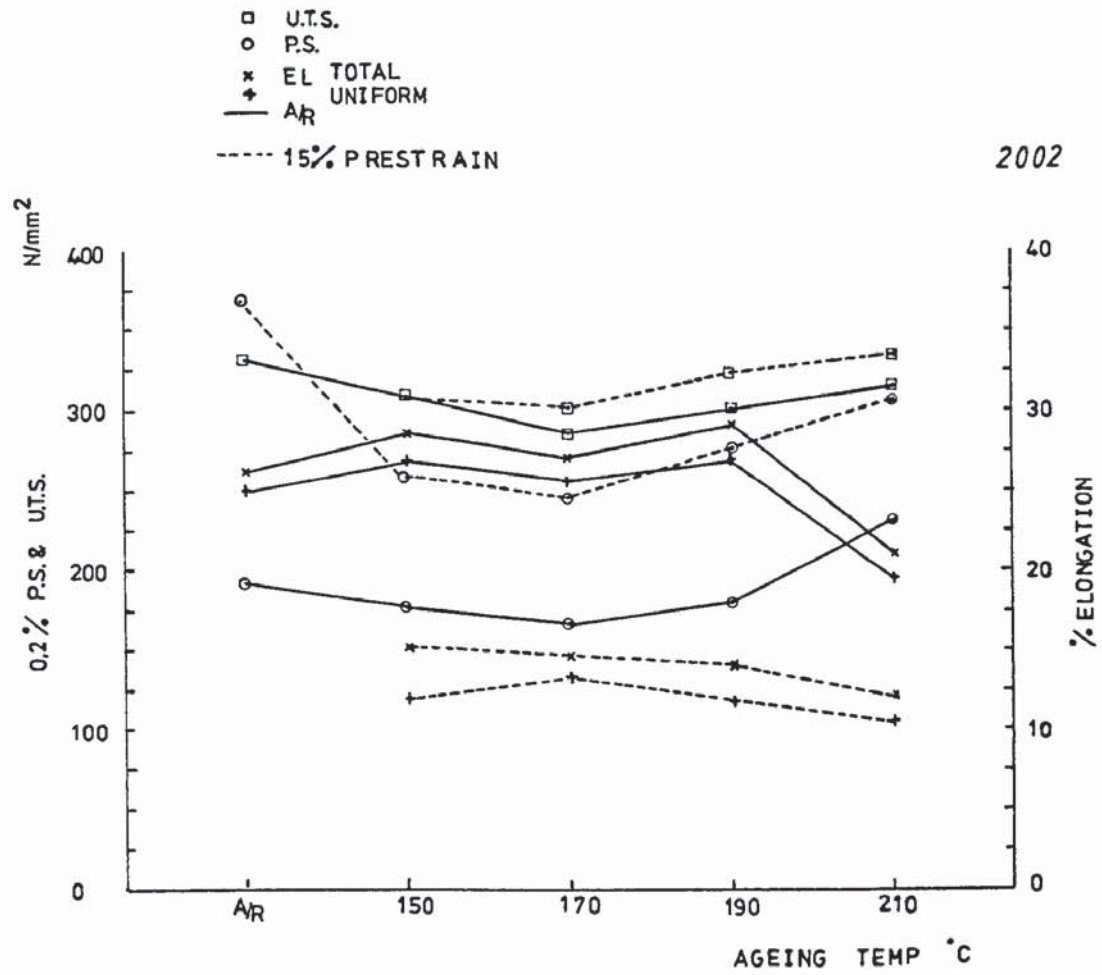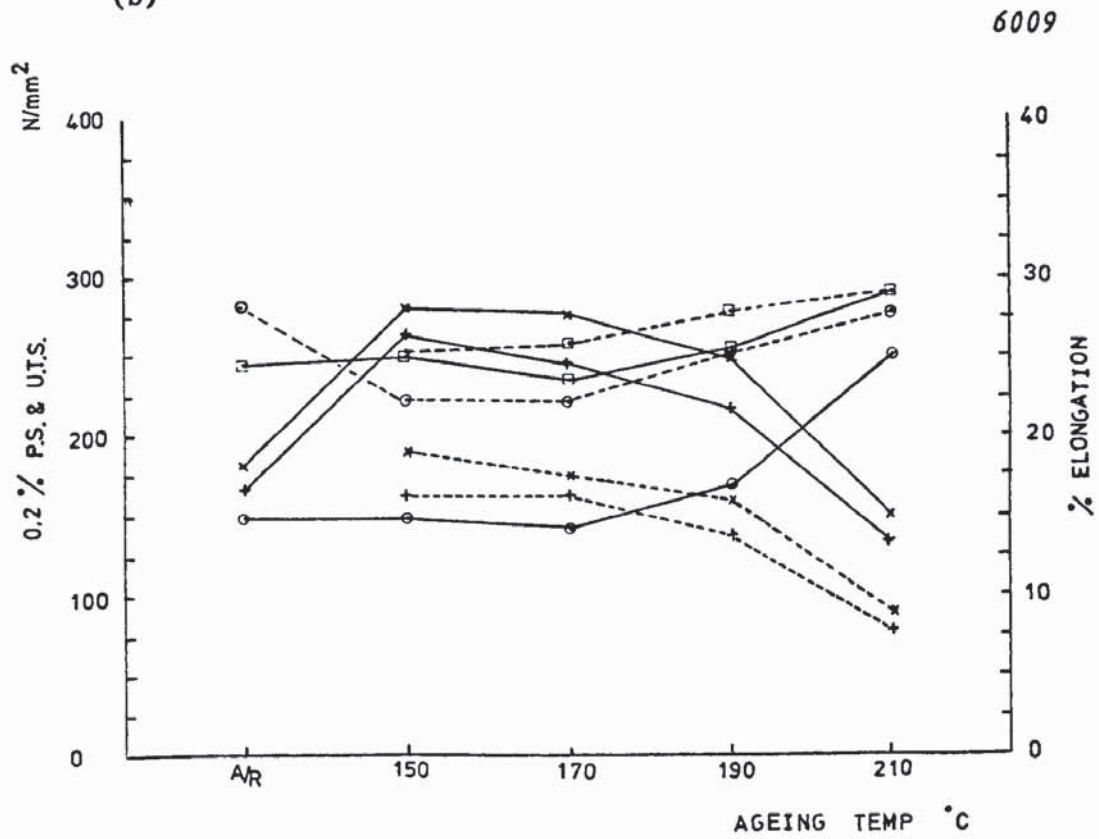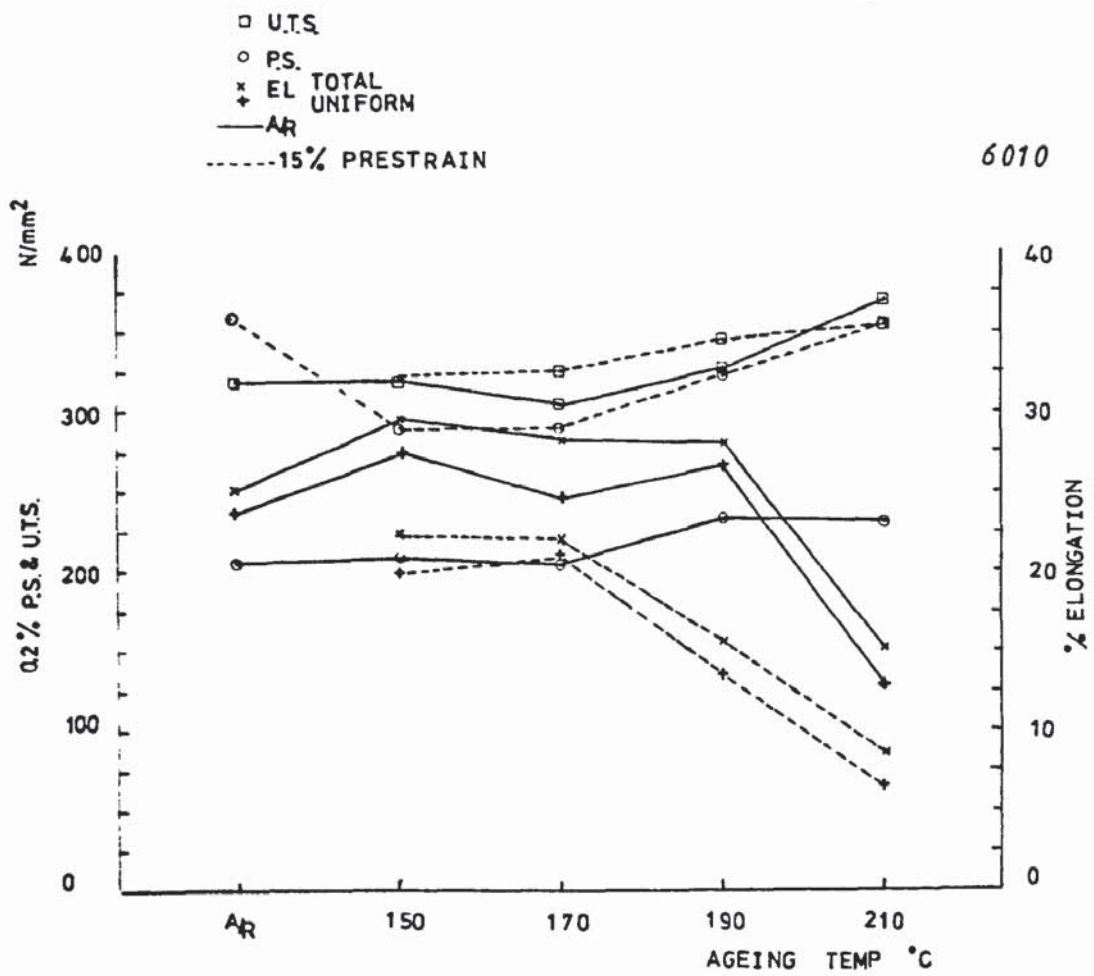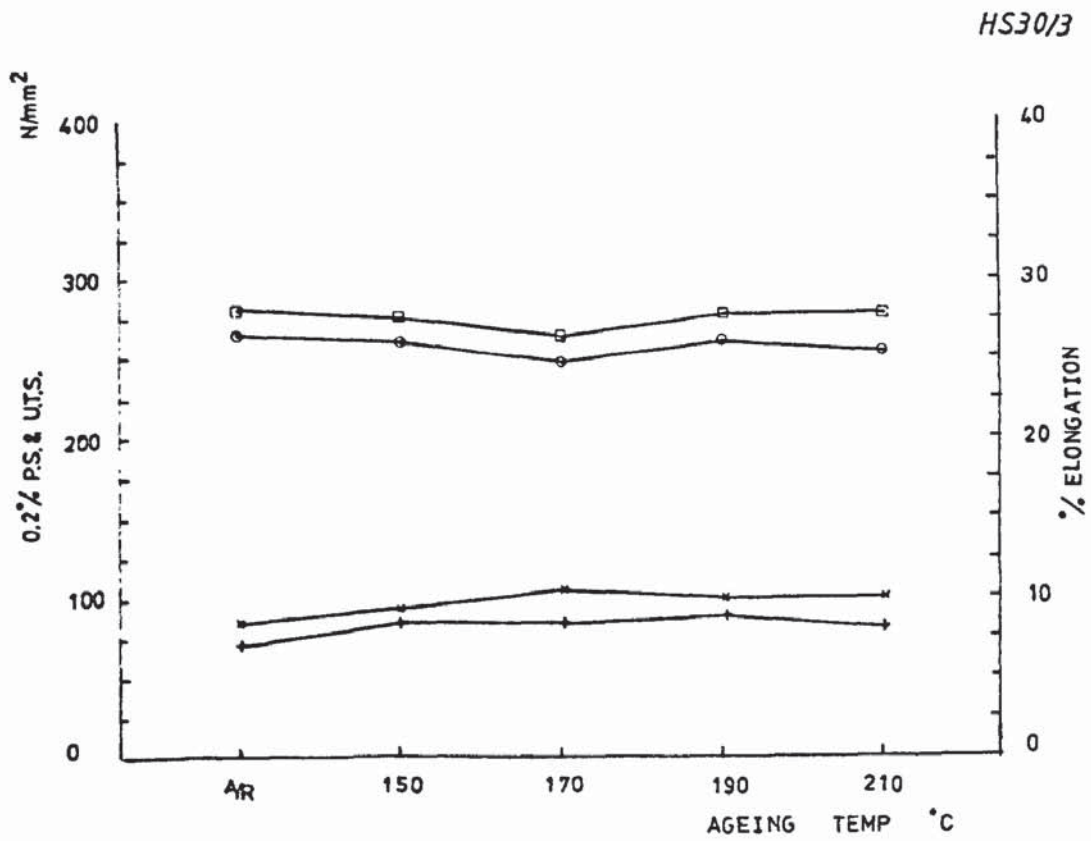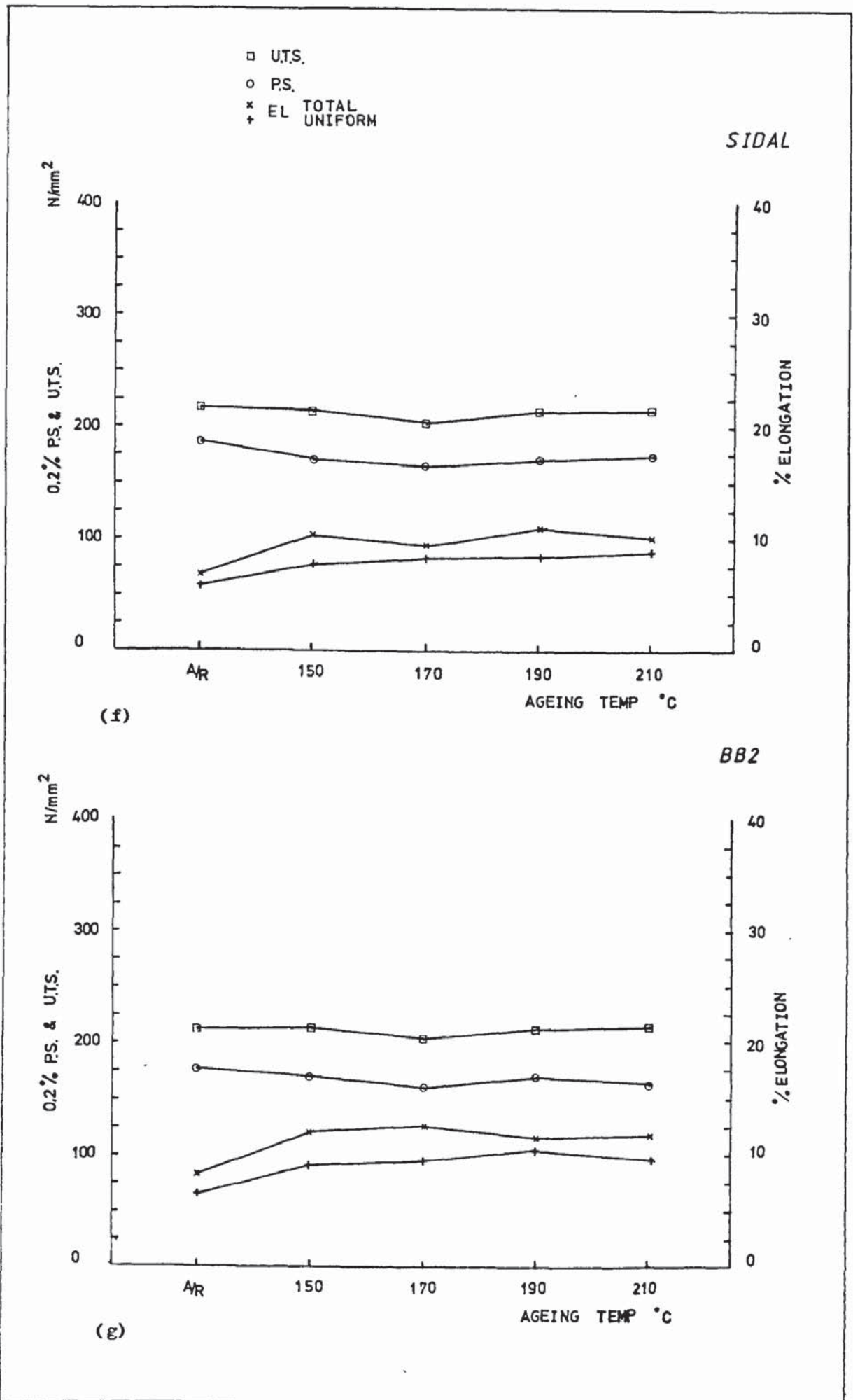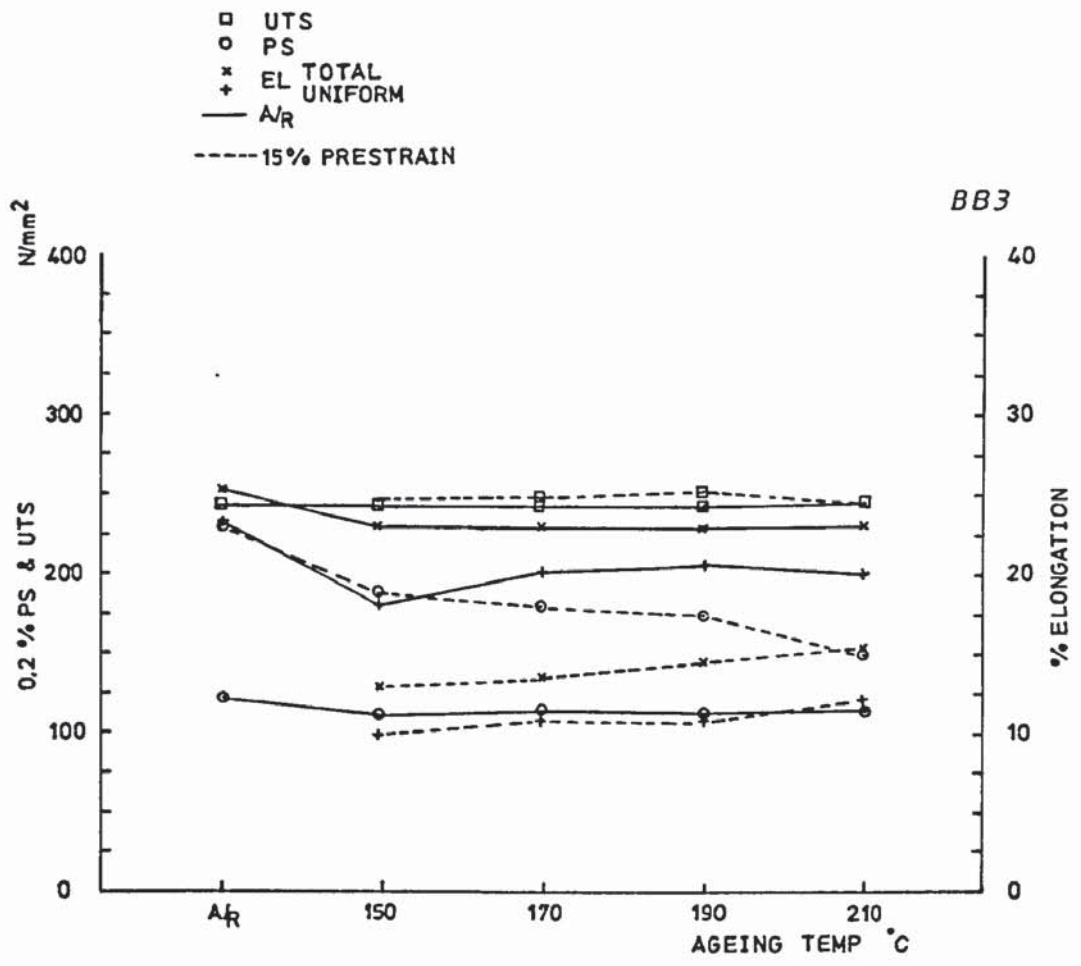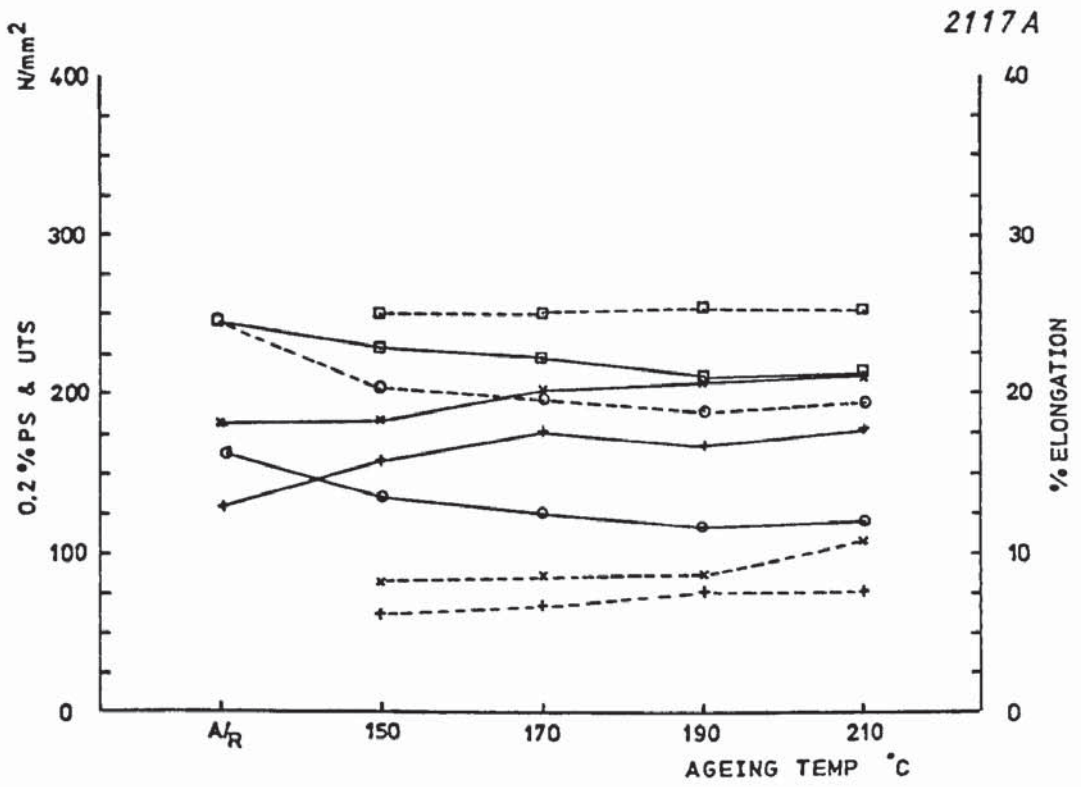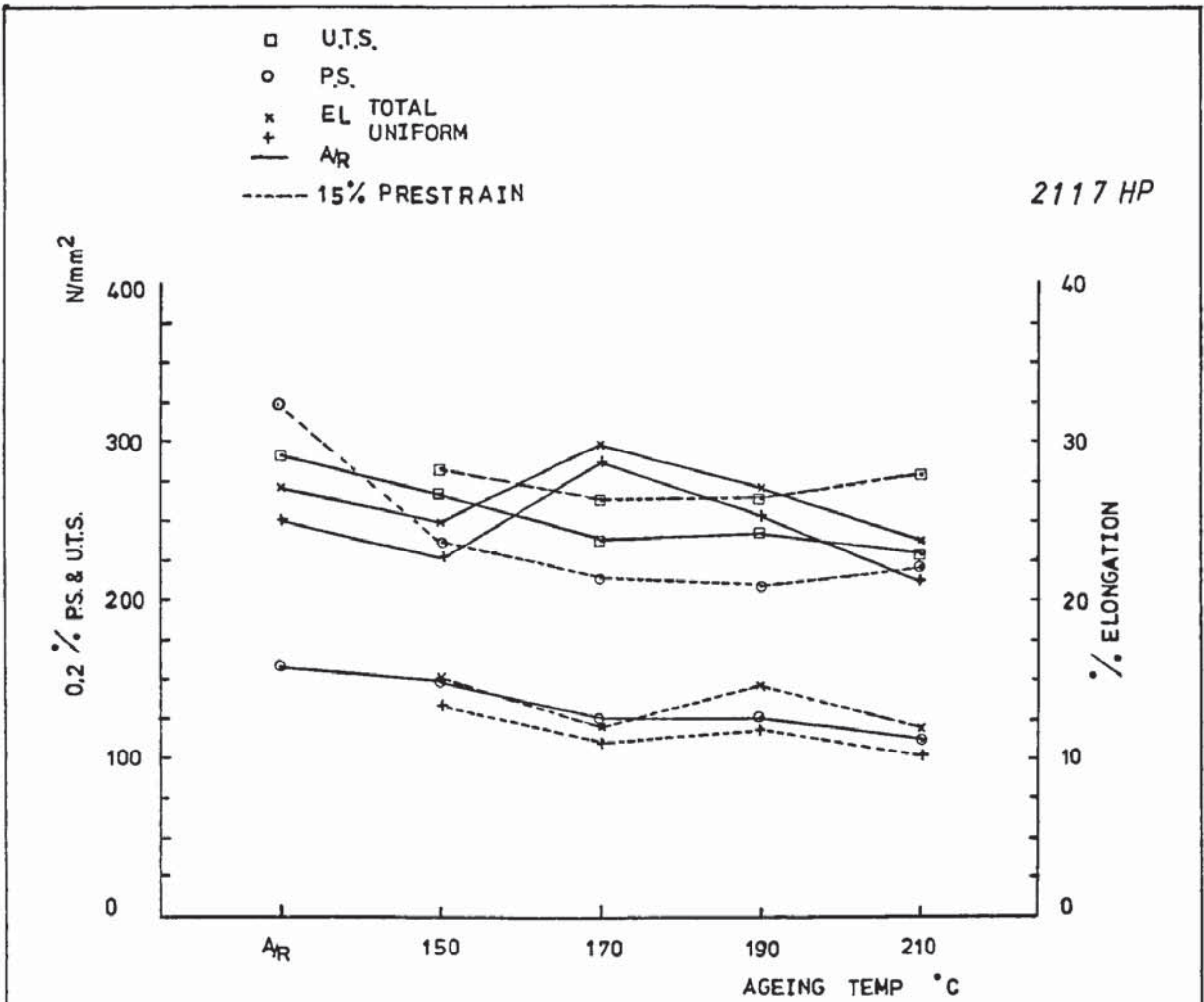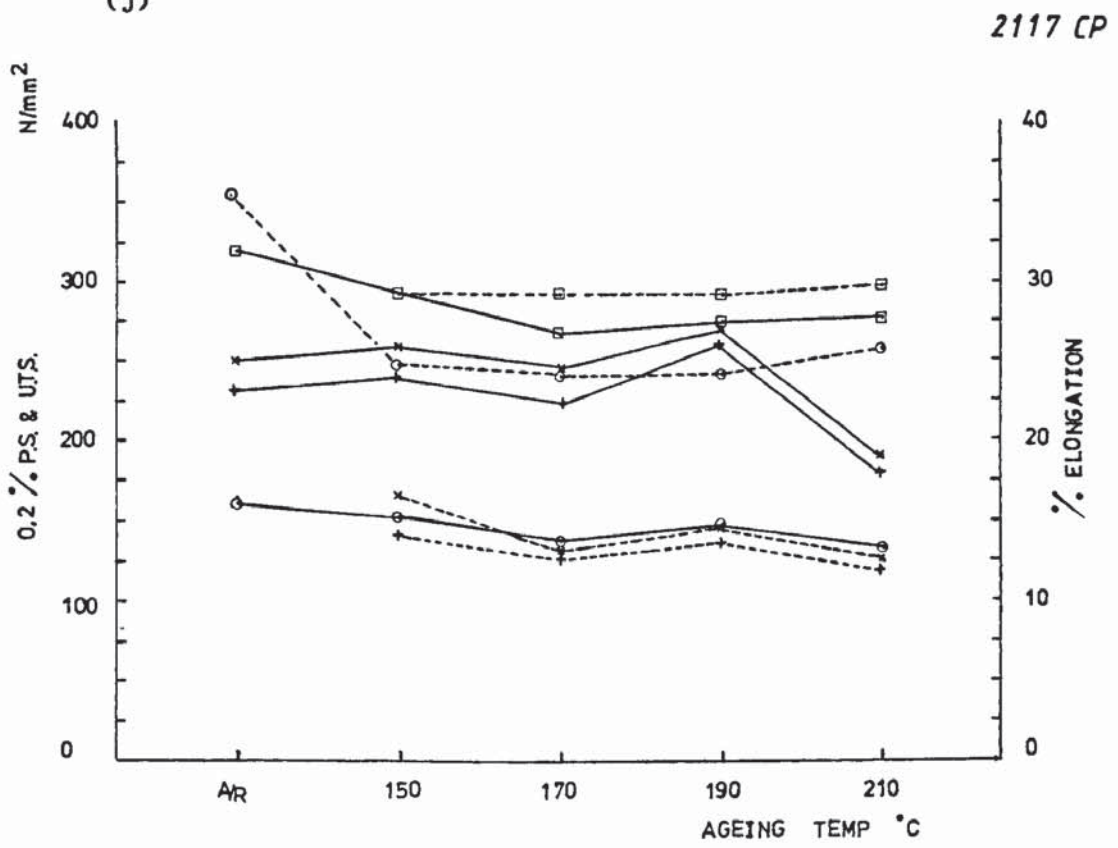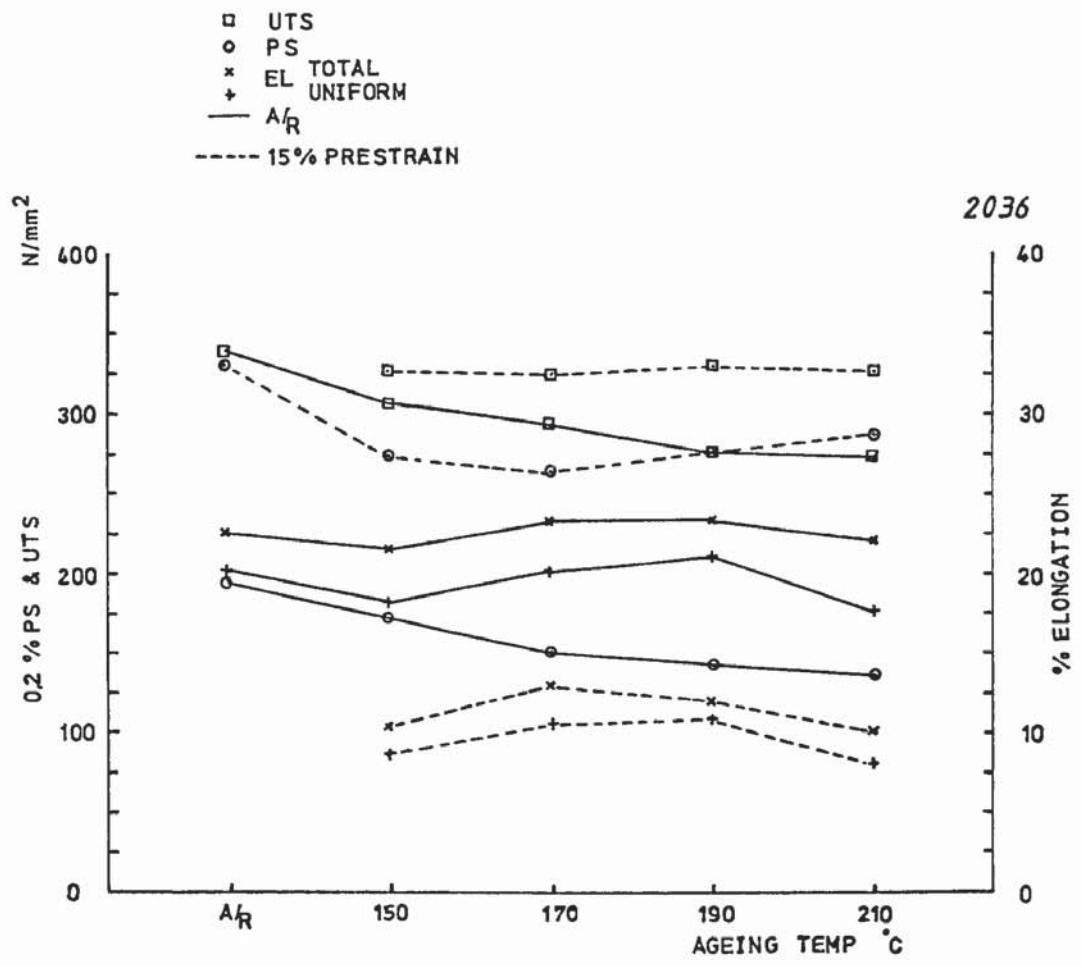
(1)
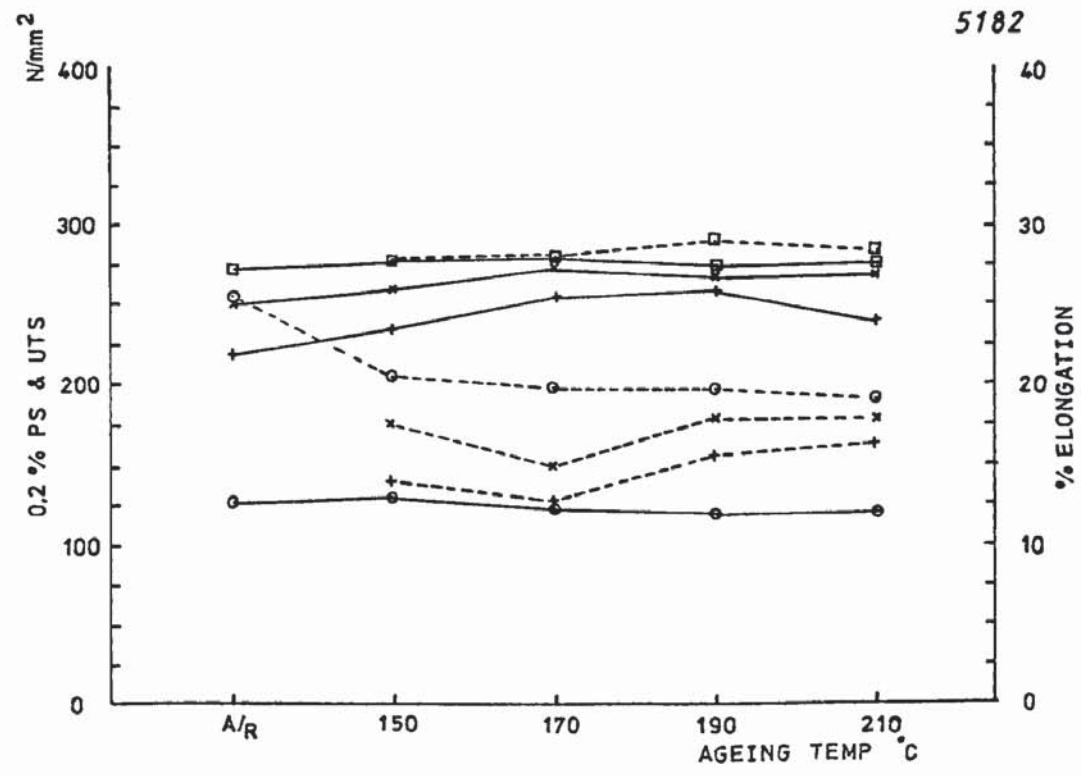
(m)

5.2   Characteristics of Materials Used in Later Work

Of the thirteen alloys investigated during the work of section 5.1,
four were chosen as promising representatives for further research.
These alloys were 6010, 5182, 2117 HP and 2117 CP. They were   .
selected on the basis of mechanical properties and material
availability.

5.2.1   Uniaxial Tensile Test Data

Table 4. restates the average tensile properties for alloys 6010,
5182, 2117 HP and 2117CP. Alloy 5182 is significantly softer than
the other three materials which all behave in a broadly similar
manner. 5182 was the only alloy to exhibit a marked yield point,
its surface showed repeated stretcher-strain lines during tensile
testing. The n-values in table 4. show alloy 6010 to have less
rapid work hardening than the others although its total elongation
is at least as good.

5.2.2 Texture

Figs 23 (a) - (1) show centre textures for alloys in the "as
received" condition. (111), (200) and (220) pole figures are
presented for each alloy.

Alloy 6010 shows a fairly weak texture overall. This consists of
a weak cube texture with weak (110) [112] and (110) [001] components.
5182 has a very weak cube texture with a (100) [001] component. In

comparison, both 2117 alloys exhibit strong textures. 2117 CP shows
a strong retained rolling texture (123) [412] with a strong (110)
[001] component while 2117 HP shows strong (110) [001] and (110)
[112] components. The two texture components identified in 2117 HP
are known to give rise to six fold symmetry. This was confirmed
during deep drawing trials by the presence of 6 fold earing on
drawn cups of this alloy.

5.2.3 Second Phase Particle Size Distributions

Figs 24 (a) - (d) show the size (diameter) distribution of second phase
particles for alloys 6010, 5182, 2117 CP and 2117 HP. Alloy 6010 has a
very narrow particle size distribution with ~ 80% content < 0.8μm and
95% <1.0μm. The number of particles in 6010 is approximately three
times that of 5182 and ten times that of 2117 HP or 2117 CP. These
variations are sufficiently great to affect the fracture behaviour and
forming limits as will be discussed later.

5.2.4 Microstructures

Typical microstructures for alloys 6010, 5182, 2117 CP and 2117 HP are
shown in Figs 25 (a) - (d). Sections were taken through the sheet
thickness. 6010, 2117 HP and 2117 CP have very similar grain sizes,
approximately 20-25μm. The grains have smooth boundaries and are
slightly elongated in the plane of the sheet which may be inpart a result
of temper rolling during production but may also have resulted from
recrystallization in the presence of second phase particles. Alloy
5182 has a grain size about half that of the other alloys.

ALLOY	0.2% Proof Stress (N/mm^2)	U.T.S. (N/mm^2)	% Elongation Uniform	Total	$\bar{r}$	$\bar{n}$	$\bar{K}$ (N/mm^2)
6010	195	327	27.2	28.6	0.59	0.18	475
5182	130	280	25.2	26.2	0.68	0.26	473
2117HP	170	340	25.2	26.4	0.86	0.21	513
2117CP	190	365	24.5	25.6	0.81	0.22	562

Table 4.   Average tensile properties of alloys 6010, 5182, 2117 HP and 2117 CP in the "as received" condition.

Fig. 23(a)-(1)   Centre textures determined for alloys 6010, 5182,
                 2117 HP and 2117 CP showing (111), (200), and (220)
                 reflections.

(d)

5182 (111)

(e)

5182 (200)

(f)

5182 (220)

2117 HP (111)

(g)

2117 HP (200)

(h)

2117 HP (220)

(i)

(j) 2111 CP (111)

(k) 2111 CP (200)

(l) 2111 CP (220)
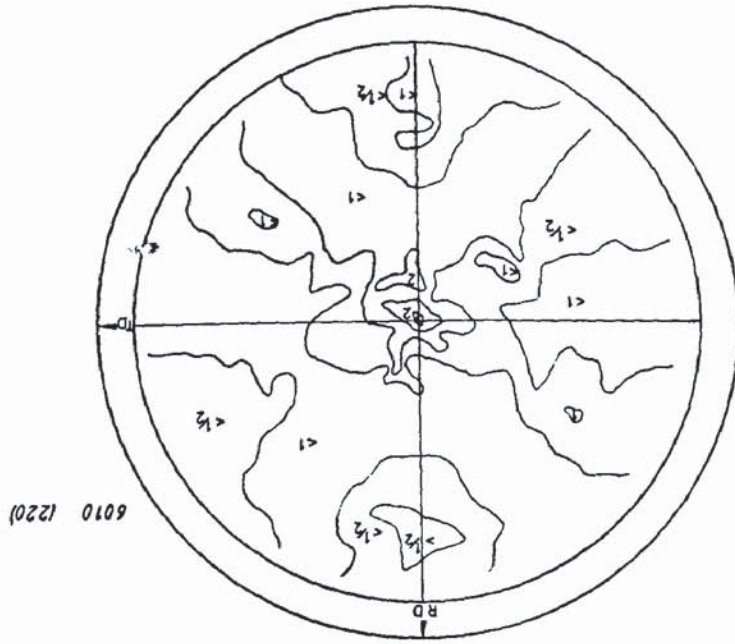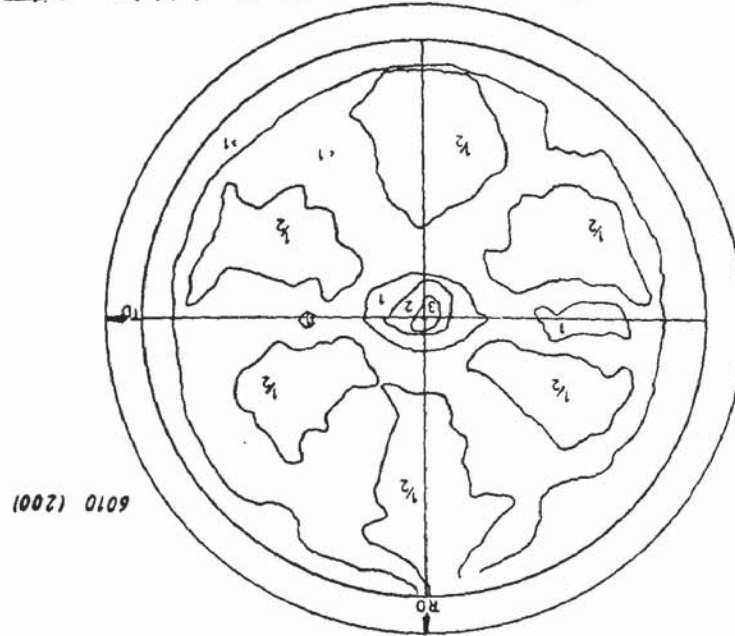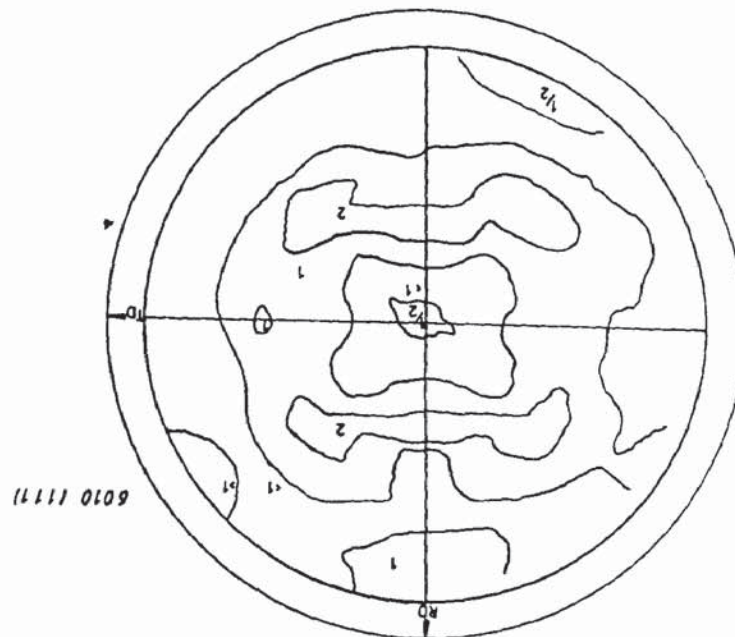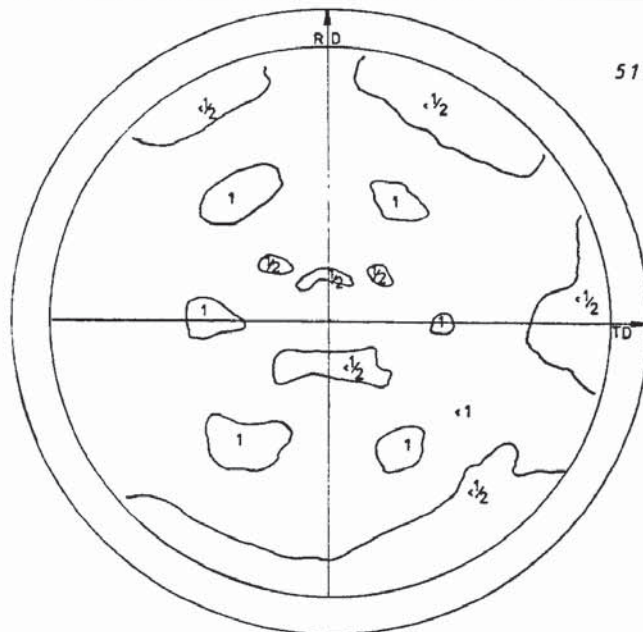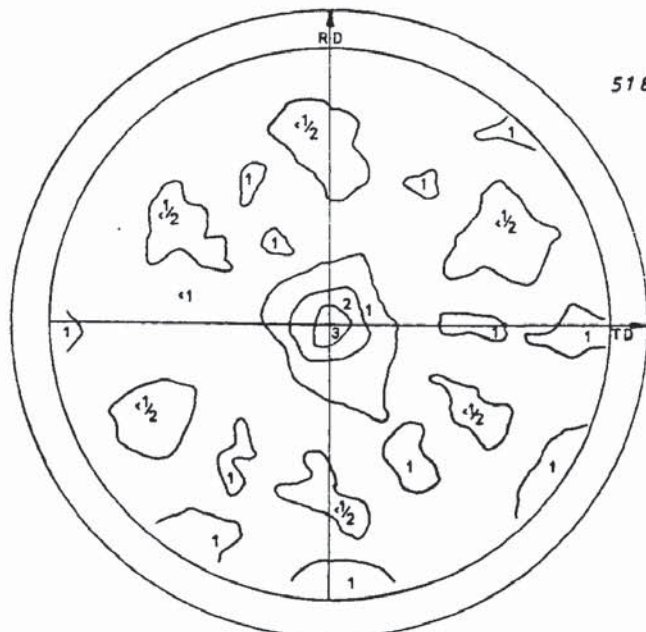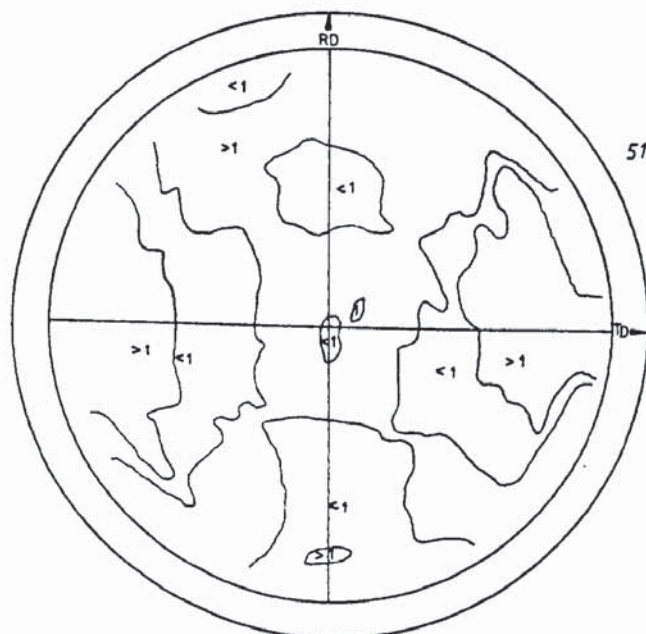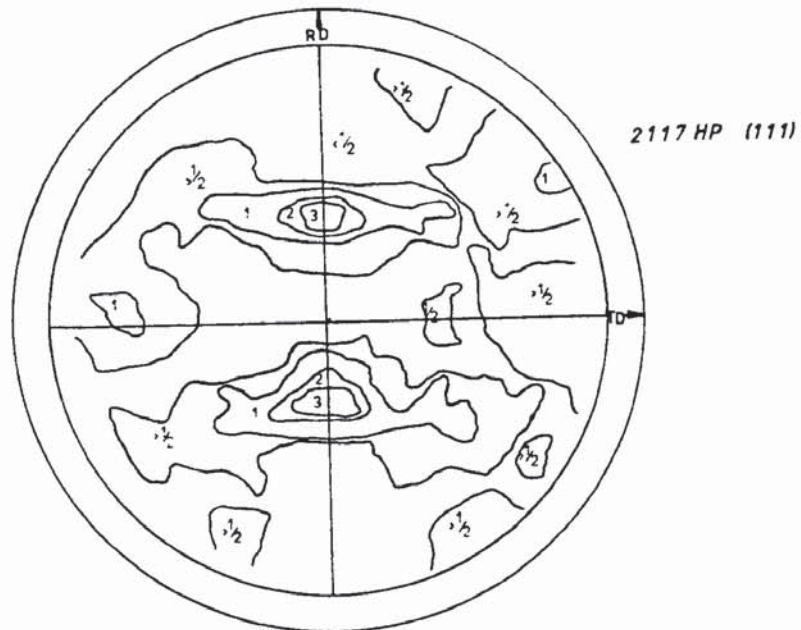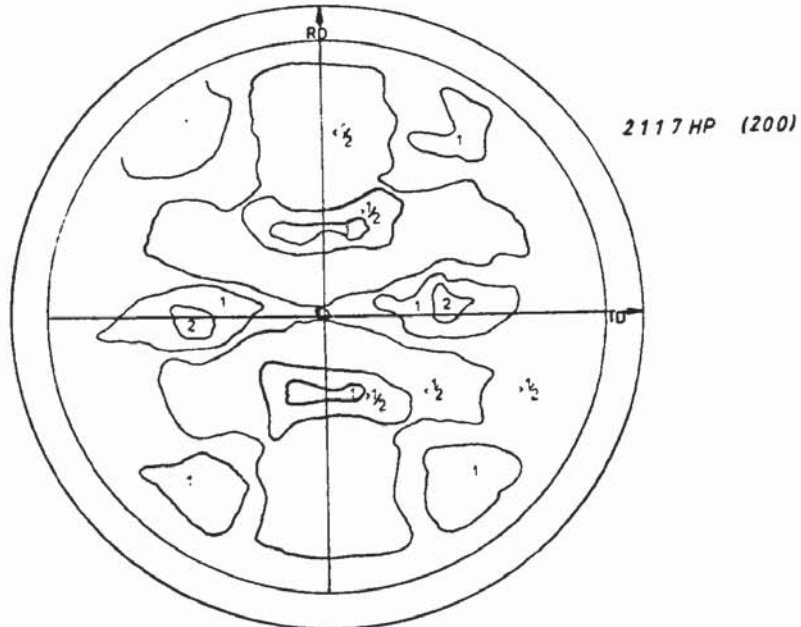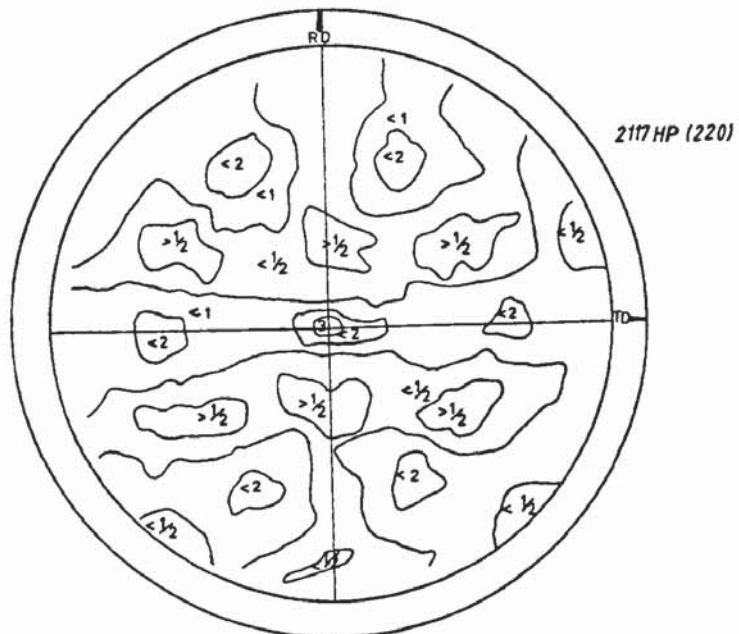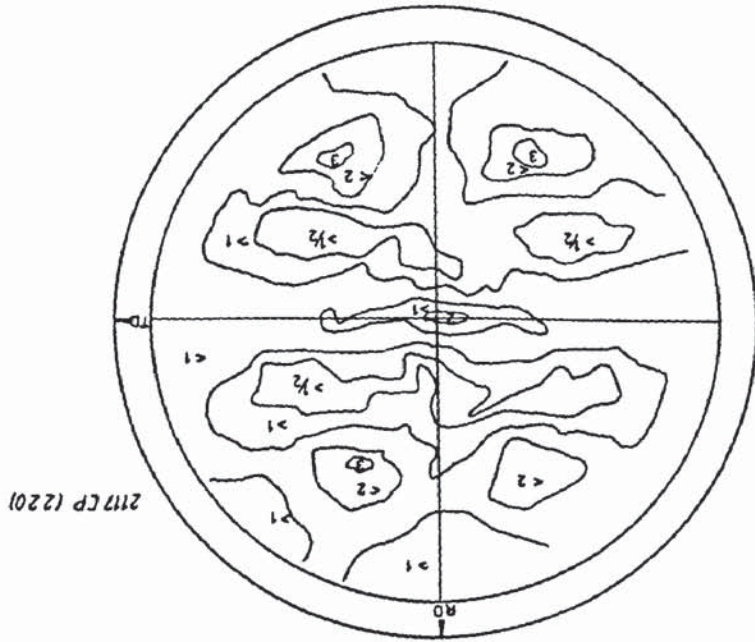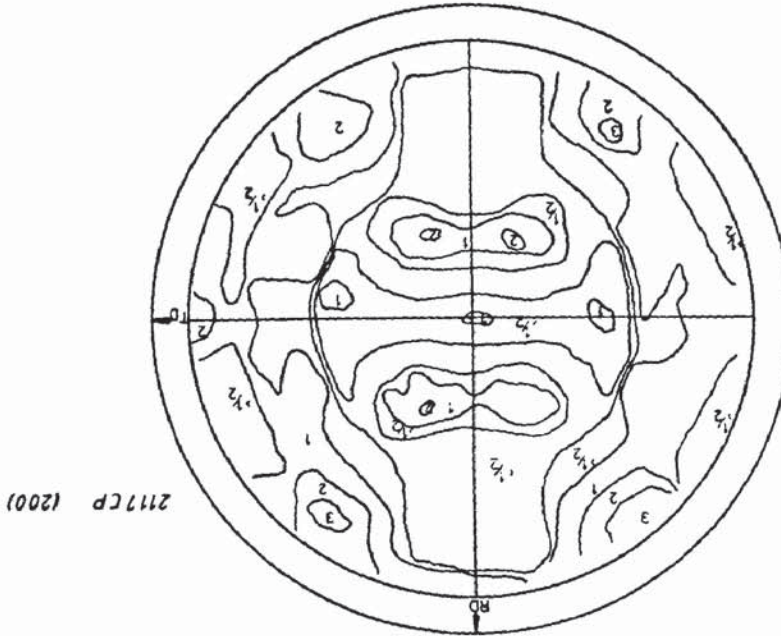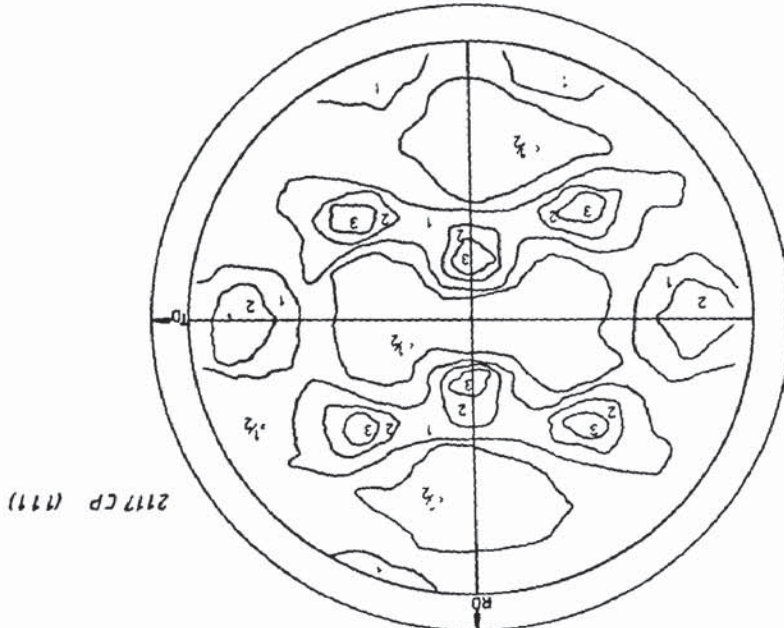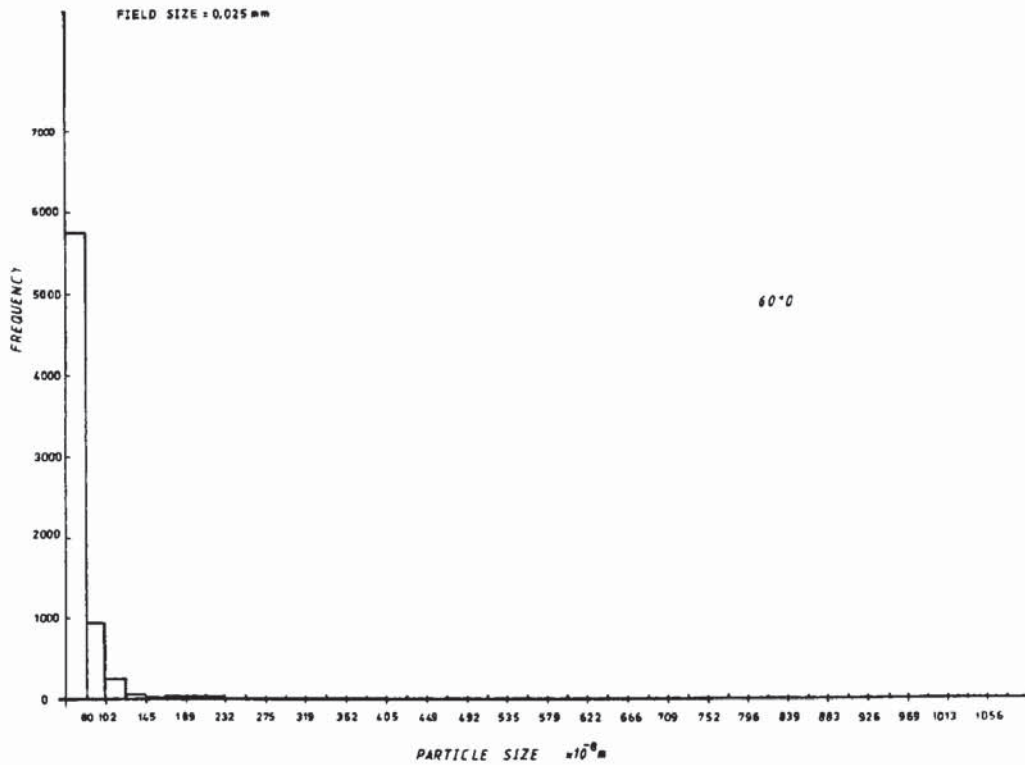
Fig. 24(a)   Size (diameter) distribution of second phase
              particles in alloys 6010, 5182, 2117HP, and
              2117CP.

(b)

FIELD SIZE = 0.025 mm

2117 HP

FREQUENCY

300

200

100

80 102 145 189 232 275 319 362 405 449 492 535 579 622 666 709 752 796 839 883 926 969 1013 1056

PARTICLE SIZE $\times 10^{-8}$ m

(c)

FIELD SIZE = 0.025 mm

2117 CP

FREQUENCY

400

300

200

100

80 102 145 189 232 275 319 362 405 449 492 535 579 622 666 709 752 796 839 883 926 969 1013 1056

PARTICLE SIZE $\times 10^{-8}$ m
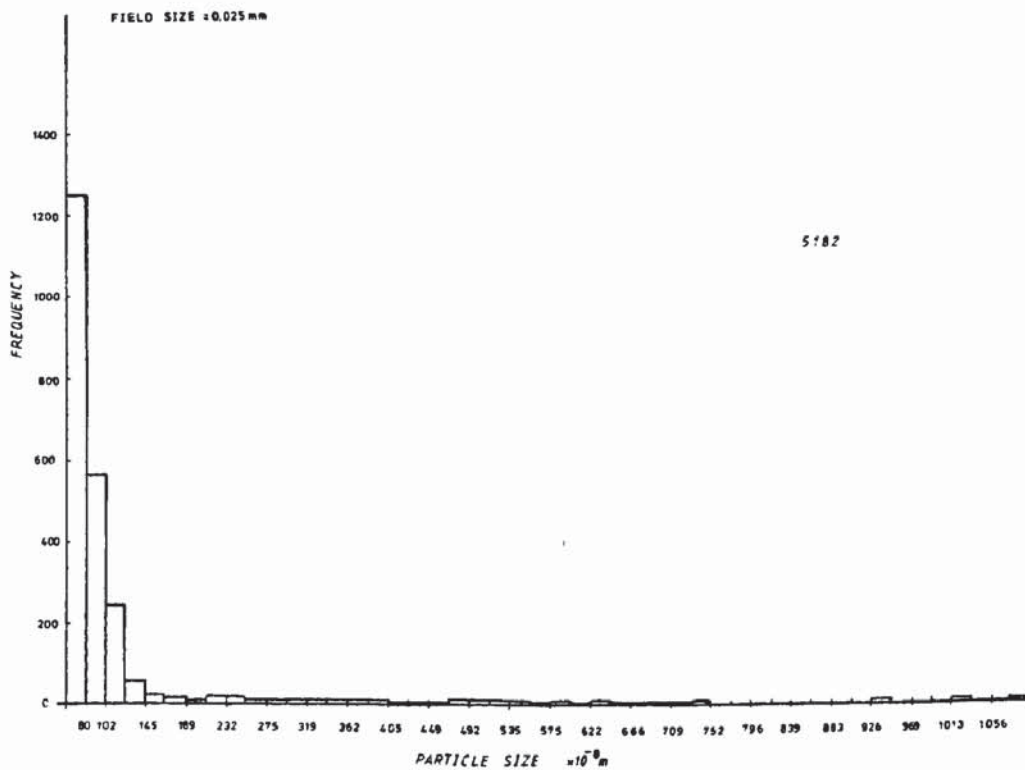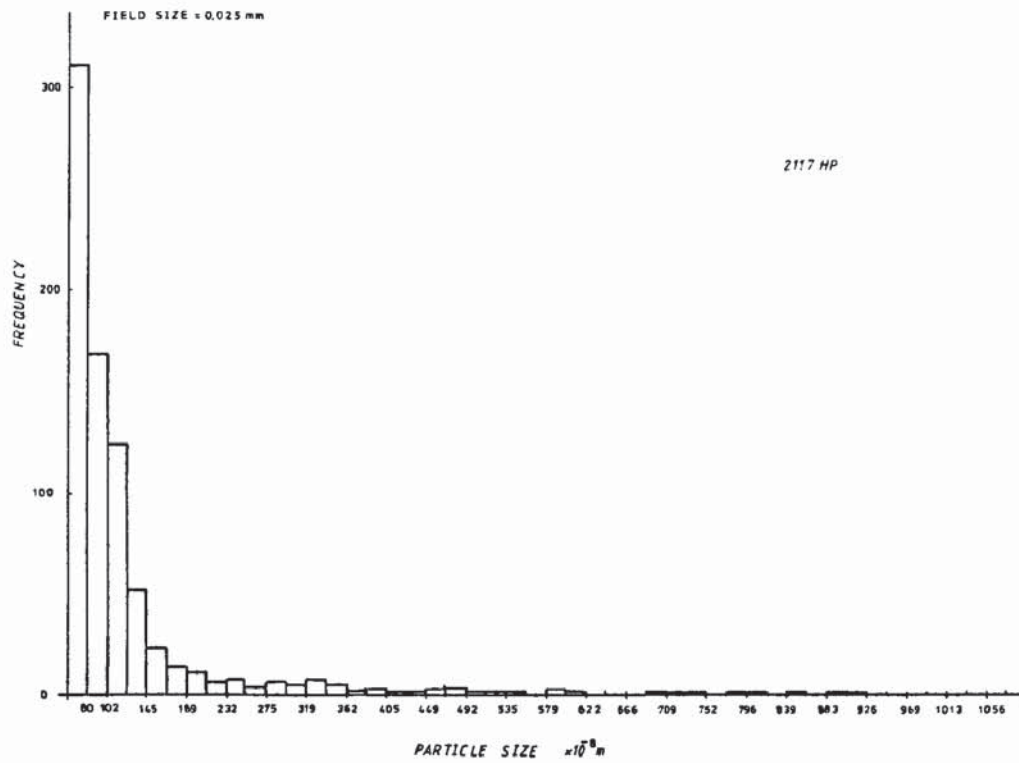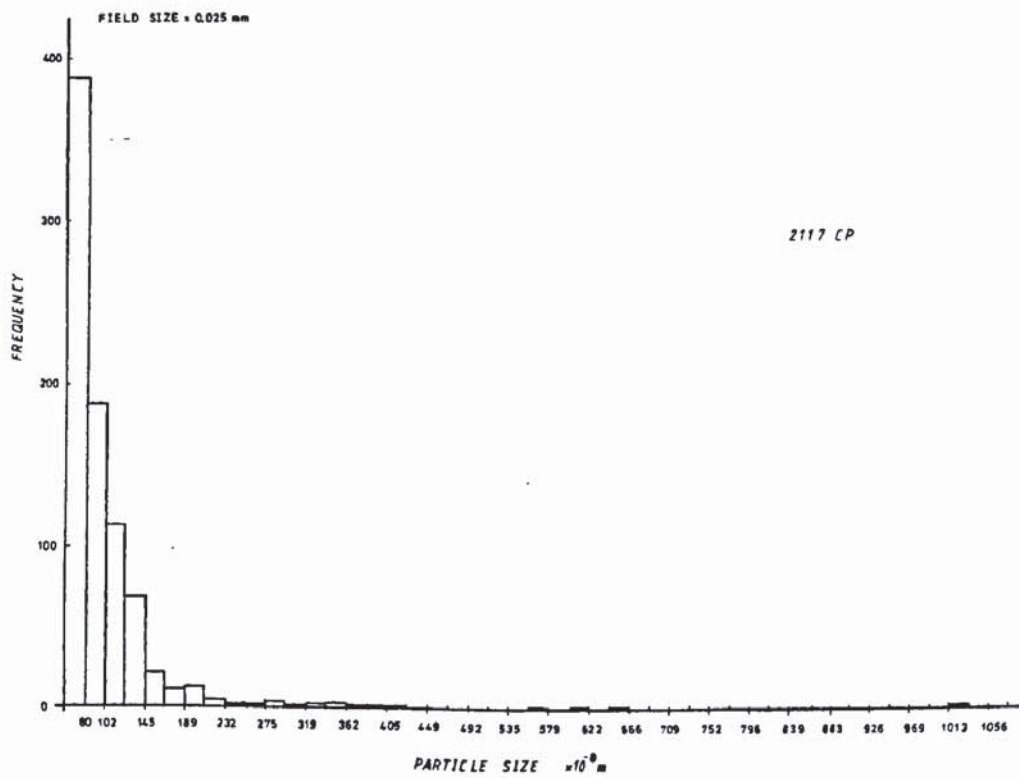
(d)

Figs 25(a)-(d)   Typical microstructures of alloys (a) 6010,
(b) 5182, (c) 2117 HP and (d) 2117 CP.
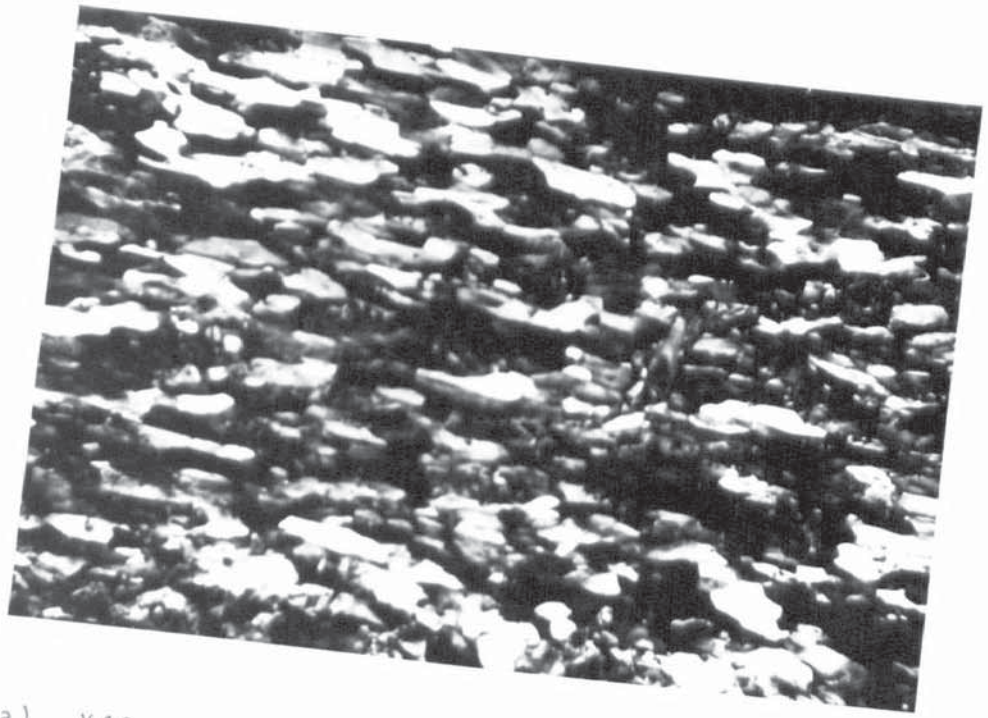
Fig. 25(a) X40
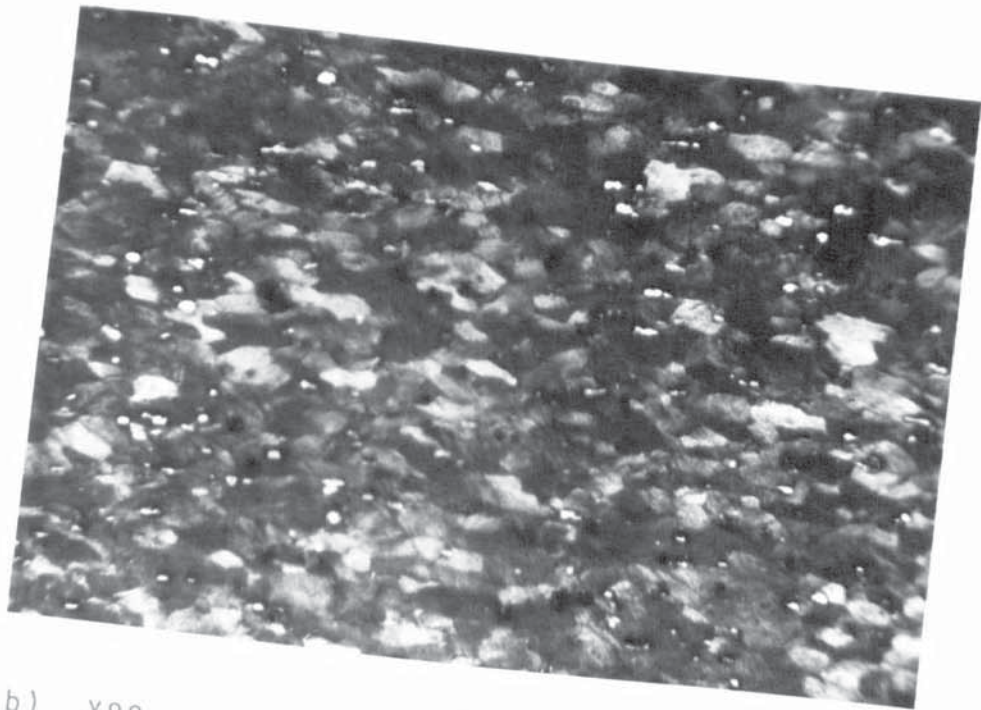
(b) X80
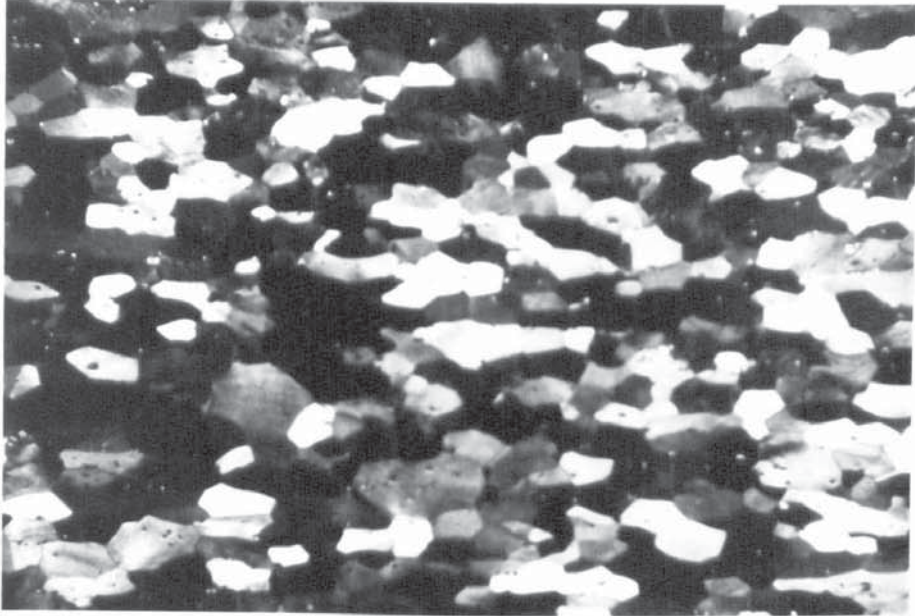
(c) X40
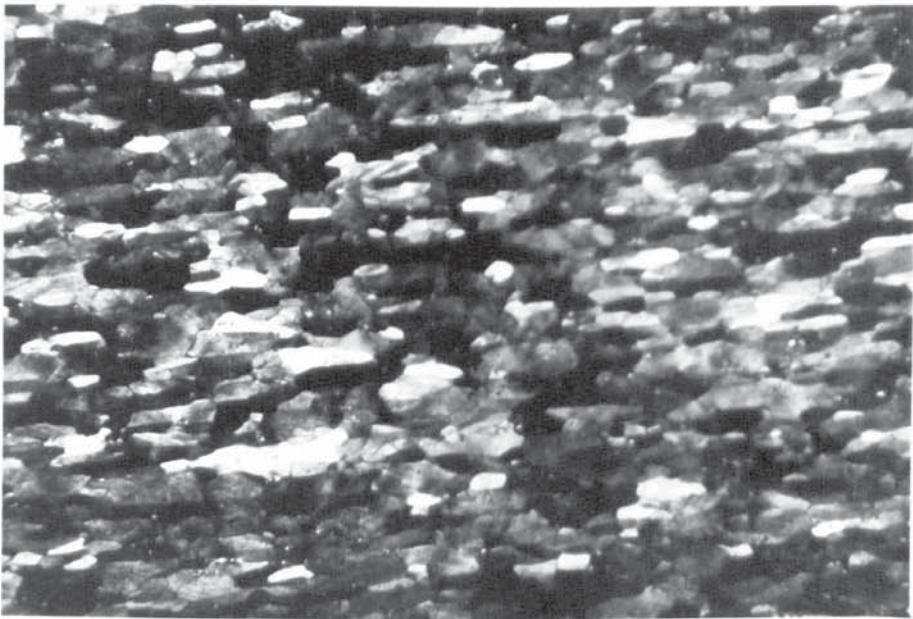
(d) X40

5.3   Strain Hardening and Strain Distribution

5.3.1   Extended Straining Beyond Load Instability

Figs 26 (a) - (c) show the nominal stress-strain curves for alloys
6010, 2117 HP and 2117 CP during extended uniaxial tensile straining.
The initial part of the curves represents data obtained during normal
uniaxial tensile testing to strains of ~ 24%. The later part of the
curves, strains above ~ 24%, represents data obtained during extended
tensile testing. It is apparent that around 25% elongation the work
hardening capacity of the alloys no longer compensates for the reduction
in cross section and at this point necking would normally occur.
However, due to the restrictions imposed on the test piece, necking is
postponed and straining continues by as much as a further 20-25%. During
this period the load is found to decrease steadily.

Curves for test pieces cut at 0° and 90° to the sheet rolling direction
are shown and the results suggest that alloy 6010 possesses very little
mechanical directionality. The other alloys show consistently that
longitudinal specimens possess increased strength and reduced ductility
when compared with specimens cut in the transverse direction. The
difference between the stress levels of the transverse and longitudinal
curves remains constant over the entire strain range indicating that
the work hardening capacity is almost identical for the two directions.

Figs 27 (a) - (c) show true stress (σ_t) - true strain (ϵ) curves for

equi-biaxial and uniaxial tensile tests. The equi-biaxial σ_t/ϵ curve remains significantly above the uniaxial tensile curves for alloy 6010 and 2117 CP. However, uniaxial and equi-biaxial curves coincide for alloy 2117 HP. No satisfactory explanation for this inconsistency has been formulated and error in the experimental technique can not be ruled out. In the case of 2117 HP a plot of σ_t vs ϵ using the Hollomon equation was found to be in excellent agreement with both the equi-biaxial and tensile curves when values of $n = 0.21$ and $k = 513$ were used. This suggests that extrapolation of tensile σ_t/ϵ curves into high strain regimes would be a valid exercise providing experimental and theoretical curves coincided over the normal tensile strain range.

Data on alloy 5182 were not included because serrated yielding prevented accurate measurements of load for this alloy. Also, due to its susceptability to Luders banding it was found that adhesion between the tensile test specimens and backing strips was limited. Usually, this alloy was found to fail at strains only marginally larger than those achieved during normal tensile testing.

5.3.2 Strain Development During Hydraulic Bulge Testing

Fig 28 shows the pattern of major strains for a row of grid circles on 2117 CP sheet bulged through a circular die (118mm diameter orifice) at various pressure increments. The radial line along which strains were measured traversed between the pole and edge of the dome and was positioned so as to cross the fracture site in the area of initiation. It can be seen that upto strains close to fracture no indication of the fracture site is apparent. The fracture is marked by a large

increase in strain similar to that shown in Fig 29. It may be concluded that failure is by a sudden catastrophic process rather than the gradual formation of a local non-uniformity.

Fig. 29 illustrates the relationship between major and minor strain versus distance from the site of fracture initiation. The results shown in this figure relate to failure in an aluminium sheet stretched over a 50mm hemispherical punch. Major strains show a much greater variation in magnitude than minor strains especially in the region immediately adjacent to the fracture site. This suggests that a plot of minor strain versus bulge height would result in a limiting dome height curve exhibiting a significantly reduced degree of scatter. The reproducability of such a curve might therefore be greatly improved.

Fig. 30 shows an almost linear variation in bulge height with increasing pressure. The curves are found to differ primarily as a consequence of varying sheet thickness.
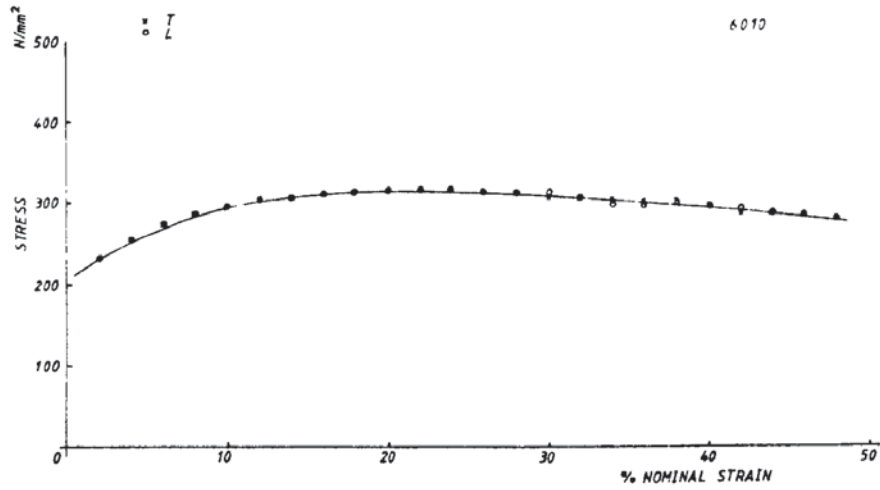
Fig. 26(a) Nominal stress – strain curves for equi-biaxial and uniaxial tensile tests.
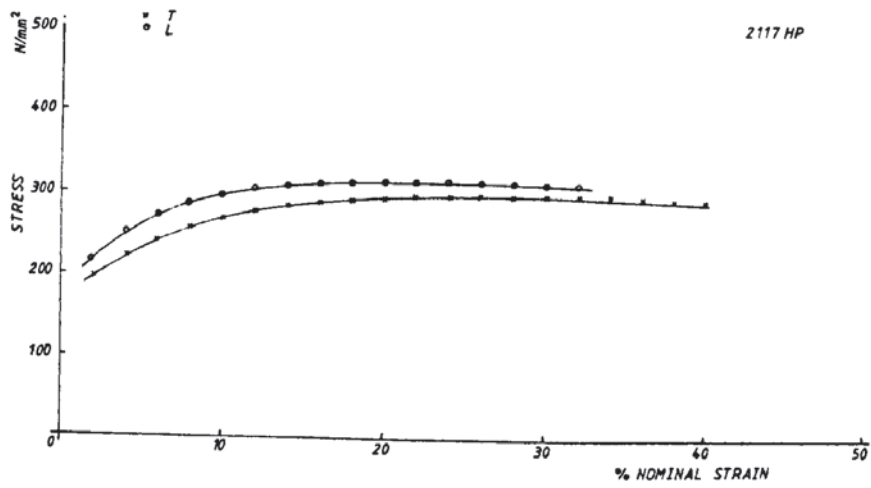
(b)
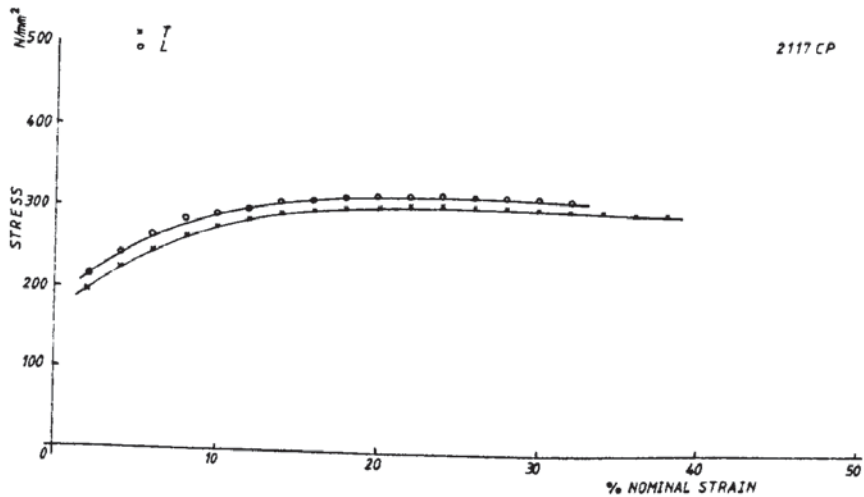
(c)
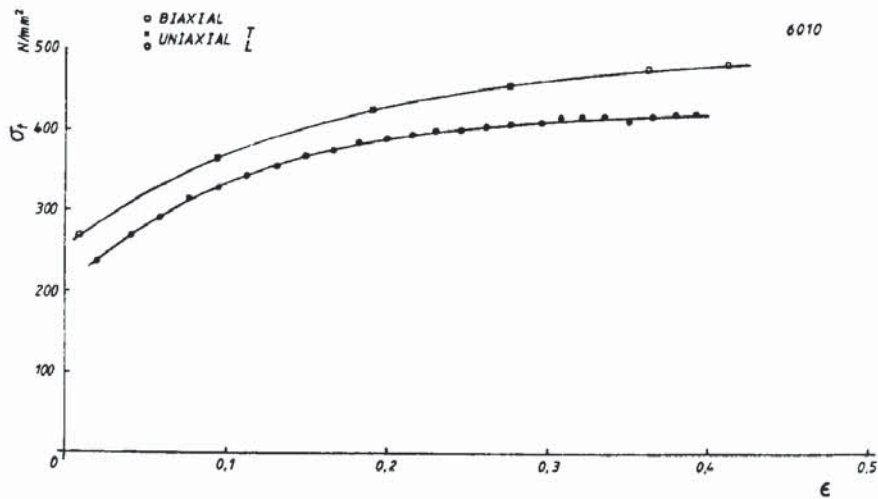
Fig. 27(a)   True stress – strain curves for equi-biaxial
              and uniaxial tensile tests.
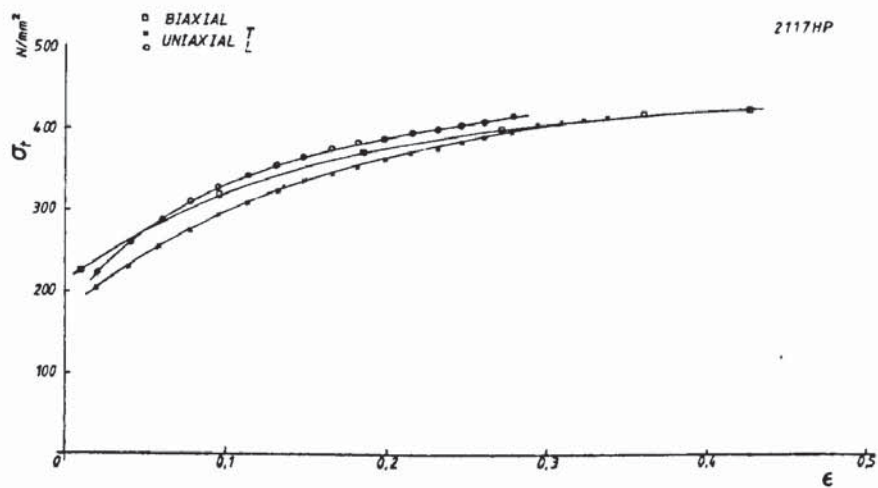
(b)
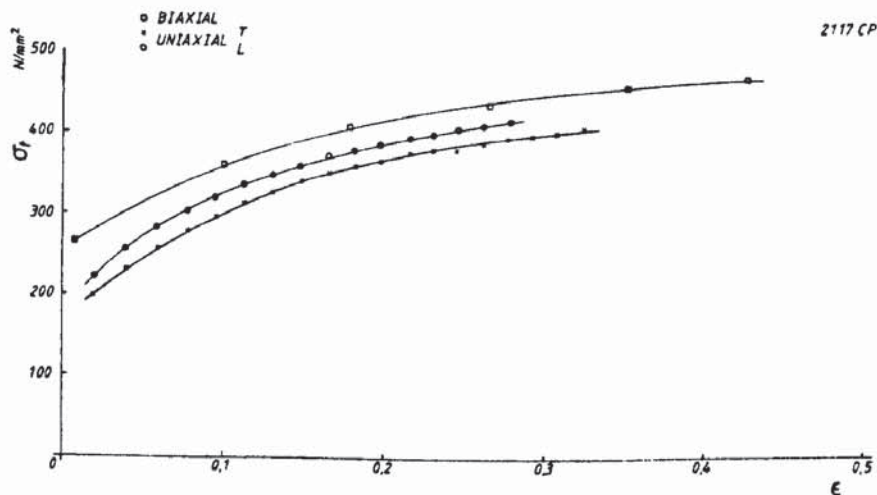
(c)
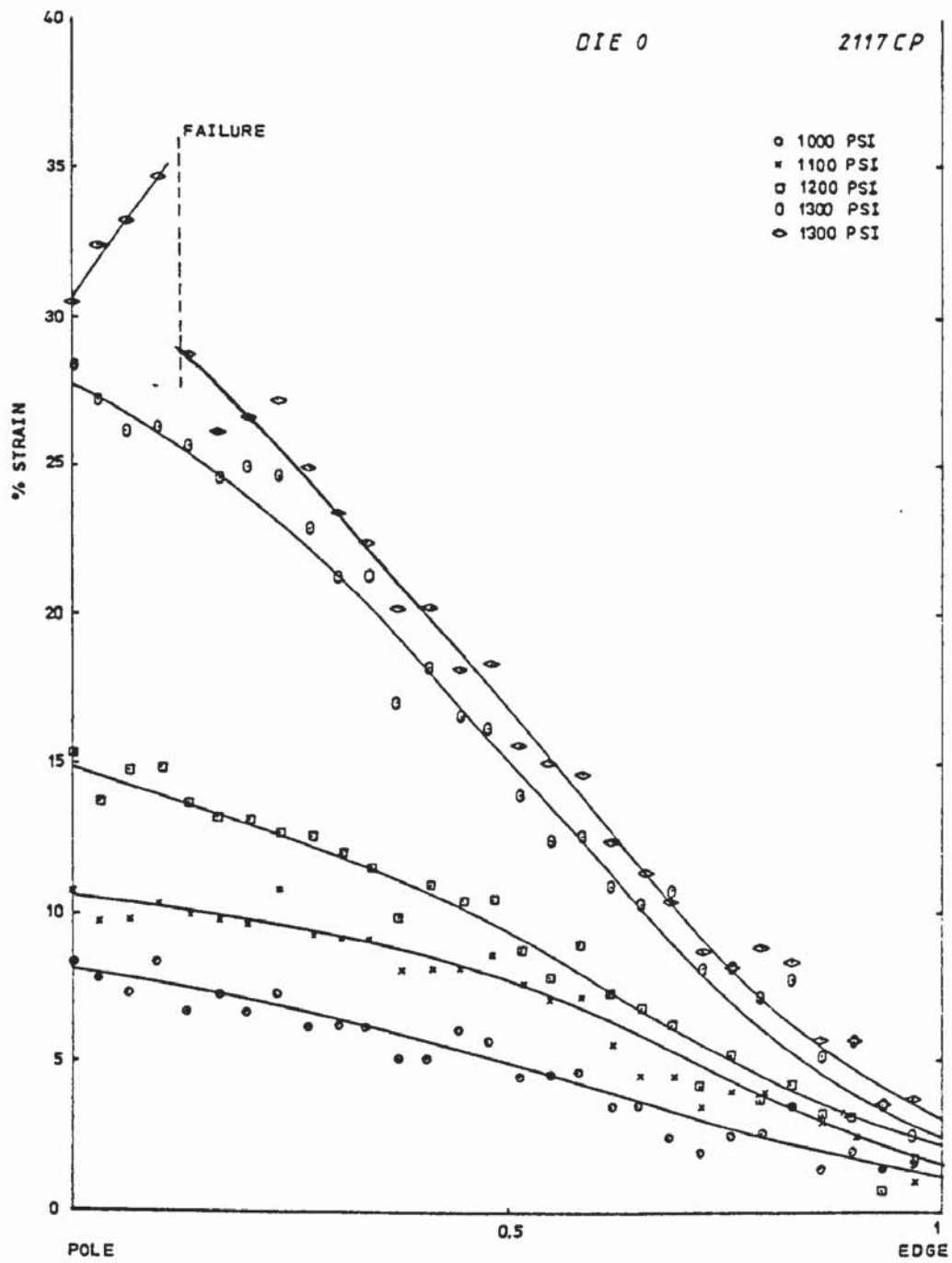
Fig. 28   Pattern of major strains for a row of grid circles
on 2117CP sheet bulged through a circular die at
various pressure increments.
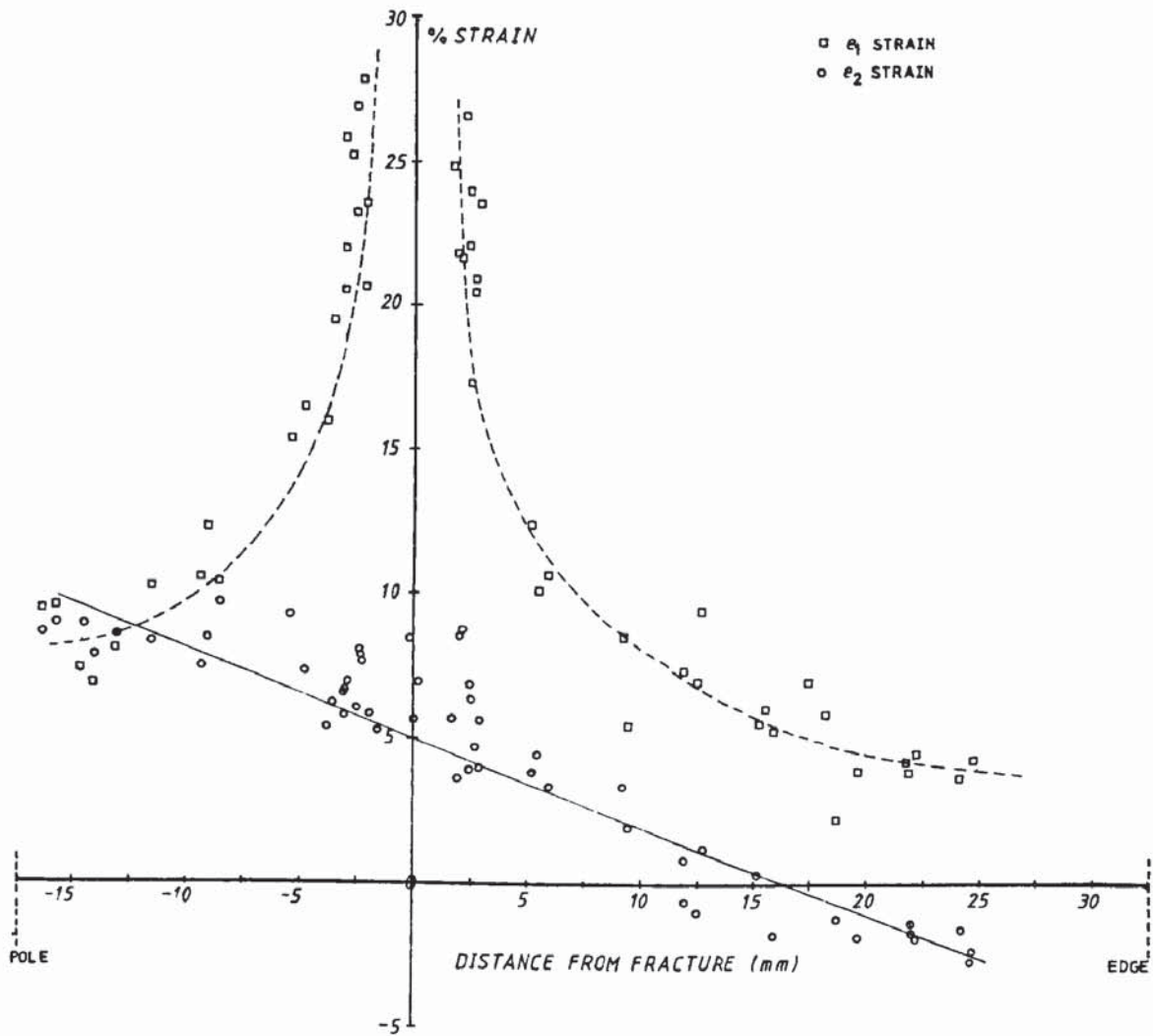
Fig. 29   Plot of major (e_1) and minor (e_2) strains versus distance, wrt fracture site, for a 50mm diameter hemispherical cup.
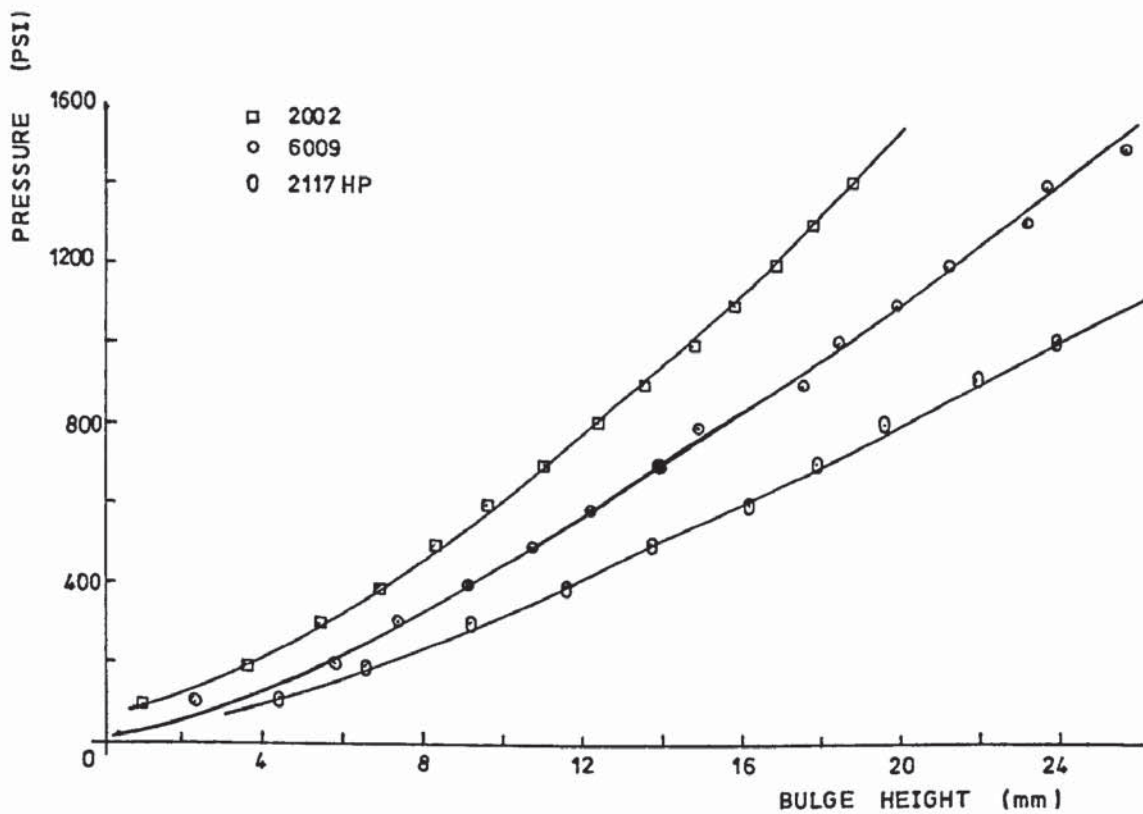
Fig. 30 Variation of bulge height with pressure for three high strength aluminium alloys hydraulically bulged through a 118 mm diameter circular die.

5.4   Factors Controlling Forming Limits

5.4.1   Effect of Test Procedure on Limit Strains

Forming limits were determined for alloys 6010, 5182, 2117 HP and
2117 CP using solid punches and non-frictional techniques. Figs 31
(a) - (d) show the forming limit diagrams for the four alloys above.
The dotted line represents limit strains determined by punch
stretching and the solid line those determined by hydraulic bulge
tests and tensile tests. The F.L.C.'s determined by punch stretching
(Nakazima strip tests) lie above those for the hydraulic bulge tests
in all cases although for 6010 both curves coincide at the point of
plane strain. This suggests that limit strains are not only determined
by the materials' inherent properties but also by the method of testing.
Contact between the sheet and punch surface appears to inhibit the
formation of a local heterogeneity until conditions are sufficient to
overcome the supportive effect of the punch.

During hydraulic bulge tests it was noticed that alloys 5182, 2117 HP
and 2117 CP consistently failed at right angles to the rolling direction
while 6010 failed parallel to the sheet rolling direction.

5.4.2   Fracture Mode

Three types of failure were generally observed during the determination
of limit strains. These are shown in the form of polished sections at
right angles to the fracture close to the points of initiation,
Figs 32 (a) - (c). The ductile fracture behaviour shown in Fig 32 (a)

was relatively uncommon for friction free testing and was only found in some cases where the minor strain e_2 was negative. With Nakazima strip specimens, ductile failure was much more common and could exist over the complete range of strain ratios, especially in the case of alloy 5182. Otherwise, separation occured by shear fracture along a band at approximately 45° to the major strain axis. In many cases local necking had evidently preceded fracture as shown in Fig 32 (b). In other cases, however, there was no detectable reduction in cross-section at the failure site and it appeared that fracture had occured abruptly without prior strain localisation, Fig 32 (c).

5.4.3 Fracture Surface Characteristics

Three types of fracture surface were observed on specimens subjected to different strain paths prior to failure. These are shown in Figs 33 (a) - (f). Ductile fracture surfaces, Figs 33 (a) - (b), were commonly observed and were invariably the type seen when examining Nakazima strip specimens. Some hydraulic bulge fracture surfaces also displayed this type of characteristic dimpled surface which corresponded to sheet cross-sections of the type shown in Figs 32 (a) - (b).

Rather more uncommon was the ductile shear fracture surface shown in Figs 33 (c) - (d). These were normally only identified on hydraulic bulge specimens with cross-sections similar to Figs 32 (b) - (c). It can be seen that the fracture surface is very similar to those shown in Figs 33 (a) - (b) except for the smearing effect produced by the shearing movement of the fracture surfaces across each other as separation occurs.

The third type of fracture surface, shown in Figs 33 (e) - (f), was only observed on hydraulically bulged specimens with cross-sections of the failure site corresponding to the type shown in Fig 32 (c).

This type of behaviour appears to be due to fast fracture (272, 273) and is characterised by tear dimples on the fracture surface. It is associated with sudden catastrophic type failures which in this case may be explained by surface defects seen to appear on the surface of some hydraulically bulged specimens prior to failure. Figs 34 (a) - (c) show the appearance of these defects on the bulge surface of, in this case, alloy 2117 CP. It will be seen that the shear surface has a roughened appearance which apparently leads to intergranular cavitation in isolated regions. Such cavities were typically 50-100 μm across.

5.4.4   Initiation of Void Growth at Instability

To determine the point at which voids begin to take part in the ductile fracture process, bulge   specimens were sectioned and examined under the optical microscope. Figs 35 (a) - (b) show the development of a neck in alloy 5182 producing a locally thinned region with fractional thickness ~ 0.85. At this stage of straining it can be seen that there is no evidence to suggest the development of void sheets. Fig 35 (c) shows a cross-section in which fracture appears to have taken place along one of two shear planes. The second shear plane is evidenced by a distinct line of voids indicated on the micrograph by an arrow. It was generally observed that void formation did not occur until almost the instant of failure. Where voids were observed in failed

specimens they were extremely localized and restricted to a region immediately adjacent to the fracture surface or on a secondary shear plane.

5.4.5   Effect of Surface Defects on Limit Strains

During hydraulic bulge testing of sheet alloys it was noticed that surface scratches, introduced into the material during handling operations, had a marked effect on the magnitude of strain at fracture. To investigate this phenomenon further, sheet alloys subjected to uniaxial tensile, punch and hydraulic bulge tests had defects introduced in the form of shallow v-notch grooves. These defects ran parallel to the normal fracture direction of the sheet in bulged and punch stretched specimens and at right angles to the gauge length in tensile samples. Figs 36 (a) - (c) show the relative cross-section and geometry of the inhomogeneities. Table 5. shows the ratio of reduced cross-section (fo) for alloys 6010, 5182, 2117 HP and 2117 CP.

These defects did not influence the strains at fracture for tensile test or Nakazima strip specimens. Alloys having multiple defects introduced were tested in an attempt to influence the position of the fracture site. This was unsuccessful and it was concluded that, in the case of tensile test or Nakazima strip specimens, failure was not influenced by surface defects in the sheet.

Prior to bulge testing the sheet was centralized in the test machine so as to position the defect as near as possible to the expected failure site. Failure was found to occur at decreasing strains with increasing defect size, illustrated in Figs 37 (a) - (d) where the principal axes

of the sheet are chosen as the reference frame. From these it can be seen that the direction of failure in 6010 was parallel to the sheet rolling direction while that of 5182, 2117 HP and 2117 CP was transverse to it. It is clear from Fig 37 that the strain ratio $\epsilon_2 : \epsilon_1$ is independent of surface treatment, being controlled solely by the die ellipticity. Scratches of increasing severity merely cause fracture to intercede sooner in the deformation process without influencing the plastic strain development itself. Figs 38 (a) - (d) show the forming limit diagrams corresponding to the results of Fig 37 (a) - (d). The limit strains decrease with increasing defect size in all alloys.

5.4.6   Effect of Surface Defects on Fracture Type

F.L.C.'s in Fig 39 (a) - (d) incorporate information relating to the type of failure process identified from cross-sections of fractured test pieces.

Where local necking was observed, Fig 32 (a), the F.L.C.'s are plotted as thin lines while conditions corresponding to no local necking, Fig 32 (c), are shown as broad bands. Failure in the Nakazima strip specimens was normally preceded by local necking. A clear pattern of behaviour is evident for all the alloys although minor differences exist between them. The tendency for abrupt fracture without prior necking is most evident in strain states approaching equi-biaxial tension. For the unscratched specimens the fracture controlled range was greatest in 2117 CP and decreased progressively in 2117 HP and 6010. In the case of alloy 5182, the virgin material showed necking failure under all

conditions. As grooves of increasing severity were introduced, limit strains were substantially reduced and the range of fracture initiated failures extended toward the plane strain condition. The tendency for fracture without prior necking was evident in 5182 as well as the other alloys when groove type defects were present.

5.4.7 Comparison of Calculated and Theoretical Forming Limits

Figs 40 (a) - (c) show the experimental (solid line) and calculated (dashed line) forming limit curves obtained with and without defects in the sheet surface. The theoretical curves have been calculated as shown in appendix A. Nominal strains measured in defect free sheet were converted to effective strain and effective stress. From these the principal and critical shear stress's were calculated. The stress concentrating factor C was introduced into the equations and new values of β (strain ratio) determined. By reversing the above procedure new values of nominal strain were computed.

The level of the F.L.C. is reduced with increasing defect size. Calculated and experimental curves were found to be of tolerably good fit in the region of equi-biaxial tension. However, as plane strain conditions are approached the discrepency between the levels of the theoretical and calculated curves is found to increase. The general form of the experimental F.L.C. may differ substantially from that calculated. The material is assumed to obey the relationship $\sigma = k\varepsilon^n$ over its entire strain range which may not infact be justified. Material and statistical effects are also introduced during testing. Therefore, for such a simple model, the discrepencies

observed when departing from equi-biaxial straining may be attributed to, amongst other things, its crudeness.
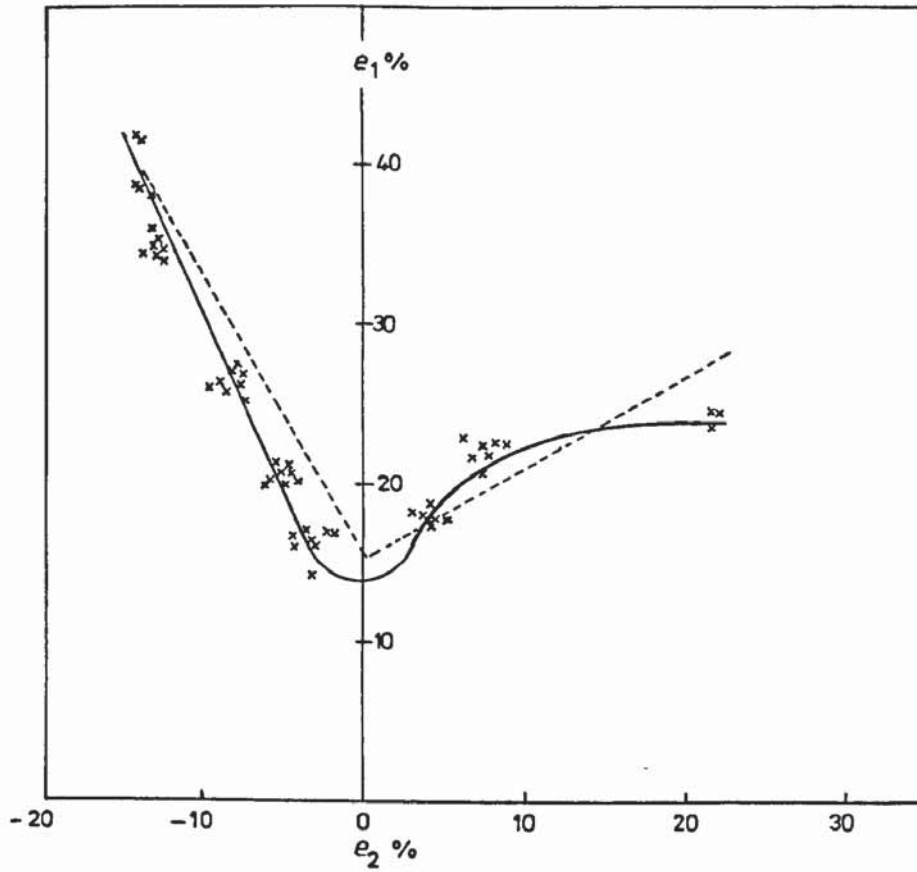
Fig. 31(a)   Forming limit curves determined by Nakazima strip
              (dotted line) and hydraulic bulge test (solid line)
              techniques.

(c)

6010

(d)
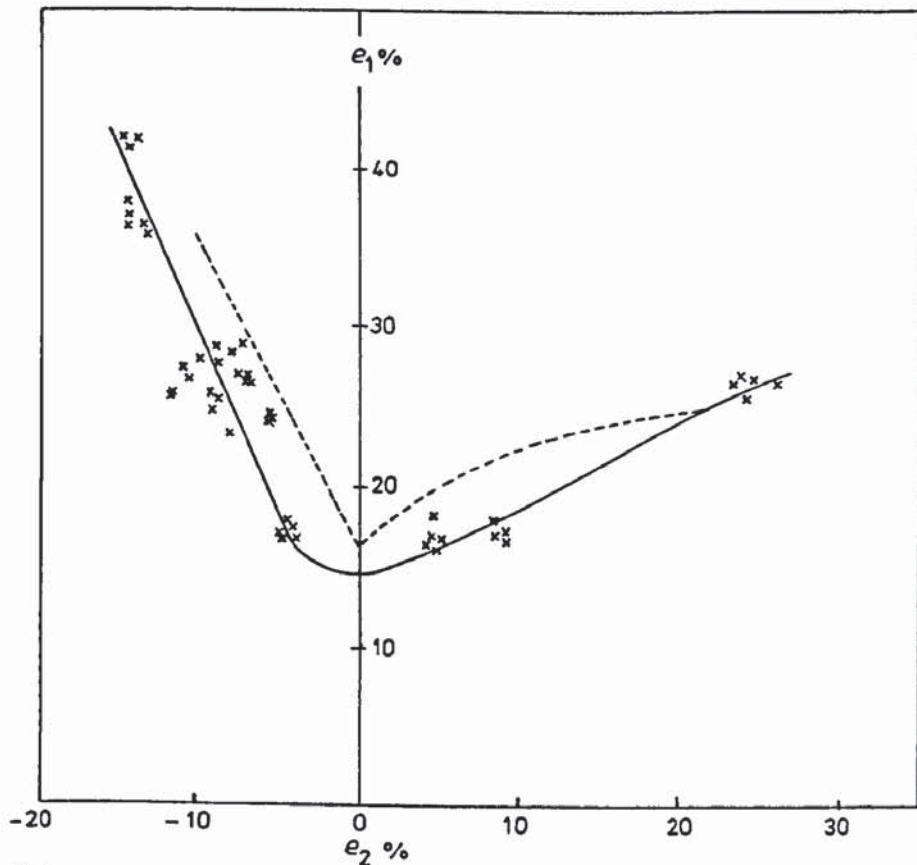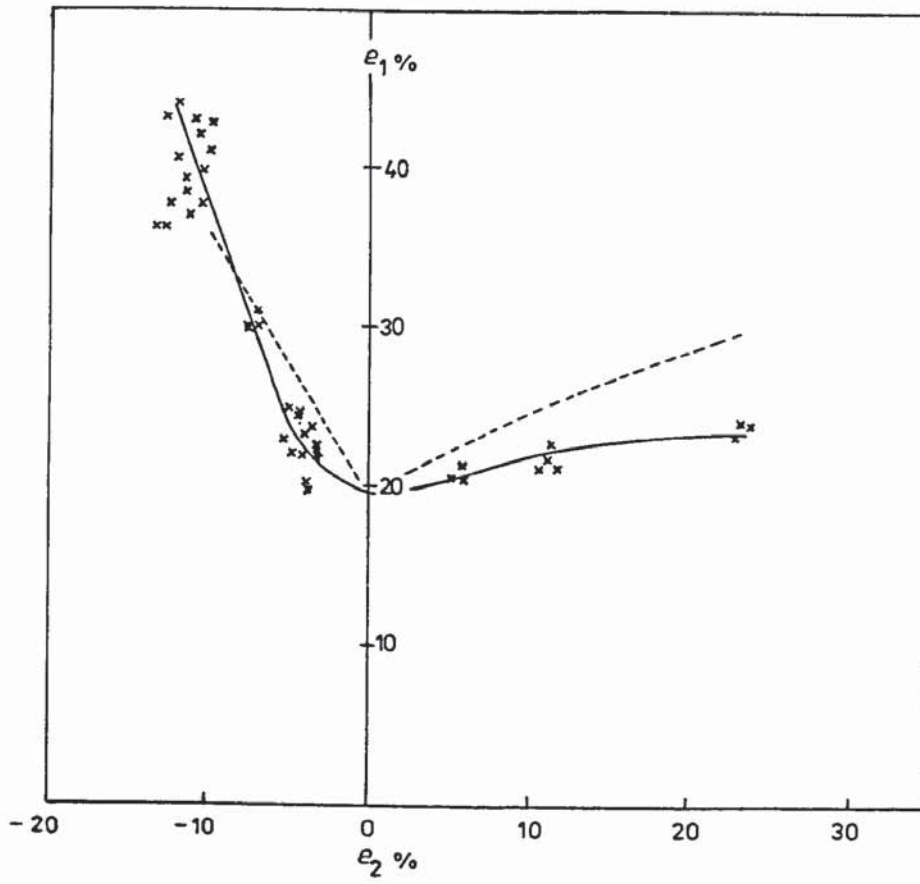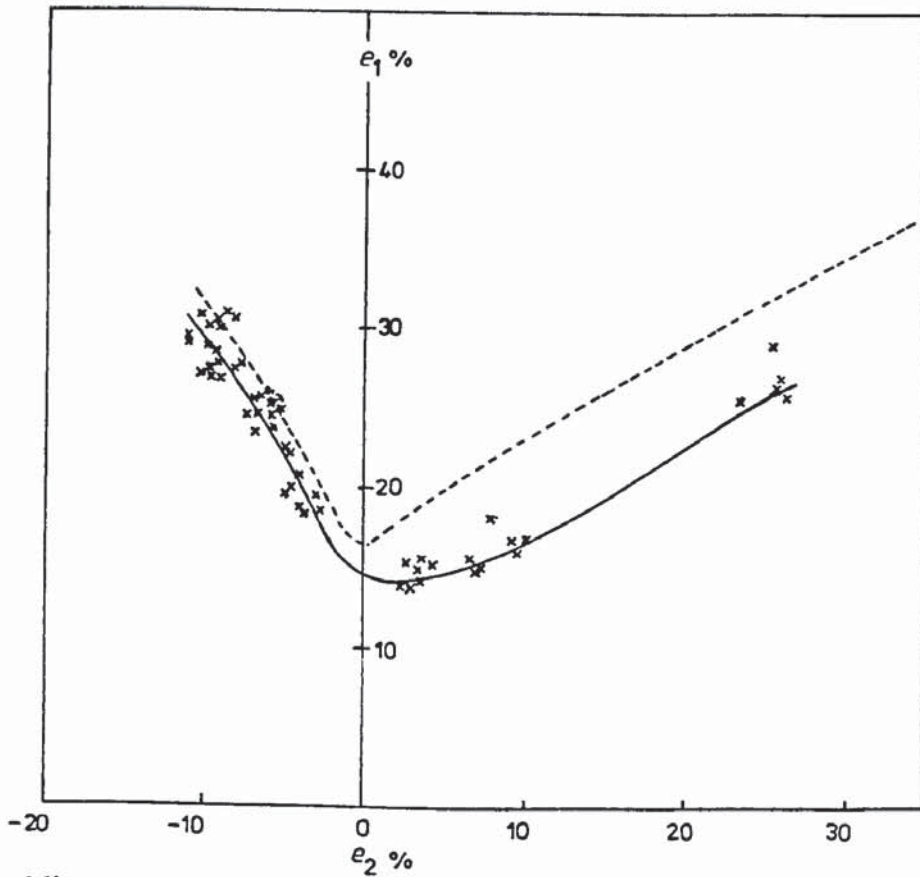
5182

Fig. 32(a) - (c)   Failure modes observed in aluminium alloys
                     subjected to strain states between uniaxial
                     and equibiaxial conditions. (a) denotes
                     ductile fracture, (b) ductile/shear fracture
                     and (c) pure shear.
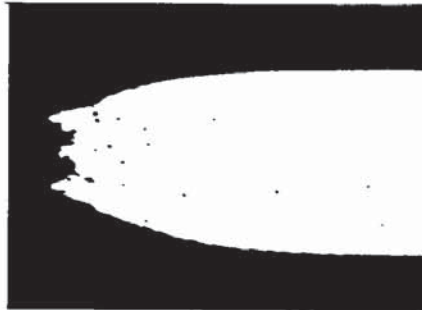
Fig. 32(a)

(b)

(c)

Fig. 33(a) - (f)   Fracture surface characteristics of aluminium
                    alloys subjected to various stress states
                    (a - b) denotes ductile fracture, (c - d)
                    ductile shear fracture and (e - f) fast fracture.
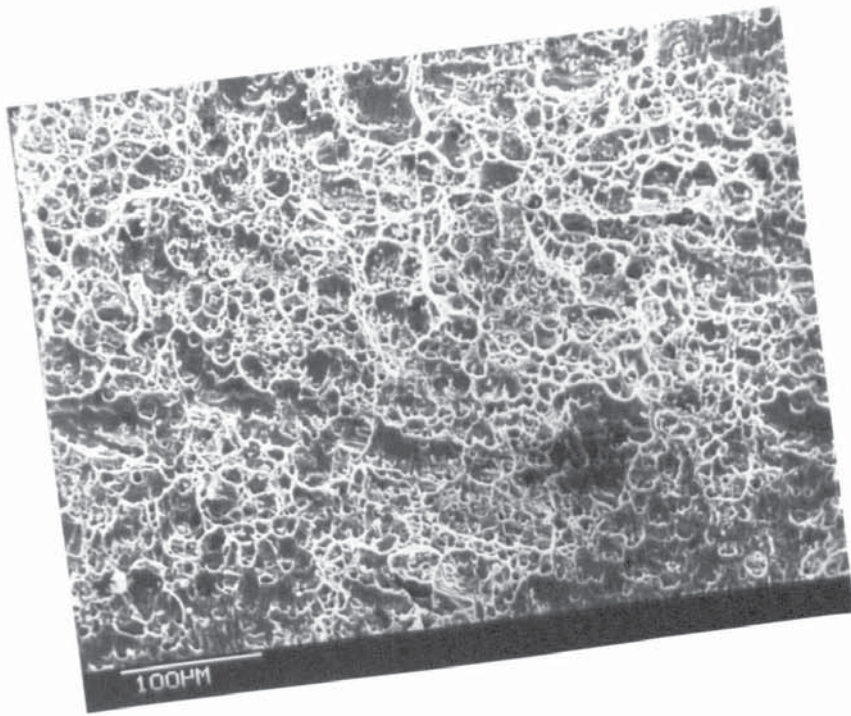
Fig. 33(a)
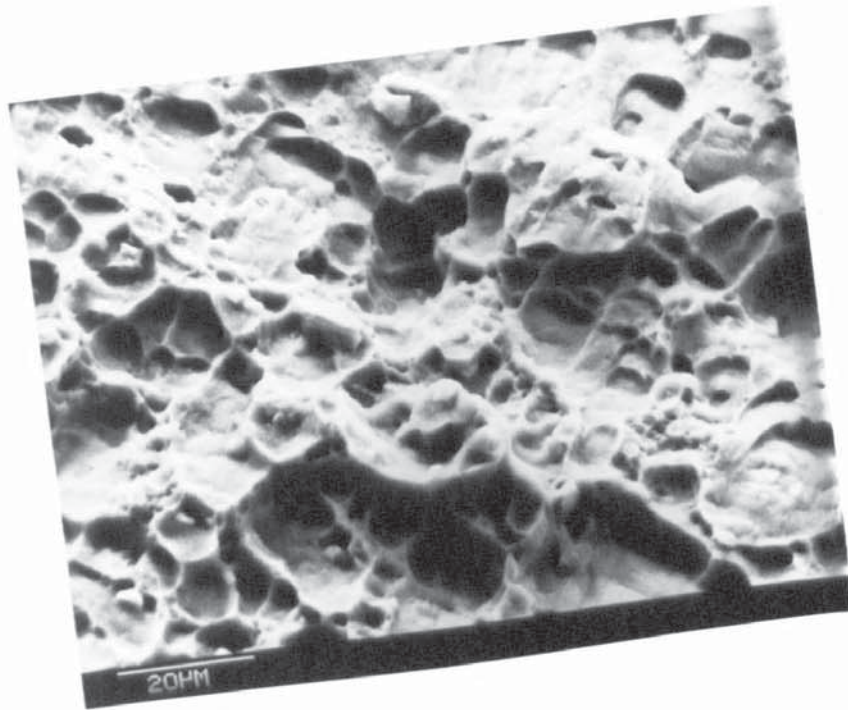
(b)
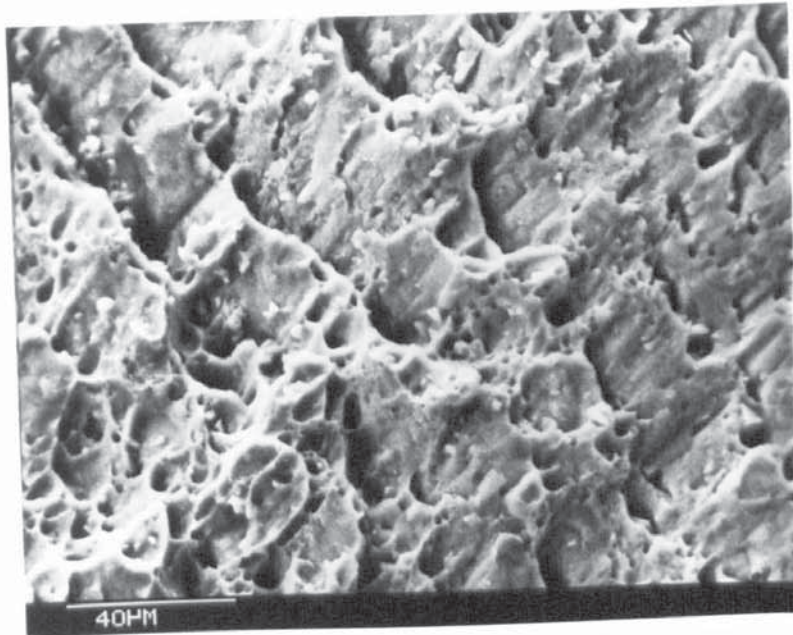
(c)
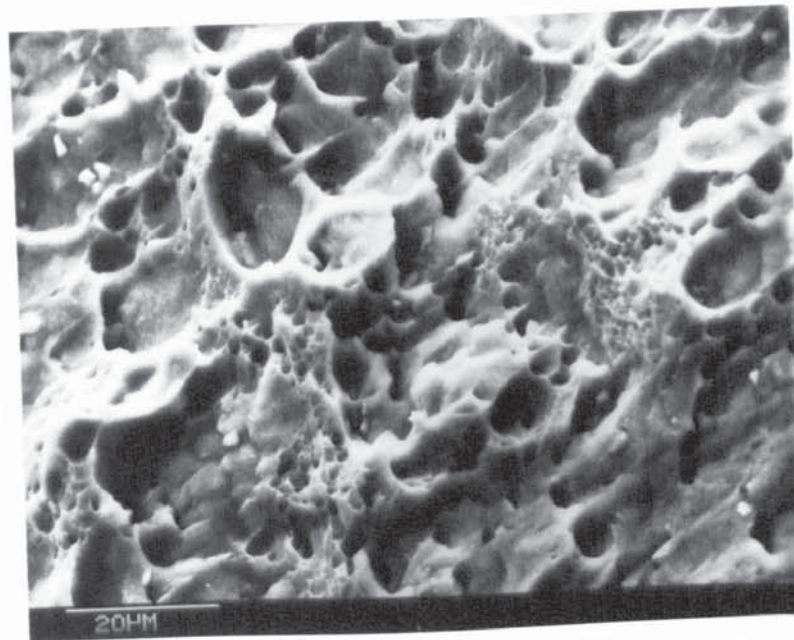
(d)
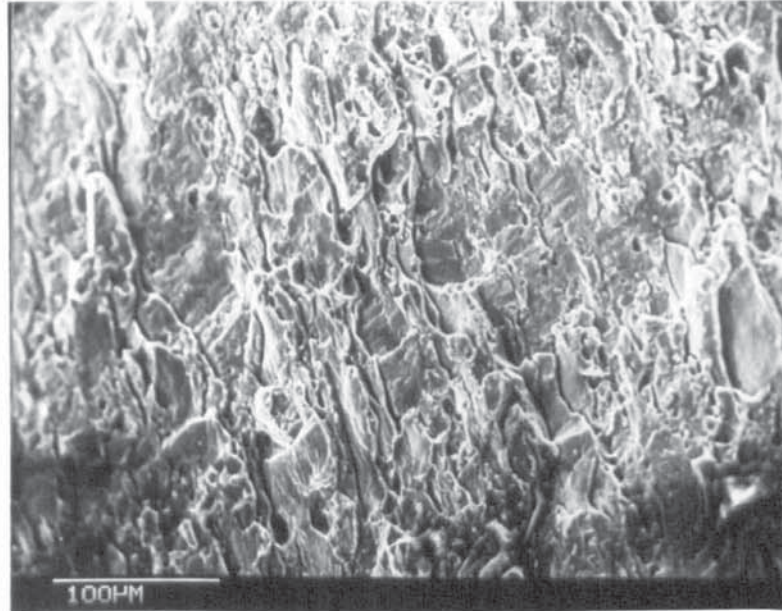
(e)
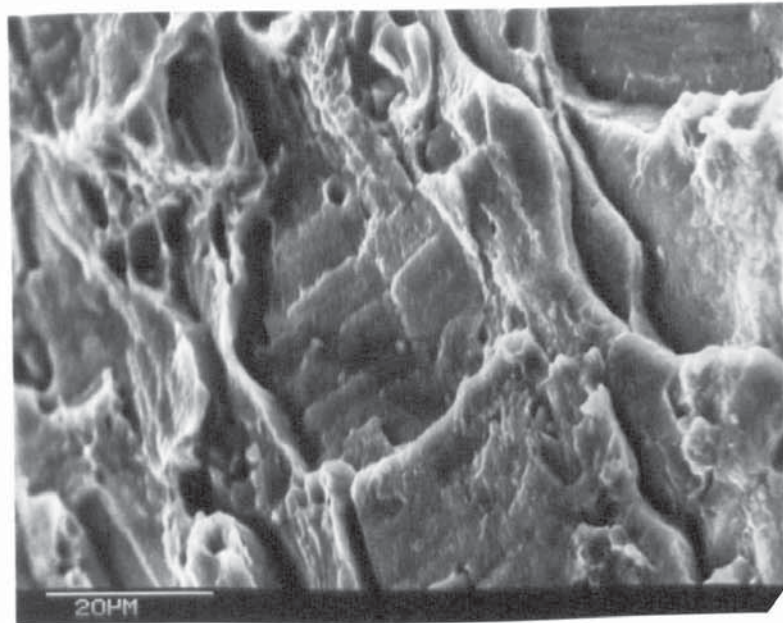
(f)
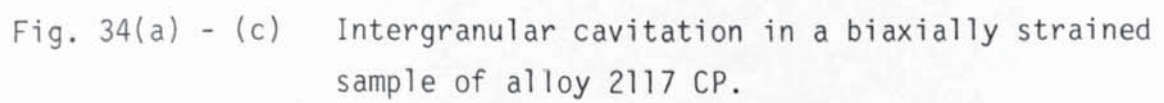
Fig. 34(a) - (c)   Intergranular cavitation in a biaxially strained
                    sample of alloy 2117 CP.
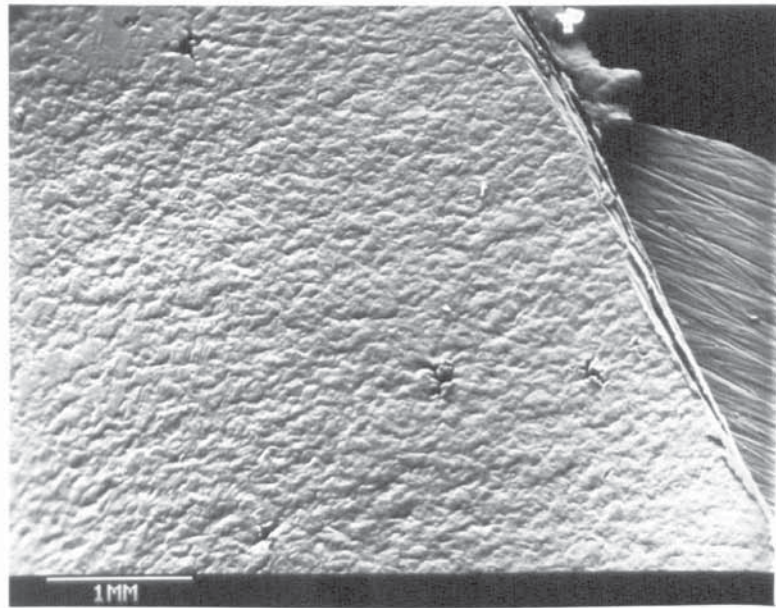
Fig. 34(a)
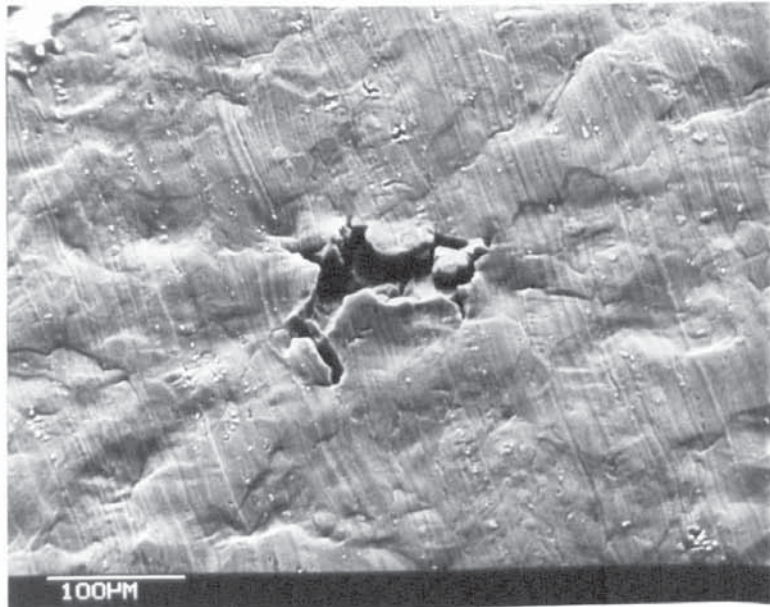
(b)
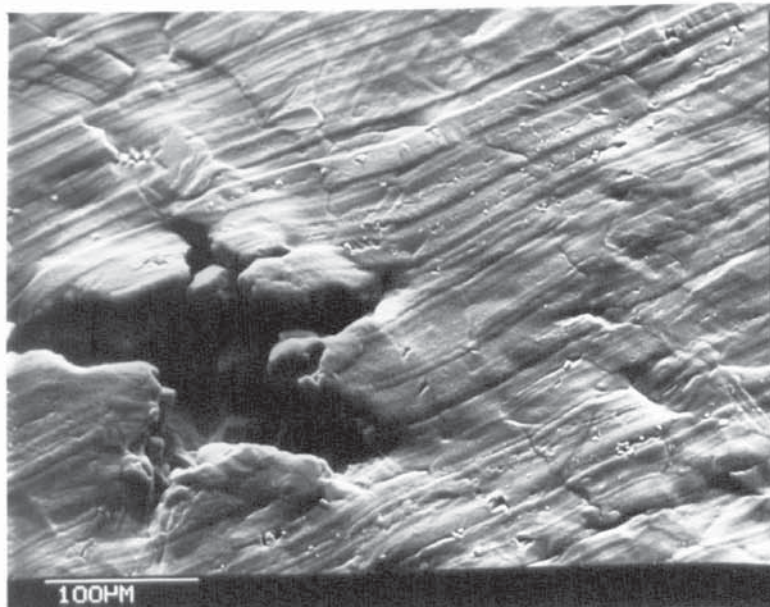
(c)
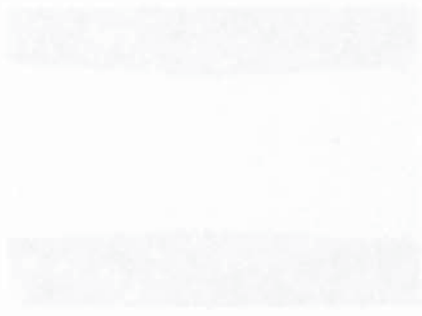
Fig. 35(a) - (c)   The development of voids in regions of localised
                    necking and fracture. (a) and (b) show no
                    indication of the presence of void sheets within
                    regions of localised necking. (c) illustrates the
                    formation of voids along a shear plane (indicated
                    by an arrow).
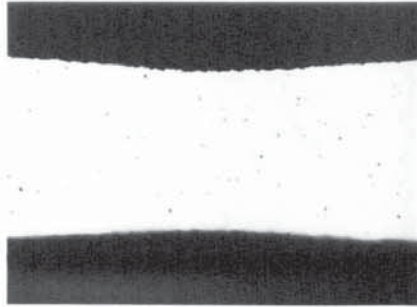
Fig. 35(a)
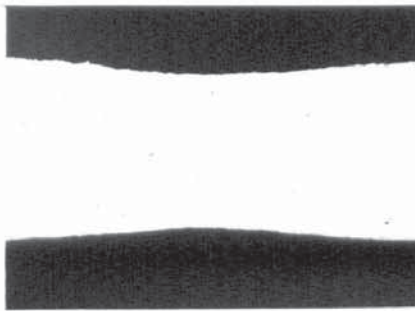
(b)
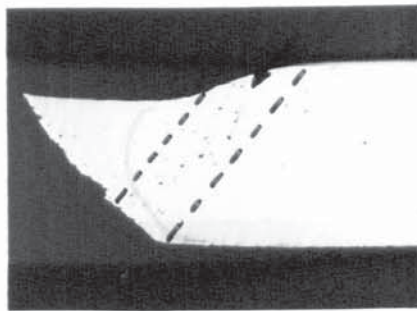
(c)

Fig. 36(a) - (c)   Relative cross-section and geometry of defects
                    introduced into the sheet surface.

Fig. 36(a)

(b)

(c)

ALLOY	TOOL LOAD (gms)	REDUCED CROSS SECTION (fo)
6010	50	0.98
	100	0.97
	300	0.94
5182	50	0.98
	100	0.97
	300	0.94
2117HP	50	0.98
	100	0.97
	300	0.94
2117CP	50	0.98
	100	0.97
	300	0.93

Table 5.   Ratio of reduced cross-section fo for alloys 6010, 5182, 2117 HP and 2117 CP.
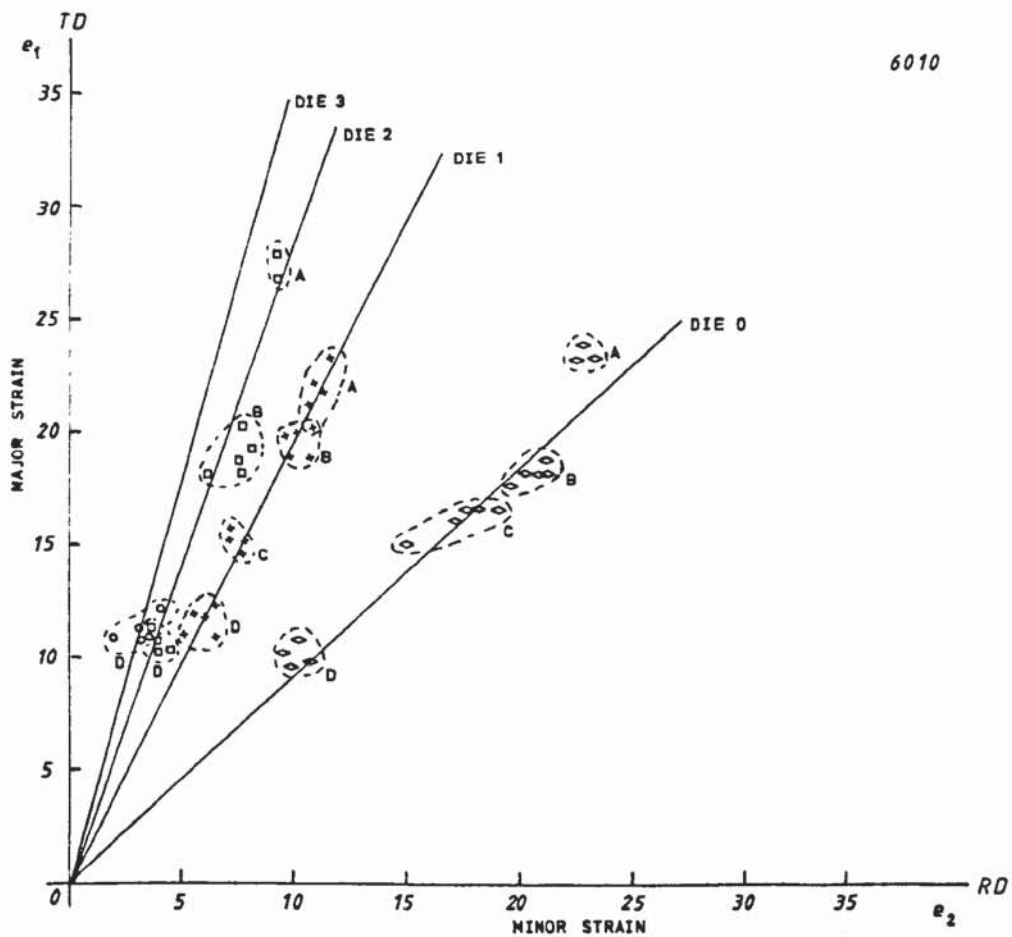
Fig. 37(a)   Strain paths followed during hydraulic bulging of thin
sheet through circular and elliptical dies. A=0 gm,
B=50 gms, C=100 gms, D=300 gms.

(d)

MAJOR STRAIN

e_2 RD

35 30 25 20 15 10 5 0

MINOR STRAIN

5 10 15 20 25 30 35

DIE 3

DIE 2

DIE 1

DIE 0

2117 CP

e_1 TD

A B C

(c)

MAJOR STRAIN

e_2 RD

35 30 25 20 15 10 5 0

MINOR STRAIN

5 10 15 20 25 30 35

DIE 3

DIE 2

DIE 1

DIE 0

2117 HP

e_1 TD

A B C
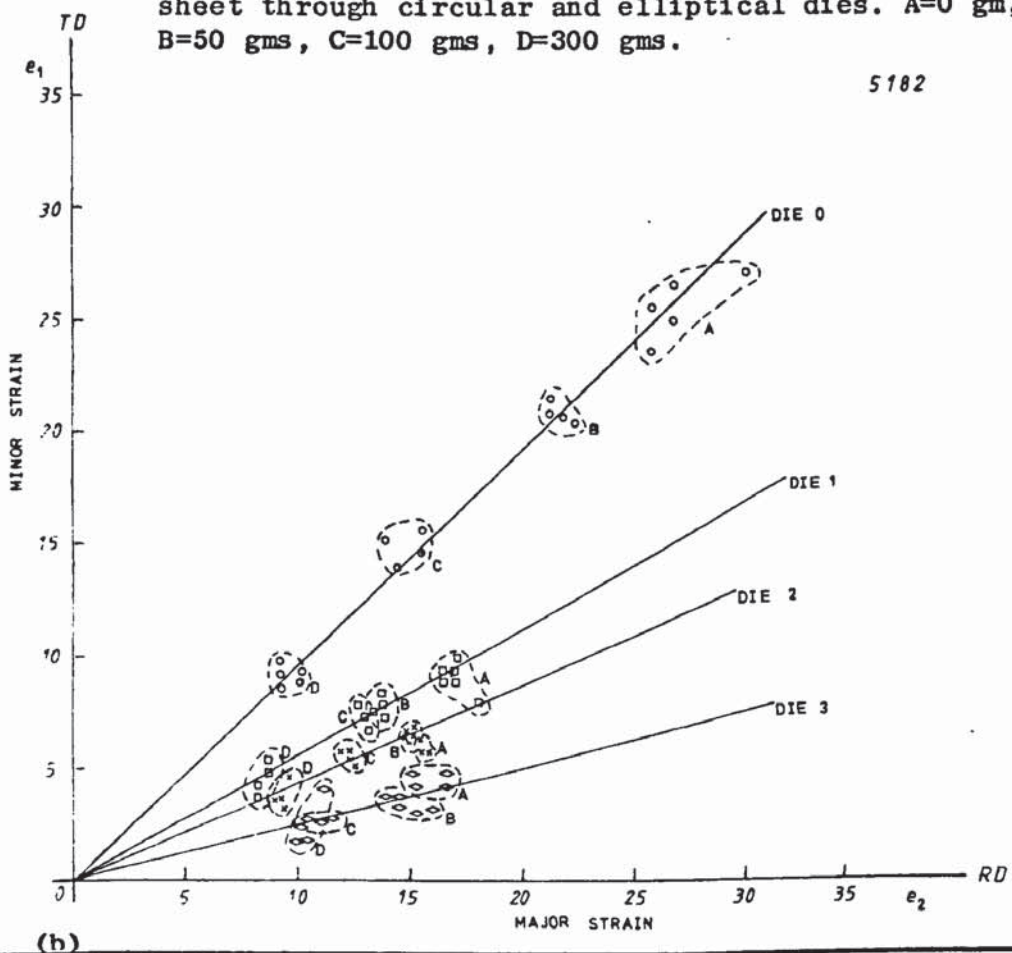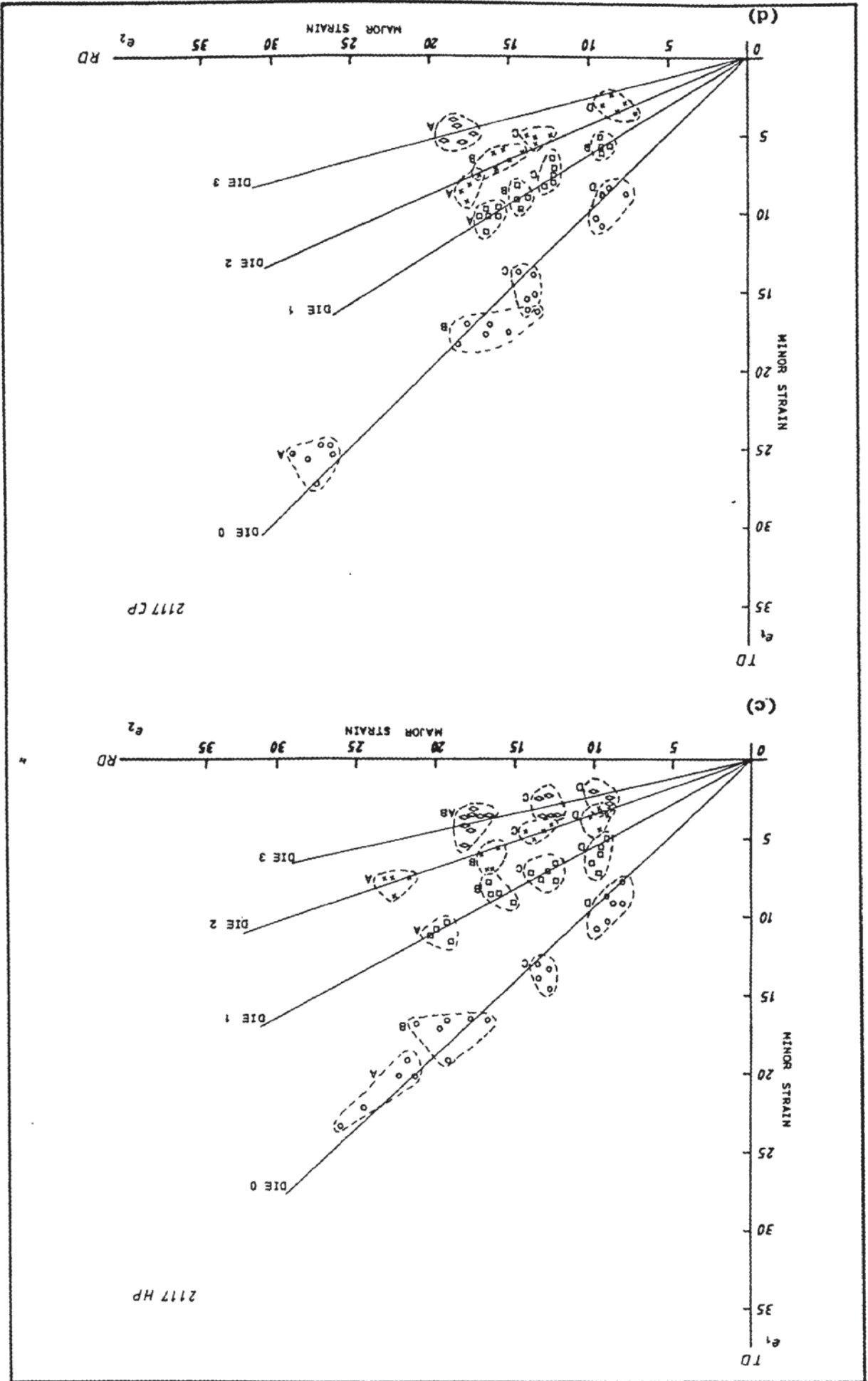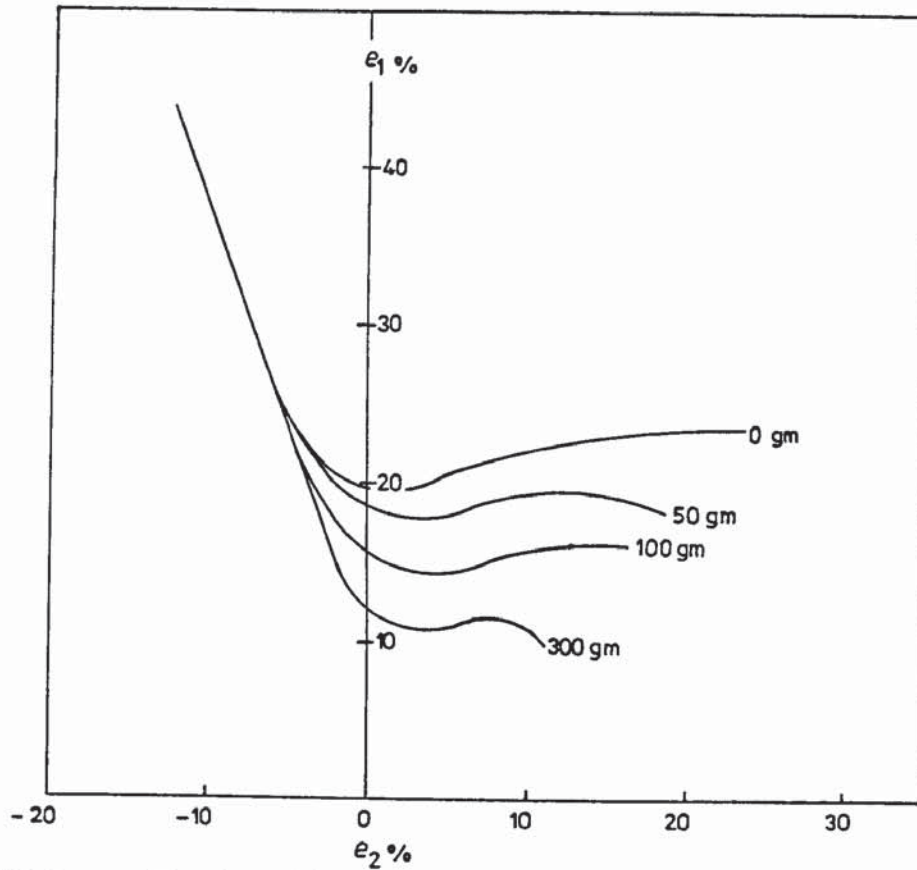
Fig. 38(a)   Forming limit curves for alloys containing local heterogeneities prior to testing.

(c)

2117 HP

(d)
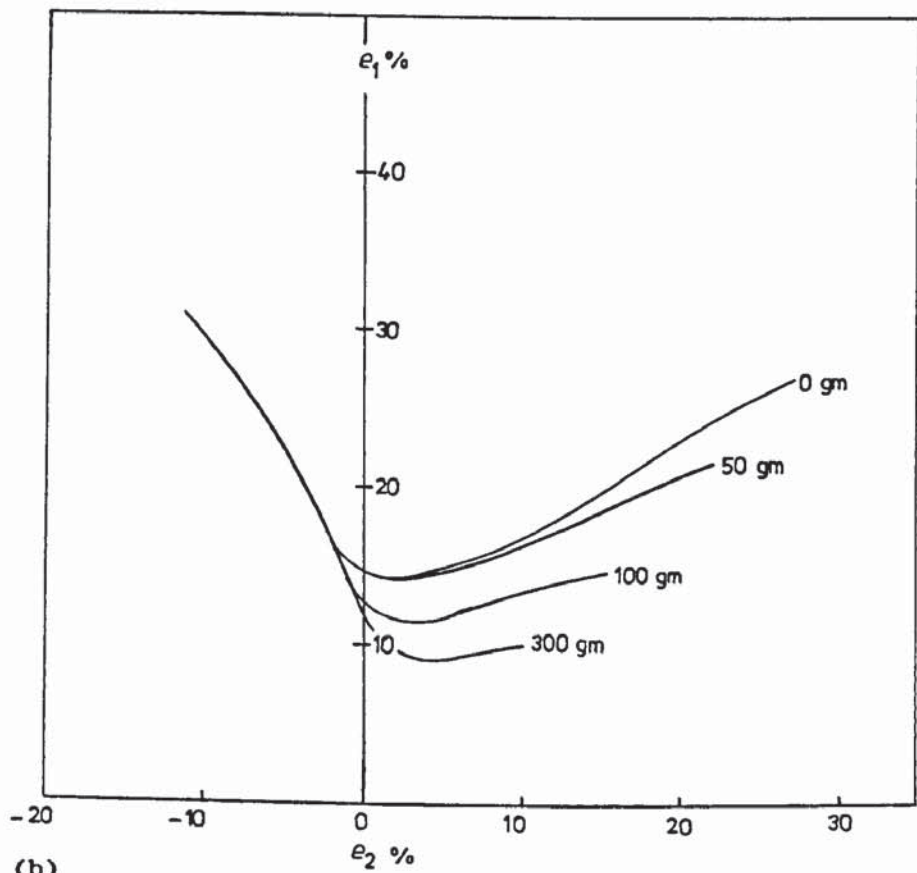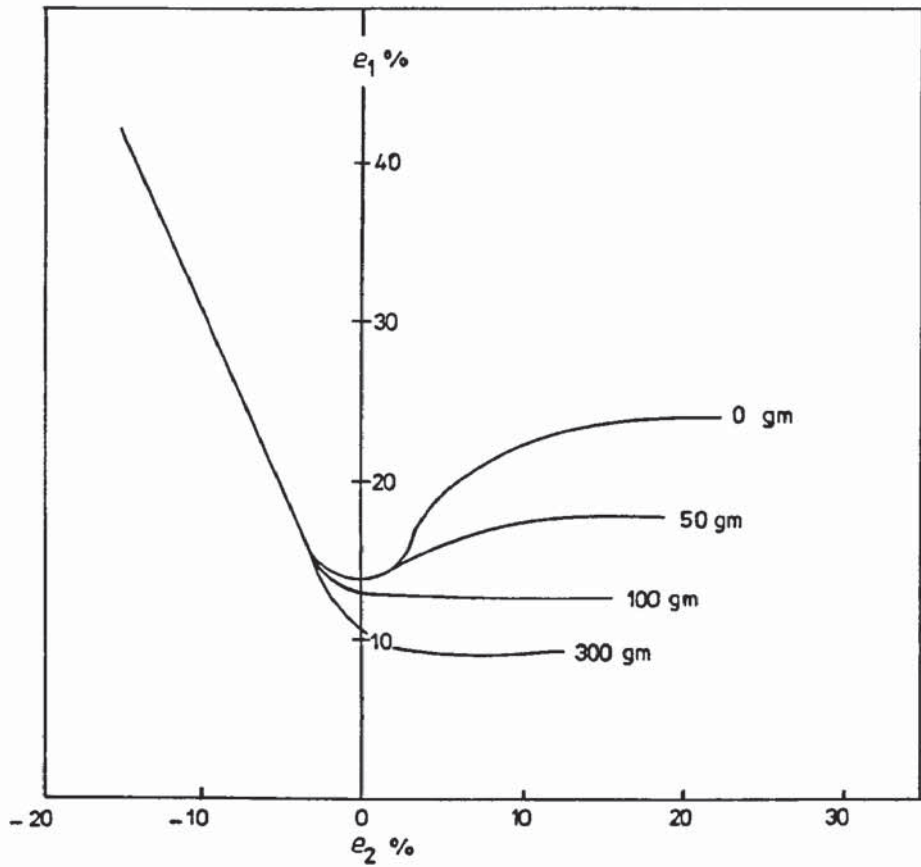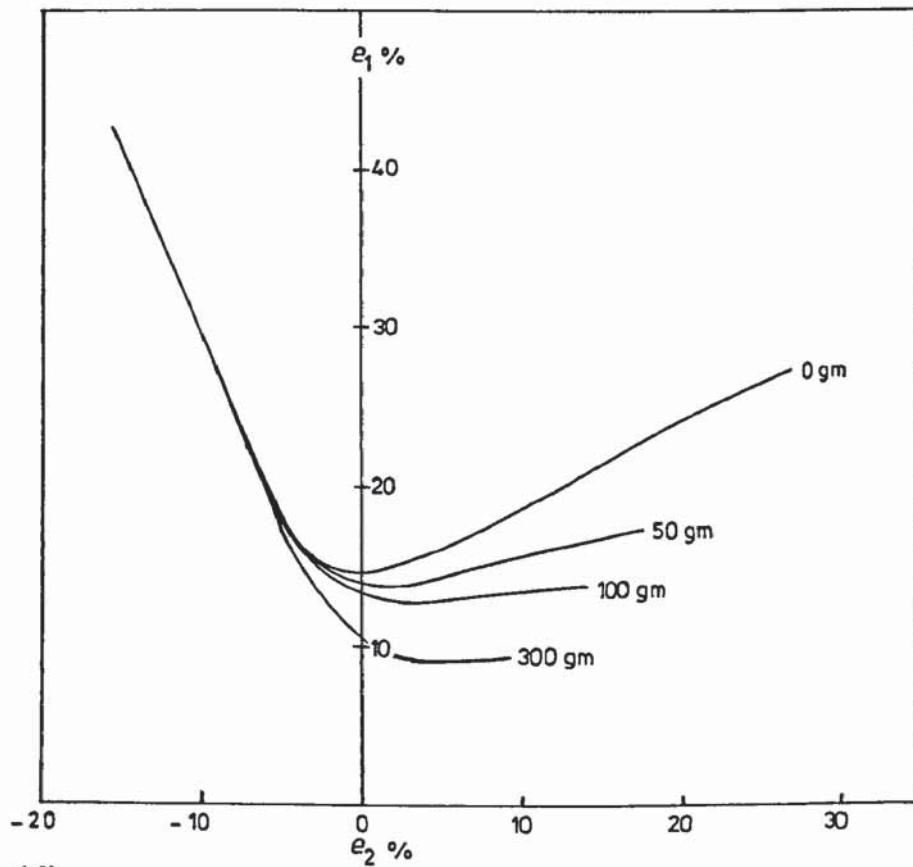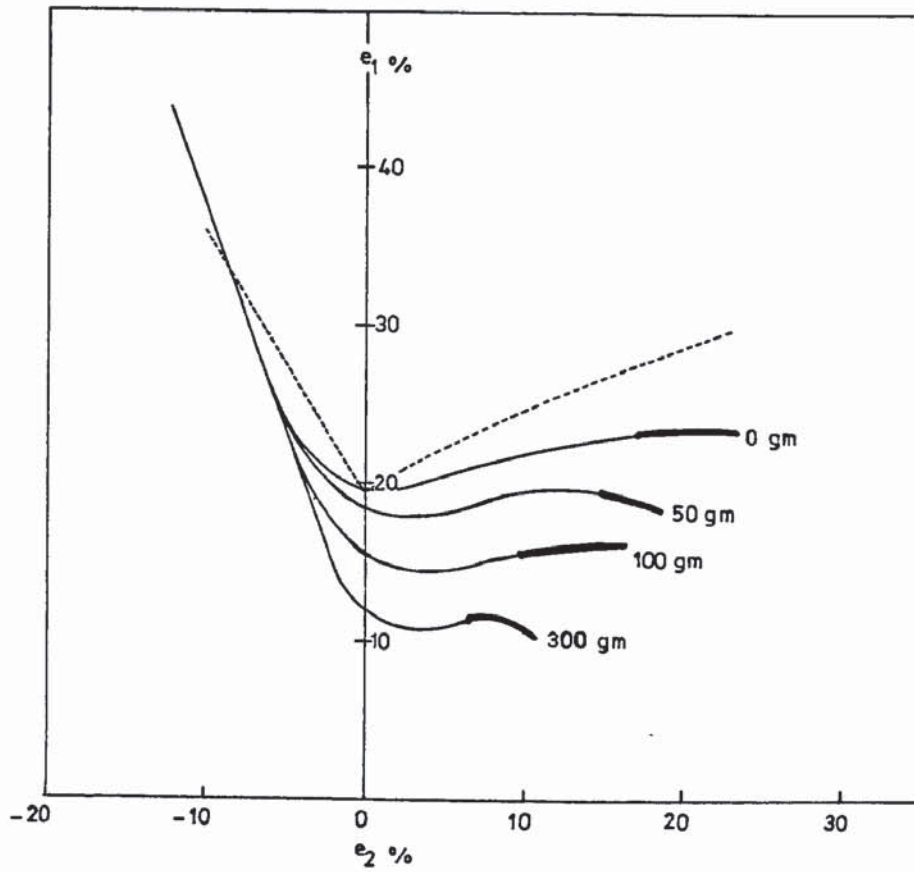
2117 CP

6010

Fig. 39(a)   Failure processes in thin sheet. Local
              necking = thin lines, no local necking = broad
              lines.

5182

(b)

(c)

2117 HP

(d)
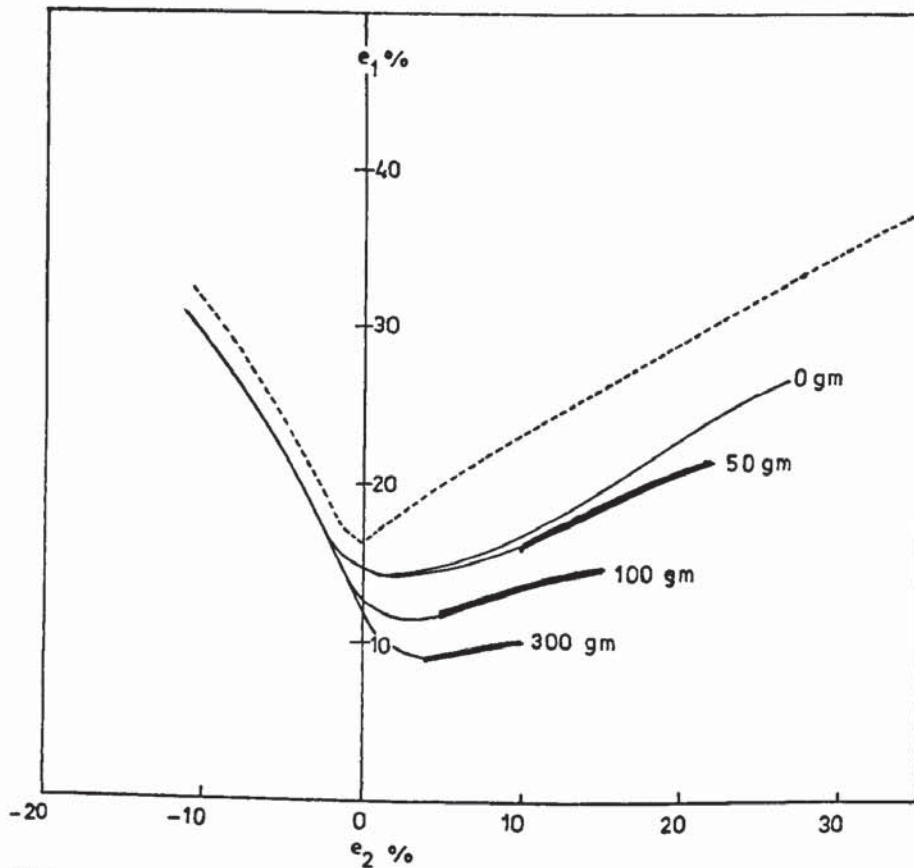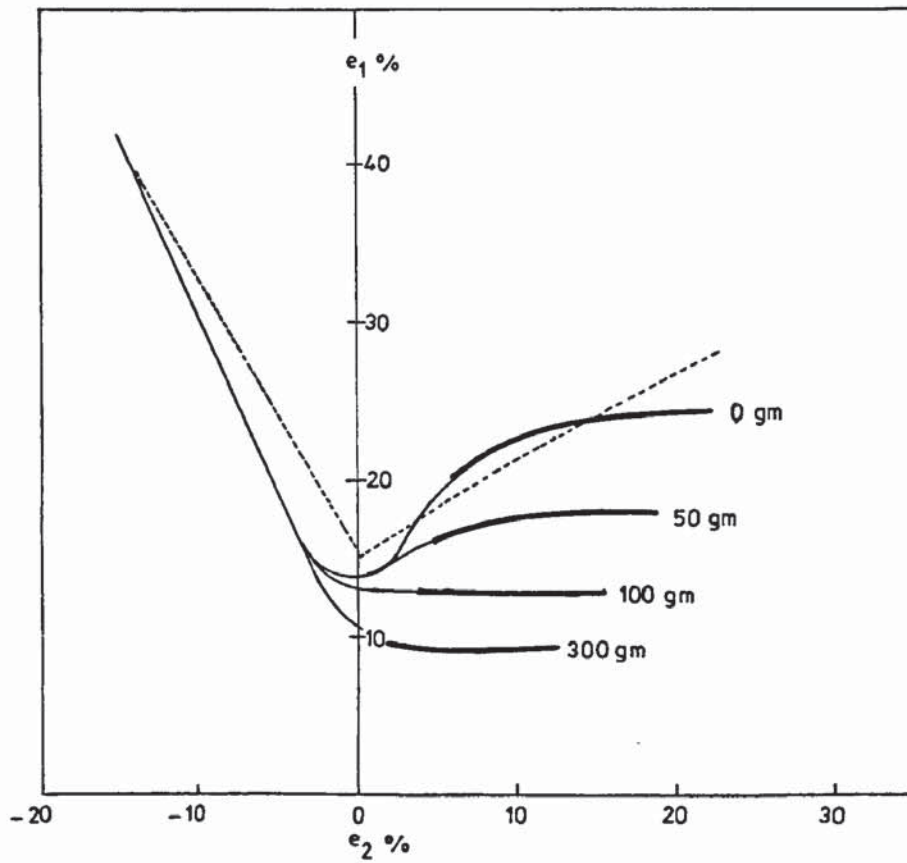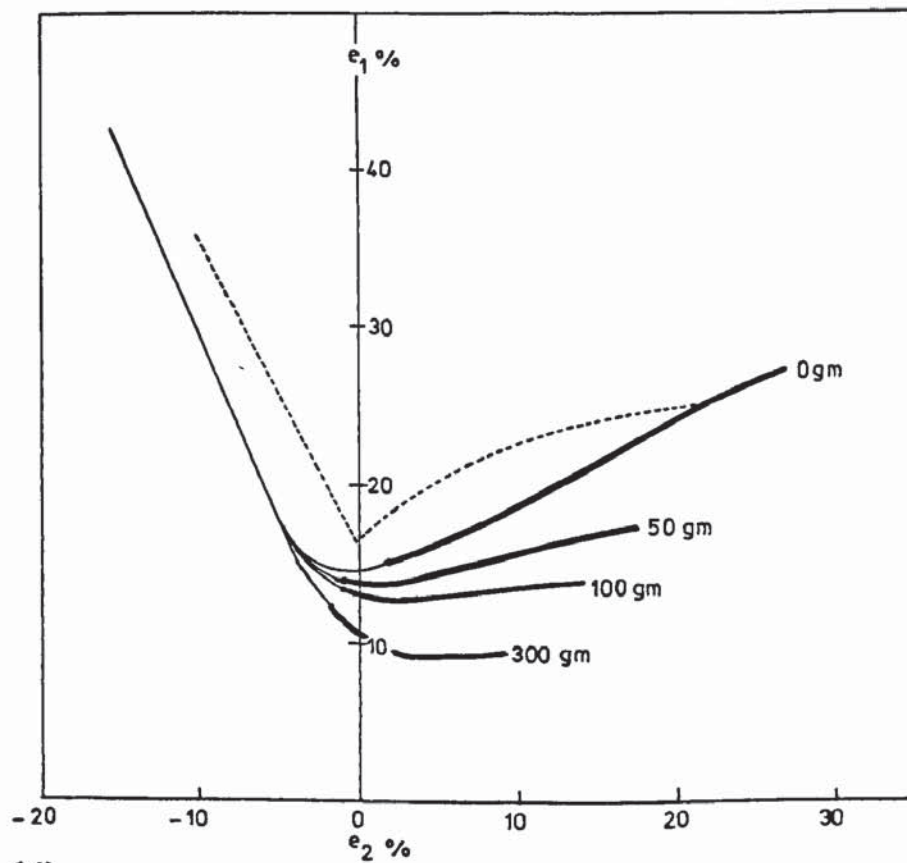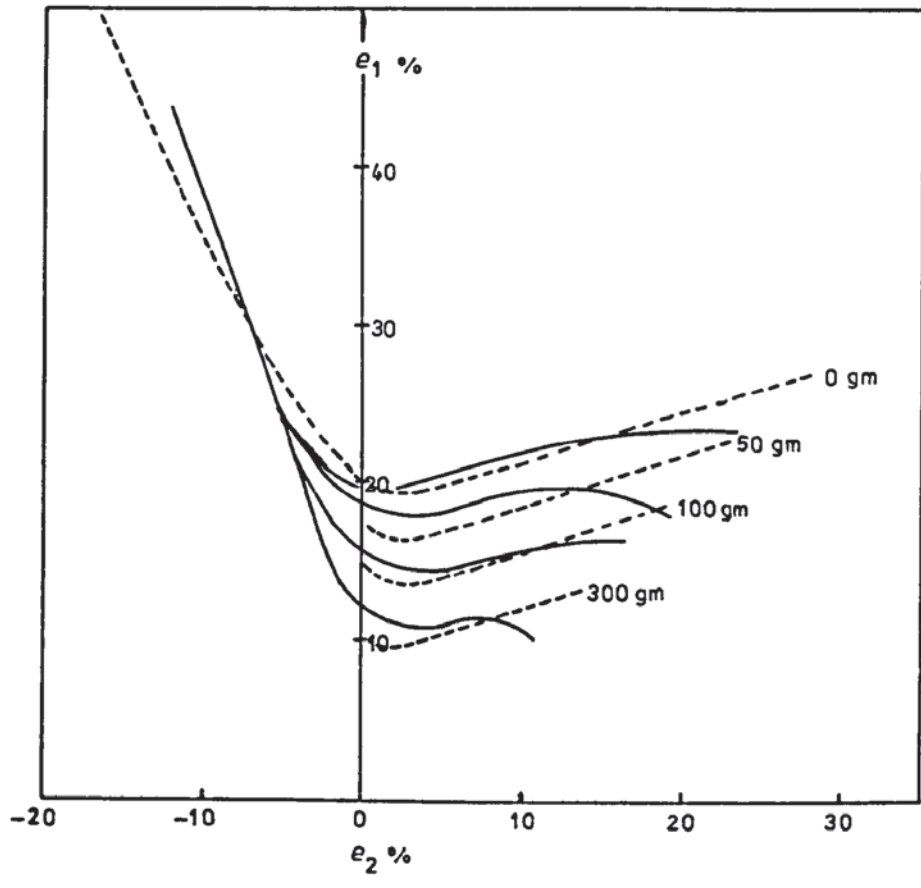
2117 CP

Fig. 40(a)   A comparison of theoretical (dotted line) and
              experimental (solid line) forming limit curves.

(b)

2 117 HP

(c)

2 117 CP

6. DISCUSSION
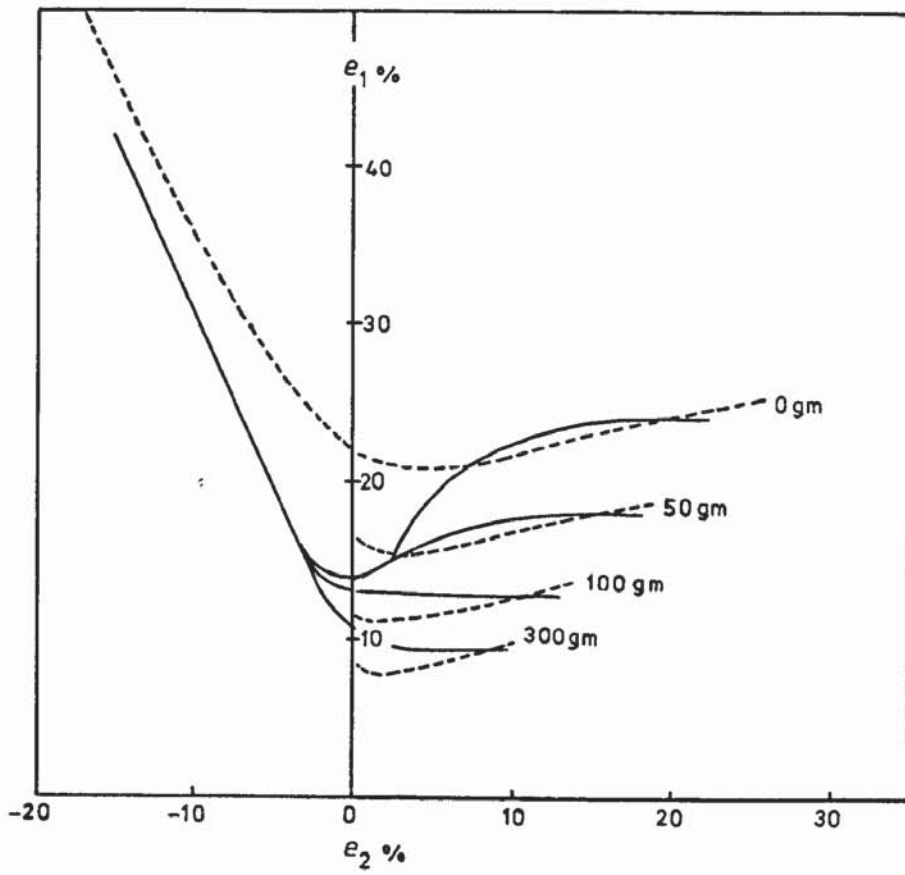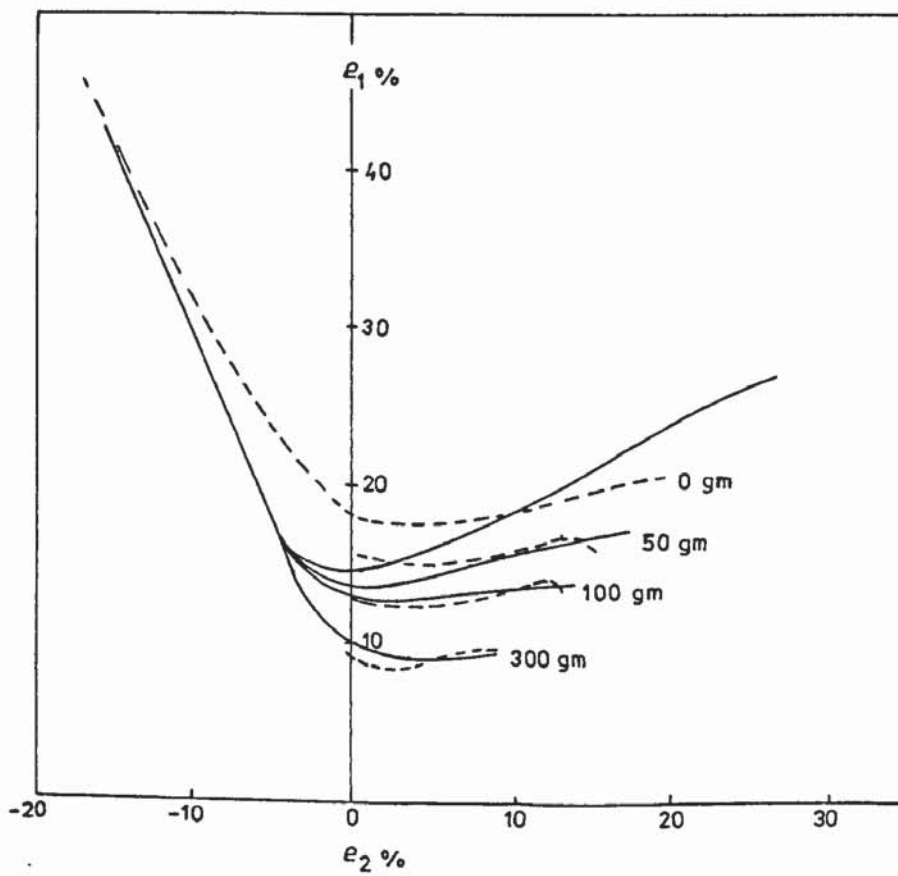
6.1 Characteristics of Commercially Available Aluminium Alloy Sheet

The alloys investigated during this research were obtained from a
wide selection of suppliers eg. B.A.C.O. supplied 2117 HP and
2117 CP (high press and commercial press); Pechiney (France)
2117A, 2002 and CP 609; Reynolds (U.S.A.) AA 2036 and 5182 S.S.F.
whilst ALCOA supplied 6009 and 6010. It will therefore be appreciated
that as well as the differences in the properties of these alloys which
result from their different compositions, the processing routes followed
during manufacture may also be expected to have a significant effect.

Figs 41 (a) - (b) show the relationship between total elongation and
U.T.S. or 0.2% proof stress for all alloys investigated in the
"as received" condition. Fig 41 (a) shows that increases in U.T.S.
may be achieved in addition to increases in elongation in some cases.
No trend is apparent. As might be expected, the 5xxx alloys which
have been rolled to temper (SIDAL, BB2) are generally found to have
lower elongation values while 5182 which was fully annealed had good
ductility. The information contained in Fig 41 (a) relates basically
to the shape of the stress-strain curve for each alloy and indicates
how fast the alloy approaches failure. The results are directly
related to the work-hardening capacity of these alloys and their
ability to sustain work-hardening as straining progresses. Elongation
values show a tendency to decrease with increasing yield stress,

Fig 41 (b), but this trend is mainly due to the presence of the three cold rolled samples. The yield stress is a structure sensitive property and depends on grain size, dislocation density and the arrangement of second phase particles. The results show HS30/3 to have the highest proof stress in the "as received" condition. This is believed to be a consequence of prior cold work together with some natural ageing response. Alloys exhibiting higher elongations were either O - temper for the 5xxx series or T4 - temper for the 2xxx and 6xxx series. Although high values of yield stress are desirable in formed components problems can arise when these values are too high prior to forming. Manufacturing experience with the same alloys as reported here has shown poor press forming characteristics and increased die problems when using materials with a yield stress in excess of 170 - 180 N/mm^2 (6010, 2036 and 2002) although their tensile elongation values are no worse than for the other alloys.

Figs 42 (a) - (b) illustrate the relationship between Erichsen value and U.T.S. or 0.2% proof stress. Although the Erichsen value is related to the percentage elongation and is a reflection of the materials ductility the method of testing introduces new variables including specimen geometry, strain state and distribution. No mathematical relationship is apparent between I.E. and U.T.S. However, a clear trend can be seen in Fig 42 (b) where Erichsen value is seen to increase with decreasing proof stress. This is in agreement with Fig 41 (b) although the alloy rankings differ considerably suggesting that some alloys may exhibit high levels of ductility under one system of imposed stresses while a different system will give rise to inferior ductility. The reason for this apparent difference may be

Fig. 41(a) - (b)   Relationship between (a) U.T.S. Vs % elongation
and (b) 0.2% proof stress Vs % elongation for
alloys in the "as received" condition.
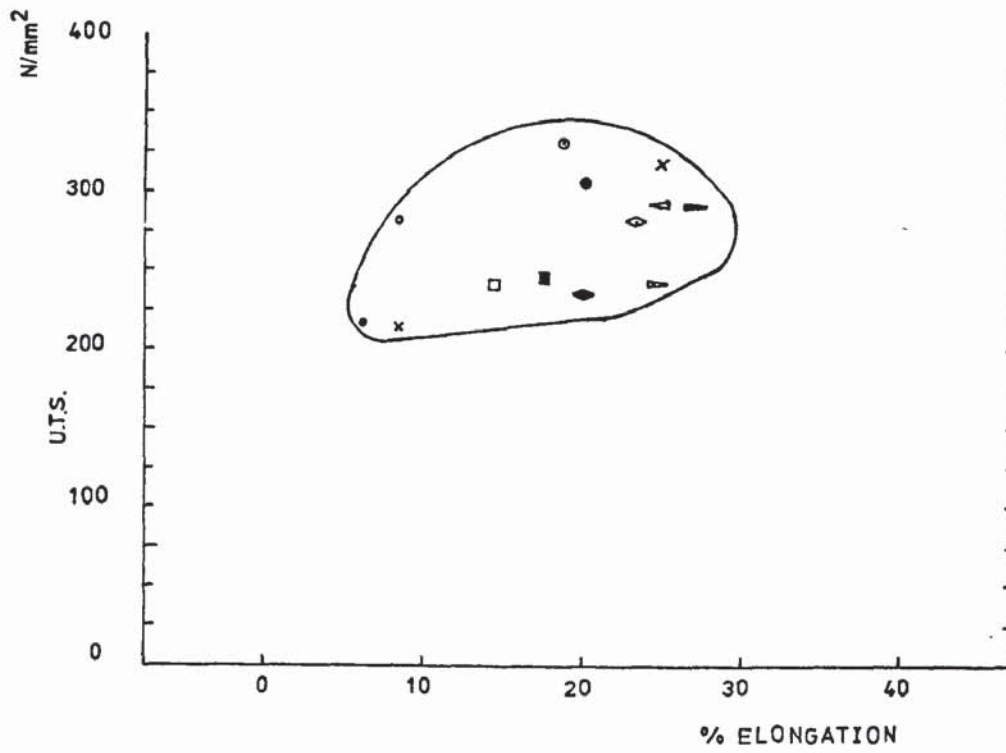
Fig. 41(a)
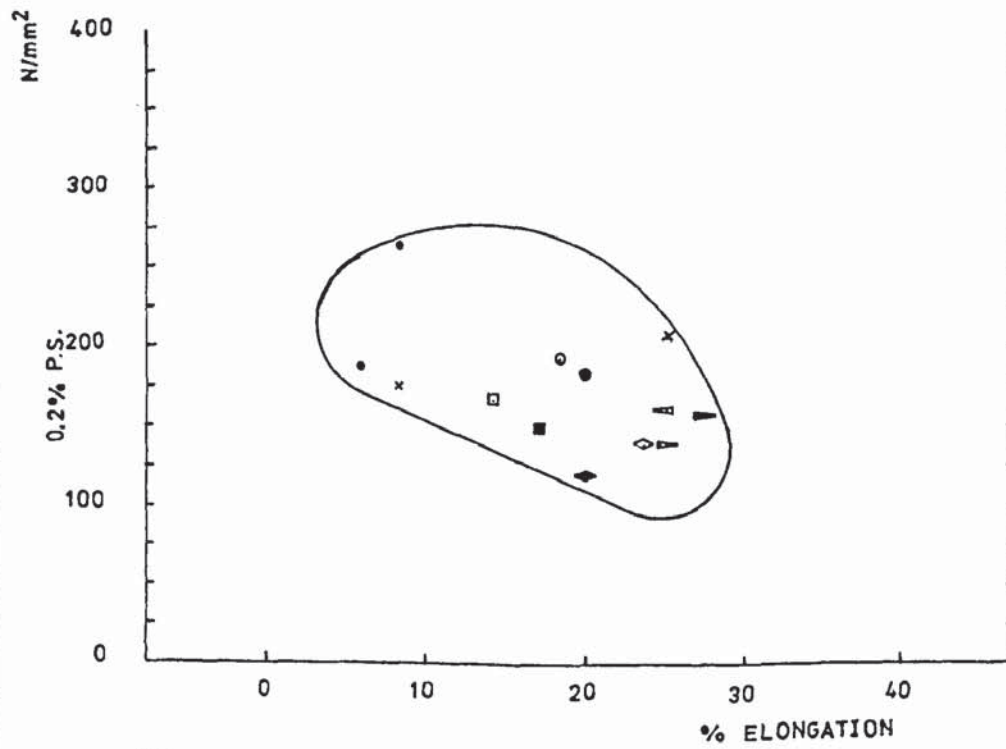
(b)

Fig. 42(a) - (b)   Relationship between (a) U.T.S. Vs IE
                      and (b) 0.2% proof stress Vs IE for
                      alloys in the "as received" condition.
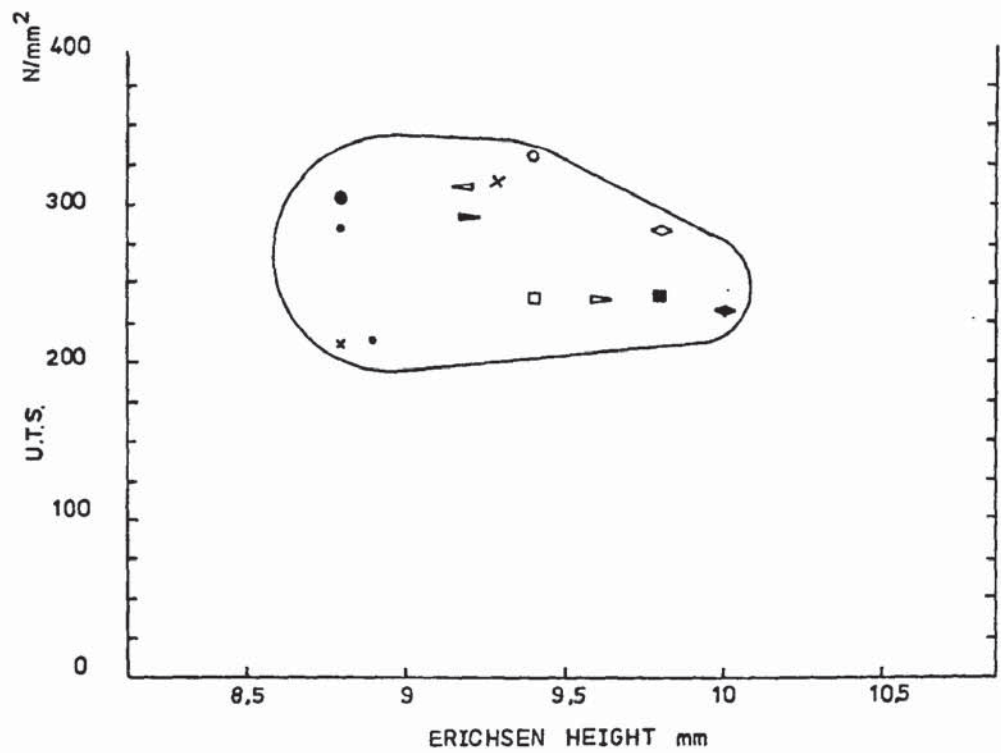
Fig. 42(a)
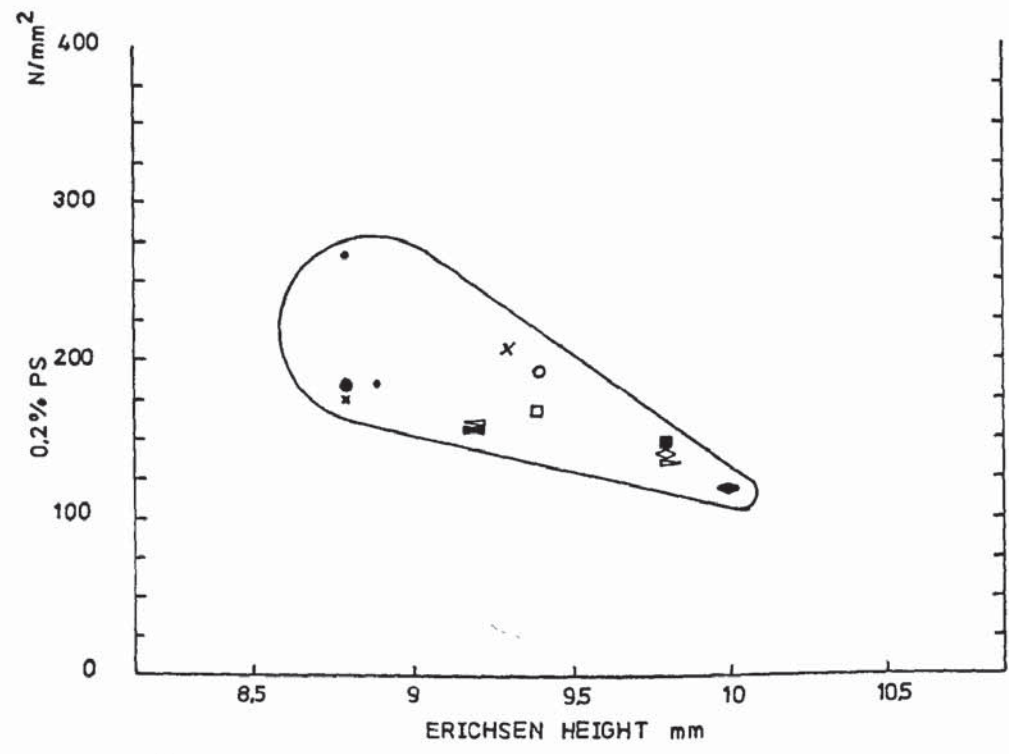
(b)

due, in part, to the initial sheet textures and the textures developed in the sheet during testing. Texture was found to influence ductility in later work and this is described further in the discussion below. It is also probable that the distribution of second phase particles influences ductility in the Erichsen test and this varies from material to material as will be discussed later. When testing the "as received" sheets in tension there were seen to be severe stretcher-strain markings on 5182 but all others were essentially free from the Luders phenomenon. It is reasonable to suppose that 5182 would be acceptable for inner panels where high formability is more important than dent-resistance and where surface defects such as stretcher-strain marks will be concealed. Taking cognisence of all the materials examined in the "as received" condition, it does not seem possible to distinguish one family of alloys as distinctly preferable to the others. There are good and bad examples of each type and even of the same nominal alloy received from different manufacturers (eg. 2117 CP and 2117 A). Evidently the details of the processing route for manufacturing the sheet are of vital importance to its press-forming quality.

Natural and artificial ageing characteristics were determined after solution heat-treatment of the alloys, Figs 20 and 21. It was found, as expected, that the age-hardening alloys and cold worked 5xxx alloys showed a considerable drop in strength properties after solution heat-treatment (in the case of the 5xxx alloys this corresponded to a recrystallization anneal). During natural ageing at room temperature both the 2xxx and 6xxx family of alloys produced an optimum ageing response after two to four days although some specific alloys were

-134-

found to continue ageing for periods in excess of one month. Hardness values of these alloys followed closely the variation in proof stress with time. The 5xxx series of alloys are generally considered to be non-heat-treatable. Slight increases in strength were observed for B164-BB3. This may be due to the gradual formation of magnesium clouds around dislocations thus increasing the stress required to produce movement (251).

Artificial ageing response highlights differences between alloy families not immediately apparent from natural ageing data. Alloys belonging to the 6xxx group all showed an increase in strength at low ageing temperatures, 150°C. This strength increase did not vary substantially between 150-190°C. Above 190°C values of strength superior to those of the "as received" condition were produced in several of these alloys. The reason for this type of behaviour is probably due to the presence of two different strengthening mechanisms. At low temperature (below 190°C) an accelerated form of natural ageing is the most likely explanation. At temperatures above 190°C a modification to the precipitation process would account for the higher strengths. The 2xxx series alloys also show strength increases at temperatures around 150°C. However, in the case of 2117 CP and 2117 HP, a loss of properties is apparent with increasing temperature, as a result of reversion to which these specific alloys are susceptible. Alloy 2002 exhibits the best artificial ageing response in its class and displays a plateau similar to that described for the 6xxx alloys between 150° to 190°C. The explanation for this phenomenon would appear to be due to the way in which alloy composition

is formulated. In 2002 the Mg and Si contents are optimized to overcome reversion. On reversion of the copper-rich zones, Mg_2Si precipitation compensates for the strength but there is a subsequent sacrifice in ductility. From table 2. it can be seen that alloys 6009 and 6010 have a significant Cu content which is probably added to provide adequate low temperature strengthening. Again, 5xxx alloys show little variation in properties with artificial ageing treatments.

As these alloys are intended for use in the automotive pressing industry, where they will be used in the "as received" condition, it is most important that alloy characteristics should be determined both for conditions that will be encountered in the press-shop and for those in service in the vehicle. Fig 43 shows the proof stress for all alloys in the "as received" condition and, where possible, values of proof stress after 15% prestrain and subsequent ageing at 190°C for 15 minutes. The prestrain is intended to simulate average strain induced in a heavily stretched panel prior to paint stoving. Paint stoving is simulated by heat-treatment of these alloys at 190°C as previously stated.

Until recently, it has been commercial practice to use anodic electro-priming of vehicle bodies which required subsequent baking around 170°C. However, a cathodic process has now been adopted which provides much better corrosion resistance and which necessitates baking at 190°C. During this heat treatment there is competition between recovery processes which tend to soften the base material and precipitation which strengthens it. Apart from 2002 which shows a small nett strengthening, the alloys become weaker as a result of the

-136-

Fig. 43   0.2% Proof stress for alloys in the "as received" condition, after 15% prestrain and after 15% prestrain + simulated paint bake cycle (15 minutes @ 190° C).
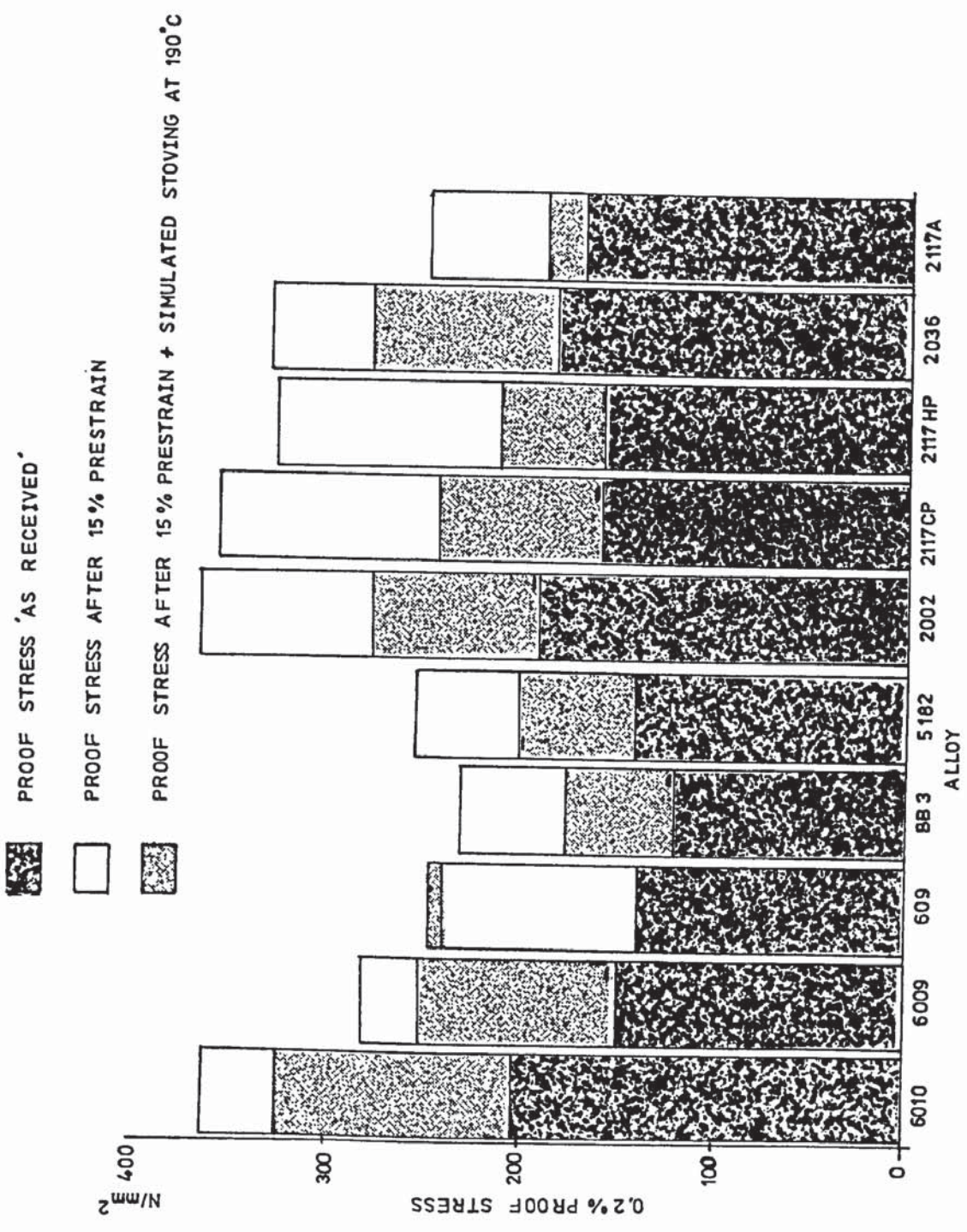
Fig. 43

190°C anneal. Generally, the 6xxx alloys are rather better than 2xxx in this respect, and 5xxx alloys which are not susceptible to precipitation show the greatest softening. The final "service" strengths of the alloys can also be ranked on the basis of Fig 43.

6.2 Properties of Alloys for Further Investigation

Of the thirteen alloys originally investigated, four were chosen for much more detailed examination of their plastic properties and formability. These were 6010, 5182, 2117 CP and 2117 HP and were selected because they represented all three classes of alloy and were broadly similar with respect to strength levels and other mechanical properties. Table 4. summarises the more important tensile properties from section 5.1.

Typical microstructures for the alloys are shown in Fig. 25. Alloy 6010 and both 2117 alloys were found to have similar grain sizes ~20-25μm while the grain size of 5182 was ~10-15μm. The latter is rather smaller than usual for formable sheet and may contribute to the severe Ludering which the alloy shows. The relationships between grain size, work-hardening behaviour, ductility and formability have not yet been clearly established. In the past these relationships have usually been based on the Hall-Petch equation which relates the yield stress σy to the reciprocal square root of the grain size (273).

$$\text{Viz.} \quad \sigma y = \sigma_i + ky\, D^{-\frac{1}{2}} \qquad (47)$$

Where D = Grain size

$\left.\begin{array}{l}\sigma i \\ \\ ky\end{array}\right\}$ depend on the detailed model applicable to the metal

At present the flow stress, grain size relationship for aluminium has not been well documented. Experimental investigations to date have produced contradictory results (274-276).

Second phase particles are known to influence material properties by interaction with dislocations during deformation as well as by creating voids which initiate fracture. Commercial heat-treatable aluminium alloys have been found to contain two kinds of insoluble incoherent particles (277). These are either coarse ($>1\mu$m) or submicron particles. The coarse second phase particles are formed during casting or subsequent processing. During solidification, Fe and Si combine with other elements giving coarse insoluble particles such as $Al_7 Cu_2 Fe$. The normally soluble $CuAl_2$ phase is not completely dissolved during fabrication and is present as particles of approximately the same size as those containing Fe or Si. These coarse particles are detrimental to properties such as toughness and ductility because they have been found to fracture when stressed (277). Submicron particles are mainly formed during heat-treatment and processing after casting. They are rich in Cr, Mn or Zr which may be added to control recrystallization and grain growth. It has been proposed that these particles promote a homogeneous mode of deformation and so avoid dislocation pile-ups at grain boundaries (277). In the present work, alloy 6010 was found to be exceptional in that it contained a very high density of sub-micron particles and none larger than 2.5μm. The average inter-particle separation on a plane of section was 1.9μm. Alloy 5182 showed the next densest particle dispersion with an average separation of 3.3μm. This and both 2117 alloys contained occasional coarse second phase particles up to 100μm diameter. The average particle

separation for 2117 CP and 2117 HP were 5.45μm and 5.7μm respectively. None of the alloys showed obvious alignment of particles along the rolling direction.

As can be seen from Fig 25 the grain structure of these alloys is slightly elongated in the plane of the sheet which may be inpart a result of temper rolling during production but may also have resulted from recrystallization in the presence of second phase particles.

When during cold working, the grains become elongated in the direction of maximum extension, the crystal lattices rotate into preferred orientations. Material with such preferred orientation is said to possess a texture and the properties of the material as a whole then become anisotropic. Any non-metallic inclusions become elongated into fibres and if these lie along the direction of maximum stress their detrimental effect is much reduced.

Fig. 23 illustrates the "as received" sheet metal textures. Alloy 6010 shows a fairly weak texture consisting of a weak cube texture with (110) [112] and (110) [001] components. Alloy 5182 exhibits only a very weak cube texture. In comparison, both 2117 alloys have strong textures. 2117 CP shows a strong retained rolling texture (123) [412] with a strong (110) [001] component while 2117 HP shows strong (110) [001] plus (110) [112] components. The two combined texture components identified in 2117 HP show an approximate six-fold symmetry in the texture. This was confirmed during deep drawing trials by the presence of six fold earing on drawn cups of this alloy.

The coefficient of plastic anisotropy is a reflection of sheet texture, its value changing according to alloy type and processing history. Preferred orientation is known to affect sheet metal behaviour in the plastic strain range and for some anisotropic metals drawing qualities have been found to be superior to those observed in isotropic sheet (58). Table 3. gives the average r-values for alloys in the "as received" condition. In all cases the r-value is less than unity indicating poor drawability. Hu (63) and others have shown that (100) textures correspond to $\bar{r}$-values less than unity and that (111) and (110) give $\bar{r} > 1$. In the present alloys it seems that the cube texture component has a dominant effect despite its low level. Both 2117 alloys which have strong (110) components show higher $\bar{r}$-values than 6010 and 5182 but these are still less than unity. Relative to steels for which $\bar{r}$-values typically range from ~1.3 to ~2.0, the present aluminium alloys are expected to show poor deep drawing performance.

6.3   Work Hardening and Strain Distribution

Values of stress and strain measured during uniaxial tensile tests are only useful in indicating the work hardening behaviour of a material over the limited range of deformation where elongation is uniform. Because of the relatively low values of effective strain achieved in uniaxial tension as compared with equibiaxial stress states it has been difficult in the past to compare the work hardening behaviour for an alloy subjected to uniaxial or equibiaxial stress at high effective strains. To be able to make such a comparison it is first necessary to establish a uniaxial tensile testing technique which will

-141-

allow values of effective strain equivalent to those reached during biaxial testing to be achieved. This is somewhat difficult since it entails deferring tensile instability over an extended strain range or else making measurements within the neck itself (278). The author believes that the procedure developed, described in section 4.1, has solved some of the problems encountered but has left others unresolved. The technique has been found to be very successful for high strength alloys which do not exhibit serrated yielding. In these alloys nominal elongation values approaching 50% have been recorded which corresponds to approximately twice the usual value. For alloys which exhibit serrated yielding characteristics, typically those alloys belonging to the 5xxx family, nominal strains approaching 35% have been achieved.

To extend the values of strain achieved during this research either smaller strain increments between backing strip changes should be used or a higher strength adhesive employed.

Fig. 26 shows the nominal stress-strain curves for alloys 6010, 2117 HP and 2117 CP. The n values for these alloys range between 0.21 and 0.31. Fig 27 shows the true stress-true strain curves for the above alloys. Both biaxial and uniaxial data are included. As can be seen from this figure the stress-strain curves for biaxial tension generally lie above those for uniaxial tension despite r being less than unity. Theoretically the stress-strain curve for an anisotropic material should be different in biaxial tension compared to uniaxial tension (227). Mellor and Bramley (279) have studied the flow behaviour

of anisotropic metals and concluded that the biaxial stress-strain curves could be predicted from uniaxial tensile test data using the relationships

$$\bar{\sigma} = (\frac{1 + \bar{r}}{2})^{\frac{1}{2}} \; \sigma_{AVE} \tag{48}$$

$$\bar{\epsilon} = (\frac{2}{1 + \bar{r}})^{\frac{1}{2}} \; \epsilon_{AVE} \tag{49}$$

where $\bar{\epsilon}$ = Biaxial true strain

$\bar{\sigma}$ = Biaxial true stress

$\bar{r}$ = Average planar anisotropy index

σ_{AVE} = Average uniaxial tensile true stress

ϵ_{AVE} = Average uniaxial tensile true strain

The yield criterion of anisotropic sheet metal under combined stresses, developed by Hill (92) from the Von Mises criterion included special types of anisotropy of engineering importance, in particular, anisotropy resulting from the textures of cold rolled sheet metals. If it is assumed that sheet texture gives rise to transversely isotropic properties (280) (as an approximation) and $\sigma_3 = 0$, the Hill yield function reduces to

$$(\sigma_1 + \sigma_2)^2 + (1 + 2r)(\sigma_1 - \sigma_2)^2 = 2(1 + r)\sigma_u^2 \tag{50}$$

where σ_1 and σ_2 = principal stresses

σ_u = uniaxial yield stress

r = strain increment ratio

-143-

Hosford and Backofen (281) simplified the above to

$$\frac{\sigma b}{\sigma u} = (\frac{\overline{r} + 1}{2})^{\frac{1}{2}} \qquad (51)$$

for the case of balanced biaxial tension

where

σb = Equibiaxial yield stress

$\overline{r}$ = Average strain ratio $\varepsilon_w / \varepsilon_t$

Table 6. Compares the ratio σ_b / σ_u calculated using Hills theory with values determined experimentally.

Alloy	$\sigma b / \sigma u$ Calculated	Experimental
6010	0.89	1.12
2117 HP	0.97	1.04
2117 CP	0.92	1.17

Table 6. Comparison of calculated and experimentally determined values of σb/σu.

These results show the same trends as those published by Woodthorpe and Pearce (95). They also calculated $\sigma b/\sigma u$ to be less than unity while the experimentally determined ratio was greater than unity. The above results indicate that Mellor and Bramleys modification of Hills theory is not valid for aluminium, a fact concluded by Woodthorpe and Pearce who suggested that the anomaly could be a result of the deformation behaviour of aluminium. Bassani (96) has found that the above discrepancy is explicable in terms of certain texture components when applying the Bishop-Hill analysis of crystal deformation (282). When r and $\sigma b/\sigma u$ are plotted for ideal transversely isotropic textures he has observed regions where $\sigma b/\sigma u$ and r lie on opposite sides of unity. Fig (44) summarises the results of his calculations.
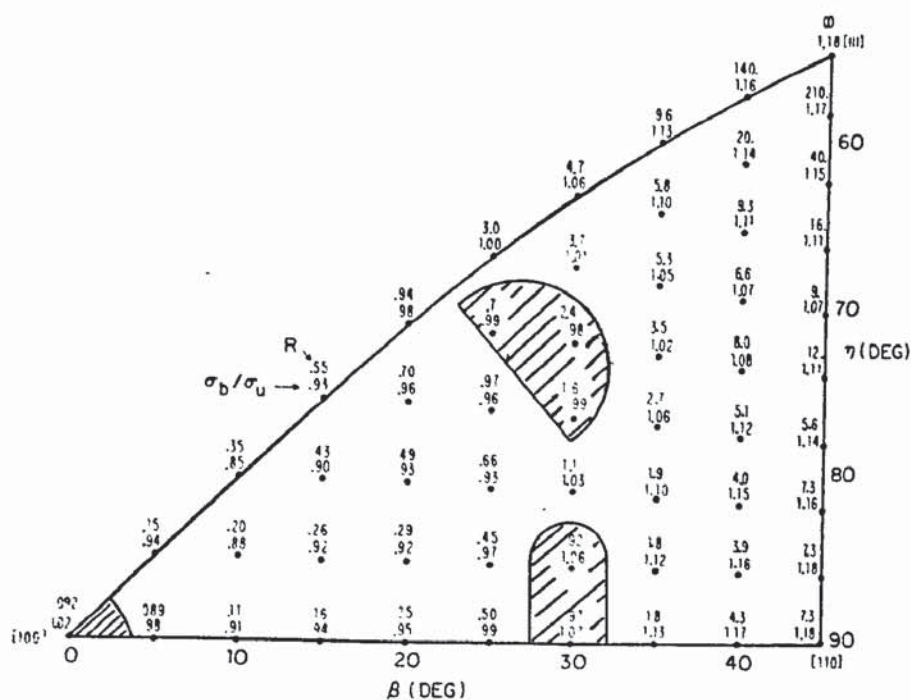
Fig. 44. r-values (top number in pair) and σb/σu for ideal textures associated with points on spherical triangle (96).

Minimum r values for ideal textures occur in the neighbourhood of
[100] and the maximum r value is at the [111] ideal texture.
Shaded regions in the unit triangle show texture components which would
demonstrate anomolous behaviour. However, the magnitude of the
observed discrepancy is much greater than that calculated even on the
basis of sharp ideal textures. When the 2117 alloys are considered
(which show strong (110) textures) it is quite inconceivable that
Bassani's explanation of the anomoly is correct.

Another possible explanation for the anomalous behaviour of aluminium
may be non-perfect planar isotropy ie. the condition for $\epsilon_1 = \epsilon_2$
in bulging does not correspond to $\sigma_1 = \sigma_2$.

Hero and Naess (283) have suggested that the differences in the stress
strain curves for aluminium when $r \leqslant 1$ may indicate that the concept
of isotropic work hardening may not be correct. Non-isotropic work
hardening could arise as a result of microscopically inhomogeneous
slip deformation. Coarse slip bands and shear bands are relatively
ineffective in biaxial stretching but can develop readily in
unconstrained simple tension. The work hardening rates for 6010,
2117 CP and 2117 HP as measured by the change in stress and change in
strain $d\sigma/d\epsilon$ were calculated from bulge test and uniaxial tensile test
data.

The results are presented in Fig 45 (a)-(c). It can be seen that for
alloy 2117 CP the work hardening rate at any given strain in biaxial
tension is greater than that in uniaxial tension. The concept of
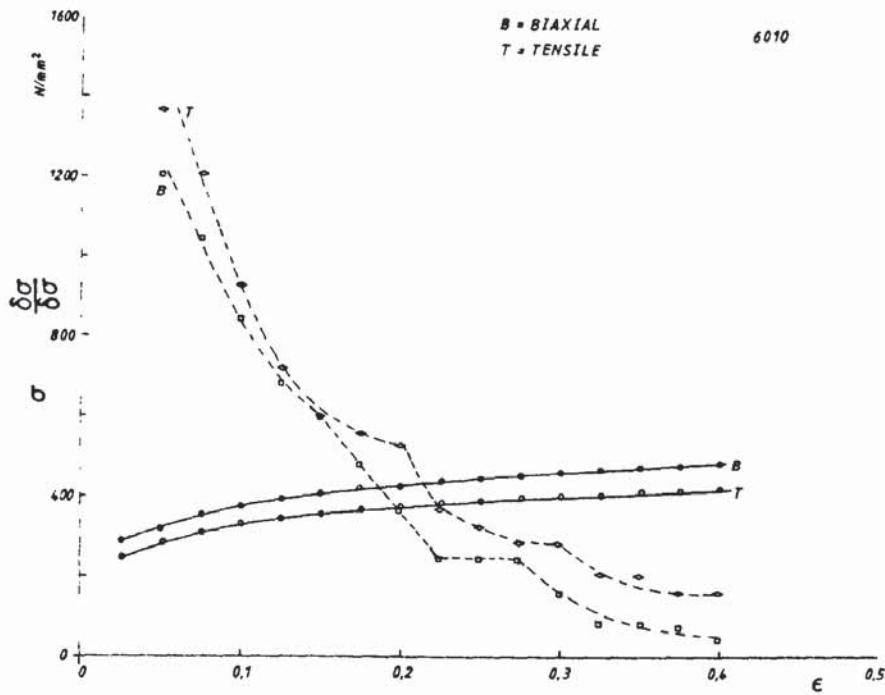
Fig. 45(a)-(c)   True stress - strain curves (solid line) and work-hardening rates (broken line) determined for uniaxial and equibiaxial stress states.
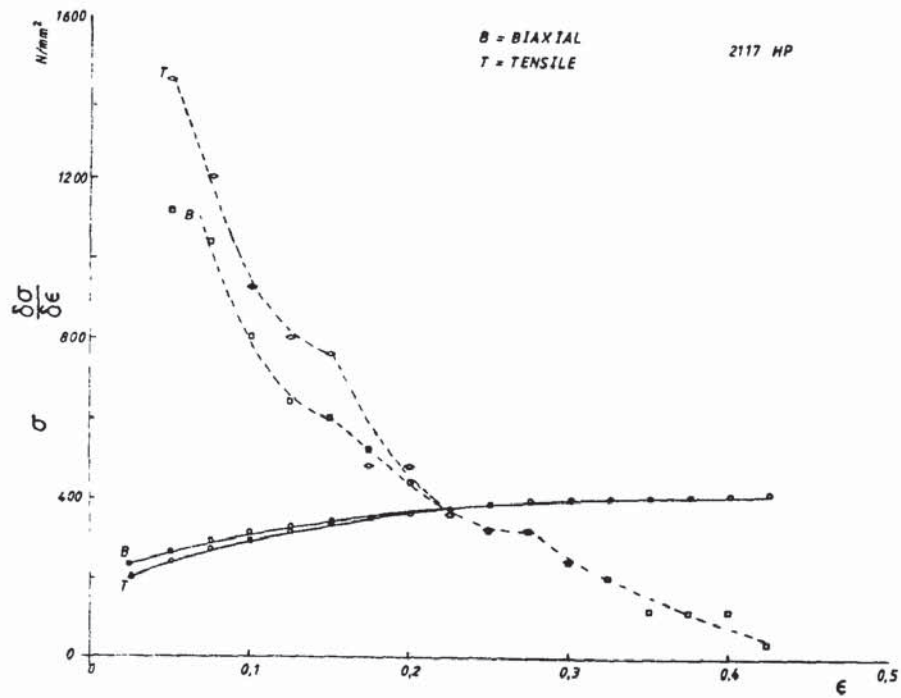
(b)
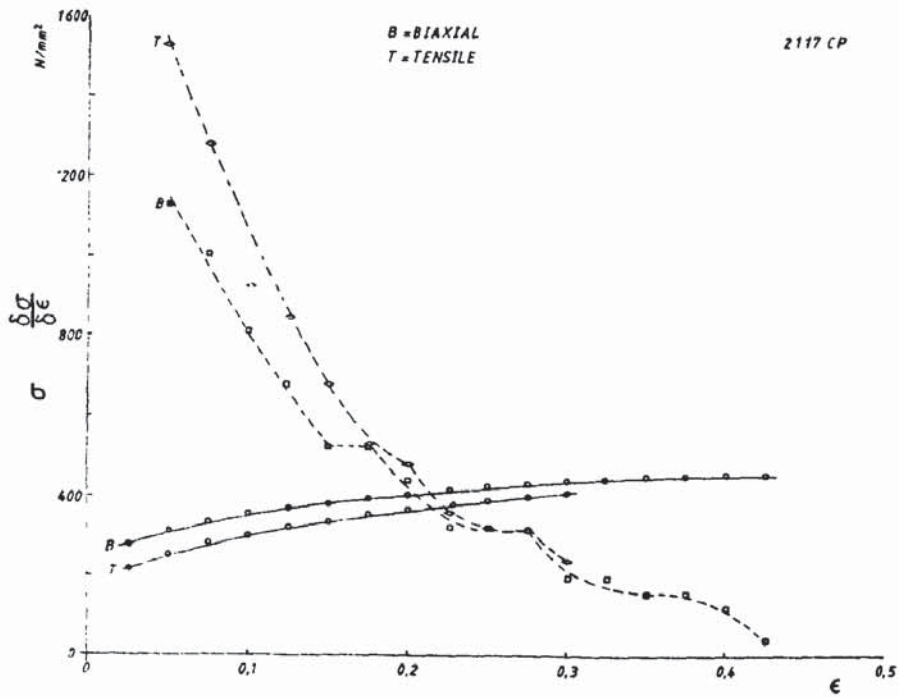
(c)

isotropic work hardening therefore does not appear to be valid for 2117 CP in agreement with the suggestion of Hero and Naess. Similarly for 2117 HP the uniaxial tensile work hardening rate is above that for biaxial up to strains of ~ 0.25 after which both $d\sigma/d\epsilon$ curves coincide. This fact would not be evident from the normal uniaxial tensile test data as uniform strains above ~ 25% are not reached. Alloy 6010 exhibits a cross-over point at $\epsilon \sim 0.12$ below which $d\sigma/d\epsilon$ is higher in uniaxial tension. The $d\sigma/d\epsilon$ curves presented are not smooth but show changes in slope - notably around the limit of uniform elongation. This rather sudden loss of work hardening capacity will contribute to instability and the rapid transition to local necking.

It seems likely that several of these observed phenomena are associated with the development of coarse slip bands and shear bands as suggested earlier by Andersson (284). The strengthening effect in age hardened alloys arising when particle size and spacing is small, such as with coherent G.P. zones, can be explained if we consider the way in which dislocations react with these particles. Slip dislocations can cut through them during the early stages of deformation. Once these particles have been cut it becomes progressively easier for further dislocations to move along the same slip plane as the particles no longer act as such effective barriers. This results in an inhomogeneous mode of deformation in the form of intense slip bands which may link together from grain to grain, especially in the presence of a suitable sharp texture, to create macroscopic shear bands. These in turn can develop into shear fractures of the types commonly found in these alloys. It seems highly probable that the relatively low tensile ductility in rolling direction specimens and the tendency for

fracture along the transverse direction in equi-biaxial bulging are due to this type of texture-induced shear band formation.

Alternatively, when the particles are large and widely spaced, such as the equilibrium precipitates, slip dislocations do not cut these particles but avoid them by cross-slip or Orowan looping mechanisms.

The theory behind these effects can be explained if we consider a dislocation line, subjected to a small shear stress, moving until it reaches an obstacle. If the stress increases, it will bow out between the obstacles and a sufficient increase in stress will cause it to break through the spaces between them. The stress required for the latter is given by the Orowan formula.

$$\sigma = \frac{2Gb}{d} \qquad (52)$$

where
σ = Stress

G = Shear Modulus

b = Burgers Vector

d = Interparticle spacing

When yielding takes place by this process a dislocation loop is left around each obstacle. This increases the effective size of the particle and consequently decreases d. It would therefore be expected that work hardening should be more rapid in a dispersion hardened system than in one that does not depend on this mechanism. Considering Fig. 24 we can see that alloy 6010 has a very high proportion of submicron particles. In contrast the 2117 alloys have much lower

particle counts but a greater proportion in excess of 1μm diameter. 5182 has a particle count approximately three times that of the 2117 alloys with an equal diameter distribution.

The strengthening increment due to second phase particles was calculated using the Orowan formula assuming an equal volume fraction of particles for each alloy. This approximation is well justified in view of the small volume of fraction of second phase. Interparticle spacing was calculated as

$$d = \sqrt{\frac{\text{Field Area}}{\text{No. of particles observed}}} \qquad (53)$$

Table 7. Summarises the increment of hardening that may be attributed to Orowan looping around the observed particles.

Alloy	Mean Inter-Particle Spacing (μm)	Strengthening increment (MPa)
6010	1.9	4.5
5182	3.3	2.6
2117 CP	5.45	1.6
2117 HP	5.7	1.5

Table 7. Hardening increment attributable to Orowan looping around observed second phase particles for alloys 6010, 5182, 2117 HP and 2117 CP.

These effects are clearly very small in comparison with the typical yield and flow stresses of the alloys (~ 200 MPa). It must therefore be considered unlikely that such particles can play a significant role in the plastic deformation of the alloys.

Fig 46 illustrates the pattern of true thickness strains for a row of grid circles on 2117 CP sheet bulged through a circular die at various pressure increments. The solid line denotes experimental strains whilst the broken line shows calculated strains. The calculated strains were computed using a finite element programme developed by Dr. P. Bate , a member of the department. An explanation of his programme has been presented elsewhere (285). It can be seen that agreement between experimental and calculated values is quite good for strains developed at the bulge periphery. However as the pole of the bulge is approached so the discrepancy between experimental and calculated strain increases. Since a state of plane strain exists at the bulge periphery which changes progressively to one of equibiaxial strain at the pole it might be expected that an equation utilizing data obtained from uniaxial tensile tests would approximate plane strain conditions more closely, in the case of aluminium, for reasons proposed earlier by Hero and Naess and discussed above.

Discrepancies between calculation and measurement become increasingly severe towards the pole of the bulge (biaxial stretching). Agreement in this region could certainly be improved if the stress-strain data used in the programme were derived from biaxial testing since the lighter flow-stress levels would lead to reduced strain values as

Fig. 46(a) Comparison of true thickness strains for a row of grid circles on 2117 CP sheet bulged through a circular die at various pressure increments (solid line) with calculated strains derived using a finite element technique (broken line).

(b) Bulge height Vs pressure curves for 2117 CP sheet; experimental values - solid line, calculated values - broken line.

Fig. 46(a)
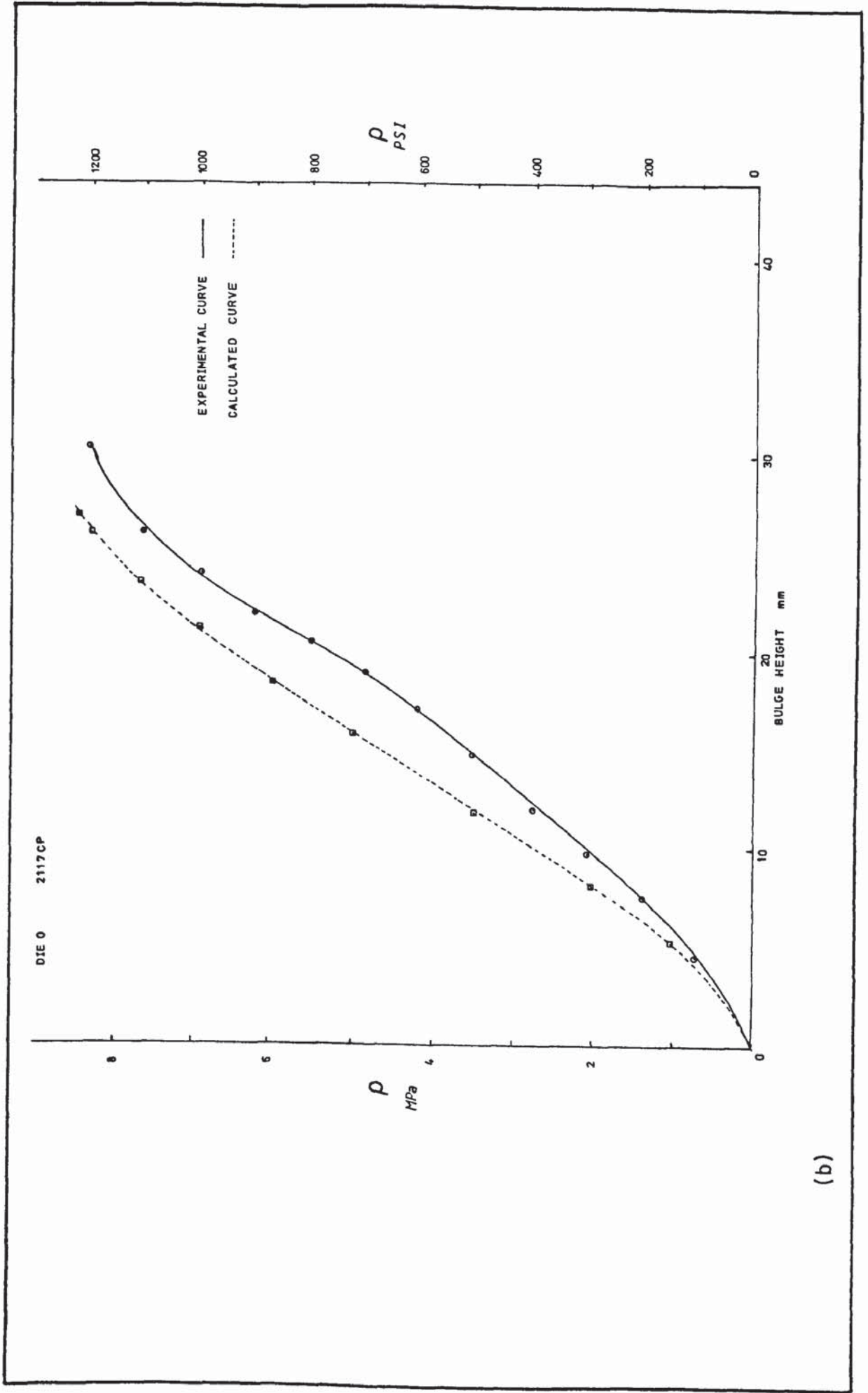
(b)

measured. Taking these results together with the earlier discussion
it does not appear that simple yield and flow criteria of the von Mises
or Hill type are adequate to describe these types of aluminium alloys.

6.4   Factors Controlling Limit Strains

Limit strains for the four alloys shown in Fig 31 were determined
using two different test techniques. In the first method varying
strain ratios were induced by bulge forming sheet specimens through a
series of elliptical dies and by the use of specially shaped tensile
specimens. The second method utilized the procedure attributed to
Nakazima. Results showed that limit strains determined using the
two methods differed significantly. Nakazima strip tests consistently
produced limit strains which were higher than those measured using
the alternative approach. Similar results have been obtained by
Pearce and Ganguli (286). Differences in test method parameters
were restricted to specimen curvature, described in section 3.5.1.3
and the effect of friction between punch and metal surface occuring in
the Nakazima strip tests. Charpentier (222) found limit strains to
increase with increasing punch curvature (1/R) at constant material
thickness. This is in agreement with the findings presented above if
we consider R to be the punch radius or bulge specimen radius.
However, it is more likely that the effect described above is a
consequence of the boundary conditions that exist between sheet and
punch and which are lacking in the hydraulic bulge test. It is
suggested that the effect of friction between the punch and sheet
surface will be to restrict straining in the contact area and so

inhibit the formation of a local discontinuity. In particular, the tendency for macroscopic shear band formation which could lead to a shear fracture will be restricted in the case of punch stretching but can occur freely in bulging.

Alloy 5182 and both the 2117 alloys show a preference for the failure line to run parallel to the transverse direction of the sheet in biaxial testing. Lower tensile ductilities were observed in specimens cut parallel to the rolling direction than in transverse direction specimens. Almost certainly these effects have their origins in the crystallographic textures of the sheets. The major peaks in the (111) pole figures, Fig 23, are approximately 40° from the sheet normal, tilted towards the rolling direction. These correspond to concentrations of crystallographic slip planes which are oriented to favour the type of shear failure that is observed in these alloys. Similar effects have been found by Andersson (284) in an Al-Zn-Mg alloy. More detailed analysis of this phenomenon is necessary but there does seem to be a clear effect of crystallographic texture on the failure process which is apparently related to the forming limits. In the case of alloy 6010, the texture is rather weak and does not show the same disposition of the (111) planes. This different texture together with the much higher inclusion density probably accounts for the fact that failure occurs preferentially parallel to the rolling direction in this alloy.

Three types of failure mode were generally observed during the determination of limit strains, Fig 32. These consisted of a ductile

fracture behaviour within a neck normally observed in punch stretched or tensile specimens where the minor strain $e_2 < 0$, shear failure in an apparent plastic neck evident in some punch stretched and hydraulically bulged samples and an abrupt shear failure without evident prior necking observed in hydraulically bulged specimens approaching equibiaxial straining.

These failure modes produced fracture surfaces of the type shown in Fig 33. The process of ductile fracture by void nucleation and coalescence is well documented and is covered in section 3.4.5. French and Weinrich (287) have examined the influence of the degree of stress triaxiality on the tensile fracture of F.C.C. metals and alloys. They found that the most common feature of deformation of these alloys was the occurence of microscopic shear zones prior to fracture. Microstructural observations in the present work suggest that shear bands develop as sharp localized instabilities and that separation occurs by linking of voids within the shear bands, Fig 35. The tendency for fracture without prior necking is greatest in the 2117 CP alloy and least for 5182 which displays serrated yielding. The characteristic directions along which shear instability bands form depends on the stress state.

In the event of fracture by either ductile or shear mechanisms, voids were not observed to develop at the site of instability until the moment of failure. This is probably due to the strong particle/matrix interface observed in aluminium alloys (117). Because of this voids develop only just prior to fracture and void coalescence occurs rapidly and only close to the fracture path.

The most significant findings of the present work are that different
failure mechanisms can operate depending on strain state and surface
condition, and that limit strains can be greatly reduced. As
previously stated, the tendency for fracture without prior necking is
greatest in the 2117 CP alloy where this occurs for all conditions of
biaxial stretching and least for 5182 where necking always occurs
unless the sheet is scratched, Fig. 39. In cases where there is no
localization of strain prior to the final failure, it is clear that
the M-K hypothesis of continuous groove development cannot apply. If
failure occurs by the linking of voids within a shear band, as has
been observed, then the criterion that defines the limit strains is
that for the initiation of a shear band. This subject has received
considerable attention in recent years and some of the effects relevant
to sheet metal forming have been recently summarised by Bird and
Duncan (288). It has been suggested that shear bands will occur if a
zero or negative work hardening rate is reached in the homogeneous
deformation behaviour. However, this condition would imply failure
at a constant value of effective strain which is quite different
from the observed behaviour. On the basis that the shear band may
be triggered by an avalanche of slip dislocations when the stress at
the tip of a pile-up reaches a critical value to overcome the resistance
of hardening-precipitates, or other obstacles, a simple critical shear
stress condition might be expected. A criterion of this type can
be applied as shown by Embury and LeRoy (237) to calculate the shape
of the F.L.C.

Calculations of forming limits, results of which are presented in
Fig 40, made use of effective stress-effective strain relationships
which were determined for each material in simple tension and
approximated by the relationship.

$$\bar{\sigma} = k\bar{\varepsilon}^n$$

A single value of critical shear stress for failure was obtained for
each alloy by fitting the calculated values to the observed F.L.C.
values for conditions of abrupt fracture in smooth sheet. This
corresponded to strain states of biaxial stretching. Alloy 5182 could
not be included since abrupt fracture was not observed under any
condition in the absence of grooves. Having determined the relevant
critical shear stress, theoretical failure strains were calculated
for all strain states relevant to the F.L.C. Fig 40 shows there is
tolerably good fit in the stretching quadrant as would be expected
from the method of calculation. Any agreement for conditions of
negative minor strains must be coincidental since instability and
necking are expected to dominate the failure process here. Limit
strains were also calculated for the grooved specimens using the
appropriate shear stress values as before but also including a
"stress concentrating factor" which was obtained in each case by
fitting the calculation to experimental values. Fig 40 again shows
that tolerable agreement can be obtained in this way. Despite the
extensive plasticity that has taken place there seems to be a residual
stress concentration arising from the shape of the grooves since these
are approximately twice as effective in the failure process as would
be expected on the basis of a simple reduction in cross-section.

Deep grooves are found to be proportionally more deleterious than shallow ones, Fig 37.

It might be expected at first sight that a transition from a necking mode to an abrupt fracture mode would be accompanied by a knee in the F.L.C. as the criterion for failure changes. Fig 39 shows this is not the case. However, examination of cross-sections of the fracture sites shows that in many cases the local neck is formed by the operation of a pair of shear bands leading to the intrusion of a rigid wedge of material. The example in Fig 32 (b) is probably of this type. If this view is correct the distinction between necking and abrupt fracture may not be fundamental in such alloys but may reflect the point at which a localized plastic shear leads to decohesion and shear fracture. As the strain state moves progressively towards biaxial tension the level of the effective strain increases and the residual ductility decreases so that conditions for abrupt fracture are established. Local necking which does not involve shear band formation may still be expected when the minor strain has a negative value.

7.   CONCLUSIONS

Investigations have been carried out on a wide variety of strong
formable aluminium sheet alloys. The chief aims have been to
evaluate their important mechanical properties and to try to
understand the factors which control their formability. The main find-
ings were as follows:

1. It is not possible to select one family of alloys as generally
superior to the others. Instead it has been found that specific alloy
composition and processing route play a significant role in determining
the final formability that an individual alloy may possess. There is
a trend towards lower ductility in alloys with higher proof stresses
but no obvious correlation with U.T.S. values.

2. Ageing characteristics of the alloys differ considerably. These
can be broadly grouped into three types of response associated with
alloy composition. The 6xxx family show the most promising results
because of their combination of good low temperature ageing
characteristics, a result of Cu content, and higher temperature
characteristics, a result of Mg-Si content. The 2xxx alloys have
inferior ageing responses at temperatures in excess of   160°C due to
stress relief or reversion effects. Alloys of the 5xxx family are not
age-hardenable and soften by recovery processes.

3. A new technique has been developed enabling uniaxial tensile stress-
strain data to be obtained at strains upto twice those normally reached.
This has allowed comparison of stress-strain relationships from

uniaxial and equibiaxial tensile tests at strains approaching failure in the latter mode of stretching.

4. It has been confirmed that a discrepancy exists between the stress-strain curves obtained from uniaxial and equibiaxial tensile tests which cannot be explained in terms of either the Hill or Bishop-Hill theories. It is concluded that the most likely explanation for this anomoly is that these materials do not show isotropic work hardening.

5. It is believed that deformation mechanisms in these alloys involve unusually coarse slip bands and shear bands. Non-isotropic work-hardening may arise as a result of microscopically inhomogeneous slip deformation which is favoured by certain states of macroscopic strain. Both instability and fracture are controlled by these mechanisms.

6. Alloy texture is important to work-hardening, ductility and formability due to its associated effect on shear band formation. It is proposed that, during inhomogeneous deformation, intense slip bands may link together from grain to grain, assisted by the presence of a suitable sharp texture, to create macroscopic shear bands. Void formation and linkage within these bands leads to shear fractures of the type observed in these alloys.

7. Forming limit curves are influenced by mode of testing, alloy type, texture and surface condition.

8. Different failure mechanisms have been found to exist which are dependant on the applied stress state. The failure modes range from necking (fibrous ductile fracture) to abrupt shear fracture with a mixed mode of fracture prevalent between the two extremes.

9. Forming limit curves for these alloys can be modelled reasonably well on the basis of a critical shear stress for fracture.

10. The stress concentrating effect of surface scratches can dominate the failure process in these sheet alloys and reduce the level of the F.L.C. The amount by which the limit strains are reduced is directly related to the severity of the surface defects introduced. Scratches produce a stress concentrating effect which promotes premature shear fracture rather than failure by gradual groove development as proposed by Marciniak.

ACKNOWLEDGEMENTS

Calculation of Theoretical Limit Strain

Assuming constancy of volume, then

$$\epsilon_1 + \epsilon_2 + \epsilon_3 = 0$$

As a starting point the major and minor strains, e_1 and e_2 respectively, are determined experimentally. True strains are then given by

$$\epsilon_1 = \ln(1 + e_1)$$

$$\epsilon_2 = \ln(1 + e_2)$$

The strain ratio β and thence the stress ratio α are determined as

$$\beta = \epsilon_2/\epsilon_1$$

$$\alpha = \sigma_2/\sigma_1 = \frac{(2\beta + 1)}{(2 + \beta)}$$

Effective strain, $\bar{\epsilon}$, is given by

$$\bar{\epsilon} = \sqrt{4/3\ (\epsilon_1^2 + \epsilon_2^2 + \epsilon_1\epsilon_2)}$$

$$\bar{\epsilon} = \epsilon_1\sqrt{4/3\ (1 + \beta + \beta^2)}$$

Assuming the material behaviour can be described by the Holloman equation, the effective stress ($\bar{\sigma}$) is

$$\bar{\sigma} = K \bar{\epsilon}^n$$

where K and n have been previously determined from uniaxial tensile test results.

The principal stresses are related to the effective stress by an equation of the form

$$\bar{\sigma} = \sqrt{\sigma_1^2 + \sigma_2^2 - \sigma_1 \sigma_2}$$

$$\bar{\sigma} = \sqrt{\sigma_1^2 - \alpha \sigma_1^2 + \alpha^2 \sigma_1^2}$$

$$\sigma = \bar{\sigma} \Big/ \sqrt{1 - \alpha + \alpha^2}$$

The critical shear stress (τ_{cr}) is given by

$$\tau_{cr} = \frac{\sigma_1}{2} \qquad \text{(for the range } \sigma_3 < \sigma_2 < \sigma_1 \text{)}$$

Having obtained a value of τ_{cr} (normally at the equi-biaxial tension condition) the calculation is carried out in reverse for different assumed values of α. This produces the values of e_1 and e_2 for various stress (strain) states which comprise the forming limit curve.

We now introduce the scratch stress concentrating factor C derived as

$$C = \frac{\text{Actual Stress}}{\text{Apparant Stress}}$$

$$\text{New } \sigma_1 = \frac{2\,\tau_{cr}}{C}$$

We now apply values of α and calculate corresponding values of β, e_1 and e_2.

REFERENCES

(1)   B.A.C.O.   "Technical Information Bulletin N° 22", April
        1976, British Aluminium Co. Ltd., London.

(2)   E.P.A. Report   "1974 Gas Mileage Ratings - Car by Car".

(3)   Huebner, G.J. (Jnr) and Gasser, D.J.   "Energy and the
        Automobile, General Factors Affecting Vehicle Fuel
        Consumption", S.A.E. Paper N° 730518, 1974.

(4)   Rolf, R.F., Sharp, M.L. and Herbein, W.C.   "Minimizing
        the Weight of Aluminium Body Panels", S.A.E. Paper N°
        790164, 1979.

(5)   Motwani, M.B.   "Application of Aluminium in Body Weight
        Reduction", S.A.E. Paper N° 770306, 1977.

(6)   Younger, D.G.   "H.S.L.A. Steels and the Weighty Auto-
        mobile Problems, Mechanical Working and Steel Processing",
        Trans. A.I.M.E., 1974.

(7)   Section 1 - "Specifications for Aluminium Structures",
        Aluminium Construction Manual,The Aluminium Association
        Inc., N.Y., 1976.

(8)   Rolf, R.L., Sharp, M.L. and Stroebel, H.H.   "Structural
        Characteristics of Aluminium Body Sheet", S.A.E. Paper
        770200, 1977.

(9)   Niemeir, B.N. and Burley, C.E.   "Hailstone Response of
        Body Panels - Real and Simulated", S.A.E. Paper N° 780398,
        1978.

(10)   DiCello, J.A. and George, R.A.   "Design Criteria for
        the Dent Resistance of Autobody Panels", S.A.E. Paper
        N° 740081, 1978.

(11)   Chang, D.C. and Justusson, J.W.   "Structural Requirements
        in Material Substitution for Car Weight Reduction",
        S.A.E. Paper N° 760023, 1976.

(12)   George, R.A., Swenson, W.E. and Adams, D.G. "Aluminium in Automobiles; Why and How it is Used", S.A.E. Paper N° 760164, 1976.

(13)   Burley, C.E., Niemeir, B.A. and Koch, G.P. "Dynamic Denting of Autobody Panels", S.A.E. Paper N° 760165, 1976.

(14)   Johnson, T.E. (Jnr) and Schaffnit, W.O. "Dent Resistance of Cold-Rolled Low-Carbon Steel Sheet", S.A.E. Paper N° 730528, 1973.

(15)   Hirth, J.P. and Weertman, J. "Work Hardening", Gordon and Breach, N.Y. 1968.

(16)   Nabarro, F.R.N., Basinski, Z.S. and Hold, D.B. "The Plasticity of Pure Single Crystals", Adv. Phy. (G.B.), 13, pp 193-323, 1964.

(17)   Lucke, K. and Mecking, H. "Inhomogeneity of Plastic Deformation", A.S.M., Metals Park, Ohio, P223, 1972.

(18)   Holloman, J.H. "Tensile Deformation", Trans. A.I.M.E., 162, pp 268-290, 1945.

(19)   Nadai, A. "Theory of Flow and Fracture of Solids", McGraw Hill Book Co. Inc., N.Y. p 77, 1950.

(20)   Freudenthal, A.M. "The Inelastic Behaviour of Engineering Materials and Structures", John Wiley and Sons Inc., N.Y., p 544, 1950.

(21)   Ghosh, A.K. "Strain Localization in the Diffuse Neck in Sheet Metal", Met. Trans., 5, pp 1607-1616, 1974.

(22)   Arbel, C. "Recherche d'une relation entre les propriétés d'emboutissage des métaux et les essais de traction", Rev. Métall. 47, pp 388-394, 1950.

(23)   Swift, H.W. "The Mechanism of a Simple Drawing Operation", Engineering, 178, pp 431-435, 1954.

(24)   Ludwik, P. "Elemente der Technologischen Mechanik", Verlag von Julius Springer, Berlin, 1909.

(25)   Swift, H.W. "Plastic Instability Under Plane Stress",
         J. Mech. Phys. Solids, 1, pp 1-18, 1952.

(26)   Voce, E. "The Relationship Between Stress and Strain
         for Homogeneous Deformation", J.I.M., 74, pp 537-562,
         1947.

(27)   Kleemola, H.J. and Nieminen, M.A. "On the Strain Hardening
         Parameters of Metals", Met. trans., 5, pp 1863-1866.

(28)   Considere, M., Annls. Ponts Chauss, 9, p 574, 1885.

(29)   Zener, C. and Holloman, J.H. "Effect of Strain Rate
         Upon Plastic Flow of Steel", J. App. Phys., 15, pp 22-32,
         1944.

(30)   Backofen, W.A. in "Fracture of Engineering Materials",
         A.S.M., Metals Park, Ohio, U.S.A., p 107, 1964.

(31)   Hillier, M.J. "Tensile Plastic Instability of Thin
         Tubes - pt. I", Int. J. Mech. Sci., 7, pp 531-538, 1965.

(32)   Hart, E.W. "Theory of the Tensile Test", Acta. met.,
         15, pp 351-355, 1967.

(33)   Argon, A.S. in "Inhomogeneity of Plastic Deformation",
         A.S.M., Metals Park, Ohio, U.S.A., p 161, 1972.

(34)   Duncombe, E. "Plastic Instability and Growth of Grooves
         and Patches in Plates or Tubes", Int. J. Mech. Sci.,
         14, pp 325-337, 1972.

(35)   Duncombe, E. "Analysis of Diffuse Plastic Stability
         in Tubes and Sheet", Int. J. Solids. Struc., 10,
         pp 1445-1458, 1974.

(36)   Ghosh, A.K. and Ayres, R.A. "On Reported Anomolies
         in Relating Strain-Rate Sensitivity (m) to Ductility",
         Met. Trans., 7, pp 1589-1591, 1976.

(37)   Azrin, M. and Backofen, W.A. "The Deformation and Failure
         of a Biaxially Stretched Sheet", Met. Trans., 1, pp 2857-
         2865, 1970.

(38)   Cambell, J.D. "Plastic Instability in Rate-Dependent
         Materials", J. Mech. Phys. Solids, 15, pp 359-370,
         1967.

(39)   Demeri, M.Y. and Conrad, H. "Instability of Plastic
         Flow in Tension", Scr. Met., 12, p 389, 1978.

(40)   Violan, P. "Stability Criterion for the Tensile Plastic
         Deformation of Cubic Centred Metals", Scr. Met., 6,
         pp 1175-1183, 1972.

(41)   Jonas, J.J., Holt, R.A. and Coleman, C.E. "Plastic
         Stability in Tension and Compression", Acta. Met., 24,
         pp 911-918, 1976.

(42)   Kocks, U.F., Jonas, J.J. and Mecking, H. "The Development
         of Strain-Rate Gradients", Acta. Met., 27, pp 419-432,
         1979.

(43)   Marciniak, Z., Kuczynski, K. and Pokora, T. "Influence
         of the Plastic Properties of a Material on the Forming
         Limit Diagram for Sheet Metal in Tension", Int. J. Mech.
         Sci., 15, pp 789-805, 1973.

(44)   Jonas, J.J., Christodoulou, N. and G'Sell C. "The Onset
         of Flow Localization in Tensile Samples Containing Geo-
         metric and Metallurgical Defects", Scr. Met., 12,
         pp 565-570, 1978.

(45)   Jonas, J.J. "Effect of Crack and Cavity Generation on
         Tensile Stability", Acta. Met., 25, pp 43-50, 1977.

(46)   Ghosh, A.K. "Tensile Instabilty and Necking in Materials
         with Strain Hardening and Strain-Rate Hardening", Acta.
         Met., 25, pp 1413-1424, 1977.

(47)   Sagat, S. and Taplin, D.M.R. "The Stability of Plastic
         Flow in Strain-Rate Sensitive Materials", Met. Sci.,
         10, pp 94-100, 1976.

(48)   Hutchinson, J.W. and Neale, K.W. "Influence of Strain-
         Rate Sensitivity on Necking Under Uniaxial Tension",
         Acta. Met., 25, pp 839-846, 1977.

(49)   Fyfe, I.M. and Rajendran, A.M. "Dynamic Pre-Strain
         and Inertia Effects on the Fracture of Metals", J. Mech.
         Phys. Solids, 28, pp 17-26, 1980.

(50) Keeler, S.P. and Backofen, W.A. "Plastic Instability and Fracture in Sheets Stretched Over Rigid Punches", Trans. A.S.M., 56, pp 25-48, 1963.

(51) Hill, R. "On Discontinuous Plastic States, with Special Reference to Localized Necking in Thin Sheets", J. Mech. Phys. Solids, 1, pp 19-30, 1952.

(52) Wilson, D.V. "The Effects of 2nd Phase Particles on the Mechanical Properties of Steels", Proc. Conf. Iron Steel Inst., Scarborough, 1971.

(53) Bridgeman, P.W. "The Stress Distribution at the Neck of a Tension Specimen", Trans. A.S.M., 32, pp 553-572, 1944.

(54) Davidenkov, N.N. and Spiridonova, N.I. "Analysis of the State of Stress in the Neck of a Tension Test Specimen", Proc. A.S.T.M., 46, pp 1147-1158, 1946.

(55) Pearce, R. "Some Aspects of Anisotropic Plasticity in Sheet Metals", Int. J. Mech. Sci., 10, pp 995-1005, 1968.

(56) Ghosh, A.K. and Backofen, W.A. "Strain Hardening and Instability in Biaxially Stretched Sheets", Met. Trans., 4, pp 1113-1123, 1973.

(57) Lankford, W.T., Snyder, S.C. and Bauscher, J.A. "New Criteria for Predicting the Press Performance of Deep-Drawing Sheets", Trans. A.S.M., 42, pp 1197-1225, 1950.

(58) Mitsukashi, T., Kimura, K. and Hosoi, Y. "Aptitude for Deep-Drawing and Anisotropy of Thin Steel Sheets", Tetsu to Hagane, 44, pp 749-754, 1958.

(59) Krupkowski, A. and Kawinski, S. "The Phenomenon of Anisotropy in Annealed Polycrystalline Metals", J. Inst. Met., 75, pp 869-880, 1948.

(60) Whitely, R.L., Wise, D.E. and Blickwede, D.J. "Anisotropy as an Asset for Good Drawability", S.M.I., 38. pp 349-353 and p 358, 1961.

(61) Truszkowski, W. "Influence of Strain on the Plastic Strain Ratio in Cubic Metals", Met. Trans., 7, pp 327-329, 1976.

(62) Atkinson, M. "Assessing Normal Anisotropic Plasticity of Sheet Metals", S.M.I., 44, pp 167-178, 1967.

(63) Hu, H. "Effect of Plastic Strain on the r-Value of Textured Sheet Steel", Met. Trans., 6, pp 2307-2309, 1975.

(64) Arthey, R.P. and Hutchinson, W.B. "The Plastic Strain Ratio of Homogeneously and Inhomogeneously Deformed Steels", Proc. I.C.O.T.O.M. 6, 2, pp 1057-1065, Iron Steel Inst. Japan, 1981.

(65) Whiteley, R.L. "How Crystallographic Texture Controls Drawability", Met. Prog., 94, pp 81-84, 1968.

(66) Burns, R.S. and Heyer, R.H., Symposium on the Annealing of Low Carbon Steel Sheet, Case Inst. of Tech., Cleveland, Ohio, 1957.

(67) Atkinson, M. and Maclean, I.M. "Normal Plastic Anisotropy in Steel Sheet", S.M.I., 42, pp 290-298, 1965.

(68) Grumbach, M. and Pomey, G. "Method of Measuring the Coefficients of Anisotropy and Work Hardening", S.M.I., 43, pp 515-529, 1966.

(69) Duncan, K., Goni, E. and Johnson, W. "Measurement of Normal Plastic Anisotropy in Sheet Metal", J. Aust. Inst. Met., 12, pp 127-137, 1967.

(70) Wilson, D.V. and Butler, R.D. "The Role of Cup Drawing Tests in Measuring Drawability", J. Inst. Met., 90, pp 473-483, 1961.

(71) Stickels, C.A. and Mould, P.R. "The Use of Youngs Modulus for Predicting the Plastic Strain Ratio of Low Carbon Steel Sheets", Met. Trans., 1, pp 1303-1312, 1970.

(72) Alders, G.A. and Liu, Y.C. "Calculation of Elastic Anisotropy in Rolled Sheet", Trans. A.I.M.E., 236, pp 482-489, 1966.

(73) Liu, Y.C. and Alders, G.A. "The Anisotropy of Youngs Modulus in Cold-Rolled Sheets of Binary Cu-Zn Alloys", Trans. A.I.M.E., 236, pp 489-495, 1966.

(74)   Alders, G.A. and Liu, Y.C. "The Nature of Transition
         Textures in Copper", Trans. A.I.M.E., 239, pp 210-216,
         1967.

(75)   Alders, G.A., Choi, S.S. and Liu, Y.C. "The Effect of
         Neutron Irradiation on the Rolling Texture of Copper",
         Trans. A.I.M.E., 239, pp 917-919, 1967.

(76)   Whiteley, R.L. "The Importance of Directionality in
         Drawing Quality Steel Sheet", Trans. A.S.M., 52,
         pp 154-163, 1960.

(77)   Lilet, L. "Suitability of Sheets for Pressing", S.M.I.,
         43, pp 949-957, 1966.

(78)   Kawai, N., Tomata, E., Moriya, K., Akaki, H., Kondo, K.
         and Fujimura, Y. "The Effects of Processing Variables
         on Formability of Aluminium Sheet", Bull. Jap. Soc.
         Mech. Eng., 12, pp 1223-1231, 1969.

(79)   Rogers, R.W. (Jnr) and Anderson, W.A. "Metal Forming",
         Ed. Hoffmanner, A.L., A.I.M.E. Plenum Press, N.Y., p 185,
         1971.

(80)   Davison, R.M. "Formability of Low-Interstitial
         18% Cr - 2% Mo Ferritic Stainless Steel", Met. Trans.,
         5, pp 2287-2294, 1974.

(81)   Goodenow, R.H. and Held, J.F. "Recrystallization of
         Low-Carbon Titanium Stabilized Steel", Met. Trans.,
         1, pp 2507-2515, 1970.

(82)   Rennhack, E.H. "How Normal Anisotropy Influences Form-
         ability of Aluminium Alloys", Met. Eng. Qrt., 16,
         pp 58-64, 1976.

(83)   Lloyd, D.H. "Anisotropy in the Press Forming Industry",
         S.M.I., 39, pp 863-875, 1962.

(84)   Stanley, J.K. "Orientation in Low-Carbon Deep-Drawing
         Steel", Trans. A.I.M.E., 158, pp 354-371, 1944.

(85)   Tucker, G.E.G. "Texture and Earing in Deep-Drawing of
         Aluminium", Acta. Met., 9, pp 275-286, 1961.

(86)   Tresca, H. "Mémoires Présentés par Divers Savants à l'Académie des Sciences", 18, pp 733-799, 1868.

(87)   Von Mises, R., Gottingen Nachrichten, Math.-Phys. Klasse, p 582, 1913.

(88)   Huber, M.T., Czasopismo Technizne, 22, p 81, 1904.

(89)   Backofen, W.A. "Deformation Processing", Met. Trans., 4, pp 2679-2699, 1973.

(90)   Hencky, H. and Angew, Z., Math. Mech., 4, pp 323-334, 1924.

(91)   Hill, R. "A Theory of Yielding and Plastic Flow of Anisotropic Metals", Proc. Roy. Soc. (LONDON), 193, pp 281-297, 1948.

(92)   Hill, R. "The Mathematical Theory of Plasticity", Clarendon Press, Oxford, Ch. 12, 1950.

(93)   Backofen, W.A. "Deformation Processing", Addison-Wesley, Mass, 1972.

(94)   Lee, D. "A Continuum Description on Anomalous Yielding in Anisotropic Metals", Met. Trans., 9, pp 1495-1497, 1978.

(95)   Woodthorpe, J. and Pearce, R. "The Anomalous Behaviour of Aluminium Sheet Under Balanced Biaxial Tension", Int. J. Mech. Sci., 12, pp 341-347, 1970.

(96)   Bassani, J.L. "Yield Characterization of Metals with Transversely Isotropic Plastic Properties", Int. J. Mech. Sci., 19, pp 651-660, 1977.

(97)   Trozera, T.A., Sherby, O.D. and Dorn, J.E. "Effect of Strain Rate and temperature on the Plastic Deformation of High Purity Aluminium", Trans. A.S.M., 49, pp 173-188, 1957.

(98)   Hockett, J.E. "On Relating the Flow Stress of Aluminium to Strain, Strain Rate and Temperature", Trans. A.I.M.E., 239, pp 969-976, 1967.

(99)   Holt, D.L., Babcock, S.G., Green, S.J. and Maiden, C.J.
         "The Strain-Rate Dependence of Flow Stress in Some
         Aluminium Alloys", Trans. A.S.M., 60, pp 152-159, 1967.

(100)   McQueen, H.J. "Deformation Mechanisms in Hot Working",
         J. Met., 20, pp 31-38, 1968.

(101)   D'Antonio, C.R., Maciag, R.J., Mukherjee, K. and Fischer, G.J.
         "The Effect of Strain Rate and Temperature on the Flow Stress
         of 7075 Aluminium", Trans. A.I.M.E., 242, pp 2295-2297, 1968.

(102)   Wilson, D.V. "Overview of Temperature and Strain-Rate
         Effects", Proc. Int. Conf. Met. Eng., Univ. Aston,
         Birmingham, U.K., 1981.

(103)   Ghosh, A.K. and Hecker, S.S. "Failure in Thin Sheets
         Stretched Over Rigid Punches", Met. Trans., 6, pp 1065-
         1074, 1975.

(104)   Lin, I.H., Hirth, J.P. and Hart, E.W. "Plastic Instability
         in Uniaxial Tension Tests", Acta. Met., 29, pp 819-827,
         1981.

(105)   Orowan, E. "Fracture and Strength of Solids", Rep. Prog.
         Phys., 12, pp 185-232, 1948.

(106)   Orowan, E., Nye, J.F. and Cairns, W.J. "Strength and
         Testing of Materials", H.M. Stationary Office, Vol. 6
         pt. 1, p 127, 1952.

(107)   Cottrell, A.H. "Fracture", Ed. Averbach, B.L., Chapman
         and Hall, London, p 20, 1959.

(108)   Meakin, J.D. and Petch, N.J. "Fracture of Solids",
         Ed. Drucker, D.C. and Gilman, J.J., Interscience, N.Y.
         p 393, 1963.

(109)   Tipper, C.F. "The Fracture of Metals", Metallurgia,
         39, pp 133-137, 1949.

(110)   Gurland, J. "Observations on the Fracture of Cementite
         Particles in a Spheroidized 1.5% C Steel Deformed at
         Room Temperature", Acta. Met., 20, pp 735-741, 1972.

(111)   Crussard, C., Plateau, J., Tamhankar, R., Henry, G.
         and Lajeunesse, D. "Fracture", Ed. Averbach, B.L.,
         Chapman and Hall, p 524, 1959.

(112)   Liu, C.T. and Gurland, J. "The Fracture Behaviour of
         Spheroidized Carbon Steels", Trans. A.S.M., 61, pp 156-
         167, 1968.

(113)   Hayden, H.W. and Floreen, S. "Observations of Localized
         Deformation During Ductile Fracture", Acta. Met., 17,
         pp 213-224, 1969.

(114)   Thomason, P.F. "Prospects of Fracture Mechanics", Ed.
         Sih, G.C., Van Elst, H.C. and Broek, D., Noordhoff,
         Netherland, p 3, 1974.

(115)   Puttick, K.E. "Ductile Fracture in Metals", Phil. Mag.,
         14, pp 964-969, 1959.

(116)   Rogers, H.C. "The Tensile Fracture of Ductile Metals",
         Trans. A.I.M.M.E., 218, pp 498-506, 1960.

(117)   French, I.E. and Weinrich, P.F. "The Shear Mode of
         Ductile Fracture in Materials with Few Inclusions",
         Met. Trans., 7, pp 1841-1845, 1976.

(118)   McClintock, F.A. "On the Mechanics of Fracture from
         Inclusions", Paper from 'Ductility', A.S.M., Metals
         Park, Ohio, pp 255-277, 1978.

(119)   Rice, J.R. and Tracey, D.M. "On the Ductile Enlargement
         of Voids in Triaxial Stress Fields", J. Mech. Phys.
         Solids, 17, pp 201-217, 1969.

(120)   Palmer, I.G. and Smith, G.C., Proc. 2nd Bolton Landing
         Conf. on Oxide Dispersion Strengthening, Gordon and
         Breach, N.Y., p 253, 1968.

(121)   Brown, L.M. and Stobbs, W.M. "The Work-Hardening of
         Copper-Silica pt. 2", Phil. Mag., 23, pp 1201-1223,
         1971.

(122)   Gurland, J. "The Fracture Strength of Sintered Tungsten
         Carbide-Cobalt Alloys in Relation to Composition and
         Particle Spacing", Trans. A.I.M.M.E., 227, pp 1146-1150,
         1963.

(123) Gurland, J. and Plateau, J. "The Mechanism of Ductile Rupture of Metals Containing Inclusions", Trans. A.S.M., 56, pp 442-454, 1963.

(124) Palmer, I.G., Smith, G.C. and Warda, R.D. Proc. Conf. "Physical Basis of Yield and Fracture", Ed. Strickland, A.C., Inst. Physics and the Phys. Soc., London, p 53, 1966.

(125) Zener, C. "Fracturing of Metals", A.S.M., Metals Park, Ohio, p 3, 1949.

(126) Ashby, M.F. "Work Hardening of Dispersion Hardened Crystals", Phil. Mag., 14, pp 1157-1178, 1966.

(127) Argon, A.S., Im, J. and Safoglu, R. "Cavity Formation From Inclusions in Ductile Fracture", Met. Trans., 6, p 825-837, 1975.

(128) Guillen-Preckler, A., Annls. C.I.R.P., 15, p 183, 1967.

(129) McClintock, F.A. and Argon, A.S. "Mechanical Behaviour of Materials", Addison-Wesley, N.Y., p 524, 1980.

(130) Edelson B.T. and Baldwin, M.M. "The Effect of Second Phases on the Mechanical Properties of Alloys", Trans. A.S.M., 55, pp 230-250, 1962.

(131) Ansell, G.S. and Lenel, F.V. "Criteria for Yielding of Dispersion-Strengthened Alloys", Acta. Met., 8 pp 612-616, 1960.

(132) McLean, D. "Mechanical Properties of Metals", John Wiley, N.Y., p 124, 1962.

(133) Roberts, C.S., Caruthers, R.C. and Averbach, B.C. "The Initiation of Plastic Strain in Plain Carbon Steels", Trans. A.S.M., 44, pp 1150-1157, 1952.

(134) Lenel, F.V., Ansell, G.S. and Nelson, E.C. "Metallography of Aluminium Powder Extrusions", Trans. A.I.M.M.E., 209, pp 117-124, 1957.

(135) Melander, A. "Ductile Fracture in a Random Distribution of Voids", Mater. Sci. Eng., 39, p 57-63, 1979.

(136)   Melander, A. and Stahlberg, U. "The Effect of Void
        Size and Distribution on Ductile Fracture", Int. J.
        Frac., 1979.

(137)   Needleman, A. and Rice, J.R. "Limits of Ductility Set
        by Plastic Flow Localization", Mechanics of Sheet Metal
        Forming: Material Behaviour and Deformation Analysis,
        Plenum Press, N.Y., 1978.

(138)   Melander, A. "Void Growth during Wire Drawing and Tensile
        Testing", Scand. J. Met., 9, pp 267-272, 1980.

(139)   Altenburger, C.L. "Some Factors in Physical Properties
        that Influence Deep-Drawing Behaviour", Proc. A.I.M.E.,
        p 73, 1957.

(140)   Lloyd, D.H. "Metallurgical Engineering in the Pressed
        Metal Industry", S.M.I., 39, pp 7-19, 1962.

(141)   Sandin, A. "The Tensile Test - A Measure of Drawability",
        Fernkontarets Annaler, 148, p 259, 1964.

(142)   Butler, R.D. "Relationship Between Sheet Metal Formability
        and Certain Mechanical Properties", S.M.I., 41, p 704-716,
        1964.

(143)   U.S.A. National Committee of the I.D.D.R.G. "Correlation
        of Deep-Drawing Press Performance with Tensile Properties",
        A.S.T.M., STP 390, 1965.

(144)   Keeler, S.P. "Ductility of Anisotropic Sheet Metal".
        Presented at A.S.M. National Met. Cong., Oct. 1967.

(145)   I.D.D.R.G. "Anisotropy and Tensile Test Properties and
        their Relationship to Sheet Metal Forming", Inst. S.M.E.,
        June 1964.

(146)   Nelson, P.G. "Simplified Methods of Determining 'r' and
        'n' Values in the Tensile Test", The Budd Co. Product
        Lab., Automotive Div., Philadelphia, Feb. 1964.

(147)   A.S.T.M. "Standard Methods and Definitions for Mechanical
        Testing of Sheet Products", A.S.T.M., A370-65, p 378,
        Feb. 1966.

(148)   Swift, H.W. "Drawing tests for Sheet Metal", Proc.
          Inst. Automobile Eng., 34, p 361, 1939.

(149)   Swift, H.W. "Two-Stage Drawing of Cylindrical Cups",
          Trans. Inst. Eng. and Shipbuilders in Scotland, 86,
          p 195, 1942.

(150)   Chung, S.Y. and Swift, H.W. "Cup Drawing From a Flat
          Blank", Proc. Inst. Mech. Eng., 165, pp 199-223, 1951.

(151)   Chung, S.Y. and Swift, H.W. "An Experimental Investigation
          into the Redrawing of Cylindrical Shells", Proc. Inst.
          Mech. Eng., 166, pp 437-447, 1952.

(152)   Loxley, E.M. and Swift, H.W. "The Wedge-Drawing Test",
          Engineering, 159, pp 38-40, 77-80, 136-138, 1945.

(153)   Swift, H.W. "The Mechanism of a Simple Deep-Drawing
          Operation", S.M.I. 31, pp 817-828, 1954.

(154)   Willis, J. "Deep-Drawing: A Review of the Practical
          Aspects of Prof. H.W. Swift's Researches", Butterworths
          Scientific Publications, London, 1954.

(155)   Jevons, J.D. "The Deep-Drawing and Pressing of Non-
          Ferrous Metals and Alloys", J. Inst. Met., 78, pp 591-601,
          1950.

(156)   Sachs, G. "Principals and Methods of Sheet Metal
          Fabricating", Reinhold pub. Corp., pp 26-39, 1951.

(157)   de Witte, G. "The Need for Specific Metal-Testing
          Methods for Deep-Drawing and Forming", S.M.I., 35,
          pp 19-20, 1958.

(158)   Yoshida, K. "Classification and Systemization of Sheet
          Metal Press Forming Processes", Sci. Paper I.P.C.R.,
          Tokyo, 53, pp 126-187, 1959.

(159)   de Witte, G. "Some Aspects of the Development of Testing
          Methods for the Formability of Sheet", S.M.I., 37,
          pp 565-571, 1960.

(160)   Erichsen, A.M. "Ein Neues Prüfverfahren fur Feinblech",
          Stahl und Eisen, 34, pp 879-882, 1914.

(161)   Kummer, H. "Untersuchung am Blechprüfapparat von Erichsen",
         Maschinenbau und Betrieb, 5, pp 657-661, 1926.

(162)   Kokkonen, V. and Nygren, G. "Investigations into the
         Accuracy of the Erichsen Cupping Test", S.M.I., 36,
         pp 167-178, 1959.

(163)   Mellor, P.B. and Loxley, E.M. "The Hydrostatic Bulging
         of Circular Metal Diaphrams", B.I.S.R.A. Research Report
         N° MW/E/36/52, 1952.

(164)   Siebel,E. and Pomp, A. "Ein Neues Prüfverfahren für
         Feinblech", Mitt. K.W. Inst. für Eisenforschung, 11,
         pp 287-291, 1929.

(165)   Siebel, E. and Pomp, A. "Die Prüfung von Feinblechen
         durch den Tiefzieh-Weitungsversuch", Mitt. K.W. Inst.
         für Eisenforschung, 12, pp 115-125, 1930.

(166)   Güth, H. "Ein Neues Streckziehverfahren", Metallwirtschaft,
         20, pp 55-58, 1941.

(167)   Patterson, W. "Streckziehfähigkeit de Al-Mg Legierungen",
         Metallwirtschaft, 21, pp 429-431, 1942.

(168)   Kasper, A.S. "Forming of Sheet Metal Parts", Amer. Soc.
         Tool and Manufacturing Eng., Paper N° MF69-516, 1969.

(169)   Beer, F. "Improving the Accuracy of the Erichsen Cupping
         Test", S.M.I., 48, pp 792-794, 1971.

(170)   Hawtin, L.R. and Parkes, G.M. "Erichsen Test for Form-
         ability of Metal Sheet", S.M.I., 47, pp 533-543, 1970.

(171)   Sachs, G. "Ein Neues Prüfgerät für Tiefziehbleche",
         Metallwirtschaft, 9, pp 213-218, 1930.

(172)   Blume, I. "Ermittlung der Ziehfahigkeit von Tiefstanz-
         blechen", Metallbörse, 12, pp 1945-1946, 1922.

(173)   Fischer, G.R. "A.E.G. - Tiefziehprufverfahren", A.E.G. -
         Mitteilungen, 7, pp 483-486, 1929.

(174)   Oehler, G. "Die Tiefziehgüte von Messingblechen nach
         dem A.E.G. - Prüfverfahren", Metallwirtschaft, 16,
         p 1059, 1937.

(175)   Schmidt, M. "Die Prüfung von Tiefziehblech", Arch.
         Eisenhüttenwesen, 3, pp 213-222, 1929.

(176)   Beisswanger, H. "Das Näpfchenziehprüfverfahren zur
         Bestimmung der Tiefzieheigenschaften von Blechen und
         Bändern", Mitt. Forsch-Ges. Blechverarbeitung, 18,
         pp 201-222, 1952.

(177)   Fukui, S., Yuri, H. and Yoshida, K. "Analysis for Deep-
         Drawing of Cylindrical Shell Based on Total Strain Theory
         and Some Formability Tests", Aeronautical Research Inst.,
         Univ. of Tokyo, Report N° 332, pp 69-75, 1958.

(178)   The Conical Cup Test Research Group, "The Conical Cup
         Test as a Method of Testing the Drawing and Forming
         Qualities of Sheet Steel", The Conical Cup Test Research
         Group, c/o Inst. of Physical and Chemical Research,
         Tokyo, 1958.

(179)   Kayseler, H. "Uber die Eigenschaften von Vershieden
         Behandeltem Bandstahl mit Besonderer Berücksichtigung
         der Tiefzieheignung und deren Prüfung" Mitt. Forsch-
         Inst. Ver. Stahlwerke, Dortmund, 4, pp 39-42, 1934.

(180)   Kayseler, H. "Prufmaschinen für das Keilzug-Tiefungsver-
         fahren", Maschinenbau U. Betrieb, 16, p 246, 1937.

(181)   Engelhardt, W. "Verfahrensgerechte Tiefziehprüfung",
         Fertigungstechnik, 8, pp 530-537, 1958.

(182)   Engelhardt, W. "Neues Verfahren Zur Prüfung der
         Tiefziehfähigkeit", Mitt. Forsch-Ges. Blechverarbeitung,
         22, pp 287-292, 1959.

(183)   Gross, H. and Engelhardt, W. "Verfahrensgerechte Bestimmung
         der Tiefziehfähigkeit von Blechen", Fertigungstechnik und
         Betrieb, 10, pp 24-32, 1960.

(184)   Gross, H., Engelhardt, W. and Melzer, K. "Prüfgerät
         und Verfahren zur Bestimmung des Natürlichen Masses
         der Tiefziehfähigkeit von Blechen", Maschinenbautechnik,
         9, pp 238-240, 1960.

(185)   Engelhardt, W. "Ein Neues Tiefzieprüfverfahren",
         Technisches Zentralblatt für Praktische Metallbearbeitung,
         54, pp 564-567, 1960.

(186)   Rickert, A. and Gross, H. "Bestimmung der Tiefzieh-
         fähigkeit von Blechen. Einheitliche Prüfung nach dem
         Verfahren von Engelhardt und Gross", Fertigungstechnik
         und Betrieb, 11, pp 384-388, 1961.

(187)   Rickert, A. and Gross, H. "Bestimmung der Tiefzieh-
         fähigkeit von Blechen. Erläuterungen zu den Standardkurven",
         Fertigungstechnik un Betrieb, 11, pp 623-626, 1961.

(188)   Gensemer, M. "Strength and Ductility", Met. Prog.,
         49, pp 731-734, 1946.

(189)   Keeler, S.P. "Determination of Forming Limits in Auto-
         motive Stampings", S.A.E. Paper N° 650535, 1965.

(190)   Goodwin, G.M. "Application of Strain Analysis to Sheet
         Metal Forming Problems in the Press Shop", S.A.E. Paper
         N° 680093, 1968.

(191)   Nakazima, K., Kikuma, T. and Hasuka, K., Yamata Technical
         Report N° 264, p 141, 1968.

(192)   Goodwin, G.M. "Strain Analysis Problems in the Press-
         Shop", Met. Ital., 60, pp 767-774, 1968.

(193)   Woodthorpe, J. and Pearce, R. "The Effect of r and n
         upon the Forming Limit Diagrams of Sheet Steel", S.M.I.,
         46, pp 1061-1067, 1969.

(194)   Grumbach, M. and Sanz, G. "Influence of Certain Parameters
         on the Deep-Drawing Limit Curves", Rev. Met., 69,
         pp 273-289,1972.

(195)   Brozzo, P. and de Luca, B. "On the Interpretation of
         the Formability Limits of Metal Sheets and their
         Evaluation by Elementary Tests", Proc. Int. Conf. Sci.
         Technol. Iron Steel, Tokyo, pp,966-968, 1971.

(196)   Habberfield, A.B. and Boyles, M.W. "Laboratory Determined
         Forming Limit Diagrams", S.M.I., 50, pp 400, 402-405, 411,
         1973.

(197)   Venter, R. and de Malmerbe, M.C.   "Theoritical Estimate
         of the Keeler-Goodwin Formability Curve", S.M.I., 48,
         pp 656-658, 1971.

(198)   Marciniak, Z. and Kuczynski, K.   "Limit Strains in the
         Processes of Stretch-Forming Sheet Metal", Int. J. Mech.
         Sci., 9, pp 609-620, 1967.

(199)   Sowerby, R. and Duncan, J.L., S.M.E. MF71-134, 1971.

(200)   Sowerby, R. and Duncan, J.L., "Failure in Sheet Metal
         in Biaxial Tension", Int. J. Mech. Sci., 13, pp 217-229,
         1971.

(201)   American Society for Metal Committee on Formability of
         Sheet Steel, " The Selection of Low Carbon Steel Sheet
         for Formability", Metals Handbook 8th Ed., A.S.M.,
         pp 319-330, 1961.

(202)   Iron and Steel Technical Committee, "Method of Determining
         Plastic Deformation in Sheet Metal Stampings", S.A.E.,
         J863.

(203)   Keeler, S.P.   "Understanding Sheet Metal Formability",
         pts. 1-6, Machinery, 1968.

(204)   Keeler, S.P.   "Use of Grid Systems for Strain Determinations",
         I.D.D.R.G., June 1964.

(205)   Miller, J.A.   "Improved Photogrid Techniques for
         Determination of Strain Over Short Gauge Lengths", Proc.
         Soc. Exp. Stress Analysis, 10, pp 29-34, 1952.

(206)   Pearce, R. and Drinkwater, I.C.   "Some Aspects of Electro-
         chemical Marking", S.M.I., 45, pp 751-755, 1968.

(207)   Palmer, D.R.   "Electrochemical Marking of Grids in Auto-
         body Press Working", S.M.I., 45, pp 198-206, 1968.

(208)   Keeler, S.P.   "Circular Grid System - A Valuable Aid
         for Evaluating Sheet Metal Formability", S.M.I., 45,
         pp, 633-641, 1968.

(209)   Mayer, B.   "Handbook of Electrochemical Marking",
         Willoughby, Ohio, The Electromark Corp., 1967.

(210) Butler, R.D., North, D. and Davies, G.M. "Metallurgical Aspects of Sheet Steel for Press Shops", S.M.I., _48_, pp 842-854, 1971.

(211) Brookes, I.C. and Davies, G.M. "Grid Marking Techniques in the Press Shop", S.M.I., _49_, pp 707-710, 1972.

(212) Larsen, B. "Photochemical Etching of Circular Grids", S.M.I., _51_, pp 139-142, 1974.

(213) Hsu, T.C. "The Characteristics of Coaxial and Noncoaxial Strain Paths", J. Strain Analysis, _1_, pp 216-230, 1966.

(214) Hsu, T.C. "A Study of Large Deformations by Matrix Algebra", J. Strain Analysis, _1_, pp 313-321, 1966.

(215) Hsu, T.C. "Velocity Field and Strain-Rates in Plastic Deformation", J. Strain Analysis, _2_, pp 196-206, 1967.

(216) Veerman, C.C., Hartman, L., Peels, J.J. and Neve, R.F. "Determination of Appearing and Admissible Strains in Cold Reduced Sheets", S.M.I., _48_, pp 678-680, 1971.

(217) Veerman, C.C. "Some Aspects of the Determination of the F.L.D. - Onset of Localized Necking", S.M.I., _49_, pp 421-423, 1972.

(218) Nakazima, K. and Kikuma, T., Tetsu-to-Hagane, _53_, p 455, 1967.

(219) Kikuma, T. and Nakazima, K. "Effects of Deforming Conditions and Mechanical Properties on the Stretch-Forming Limits of Steel Sheets", Proc. Int. Conf. Sci. Technol. Iron Steel, pp 827-831, 1971.

(220) Parmar, A. and Mellor, P.B. "A New Model for the Prediction of Instability and Limit Strains in Thin Sheet Metal", Int. J. Mech. Sci., _19_, pp 389-398, 1977.

(221) Yamaguchi, K. and Mellor, P.B. "Thickness and Grain Size Dependence of Limit Strains in Sheet Metal Stretching", Int. J. Mech. Sci., _18_, pp 85-90, 1976.

(222) Charpentier, Ph. 1. "Influence of Punch Curvature on the Stretching Limits of Sheet Steel", Met. Trans., _6_, pp 1665-1669, 1975.

(223) Hiam, J. and Lee, A. "Factors Influencing the Forming Limit Curves of Sheet Steel", S.M.I., 55, pp 631-641, 1978.

(224) Hobbs, R.M. "Use of Grid Strain Analysis for Die Development and Process Control in Australian Press Shops", S.M.I., 55, pp 451-476, 1978.

(225) Kleemola, H., Kumpulainen, J. and Ranta-Eskola, A. "Factors Influencing the Forming Limits of Sheet Metals", Mem. Sci. Rev. Met. N° 3, pp 203-222, 1980.

(226) Ayres, R.A. and Wenner, M.L. "Strain and Strain-Rate Hardening Effects in Punch Stretching of 5182-0 Aluminium at Elevated Temperatures", Met. Trans., 10, pp 41-46,

(227) Duncan, J.L., Kolodziejski, J. and Glover, G. "Sheet Metal Forming and Energy Conservation", A.S.M., Metals Park, Ohio, p 131, 1976.

(228) Lloyd, D.J., McLaughlan, B.D. and Sang, H. "The Stress-Strain Behaviour of Aluminium Alloys at Large Strains", Scr. Met., 11, pp 297-300, 1977.

(229) Ghosh, A.K. and Hecker, S.S. "Stretching Limits in Sheet Metals: In-Plane Versus Out-of-Plane Deformation", Met. Trans., 5, pp 2161-2164, 1974.

(230) Van Minh, H., Sowerby, R. and Duncan, J.L. "Probablistic Model of Limit Strains in Sheet Metal", Int. J. Mech. Sci., 17, pp 339-349, 1975.

(231) Gronostajski, J.Z. and Sobis, T.J. "Formability of H.S.L.A. Steel Sheet", Int. Cong. Met. Eng., Univ. Aston. 1981.

(232) Van Minh, H., Sowerby, R. and Duncan, J.L. "Variability of Forming Limit Curves", Int. J. Mech. Sci., 16, pp 31-34, 1974.

(233) Yamamoto, H. "Conditions for Shear Localization in the Ductile Fracture of Void Containing Materials", 14, pp 347-365, 1978.

(234) Kaftanoglu, B. "Plastic Instability of Thin Shells Deformed by Rigid Punches and by Hydraulic Pressure", J. Eng. Mat. Tech., 95, pp 36-40, 1973.

(235)   Kaftanoglu, B. and Alexander, J.M. "On Quasistatic Axi-symmetrical Stretch Forming", Int. J. Mech. Sci, 12, pp 1065-1084, 1970.

(236)   Wilson, D.V. and Acselrad, O. "Effects of Microstructure on Forming Limits in Biaxial Stretching", I.D.D.R.G. 10th Biennial Congress, pp 155-166, 1978.

(237)   Embury, J.D. and Le Roy, G.H. "Failure Maps Applied to Metal Deformation Processes", Fracture, I.C.F.4, Waterloo, Canada, pp 15-42, 1977.

(238)   Glover, G., Duncan, J.L. and Embury, J.D. "Failure Maps for Sheet Metal", Met. Technol., pp 153-159, 1977.

(239)   Azrin, M. and Backofen, W.A., Met. Trans., 20, p 2, 1975.

(240)   Bramley, A.N. and Mellor, P.B. "Plastic Anisotropy of Titanium and Zinc Sheet - Macroscopic Approach", Int. J. Mech. Sci., 10, pp 211-219, 1968.

(241)   Horta, R.M.S.B., Roberts, W.T. and Wilson, D.V. "Effects of Plastic Anisotropy on the Biaxial Stretching Performance of Low-Carbon Steels", Int. J. Mech. Sci., 12, pp 231-243, 1970.

(242)   Yoshida, K., Yoshii, K., Komorida, H., Usuda, M. and Watanabe, H. "Significance of the X-value and the Work Hardening Exponent (n) Under Equibiaxial Tension in the Assessment of Sheet Metal Formability", S.M.I., 48, pp 772-783, 1971.

(243)   Hill, R. "Theoretical Plasticity of Textured Aggregates", Math. Proc. Cambridge Philos. Soc., 85, pp 179-191, 1979.

(244)   Hutchinson, W.B., Arthey, R. and Malmstrom, P. "On Anomalously Low Work Hardening in Pre-Strained Metals", Scripta. Met., 10, pp 673-675, 1976.

(245)   Ranta-Eskola, R.J. "Effect of Loading Path on Strss-Strain Relationships of Sheet Steel and Brass", Met. Technol., 7, pp 45-49, 1980.

(246)   Ronde-Oustau, F. and Baudelet,B. "Microstructure and Strain Path in Deep-Drawing", Acta. Met. 25, pp 1523-1529, 1977.

(247)   Hillier, M.J. "Tensile Plastic Instability of Thin
         Tubes - pt. 2 ", Int. J. Mech. Sci, $\underline{7}$, pp 539-549, 1965.

(248)   Negroni, F., Kobayashi, S. and Thomsen, E.G. "Plastic
         Instability in Simple Stretching of Sheet Metals", Trans.
         A.S.M.E., $\underline{90}$, pp 387-392, 1968.

(249)   Kobayashi, T., Ishagaki, H. and Abe, T. "Relations Between
         Deformation Behaviours and Geometrical Factors of Autobody
         Parts in Press Forming", Proc. Int. Conf. Sci. Technol.
         Iron Steel, Tokyo, pp 837-841, 1971.

(250)   Laukonis, J.V. and Ghosh, A.K. "Effects of Strain Path
         Changes on the Formability of Sheet Metals", Met. Trans.,
         $\underline{9}$, pp 1849-1855, 1978.

(251)   Mondolfo, L.F. "Aluminium Alloys: Structure and Properties",
         Butterworths, London, 1976.

(252)   Thomas, G. and Whelan, M.J. "Precipitation in Aluminium
         - 4% Copper Alloy", Proc. European Conf. on Electron
         Microscopy, Delf, pp 452-455, 1960.

(253)   Doi, K. "The Structure Analysis of a Guinier-Preston
         Zone by Means of a Fourier Method", Acta. Crys., $\underline{13}$,
         pp 45-49, 1960.

(254)   Rakin, V.G. and Buinov, N.N. "Effect of Plastic Deformation
         on the Stability of Precipitation Particles in an Aluminium
         - (4%) Copper Alloy", Physics Metals Metallography, $\underline{11}$,
         pp 61-73, 1961.

(255)   Hardy, H.K. and Heal, T.J. "Nucleation and Growth Processes
         in Metals and Alloys", Inst. of Metals Monograph and Report
         Series A N° 18, 1956.

(256)   Mahl, H. "Ultramicroscopic Surface (Structure) Deter-
         mination by Means of the Film Printing Method", Naturwiss,
         $\underline{30}$, pp 207-217, 1942.

(257)   Franz, H. and Kröner, E. "The Stability of Guinier-Preston
         Zones in Aluminium Copper Alloys", Z. Metallkunde, $\underline{46}$,
         pp 639-646, 1946.

(258)   Gerold, V. "The Structure of Guinier-Preston Zones in
         Aluminium Copper Alloys", Acta. Crys., $\underline{11}$, p 230,
         1958.

(259)   Castaing, R. and Laborie, P. "Particular Aspects of
         the Study of Thin Sections of Metals", Met. Abs., 22,
         p 117, 1954.

(260)   Buinov, N.N. and Shaskov, O.D. "An Investigation of
         the Structure of the Deformed Aluminium -(4%) Copper
         Alloy by Means of the Electron Microscope", Met. Abs.,
         24, p 813, 1956.

(261)   Gayler, M.L.V. "Some Characteristics of Copper - Aluminium
         Alloys Made from Aluminium of Very High Purity", J. Inst.
         Met., 63, pp 67-82, 1938.

(262)   Nicholson, R.B. and Nutting, J. "Direct Observation of
         the Strain Field Produced by Coherent Precipitated
         Particles in an Age-Hardened (Al - 4% Cu) Alloy", Phil.
         Mag., 3, pp 531-535, 1958.

(263)   Dehlinger, U. and Pfleiderer, H. "Structure Relationships
         of $CuAl_2$ and the Precipitation Lattice of Aluminium -
         Copper Alloys", Z. Metallkunde, 47, pp 229-231, 1956.

(264)   Samans, C.H. "The Process of Precipitation from Solid
         Solutions", Trans. Amer. Inst. Min. Met. Eng., 137,
         pp 85-94, 1940.

(265)   Nemoto, M. and Koda, S. "Direct Observation of the
         Change from the θ' Phase to the θ Phase on Precipitation
         in an Aluminium - Copper Alloy ", Nippon Kinzoku Gakkai-Si,
         27, pp 599-604, 1963.

(266)   Silcock, J.M. "The Structural Ageing Characteristics
         of Aluminium - Copper - Magnesium Alloys with Cu-Mg
         Weight Ratios of 7:1 and 2.2:1", J. Inst. Met., 89,
         pp 203-210, 1960.

(267)   Lutts, A. "Pre-Precipitation in Al-Mg-Ge and Al-Mg-Si
         Alloys", Acta. Met., 9, pp 577-586, 1961.

(268)   Castaing, R. "Investigations into the Ageing of Light
         Alloys by the Use of the Electron Microscope", Met. Abs.,
         17, p 813, 1949.

(269)   Hecker, S.S. "Simple Technique for Determining Forming
         Limit curves", S.M.I., 52 pp 671-676, 1975.

(270) Schulz, L.G. "A Direct Method of Determining Preferred Orientation for a Flat Reflection Sample Using a Geiger Counter X-Ray Spectrometer", J. App. Phys., 20 pp 1030-1033, 1949.

(271) Zinkham, R.E. and Dedrick, J.H. "Fracture", 6, Ed. Liebowitz, H., pp 299-370, Academic Press, N.Y., 1969.

(272) "Metals Handbook", 9, A.S.M., Ohio, 1961

(273) Hall, E.O. "The Deformation and Ageing of Mild Steel", Proc. Phys. Soc., 64B, pp 747-753, 1951.

(274) Carrecker, R.P. and Hibbard, W.R. "Tensile Deformation of Al as a Function of Temperature, Strain Rate and Grain Size", Trans. A.I.M.E., 209, pp 1157-1163, 1957.

(275) Fujita, H. and Tabata, T. "The Effect of Grain Size and Deformation Substructure on Mechanical Properties of Poly-crystalline Al", Acta. Met., 21, pp 355-365, 1973.

(276) Thompson, A.W. and Baskes, M.I. "The Influence of Grain Size on the Work Hardening of Face Centred Cubic Polycrystals", Phil. Mag., 28, pp 301-308, 1973.

(277) Dunwoody, B.J., Moore, D.M. and Thomas, A.T. "The Effect of Incoherent Particles on the Toughness of an Al-Mg-Si Alloy", J. Inst. Met., 101, pp 172-175, 1973.

(278) Saka, K., Painter, M.J. and Pearce, R. "The Uniaxial Strain-Hardening Behaviour of Sheet Metal From Zero Strain to Failure", Proc. 10th Biennial Cong. I.D.D.R.G., pp 167-174, 1978.

(279) Mellor, P.B. and Bramley, A.N. "Plastic Flow in Stabilizing Sheet Metal", Int. J. Mech. Sci., 8, pp 101-114, 1966.

(280) Hosford, W.F. (JR) and Backofen, W.A. "Fundamentals of Deformation Processing", Ed. Hosford W.F. et al, p 259, Syracuse University Press, Syracuse, 1964.

(281) Hosford, W.F. (JR) and Backofen, W.A., Proc. 9th Sagamore Ordnance Materials Research Conference, Syracuse University Press, Syracuse, 1965.

(282)   Bishop, J.F.W. and Hill, R., Phil. Mag., 42, pp 414 and
         1298, 1951.

(283)   Hero, H. and Naess, S.E. "Drawing Loads and Anisotropy in
         Aluminium", Met. Technol., 5, pp 264-269, 1978.

(284)   Andersson, B. "Plastic Instability in Stretch Forming
         of Al Zn Mg Alloys", Mem. Sci. Rev. Metall., pp 391-396,
         MARCH, 1980.

(285)   Bate, P. "Finite Element Modelling of the Hydraulic Bulging
         of Sheet Metal", Numerical Methods in Industrial Forming
         Processes", Eds. Wood, Pittman, Alexander and Zienkiewiez ,
         Pineridge, 1982.

(286)   Pearce, R. and Ganguli, D. "The Forming Limits of Al-Mg
         Alloy Sheet in Biaxial Tension", J. Inst. Met., 100,
         pp 289-295, 1972.

(287)   French, I.E. and Weinrich, P.F. "The Tensile Fracture
         Mechanisms of F.C.C. Metals and Alloys - A Review of the
         Influence of Pressure", J. Aust. Inst. Met., 22, pp 40-50,
         1977.

(288)   Bird, J.E. and Duncan, J.L. "Strain Hardening at High Strain
         in Aluminium Alloys and its Effect on Strain Localization",
         Met. Trans., 12, pp 235-241, 1981.